NASA/TM—2017-219437

# Chemical and Microstructural Changes in Metallic and Ceramic Materials Exposed to Venusian Surface Conditions

*Gustavo C. C. Costa*
*Vantage Partners, LLC, Brook Park, Ohio*

*Nathan S. Jacobson*
*Glenn Research Center, Cleveland, Ohio*

*Dorothy Lukco*
*Vantage Partners, LLC, Brook Park, Ohio*

*Gary W. Hunter and Leah Nakley*
*Glenn Research Center, Cleveland, Ohio*

*Brandon G. Radoman-Shaw and Ralph P. Harvey*
*Case Western Reserve University, Cleveland, Ohio*

June 2017

# NASA STI Program . . . in Profile

Since its founding, NASA has been dedicated to the advancement of aeronautics and space science. The NASA Scientific and Technical Information (STI) Program plays a key part in helping NASA maintain this important role.

The NASA STI Program operates under the auspices of the Agency Chief Information Officer. It collects, organizes, provides for archiving, and disseminates NASA's STI. The NASA STI Program provides access to the NASA Technical Report Server—Registered (NTRS Reg) and NASA Technical Report Server—Public (NTRS) thus providing one of the largest collections of aeronautical and space science STI in the world. Results are published in both non-NASA channels and by NASA in the NASA STI Report Series, which includes the following report types:

- TECHNICAL PUBLICATION. Reports of completed research or a major significant phase of research that present the results of NASA programs and include extensive data or theoretical analysis. Includes compilations of significant scientific and technical data and information deemed to be of continuing reference value. NASA counter-part of peer-reviewed formal professional papers, but has less stringent limitations on manuscript length and extent of graphic presentations.

- TECHNICAL MEMORANDUM. Scientific and technical findings that are preliminary or of specialized interest, e.g., "quick-release" reports, working papers, and bibliographies that contain minimal annotation. Does not contain extensive analysis.

- CONTRACTOR REPORT. Scientific and technical findings by NASA-sponsored contractors and grantees.

- CONFERENCE PUBLICATION. Collected papers from scientific and technical conferences, symposia, seminars, or other meetings sponsored or co-sponsored by NASA.

- SPECIAL PUBLICATION. Scientific, technical, or historical information from NASA programs, projects, and missions, often concerned with subjects having substantial public interest.

- TECHNICAL TRANSLATION. English-language translations of foreign scientific and technical material pertinent to NASA's mission.

For more information about the NASA STI program, see the following:

- Access the NASA STI program home page at http://www.sti.nasa.gov

- E-mail your question to help@sti.nasa.gov

- Fax your question to the NASA STI Information Desk at 757-864-6500

- Telephone the NASA STI Information Desk at 757-864-9658

- Write to:
  NASA STI Program
  Mail Stop 148
  NASA Langley Research Center
  Hampton, VA 23681-2199

NASA/TM—2017-219437

# Chemical and Microstructural Changes in Metallic and Ceramic Materials Exposed to Venusian Surface Conditions

*Gustavo C. C. Costa*
*Vantage Partners, LLC, Brook Park, Ohio*

*Nathan S. Jacobson*
*Glenn Research Center, Cleveland, Ohio*

*Dorothy Lukco*
*Vantage Partners, LLC, Brook Park, Ohio*

*Gary W. Hunter and Leah Nakley*
*Glenn Research Center, Cleveland, Ohio*

*Brandon G. Radoman-Shaw and Ralph P. Harvey*
*Case Western Reserve University, Cleveland, Ohio*

National Aeronautics and
Space Administration

Glenn Research Center
Cleveland, Ohio 44135

June 2017

## Acknowledgments

We are grateful to Dr. R. Rogers (NASA Glenn) for assistance with X-ray diffraction. Support from NASA Grant NNX14AN54G "Alteration of Basaltic Materials under simulated Venus Surface Conditions" is appreciated.

This report contains preliminary findings, subject to revision as analysis proceeds.



*Level of Review*: This material has been technically reviewed by technical management.

Available from

NASA STI Program
Mail Stop 148
NASA Langley Research Center
Hampton, VA 23681-2199

National Technical Information Service
5285 Port Royal Road
Springfield, VA 22161
703-605-6000

This report is available in electronic form at http://www.sti.nasa.gov/ and http://ntrs.nasa.gov/

# Contents



# List of Tables

## List of Figures

# Chemical and Microstructural Changes in Metallic and Ceramic Materials Exposed to Venusian Surface Conditions

Gustavo C. C. Costa
Vantage Partners, LLC
Brook Park, Ohio 44142

Nathan S. Jacobson
National Aeronautics and Space Administration
Glenn Research Center
Cleveland, Ohio 44135

Dorothy Lukco
Vantage Partners, LLC
Brook Park, Ohio 44142

Gary W. Hunter and Leah Nakley
National Aeronautics and Space Administration
Glenn Research Center
Cleveland, Ohio 44135

Brandon G. Radoman-Shaw and Ralph P. Harvey
Case Western Reserve University
Cleveland, Ohio 44106

## Summary

The chemical and microstructural behavior of steels (304, 310, 316, and 1018), nickel-based alloys (β-NiAl, G30, and 625), gold, coatings (4YSZ, SilcoNert® 1040 (SilcoTek Co.), Dursan® (SilcoTek Co.), and porcelain), and bulk ceramics (α-$Al_2O_3$, fused quartz, β-SiC, and α-$Si_3N_4$) were probed after exposure to supercritical fluid with temperature, pressure, and composition mimicking the Venus lower atmosphere. Exposures were carried out in the Glenn Extreme Environments Rig (GEER) chamber with the Venusian gas mixture (96.5% $CO_2$, 3.5% $N_2$, 30 ppm $H_2O$, 150 ppm $SO_2$, 28 ppm CO, 15 ppm OCS, 3 ppm $H_2S$, 0.5 ppm HCl, and 5 ppb HF) at 92 bar (1330 psi) and 467 °C (873 °F) for durations of 10 and 42 days. An additional 21-day exposure was done to stainless steel uncoated and coated with SilcoNert® and Dursan®. Samples were characterized before and after the experiment by gravimetric analysis, X-ray diffraction, X-ray photoelectron and Auger electron spectroscopies, and cross section electron microscopy analysis. All steels exposed for 10 and 42 days formed double-layered scales consisting mainly of metal (Cr, Fe, Ni) oxides and sulfides showing different chemistry, microstructure, and crystalline phases. The alloys G30 and 625 formed double-layered scales consisting mainly of nickel sulfides. After 10 days, the β-NiAl exhibited no detectable scale, suggesting only a very thin film was formed. The 304 and 316 stainless steels coated with 4YSZ that were exposed for 10 and 42 days exhibited no significant oxidation. Steel 1018 coated with 4YSZ exhibited a corrosion scale of iron and/or chromium oxide formed at the base of the alloy. The 304 steel coated with porcelain did not exhibit corrosion, although the coating exhibited recession. SilcoNert® exposed for 10 and 42 days exhibited recession, although no oxidation was found to occur at the base of the alloy. Stainless steel 316 coated with Dursan® exhibited corrosion at the base of the alloy. All ceramics tested showed no clear evidence of reaction. The weight-gain-per-area performance of the materials exposed in the GEER for 10 and 42 days are reported from the lowest to the highest weight gain per area as follows: gold did not exhibit any weight change; nickel-based alloys: β-NiAl < G30 < 625; steels: 304 < 310 < 316 < 1018; ceramics: considering the experimental uncertainties, no weight change was observed for all ceramics of this work (α-$Al_2O_3$, $Si_3N_4$, SiC, and amorphous $SiO_2$).

# 1.0 Introduction

Degradation of materials (Ref. 1) by supercritical fluids in extreme environments is a current and future concern for understanding the stability of materials. In the case of materials the lack of knowledge of these properties limits their use for energy and planetary and space exploration applications (e.g., nuclear reactors (Ref. 2), New Frontiers Missions: Venus In Situ Explorer (VISE) (Refs. 3 and 4). Such degradation processes generally occurs via several steps (Ref. 5):

(1) Transport of reactive species through the fluid or gas
(2) Transport of reactive species through a growing (usually oxide) scale
(3) Reaction at the oxide/substrate or oxide/fluid interface
(4) Transport of any additional products away from sample

The kinetics of oxidation is generally followed by recording either scale thickness as a function of time or weight change per unit area as a function of time. In general, oxidation kinetics follow either linear or parabolic rate laws (Ref. 5). These are shown in Figure 1. The most desirable is a parabolic rate law, which indicates that solid-state diffusion through the scale is rate limiting and as the scale grows, the reaction slows. The best method of recording kinetics is with a continuous weighing mechanism, which measures weight change throughout the course of the reaction. However, in many cases this is not possible, and the sample must be removed from the exposure chamber for weight measurements. In the latter case, more measurements are better for an accurate representation of kinetics.

Following is an overview of the interaction of metallic materials and ceramics in pure supercritical $CO_2$, which is less complex than the current study involving the atmosphere and temperature of Venus simulated in the Glenn Extreme Environments Rig (GEER). The GEER atmosphere consists of a supercritical mixture of $CO_2$ and $N_2$ as well as other minor gases and vapors ($SO_2$, $H_2O$, CO, OCS, HCl, HF, and $H_2S$).

The effects of pure supercritical $CO_2$ on alloys has been explored since the 1970s because of the use of supercritical $CO_2$ as coolants in nuclear power plants (Ref. 6). The oxidation of a metal in a particular alloy occurs when metal is transported to the metal/oxygen interface, and oxygen, to the oxide/oxygen interface (Ref. 7). This process depends on the redox potentials and diffusion characteristics of the chemical species and charge carriers that are approaching and at the interfaces (Fig. 2).

Assuming that the processes occurring at the interfaces are kinetically rapid and thermodynamic governed, it is possible to predict the formation of the stable phases (metal oxides) on a metal through Ellingham diagrams (Ref. 8). In these diagrams, the Gibbs free energies of different reactions between metals and gaseous phase of $CO_2$, CO, and $O_2$ are related at different partial pressures and temperatures. In an oxidation process, it is desirable that one of the elements in an alloy forms a stable, dense, and protective oxide scale that prevents or significantly diminishes material loss at the surface at the alloy (Ref. 9). It is undesirable to form an oxide with porosity, high thermal coefficient mismatch between the metal and metal oxide, or with a high concentration of point defects (Ref. 9). Porosity and high concentration of point defects in oxides provides the ideal condition for the diffusion of molecular and ionic species, leading to continuous reaction between the supercritical and solid phases. Different thermal coefficient mismatch and rapid oxide growth leads to spallation of the oxide scale. In the case of exposure of austenitic alloys to pure supercritical $CO_2$, it is commonly expected that the following reactions will occur (Refs. 1 and 9):

$$xM + yCO_2 = M_xO_y + yCO \quad (1)$$

$$CO = CO_2 + C \quad (2)$$

$$xM + yCO = M_xO_y + yC \quad (3)$$

For an Fe-Cr alloy (stainless steel), M represents Fe, and another set of reactions may be written where M represents Cr. In these reactions a double-layered scale consisting of $Fe_3O_4$ (magnetite, outer layer) and $Cr_2O_3$ or $(Fe_xCr_y)O_4$ spinels (inner, protective layer) are formed during the oxidation process (Refs. 6 and 9). It is also possible that the carbon released by Reaction (2) causes a rapid increase of the carbon concentration in the alloy, which can lead to the formation of insoluble chromium carbides at the grain boundaries (Ref. 10). In addition to preventing the formation of a protective chromium oxide layer, the formation of carbides "weakens" the bonds between grains of the alloy, which can lead to the cracking and collapse or failure of the material. In general, the high content of chromium added to the austenitic steels enables a rapid formation of protective chromium-based oxide scales that minimizes the formation of carbides (Ref. 9). The addition of sulfur, nickel, and silicon in alloys has been reported to improve oxidation resistance of these materials exposed to supercritical $CO_2$ (Refs. 6, 9, 11, and 12). It has also been reported that nickel-based alloys exposed to supercritical $CO_2$ form a protective oxide layer that follows parabolic kinetics (Ref. 9).

In case of ceramic materials, although the reactivity of the ceramic might be low in pure supercritical $CO_2$, the presence of other gases and vapors in the Venusian atmosphere as well as their higher density and temperature significantly increases their solubility (Ref. 13). Chloride, fluoride, sulfite (from HCl, HF, and $H_2S$), and water also play a key role as ligands in providing charge stability for metallic ions, which increases the solubility or enhances the transport of chemical species in and out of the ceramic materials. Thus the species present in the Venus simulated atmosphere in the GEER are expected to have a detrimental effect on the oxidation or reactivity of the ceramics as well. These processes involving transfer of the ceramic material into the supercritical phase may lead to recession and failure of the ceramics, including the coatings. Moreover, it is well known that anions such as chloride, fluoride, and sulfide are good catalysts to increase the rate of corrosion of alloys since they work as electrolytes.

The goal of this work is to study the chemistry, structure, microstructure, and kinetics of metallic materials, coatings, and bulk ceramics exposed to supercritical fluid consisting of the chemical composition and temperature and pressure conditions of the Venus atmosphere (96.5% $CO_2$, 3.5% $N_2$, 30 ppm $H_2O$, 150 ppm $SO_2$, 28 ppm CO, 15 ppm OCS, 3 ppm $H_2S$, 0.5 ppm HCl, and 5 ppb HF at 92 bar (1330 psi) and 467 °C (873 °F).

# 2.0 Experimental

## 2.1 Materials

The materials used in this work are divided into three groups:

Group I—metallic materials
- steels 304, 310, 316, and 1018
- nickel-based alloys consisting of β-NiAl, G30, and 625
- gold

Group II—coatings
- 4 mol% yttria-stabilized zirconia (4YSZ)
- SilcoNert® 1040 (amorphous-based carboxysilane material from SilcoTek Co.)
- Dursan® (amorphous-based silicon material from SilcoTek Co.)
- porcelain

Group III—ceramics
- α-$Al_2O_3$
- fused quartz ($SiO_2$)
- polycrystalline monolithic CVD β-SiC
- CVD α-$Si_3N_4$

The metallic materials are described in Table 1, and their chemical composition provided by their manufacturers are in Table 2. The β-NiAl disc-like samples were cast in-house and were 0.3 cm thick and 1.2 cm in diameter. Gold wire samples (99.999% pure) were approximately 8 cm long and 0.2 cm in diameter. The ceramic materials are described in Table 3. The coatings SilcoNert® and Dursan® were applied on the steels 304 and 316 by SilcoTek Co. (Bellefonte, PA). According to SilcoTek Co., the SilcoNert® is a 180- to 800-nm-thick coating consisting of amorphous silicon material interdiffused with the host substrate, and its surface is passivated with covalently bonded hydrocarbon molecules. Dursan® is a 0.4- to 1.6-μm-thick coating consisting of carboxysilane material interdiffused with the host substrate. Stainless steels 304 and 316 and steel 1018 coupons were coated with commercial 4YSZ (4 mol% $Y_2O_3$: 96 mol% $ZrO_2$, or $Zr_{0.92}Y_{0.08}O_2$) powder using conventional air plasma spray (APS, Oerlikon Metco) at the NASA Glenn Research Center. The plasma torch was run at 40 kW using $Ar/N_2$. The standoff distance was ~100 mm, and the samples were preheated by passing the torch across the samples twice before deposition. The porcelain coating, or SE 2720 glass, was applied on stainless steel 304 by Prince Minerals LLC, Leesburg, AL.

All samples were cleaned with a detergent solution, rinsed with deionized water, and ultrasonicated in acetone and ethanol prior the experiments. Samples were weighed on an analytical balance (Sartorius model 1712 MP8, Göttingen, Germany) (±0.0003) before and after the exposure in the GEER.

## 2.2 Exposure Procedure in GEER

Samples were placed on a sample holder illustrated in Figure 3. The sample holder consisted of a U-shaped bracket with an alumina rod between the two ends. Samples were different sizes (see Tables 1 and 2) and directly suspended from the rod or with Au wire. This sample holder was placed on a stainless steel 316 rail and loaded into the GEER through a port near the geometric center of the main chamber (a cylinder roughly 3 by 4 ft) (Fig. 3). The chamber was sealed and brought to low pressures at ambient temperature. Deionized water was weighed and added manually through a fill port on the vessel. High-accuracy mass flow controllers were used to add the other constituents of Venus gas mixture (30 ppm $H_2O$, 150 ppm $SO_2$, 28 ppm CO, 15 ppm OCS, 3 ppm $H_2S$, 0.5 ppm HCl, and 5 ppb HF) to the vessel to approximately 34.5 bar (500 psi). Then the heating elements were turned on and the pressure increased to bring the system to the desired steady-state operating point of 92 bar (1330 psi) and 467 °C (873 °F). Two separate exposures of 10 and 42 days were conducted in the chamber under the Venusian atmosphere conditions. An additional 21 days of exposure was done to the stainless steels 304 and 316 coated with Dursan® and SilcoNert®. The chemical composition of the supercritical fluid in the chamber was monitored by removing aliquots at specified intervals for mass spectrometric analysis. The chamber is equipped with a boost system, which allowed the injection of high-pressure gases during the experiment to adjust the composition or to top off the system pressure with the original mixture in case of small leaks. For each exposure a new batch of duplicate samples were loaded into the chamber. A batch of pristine, unexposed samples were retained for examination as reference points with no corrosion.

## 2.3 Sample Characterization

Figure 4 represents the process of sample preparation. After exposure, a triangle piece was cut from each sample. This piece was analyzed by X-ray diffraction (XRD) on a Bruker D8 Discover diffractometer (Bruker-AXS GmbH, Karlsruhe, Germany), by Auger electron spectroscopy (AES) RBD Instruments refurbished PHI 660 scanning Auger microprobe, and by X-ray photoelectron spectroscopy (XPS) PHI 5000 Versaprobe (ULVAC-PHI). After XRD and XPS analyses, these triangle samples were mounted in a PolyFast® resin (Struers Inc., Cleveland, OH), finished (polished) using a nonaqueous solution and analyzed by a field emission scanning electron microscope (FE-SEM) Hitachi S4700-II (Hitachi High Technologies, Gaithersburg, MD) equipped with energy dispersive X-ray spectroscopy (EDS) (EDAX, Mahwah, NJ), a secondary electron (SE) detector, and a backscattered-electron (BSE)

detector. A focused ion beam scanning electron microscope (FIB-SEM) equipped with Gemini electron beam column (Carl Zeiss AG, Oberkochen, Germany) was also used to characterize some of the samples. Prior to electron microscopy, a thin layer of gold, platinum, or carbon was deposited on the ceramic and coated metallic samples.

The initial surface treatment of an alloy (e.g., electrolytic polishing, mechanical polishing, milling, lathe-turning, or grinding, etc.) may have a major effect on oxidation rate (Ref. 14). In order to evaluate and understand the role played by polishing the surface of the 304 and 316 stainless steel samples, their microgeometric characteristic roughness was measured by an optical three-dimensional surface profilometer (Wyko NT9100, Town of Oyster Bay, NY).

# 3.0 Results

## 3.1 Microgeometric Characterization

The total roughness measured for the polished side of the 304 stainless steel sample is 780.62 nm (Fig. 5), and for the unpolished side it is 3.57 μm (Fig. 6). The roughness of the untreated or unpolished side of the 316 stainless steel sample is 4.78 μm (Fig. 7). Both sides of the 316 stainless steel sample were unfinished and are considered to have the same roughness.

## 3.2 Gravimetric Analysis

The samples were weighed before and after exposure to the Venusian atmospheric conditions in the GEER for 10 and 42 days and then normalized to unit area by dividing the weight change by the total area of a particular sample. This analysis is used to determine weight gain or loss per area of the samples due to reactions occurring between the supercritical Venusian phase and the solid phase. The assessment of the results of the gravimetric analysis can be used to determine the potential material candidates for use in the Venusian atmospheric conditions.

### 3.2.1 Alloys and Au

In general, alloys form a thin oxide protective layer or scale in oxidizing atmospheres such as the Venusian atmosphere simulated in the GEER. Ideally, this oxide layer grows following parabolic kinetics with no breakaway behavior (fast weight gain and thickness increase of the scale resulting in oxide spallation) (Ref. 5). The reaction of oxygen with the surface of the alloy (e.g., high-temperature oxidation) is easily observed by weight gain and is tracked by gravimetric analysis. Excessive and rapid weight gains indicate that the alloy oxidizes readily.

Figure 8 shows the weight change (weight gain for all alloys) per area of each sample. Considering the experimental uncertainties, no weight change, $-1\pm8\cdot10^{-4}$ ($mg\cdot cm^{-2}$), was observed for the Au sample exposed in the GEER for 42 days. In the case of the austenitic stainless steels, 316 exhibited the highest weight gain per area ($1.760\pm0.007$ $mg\cdot cm^{-2}$ after 10 days exposure and $3.113\pm0.008$ $mg\cdot cm^{-2}$ after 42 days exposure), and stainless steel 304 exhibited the lowest ($0.040\pm0.007$ $mg\cdot cm^{-2}$ after 10 days exposure and $0.134\pm0.007$ $mg\cdot cm^{-2}$after 42 days exposure). In the case of the nickel-based alloys, alloy 625 exhibited the highest weight gain per area ($0.392\pm0.006$ $mg\cdot cm^{-2}$ after 10 days exposure and $0.624\pm0.006$ $mg\cdot cm^{-2}$ after 42 days exposure), and alloy G30 exhibited the lowest ($0.247\pm0.006$ $mg\cdot cm^{-2}$ after 10 days exposure and $0.253\pm0.006$ $mg\cdot cm^{-2}$after 42 days exposure). The carbon steel 1018 exhibited the highest weight gain per area ($4.045\pm0.009$ $mg\cdot cm^{-2}$ after 10 days exposure and $11.36\pm0.02$ $mg\cdot cm^{-2}$ after 42 days exposure) among all the metallic materials exposed to the Venusian atmosphere in the GEER.

The formation of the scales or metal oxides in the stainless steel 304 is accompanied by weight gain, which was used to calculate the weight gain rate. For this material, weight gain data were available at three times and an approximate kinetic plot could be constructed as shown in Figure 9.

### 3.2.2 Coatings on Carbon and Austenitic Steels

The weight change per area of four different coating materials (4YSZ, Dursan®, SilcoNert®, and porcelain) deposited on steel substrates and exposed to the Venusian supercritical fluid for 10 and 42 days was also measured. In order to evaluate the coatings presented in Figure 10, three main properties must be considered: (1) thermal coefficient mismatch between the substrate and the coating, (2) porosity or density of the coating, and (3) point defects intrinsic from the coating material. The 4YSZ-coated steels approximately follow the same trend as observed for the uncoated steels 304, 316, and 1018 in Figure 8, although they exhibit lower weight gain per area. As observed in the cross-sectional analysis in Section 3.3.2, "Coatings on Carbon and Austenitic Steels," the high porosity or low density of the 4YSZ provides a path for gaseous diffusion of the constituents present in the supercritical fluid. In addition to porosity, oxygen vacancies provide a diffusion path for oxygen (e.g., from $CO_2$, $SO_2$, etc.) to migrate from the supercritical fluid phase to the metal/4YSZ interface. Stainless steels 304 and 316 coated with SilcoNert® (amorphous-based silicon material) exhibited the same weight gain per area ($0.015\pm0.007$ mg·cm$^{-2}$ and $0.011\pm0.007$ mg·cm$^{-2}$, respectively, after 10 days exposure and $0.016\pm0.007$ mg·cm$^{-2}$ and $0.021\pm0.007$ mg·cm$^{-2}$, respectively, after 42 days exposure), considering the experimental uncertainties. Stainless steel 304 samples coated with Dursan® (amorphous carboxysilane material) exhibited no weight change per area ($0.007\pm0.007$ mg·cm$^{-2}$ after 10 days exposure and $-0.005\pm0.007$ mg·cm$^{-2}$ after 42 days exposure), considering the experimental uncertainties. In contrast to stainless steel 304 coated with Dursan®, stainless steel 316 samples coated with Dursan® exhibited weight gain per area of $0.100\pm0.007$ mg·cm$^{-2}$ after 10 days exposure and $0.166\pm0.007$ mg·cm$^{-2}$ after 42 days exposure. Since only one side of the stainless steel samples were coated with porcelain, their weight gain per area was calculated by subtracting the weight gain contribution of the uncoated area. With this correction, stainless steel 304 samples coated with porcelain exhibited weight gain per area of $0.09\pm0.01$ mg·cm$^{-2}$ after 10 days exposure and no weight changes ($-0.01\pm0.01$ mg·cm$^{-2}$) after 42 days exposure.

### 3.2.3 Ceramic Materials

Allowing for experimental error, no weight change was observed for the ceramic materials $\alpha$-$Al_2O_3$, $Si_3N_4$, SiC, or amorphous $SiO_2$ exposed to the Venusian atmosphere in the GEER (Fig. 11). In addition to gravimetric analysis, XPS was used to analyze these ceramic materials in order to probe possible changes in their surface chemistry.

## 3.3 Cross Section Microstructural, Structural, and Surface Characterization

### 3.3.1 Alloys and Au

Cross-sectional analysis using scanning electron microscopy (SEM) coupled with EDS was used to probe possible microstructural (e.g., oxide or sulfide layer(s) if present) and elemental changes in the materials exposed to the Venusian atmosphere in the GEER. Fast elemental mapping results are also provided here for the samples, although fast scans performed on the samples resulted in low resolution and poor definition of the microstructural features for some of the sample images. The SEM–EDS analysis results presented in this work are for samples exposed in the GEER for 10 and 42 days. The EDS results for this work are qualitative, and carbon was detected in all samples since carbon dioxide is always found adsorbed on the samples or are present in the SEM chamber even at low vacuum.

The cross-sectional SEM and BSE images of the stainless steel 304 samples that were unexposed and exposed to the Venusian atmosphere in the GEER for 10 and 42 days are shown in Figures 12 to 17. As observed in Figures 14 and 15, no oxide or sulfide layers or scales are detected on either the polished or unpolished side of the stainless steel 304 exposed for 10 days. The surface of the unpolished side, where the mounting material detached from its base, is irregular; this correlates with the surface roughness of the sample before the exposure experiment (see Fig. 16). A double-layer scale formed on the unpolished side

of the stainless steel 304 sample exposed to the Venusian atmosphere in the GEER for 42 days (Fig. 17). The inner layer of this scale is 0.84±0.10 μm thick, and the outer layer is 1.56±0.13 μm thick. No scale at a magnification of 8000× was found on the polished side of this sample exposed in the GEER for 42 days. Comparing the SEM results of the polished and unpolished sides of the stainless steel sample exposed in the GEER for 42 days, it is evident from the SEM cross-sectional images that surface polishing improves corrosion resistance of this alloy significantly.

Although no scale was observed in the SEM images of the stainless steel 304 exposed in the GEER for 10 days (Figs. 14 and 15), EDS elemental analysis of the surface of the 304 sample (Fig. 15(a)) revealed the presence of a high content of oxygen (27 wt%) and low content of sulfur aside from the main constituents of this alloy. Spot EDS analyses were performed on area I, Figure 15(a), for the surface and area II for the bulk of the alloy, and the weight percentage of the elements obtained from this analysis is presented in Table 4. The weight percentage obtained of the bulk of the alloy obtained by EDS (Figs. 18 and 19) is consistent with that provided by the manufacturer (Table 2). The scale formed on the stainless steel 304 sample exposed for 42 days is composed of oxygen (27.7 wt%), sulfur (8 wt%), chromium (34.1 wt%), and iron (27.1 wt%) (Table 5).

The X-ray elemental mapping of the unpolished side of the stainless steel 304 coupon exposed to the Venusian atmosphere in the GEER for 10 and 42 days in Figures 20 and 21 shows that the distribution of the main elements (Fe, Cr, and Ni) is homogeneous throughout the bulk of the 304 sample. The high content of oxygen near the edge of the surface 304 exposed for 10 days in the GEER is probably due to the formation of an oxide nanometer-thickness scale containing iron and chromium. The elemental mapping images of the 304 sample exposed for 42 days (Fig. 21) show iron- and oxygen-rich layers formed on the base of this sample, which correspond to the scale observed in Figure 17. XPS analysis that better reveals the surface chemistry of this sample is discussed below. High chromium and nickel amounts are usually added to the stainless steel 300 series to form a protective layer of chromium containing oxides (spinels), which improves oxidation resistance.

The XRD patterns of the unpolished 304 stainless steel samples that were unexposed and exposed in the GEER for 42 days are presented in Figure 22. Only γ austenite (PDF card 04-014-0264) and α ferrite (PDF card 04-014-0258) phases were detected by XRD analysis in the as-received sample. Magnetite ($Fe_3O_4$, PDF card 04-012-7038) and nickel sulfide ($Ni_{0.96}S$, PDF card 00-050-1791) phases were detected, in addition to the γ and α phases, on the sides of the sample exposed in the GEER for 42 days. Note that Auger analysis (discussed later in this section) detected first a layer of iron oxide followed by a layer of chromium oxide in the scale of the sample and that XRD had detected the magnetite ($Fe_3O_4$) crystalline phase. It is also possible that chromium occupies the same position of iron in the octahedral sites of the magnetite crystal structure, and thus its formula can be represented as $Fe_{3-x}Cr_xO_4$.

The elemental depth profile obtained by XPS of the polished side of the stainless steel 304 exposed in the GEER for 10 days is shown in Figure 23. From the surface sputtering inward the bulk of the sample, Figure 23 indicates that the first layer is carbon (~10 nm) and the second and third are a ~20-nm layer of iron oxide and a ~150-nm layer of chromium oxide, respectively. These oxide layers are followed by a thin layer of sulfide at the reaction front, a layer of the alloy depleted in chromium, and finally the bulk composition of the stainless steel 304 sample. The total thickness of the scale, which is around 150 nm (or 0.15 μm) as measured by XPS, was not detected by electron microscopy as observed in Figure 14 at 8000×. This is in fact because XPS is a surface technique that is much more sensitive to the first atomic layers down to a few tens of nanometers with sputtering profiling. Although the unpolished side of the stainless steel sample was too rough for an accurate depth profile XPS measurement, it exhibited the presence of iron oxide. Pt present on the samples is from the coating process that was required for charge dissipation in electron microscopy.

The elemental depth profile obtained by XPS of the polished side of the stainless steel 304 exposed in the GEER for 42 days is shown in Figure 24. The area analysis (200 μm) is shown in the image inserted in Figure 24. This depth profile covers different topographies, including the rough scales on the surface. As a result of the uneven surface topography, the material being sputtered away leads to broadening and

tailing of the interfaces in the profile. The scale, which consists of iron and chromium oxides, is roughly 0.7 μm. This scale measured by XPS was not detected by electron microscopy at 8000× (Fig. 16), which is related to the much higher sensitivity of the former technique. An ~80-nm layer of carbon was also detected by XPS depth profiling.

The elemental depth profile obtained by XPS of the unpolished side of the stainless steel 304 exposed in the GEER for 42 days is shown in Figure 25. Although the unpolished side of the stainless steel sample was too rough for an accurate depth profile XPS measurement, it exhibited the presence of 2.5- to 3-μm-thick iron oxide scale. The thickness of the scale measured by XPS is the same within the experimental uncertainty as that measured by electron microscopy shown in Figure 17 (inner layer 0.84±0.10 μm plus outer layer 1.56±0.13 μm totaling 2.40±0.16 μm).

An Auger depth profile was obtained in a point area (submicrometer) where there were no particulate material on the surface of the polished side of the stainless steel 304 exposed to the Venusian atmosphere for 42 days (Fig. 26). The analysis detected ~0.5-μm-thick iron oxide scale on the surface and ~0.1-μm-thick nickel sulfide scale at the interface between the base of the alloy and the iron oxide scale. The total thickness of the scale (~0.6 μm) measured by this technique is consistent with that measured by XPS analysis (~0.7 μm). Furthermore, no scale on this sample was detected by electron microscopy at 8000× (Fig. 16), which is related to the much higher surface sensitivity of the Auger technique. The slight difference between the thickness measured by XPS and Auger is due to the size of the areas of analysis, which covered different topographies. XPS probed a 200-μm-spot size, which included particulates and scales, whereas Auger probed a submicrometer point area where no particulate material or oxide scale was observed by electron microscopy.

The elemental depth profile obtained by Auger of the unpolished side of the stainless steel 304 exposed in the GEER for 42 days is shown in Figure 27. The point area probed by the Auger analysis where there was no particulate material on the surface is shown in the image insert. From the surface to the base of the alloy, the profile clearly shows the formation of carbon (~0.02 μm), iron oxide (~0.05 μm), chromium oxide (~0.6 μm), nickel sulfide and oxide (~0.4 μm), and chromium carbide (~0.2 μm) at the interface. The total thickness of the scale (~0.8 μm) measured by Auger in a point area (submicron) with no particles corresponds to the first layer of the scale measured by electron microscopy, which is 0.8 μm thick (Fig. 17). The particles on this sample are actually scales/oxides that grew faster on some areas than others giving a different topography as observed in the images of the surface of the samples inserted in the Auger and XPS graphs. This different topography is better observed in the cross-sectional SEM image of Figure 17.

Another Auger depth profile was carried out in a point area where there was particulate material on the surface of the unpolished side of the stainless steel 304 exposed to the Venusian atmosphere for 42 days (Fig. 28). The Auger depth profile confirms that the particles are composed of iron oxide. The total thickness of the scale measured by Auger spectroscopy (>2.0 μm) corroborates well with that measured by electron microscopy shown in Figure 17 (~2.40±0.16 μm).

The cross-sectional SEM and BSE images of the stainless steel 316 samples that were unexposed and exposed to the Venusian atmosphere in the GEER for 10 and 42 days are shown in Figures 29 to 31. As observed in Figures 30 and 31, a double-layered scale was formed in the surface of the stainless steel 316 samples exposed to the Venusian atmosphere. The outer layers of the samples exposed for 10 and 42 days are 8±2 and 16±1 μm thick, respectively. These outer layers are porous and they are irregular, or rough. The inner layers are 4.8±0.6 and 9.2±0.2 μm thick in the samples exposed for 10 and 42 days, respectively. They are dense, well bonded to the alloy, and free of porosity. Figures 30(a) and 31(a) indicate that indeed the outer layer is composed of two phases. These phases stand out even more in the BSE images in Figures 30(b) and 31(b). The cross-sectional image obtained by focused ion beam (FIB) in Figure 32 shows that the grains in the outer layer are formed by trapezoid-like dense stacked platelets.

The elemental analyses of the stainless steel 316 samples exposed to the Venusian atmosphere in the GEER for 10 and 42 days are shown in Figures 33 and 34, respectively, and the weight percentage of the elements are presented in Tables 6 and 7, respectively. High contents of oxygen (26.2 and 27.5 wt%) and iron (67.9 and 72.5 wt%) were detected by EDS elemental analysis in the metal oxide outer layer formed in the 316 sample exposed in the GEER for 10 and 42 days. The inner layer formed in the sample exposed for 10 days is mainly composed of iron (21.1 wt%), chromium (34.7 wt%), and oxygen (27.7 wt%). High contents of nickel (51.7 wt%) and sulfur (37.5 wt%) were detected in the secondary phase (location II, Fig. 31(b)) formed in the outer layer of the sample exposed for 42 days. For the inner metal oxide layer in the 316 sample (location III, Fig. 31(b)) high contents of chromium (34.8 wt%), iron (27.7 wt%), and oxygen (26.9 wt%) were detected by EDS analysis. There are also small amounts of sulfur (4.1 and 1.1 wt%) present in the inner and outer layers, respectively, of the sample exposed for 10 days. Large amounts (37.5 and 7.3 wt%) are present in the corresponding layers of the sample exposed for 42 days.

X-ray elemental mappings in Figures 35 and 36 confirm that inner layers are chromium and oxygen rich whereas the outer layers are rich in iron and oxygen. Figures 35 and 36 also show that the secondary minor phases present in the outer layer are rich in sulfur and molybdenum. Since the Kα line of sulfur and Lα line of molybdenum overlap, XRD analysis was performed on the sample exposed for 42 days in order to elucidate the presence of these elements by crystalline-phase identification (see the XRD discussion below). From EDS, elemental mapping, and XRD and according to the studies of stainless steel alloys reported in the literature, we can conclude that outer layers are mainly composed of iron oxide and the inner layers composed of iron, chromium oxide. The presence of sulfur dioxide and its small abundance in the supercritical fluid leads to the formation of small amounts of sulfides in the inner and outer layers as confirmed by XRD analysis (Fig. 37). The formation of a dense, protective layer of chromium-rich oxide at the base of the alloy is desirable since it improves oxidation resistance and protects the alloy against carbon (from the $CO_2$) diffusion into the alloy and formation of carbides.

The cross-sectional FIB image of the stainless steel 316 samples after exposure to the Venusian atmosphere in the GEER for 10 days is shown in Figure 32. As observed in Figure 32, a double-layered scale was formed in the surface of the 316 sample exposed to the Venusian atmosphere in the GEER for 10 days, which corroborates well with those images obtained by SEM.

The XRD patterns of the 316 stainless steel samples that were unexposed and exposed in the GEER for 42 days are shown in Figure 37. Only two γ austenite (γ-Fe, PDF card 98-001-3668 and γ*-Fe, PDF card 98-000-6230) phases were detected by XRD analysis in the sample unexposed in the GEER. These phases have the same space group *Fm3m* and have the same cubic symmetry and only differ in their unit cell volumes (γ-Fe = 46.6 Å and γ*-Fe = 43.0 Å). Magnetite ($Fe_3O_4$, PDF card 01-080-6402, cubic symmetry), chromium iron oxide (PDF card 04-005-8771, tetragonal symmetry), and nickel sulfides (NiS, PDF card 98-001-9442, hexagonal symmetry, and PDF card 98-001-5653, rhombohedral symmetry) phases were detected in the stainless steel sample exposed in the GEER for 42 days by XRD analysis in addition to the γ and α phases.

The elemental depth profile obtained by XPS of the stainless steel 316 unpolished surface exposed in the GEER for 10 days is shown in Figure 38. The 316 sample exhibited a thick layer (>1.8 μm) of iron oxide with trace amounts of other elements (Fig. 38). The XPS profile was stopped at the depth of 1.8 μm, although the total thickness of the scale measured by electron microscopy is 13±2 μm (Fig. 30). Carbon is also detected by XPS on the first layer formed on this sample.

The cross-sectional SEM and BSE images of the stainless steel 310 samples that were unexposed and exposed to the Venusian atmosphere in the GEER for 10 and 42 days are shown in Figures 39 to 41. Figure 40 shows that a double-layered scale was formed in the surface of the 310 samples exposed to the Venusian atmosphere in the GEER for 10 days and is clearly noticed in the BSE image of Figure 40(b). The outer and inner layers of the sample exposed for 10 days, are 1.3±0.2 μm and 0.6±0.1 μm thick, respectively. The inner layer of the sample exposed for 10 days exhibits high porosity. The scale formed on the surface of the sample exposed for 42 days apparently (Fig. 41) consists of only one layer and is 3.7±0.2 μm thick. The high porosity of the scale formed on 310 is undesirable for its oxidation resistance.

The elemental analyses of the stainless steel 310 exposed for 10 and 42 days are shown in Figures 42 and 43, respectively, and the weight percentage of the elements are presented in Tables 8 and 9, respectively. High contents of oxygen (18.0 wt%), sulfur (14.0 wt%), nickel (16.1 wt%), and iron (42.1 wt%) were detected by EDS elemental analysis in the outer layer formed in the 310 sample exposed in the GEER for 10 days. The inner layer exhibits high contents of oxygen (18.0 wt%), iron (33.3 wt%), and chromium (28.7 wt%). There is also a small amount of sulfur (5.5 wt%) present in the inner layer. The scale formed on the 310 exposed for 42 days exhibits high contents of oxygen (16.5 wt%), iron (59.3 wt%), and nickel (12.6 wt%). Sulfur was also detected in small amounts (7.7 wt%) in this scale.

From the X-ray elemental mappings in Figures 44 and 45, the scale formed on the stainless steel 310 exposed for 10 and 42 days exhibits some localized or rich areas of sulfur and nickel whereas the oxygen- and iron-rich areas of the outer layer are homogenous. It is also observed in Figures 44 and 45 that the outer layers are iron rich while the inner layers are iron and chromium rich. XRD analyses (discussed later in this section) give more detailed information about the crystalline phases present in these layers.

The XRD patterns of the of the 310 stainless steel samples that were unexposed and exposed in the GEER for 42 days are shown in Figure 46. In addition to the Fe-Ni alloy crystalline phase ($Fe_3Ni_2$, PDF card 03-065-5131, cubic symmetry) detected by XRD, magnetite ($Fe_3O_4$, PDF card 01-078-3149, monoclinic symmetry) and nickel sulfide (PDF card 03-065-3419, hexagonal symmetry) formed on the base of the alloy after exposure. Only the Fe-Ni phase was detected by XRD in the unexposed sample.

The cross-sectional SEM and BSE images of the 1018 carbon steel samples that were unexposed and exposed to the Venusian atmosphere in the GEER for 10 and 42 days are shown in Figures 47 to 49. The double-layered scale formed in the exposed samples are separated and porous. In addition to porosity, the inner layer of the sample exposed for 10 days exhibited cracks and is slightly detached from the alloy. The outer and inner layers of the sample exposed for 10 days are 23±3 and 14.0±0.9 μm thick, respectively. The outer and inner layers of the sample exposed for 42 days are 42±3 and 22.8±0.9 μm thick, respectively. From the BSE images in Figures 48(b) and 49(b) it is evident that the two layers on the 1018 steel sample are a single phase, which is confirmed to be magnetite ($Fe_3O_4$) by XRD analysis. The thick scale is the result of rapid weight gain and growth of the double-layered scale. Considering the detrimental aspects (rapid scale growth, cracks, porosity, and the double layer not being well bonded to the alloy) found in the exposed 1018 steel, we can conclude that 1018 steel is not appropriate for this supercritical environment.

The elemental analyses are shown in Figures 50 and 51, and the weight percentage of each element in the layers is presented in Tables 10 and 11. The amounts of the elements measured by EDS analysis of the layers formed on the 1018 steel sample exposed for 10 days are slightly different from each other: sulfur, 1.3 wt% in outer layer and 2.7 wt% in inner layer; oxygen, 25.1 wt% in outer and 25.7 wt% in inner; and iron, 70.8 wt% in outer and 67.8 wt% in inner. EDS analysis detected oxygen (24.4 wt%), sulfur (5.5 wt%), and iron (67.7 wt%) in the inner layer of the 1018 steel sample exposed for 42 days. Sulfur was not detected by EDS analysis in the outer layer; however, high contents of iron (71.9 wt%) and oxygen (27.7 wt%) were detected in the outer layer.

The X-ray elemental mappings in Figures 52 and 53 show that the inner and outer layers of the 1018 steel samples exposed for 10 and 42 days are iron and oxygen rich whereas their interfaces are sulfur rich. The distribution of iron and oxygen in the inner and outer layers is homogenous.

The XRD patterns of the 1018 steel samples that were unexposed and exposed in the GEER for 42 days are shown in Figure 54. XRD detected only magnetite ($Fe_3O_4$, PDF card 01-080-6402, cubic symmetry) on the base of the alloy after exposure in the GEER in addition to α ferrite (PDF card 04-014-0258).

Figures 55 to 57 show the cross-sectional SEM and BSE images of the alloy G30 samples that were unexposed and exposed to the Venusian atmosphere in the GEER for 10 and 42 days. The formation of a double-layered scale is also observed on the alloy G30. This double-layered scale is also slightly porous, as indicated in Figures 56 and 57. The thickness of the outer layers of the samples exposed for 10 and 42 days are 1.4±0.2 and 1.7±0.2 μm, respectively. These outer layers are very irregular and rough and are

missing in some areas. This may be due to spallation. The inner layers are 0.49±0.01 and 0.65±0.04 μm thick for the samples exposed for 10 and 42 days, respectively, and are slightly uniform along with the surface of the alloy. The BSE images in Figures 56(b) and 57(b) reveal that the double-layered scales formed on the G30 alloys are composed of two distinct crystalline phases. The porosity in the double-layered scale and the missing of material from the outer scale are not desirable for improving oxidation resistance of the alloy G30.

The EDS elemental analyses of the alloy G30 samples are shown in Figures 58 and 59, and the weight percentage of the elements are presented in Tables 12 and 13. The outer layer of the sample exposed for 10 days exhibits high contents of nickel (30.5 wt%), iron (12.9 wt%), and sulfur (32.6 wt%), while the inner layer has high contents of chromium (32.6 wt%), Ni (11.4 wt%), Mo (11.5 wt%), iron (7.3 wt%), oxygen (15.6 wt%), and sulfur (9.9 wt%). In case of the sample exposed for 42 days, its outer layer exhibits high contents of nickel (50.8 wt%) and sulfur (29.8 wt%), and the inner layer has high contents of chromium (31.4 wt%), Ni (8.2 wt%), Mo (11.9 wt%), oxygen (20.6 wt%), and sulfur (10.3 wt%).

The X-ray elemental mappings in Figures 60 and 61 show that the outer layers formed on the alloy G30 are iron-, nickel-, molybdenum-, and sulfur-rich, while the inner layers are rich in oxygen, iron, and chromium. Since the Kα line of sulfur and Lα line of molybdenum overlap, XRD analysis was carried out on the G30 alloy sample exposed for 42 days to reveal the crystalline phases present in the double-layered scale.

The XRD patterns of the G30 alloy samples that were unexposed and exposed in the GEER for 42 days are shown in Figure 62. Nickel sulfide (PDF card 00-050-1791, hexagonal symmetry), iron nickel sulfide (PDF card 04-002-6332, hexagonal symmetry), and magnetite ($FeCr_2O_4$, PDF card 98-000-0161, cubic symmetry) were detected by XRD on the base of the alloy after exposure in the GEER in addition to the chromium-iron phase (PDF card 04-004-8469, cubic symmetry).

The cross-sectional SEM and BSE images of the alloy 625 samples that were unexposed and exposed to the Venusian atmosphere in the GEER for 10 and 42 days are shown in Figures 63 to 65. This alloy also exhibits the formation of a double-layered scale with low porosity. The outer layers are 2.1±0.3 and 3.8±0.2 μm thick, and the inner layers are 1.3±0.3 and 1.5±0.2 μm thick for the samples exposed for 10 and 42 days, respectively. Both layers are relatively dense, irregular, and rough following the pattern of the surface of the alloy samples. It is also clear from the BSE images (Figs. 64(b) and 65(b)) that the double-layered scale is formed by two crystalline phases.

The elemental analyses are shown in Figures 66 and 67, and the weight percentage of the elements are presented in Tables 14 and 15. The major constituents of the outer layer are nickel (55.0 wt% for 10 days exposure and 58.9 wt% for 42 days) and sulfur (34.1 wt% for 10 days and 34.5 wt% for 42 days), and those of the inner layer are Mo (33.7 wt% for 10 days and 30.7 wt% for 42 days), Cr (25.9 wt% for 10 days and 26.7 wt% for 42 days), and oxygen (23.6 wt% for 10 days and 20.8 wt% for 42 days). Small amounts of other elements are also present in the inner layer and outer layers.

The X-ray elemental mappings in Figures 68 and 69 confirm that the outer layers are nickel- and sulfur-rich whereas the inner layers are rich in chromium and oxygen. It can also be observed in the elemental mappings that the outer layers are rich in molybdenum. Since the Kα line of sulfur and the Lα line of molybdenum overlap, XRD analyses were carried out in the samples exposed for 42 days to reveal the crystalline phases present in the double-layered scale.

The XRD patterns of the alloy 625 samples that were unexposed and exposed in the GEER for 42 days are shown in Figure 70. Nickel sulfides (NiS, PDF card 98-000-0308, hexagonal symmetry and $Ni_{53}S_{54}$, PDF card 98-001-1778, hexagonal symmetry), nickel molybdenum oxide (PDF card 00-016-0291, monoclinic symmetry) and chromite (PDF card 98-000-0161, cubic symmetry) were detected by XRD on the base of the alloy after exposure in the GEER in addition to the chromium nickel phase (PDF card 04-004-8469, cubic symmetry).

The cross-sectional SEM and BSE images of the β-NiAl alloy samples that were unexposed and exposed to the Venusian atmosphere in the GEER for 10 and 42 days are shown in Figures 71 to 73. Figures 72 and 73 show no clear scales on the β-NiAl alloy samples exposed for 10 and 42 days.

Figures 72 and 73 also indicate that mounting material is detached from the sample and that the surfaces of the samples are irregular, which is related to the surface roughness of the samples before exposure.

The elemental analyses are shown in Figures 74 and 75, and the weight percentage of the elements are presented in Tables 16 and 17. EDS elemental analysis performed on the surface of the β-NiAl alloy sample exposed for 10 days (Fig. 72(a)) revealed the presence of high contents of oxygen (23 wt%) and fluorine (19.5%) and a low content of sulfur (3.7 wt%) besides the main constituents of this alloy. The surface of the sample exposed for 42 days (Fig. 73(a)) exhibited only the presence of a high content of oxygen (7.9 wt%) besides the constituents of this alloy. Spot EDS analyses were performed on area I in Figures 72(a) and 73(a) for the surface and area II for the bulk of the alloy.

The X-ray elemental mapping in Figures 76 and 77 show that the distribution of the main elements (Ni and Al) is homogeneous throughout the bulk of the samples exposed for 10 and 42 days in the GEER. Areas at the edge of the surface of the β-NiAl alloy sample exposed for 10 days (Fig. 72) are rich in aluminum, sulfur, oxygen, and fluorine (Fig. 76).

The XRD patterns of the β-NiAl samples that were unexposed and exposed in the GEER for 42 days are shown in Figure 78. Only nickel sulfide (PDF card 00-012-0041, hexagonal symmetry), in addition to the aluminum nickel phase (PDF card 03-065-3199, cubic symmetry), was detected by XRD on the base of the alloy after exposure in the GEER.

Figures 79 to 81 are cross-sectional SEM and BSE images of the Au wire samples that were unexposed and exposed to the Venusian atmosphere in the GEER for 10 and 42 days. Although the Au wire samples show some porosity, scales or microstructural changes are not observed on these samples (Figs. 80 and 81), as expected since Au is inert to oxygen.

The elemental analysis is shown in Figure 82 and the weight percentage of the elements are presented in Table 18. Composition changes were not detected by EDS analysis on the Au wire sample exposed in the GEER for 10 and 42 days.

The X-ray elemental mapping in Figure 83 shows that the distribution of Au is homogeneous throughout the bulk of the sample exposed for 10 days in the GEER.

XPS analysis of the gold wire surface (Table 19) detected Ni, Cl, Ca, Na, O, and S that were soluble in deionized water. In addition to these elements, XPS analysis detected an organic (C, O, and F) layer on the gold wire surface, which was apparently not soluble in water.

### 3.3.2 Coatings on Carbon and Austenitic Steels

The cross-sectional SEM and BSE images of the unexposed 304 stainless steel samples coated with 4YSZ and after exposure to the Venusian atmosphere in the GEER for 10 and 42 days are shown in Figures 84 to 87. The thickness of the 4YSZ coatings on 304 are 138±8 μm for the unexposed sample, and 114±11 and 188±7 μm after the exposure in the GEER for 10 and 42 days, respectively. The air plasma spray deposition process itself might have led to uneven coating thickness on the substrates. The cross-sectional SEM images (Figs. 86 and 87) show no presence of oxidation products in the interface between the 4YSZ coating and the base of the alloy even though the coating is porous and has high oxygen vacancy concentration. Figures 84 to 87 show that coating is well bonded to the base of the alloy (substrate), except for the sample exposed in the GEER for 10 days. The preparation and polishing of the sample for SEM analysis might have caused the detachment of the coating from the substrate.

The elemental analyses of the 4YSZ-coated 304 stainless steel samples that were unexposed and exposed in the GEER for 10 and 42 days are shown in Figures 88 to 90, and the weight percentages of the elements are presented in Tables 20 to 22. EDS elemental analysis of the 4YSZ coating of the exposed samples (Figs. 89(b) and 90(b)) detected only the main constituents of this alloy (Fe: 72.2 wt%, Cr: 17.2 wt%, and Ni: 8.8 wt% for 10 days exposure and Fe: 73.4 wt%, Cr: 18.2 wt%, and Ni: 8.4 wt% for 42 days exposure) and of the yttria-stabilized coating (Zr: 86.2 wt%, Y: 1.8 wt%, and O: 3.2 wt% for 10 days exposure and Zr: 70.2 wt%, Y: 15.6 wt%, and O: 14.2 wt% for 42 days exposure).

The X-ray elemental mappings of 4YSZ-coated 304 stainless steel coupon exposed in the GEER for 10 and 42 days in Figures 91 and 92 show that the distribution of the main elements in the bulk (Fe, Cr, and Ni) and in the coating (Zr, Y, and O) of the sample exposed in the GEER is homogenous.

The XRD patterns of the 304 samples coated with 4YSZ that were unexposed and exposed in the GEER for 42 days are shown in Figure 93. Only tetragonal YSZ ($Zr_{0.9}Y_{0.1}O_{1.95}$, PDF card 98-000-0308) and monoclinic zirconia (PDF card 00-037-1484) crystalline phases were detected by XRD. The depth penetration of the X-rays were not enough to reach the substrate, so no other crystalline phases were detected underneath the YSZ coating.

The cross-sectional SEM and BSE images of the 316 stainless steel samples coated with 4YSZ unexposed and after exposure to the Venusian atmosphere in the GEER for 10 and 42 days are shown in Figures 94 to 97. The thickness of the 4YSZ coatings on 316 are 144±5 for the unexposed sample and 137±9 and 141±10 μm after the exposure in the GEER for 10 and 42 days, respectively. Considering the experimental uncertainties, the thickness of the 4YSZ coating on the 316 has not changed after exposure in the GEER. The cross-sectional SEM images (Figs. 96 and 97) show no presence of oxidation products in the interface between the 4YSZ coating and the base of the alloy even though the coating is porous and has a high oxygen vacancy concentration. Figure 94 indicates that there is a missing area of the coating on the face of the alloy and Figure 95 shows that the same coating is slighted detached from the base of the alloy. The loss and detachment of the coating material might be due to exposure or to sample preparation (cutting, mounting, or polishing).

The elemental analyses of the 4YSZ-coated 316 stainless steel coupons that were unexposed and exposed in the GEER for 10 and 42 days are shown in Figures 98 to 100 and the weight percentages of the elements are presented in Tables 23 to 25. EDS elemental analysis of the 4YSZ coating of the exposed samples detected only the main constituents of this alloy (Fe: 22.8 wt%, Cr: 6.2 wt%, and Ni: 3.3 wt% for 10 days exposure and Fe: 69.3 wt%, Cr: 16.3 wt%, and Ni: 10.7 wt% for 42 days exposure) and of the 4YSZ coating (Zr: 35.7 wt%, Y: 1.8 wt%, and O: 0.9 wt% for 10 days exposure and Zr: 78.5 wt%, Y: –65.7 wt%, and O: 15.0 wt% for 42 days exposure).

The X-ray elemental mapping of the 4YSZ-coated 316 stainless steel coupons in Figures 101 and 102 show that the distribution of the main elements in the bulk (Fe, Cr, and Ni) and in the coating (Zr, Y, and O) of the samples exposed for 10 and 42 days in the GEER is homogenous.

The XRD patterns of the stainless steel 316 samples coated with 4YSZ that were unexposed and exposed in the GEER for 42 days are shown in Figure 103. Only tetragonal yttria-stabilized zirconia ($Zr_{0.9}Y_{0.1}O_{1.95}$, PDF card 98-000-0308) and monoclinic zirconia (PDF card 00-037-1484) crystalline phases were detected by XRD on these. The depth penetration of the X-rays was not enough to reach the substrate, so no crystalline phases were detected underneath the YSZ coating.

The cross-sectional SEM and BSE images of the 1018 steel samples coated with 4YSZ unexposed and after exposure to the Venusian atmosphere in the GEER for 10 and 42 days are shown in Figures 104 to 107. The average thicknesses of the 4YSZ coatings are 76±2 for the unexposed samples and 66±2 and 130±5 μm for the samples exposed for 10 and 42 days, respectively. These differences may be due to deposition processes that resulted in uneven deposition of 4YSZ material. Figures 106 and 107 show that a secondary phase formed between the 4YSZ coating and the base of the alloy. This phase has interdiffused through the pores of the 4YSZ coating. The detachment of the 4YSZ seen in Figure 107 is probably due to sample mounting in the Polyfast® material and polishing.

The elemental analyses of the 4YSZ-coated 1018 steel sample exposed in the GEER are shown in Figures 108 to 110, and the weight percentage of the elements are presented in Tables 26 to 28. EDS elemental analysis of the 4YSZ-coated 1018 steel sample exposed for 10 days (Fig. 106) detected the main constituents of this alloy (Fe: 98.1 wt% and C: 1.9 wt% for 10 days exposure and Fe: 90.4 wt% and C: 9.6 wt% for 42 days exposure) and of the yttria-stabilized coating (Zr: 35.7 wt%, Y: 1.8 wt%, and O: 0.9 wt% for 10 days exposure). 90.7 wt% iron and 7.2 wt% oxygen were detected in the secondary phase of the sample exposed for 10 days. In addition to the elements listed here, EDS analysis detected the presence of 13.4% sulfur in the inner layer formed between the base of the alloy and the 4YSZ coating

in the sample exposed for 42 days. The secondary phases in Figures 106 and 107 are likely iron oxides. Small amounts of iron sulfide may also be formed in the inner layer of the sample exposed for 42 days.

The X-ray elemental mappings of 4YSZ-coated 1018 steel samples exposed for 10 and 42 days in Figures 111 and 112, respectively, show that the distribution of the main elements in the bulk (Fe and C) of the sample exposed for 10 days in the GEER is homogenous. They also show that the interface area between the coating and the base of the alloy as well as the pores of the coating are iron and oxygen rich. Figure 112 also shows sulfur in the inner layer.

The XRD patterns of the 1018 samples coated with 4YSZ that were unexposed and exposed in the GEER for 42 days are shown in Figure 113. Only tetragonal yttria-stabilized zirconia ($Zr_{0.9}Y_{0.1}O_{1.95}$, PDF card 98-000-0308) and monoclinic zirconia (PDF card 00-037-1484) crystalline phases were detected by XRD on these samples. The depth penetration of the X-rays was not enough to reach the substrate, so no crystalline phases were detected underneath the YSZ coating.

The thickness of the SilcoNert® and Dursan® coatings on stainless steel 304 and 316 samples unexposed and exposed to the Venusian atmosphere in the GEER for 10 days and 42 days are presented in Table 29 and Figure 114. The images obtained by electron microscopy, elemental analyses, X-ray mapping images and XRD patterns of the samples are shown in Figures 115 to 155. The thicknesses of the coatings were not the same for unexposed and exposed samples, and no conclusion could be made regarding coating thickness changes based on the SEM cross-sectional images. In order to circumvent this problem for the 21-day samples, the samples were ion milled and imaged with a FIB for coating thickness measurements before exposure in the GEER for 21 days. After exposure, the samples were imaged at the same ion-milled area, and the thicknesses of the coatings were measured again. The FIB cross-sectional images and the coating thicknesses measured by this technique are discussed next.

The cross-sectional FIB images of the stainless steel 304 and 316 samples before and after exposure to the Venusian atmosphere in the GEER for 21 days are shown in Figures 118, 127, 136, and 148, and the thickness of the coatings are presented in Table 30. A slight decrease in thickness of the SilcoNert® and Dursan® coatings took place after the samples were exposed in the GEER for 21 days (Table 30). The recession of the coatings may partially be due to crystallization of the amorphous coatings and/or diffusion of elements from the alloy to the coating, forming other crystalline phases (see XRD patterns below). It is also possible that the low resolution of the images at the edges of the coatings added more uncertainty to the coating measurements. The FIB images (Figs. 118, 127, 136, and 148) also show that there is no loss of materials or changes in the microstructural morphology of the coatings.

The elemental analyses of the stainless steels 304 and 316 samples coated with Dursan® and SilcoNert® exposed in the GEER are shown in Figures 119, 120, 128, 129, 138, 139, 149, and 150, and the weight percentage of the elements are presented in Tables 31 to 38. EDS elemental analysis of the coatings detected mainly silicon and oxygen in the Dursan® coating and mainly silicon in the SilcoNert® coating. The oxygen detected in the Dursan® coating is related to the oxygen present in the carboxysilane groups. Minor amounts of other elements detected in the coating are due to the beam size (0.5 to 1 μm diameter), which is larger than the thickness of the coatings. In addition to the elemental constituents of the alloys, no other elements or significant changes in the composition were detected in the samples except for the 316 sample coated with Dursan® exposed for 42 days in the GEER: A 1.09±0.06-μm-thick layer composed of iron and chromium oxides was found to be formed between the Dursan® coating and the base of the alloy. A small amount of sulfur (4.5 wt%) was also detected on the surface of this coating.

The X-ray elemental mapping of the stainless steels 304 and 316 samples coated with SilcoNert® and Dursan® exposed in the GEER for 10 and 42 days (Figs. 121, 122, 130, 131, 140, 141, 151, and 152) shows that the distribution of the main elements in the bulk and in the coating of the samples exposed for 10 and 42 days in the GEER is homogenous.

The XRD patterns of the unpolished side of the 304 stainless steel samples coated with Dursan® that were unexposed and exposed in the GEER for 42 days are shown in Figure 123. Only γ austenite (PDF card 04-014-0264) and α ferrite (PDF card 04-014-0258) phases were detected by XRD analysis in the sample that was unexposed in the GEER. Iron silicon oxide ($Fe_{2.95}Si_{0.05}O_4$, PDF card 00-052-1140)

phase was detected by XRD analysis on the sample exposed in the GEER for 42 days in addition to the γ and α phases. The amorphous silicon-based coatings were too thin to be detected by XRD analysis so amorphous humps were not observed in the XRD patterns.

The XRD patterns of the 316 stainless steel samples coated with Dursan® that were unexposed and exposed in the GEER for 42 days are shown in Figure 132. Only two γ austenite (γ-Fe, PDF card 04-014-0264 and γ*-Fe, PDF card 04-014-0258) phases were detected by XRD analysis in the sample unexposed in the GEER. Iron silicon oxide ($Fe_{2.91}Si_{0.09}O_4$, PDF card 04-013-7315) and iron nickel silicide ($Fe_{0.70}Ni_{0.20}Si_{0.10}$, PDF card 04-017-2358) crystalline phases were detected by XRD analysis on the sample exposed in the GEER for 42 days in addition to the γ and α phases.

Figure 137 shows the SEM image of the surface of the 304 stainless steel coated with SilcoNert® exposed in the GEER for 21 days. After exposure, particulate material composed of an iron oxide was found on the surface of the sample. The particulate material is the main corrosion product of the inner wall of the GEER chamber, which is made of unpolished 304.

The XRD patterns of the unpolished side of the 304 stainless steel samples coated with SilcoNert® that were unexposed and exposed in the GEER for 42 days are shown in Figure 142. Only γ austenite (PDF card 04-014-0264) and α ferrite (PDF card 04-014-0258) phases were detected in the sample that was unexposed in the GEER. Two iron silicide ($Fe_3Si$, PDF card 00-042-1329 and FeSi, PDF card 04-006-7758) crystalline phases were detected on the sample exposed in the GEER for 42 days in addition to the γ and α phases.

The elemental depth profiles obtained by XPS of the polished side of the stainless steel 304 coated with SilcoNert® before and after exposure in the GEER for 21 days are shown in Figure 143. The two rectangular dark areas shown in the image inserted in Figure 143(b) are the areas sputtered and probed by the XPS analysis. XPS analysis on the sample before exposure (Fig. 143(a)) going from surface to bulk showed a thin coating of carbon and oxygen on the surface, followed by a 700-nm-thick layer of silicon on top of the 304 from the SilcoNert® coating. There is evidence for an iron or chromium oxide at the coating/steel interface, suggesting that the metal surface had not been stripped clean of oxide prior to the coating deposition. After exposure for 21 days (Fig. 143(b)), XPS analysis showed a thin layer of silicon oxide on the surface, followed by the original 700-nm layer of silicon coating. There was some reaction of the silicon from the coating with the iron and chromium of the steel at the interface; however, there was no evidence of Venus gas penetration into the bulk.

The elemental depth profile obtained by XPS of the stainless steel 304 coated with Dursan® exposed in the GEER for 21 days is shown in Figure 144. The rectangular bright area shown in the image inserted in Figure 144(b) is the area sputtered and probed by the XPS analysis. Before exposure, a 700-nm layer of the silicon, oxygen, and carbon from the Dursan® coating was found on the surface with evidence, once again, for a thin layer of residual metal oxide at the coating/steel interface. After exposure, XPS shows a decrease in the carbon concentration within the Dursan® coating as well as some tailing of oxygen into the steel substrate.

The XRD patterns of the unpolished side of the 316 stainless steel samples coated with SilcoNert® that were unexposed and exposed in the GEER for 42 days are shown in Figure 153. The γ austenite (γ-Fe, PDF card 04-014-0264, γ*-Fe, PDF card 04-014-0258), silicon (Si, PDF card 98-001-9304), and dickite ($Al_2Si_2O_5(OH)_4$, PDF card 00-058-2002) phases were detected on the unexposed sample in the GEER. Two iron silicide ($Fe_3Si$, PDF card 00-042-1329 and FeSi, PDF card 04-006-7758) crystalline phases were detected on the sample exposed in the GEER for 42 days in addition to the γ and silicon (Si) phases.

The elemental depth profiles obtained by XPS of the stainless steel 316 coated with SilcoNert® before and after exposure in the GEER for 21 days are shown in Figure 154. The two rectangular dark areas shown in the image inserted in Figure 154(b) are the areas sputtered and probed by the XPS analysis. The depth profile of the unexposed sample (Fig. 154(a)) shows a thin surface layer of carbon and oxygen on the surface, and underneath is a ~700-nm layer of silicon from the SilcoNert®coating, followed by the

elements from the bulk composition of the 304 steel. A fairly sharp interface exists between the coating and steel. For the sample exposed for 21 days, Figure 154(b) indicates that the surface and the silicon coating layers still have approximately the same thickness and composition as those of the unexposed sample (Fig. 154(a)); however, there is evidence for reaction occurring between the silicon coating and the iron, nickel, and possibly some residual oxygen from the 316 steel in a third layer at the interface ~900 nm thick.

The elemental depth profile obtained by XPS of the stainless steel 316 coated with Dursan®, exposed in the GEER for 21 days, is shown in Figure 155. The rectangular bright area shown in the image inserted in Figure 155(b) is one of the areas sputtered and probed by the XPS analysis. Before exposure, the silicon, oxygen and carbon from the Dursan® coating layer (~325 nm thick) can be seen on top of the 316 steel. The coating/metal interface of this sample is slightly broadened because of the roughness of the initial metal surface. After exposure, obvious reaction has taken place between the Dursan® coating and the metal under the layer. Figures 155(a) and (b) show the oxygen and silicon from the coating have reacted with the iron from the steel and the amount of carbon has decreased. There is also evidence of metal sulfide at the coating/steel interface, suggesting penetration of the Venus gases through the Dursan® coating.

The cross-sectional SEM and BSE images of the 304 stainless steel samples coated with porcelain that were unexposed and exposed to the Venusian atmosphere in the GEER for 10 and 42 days are shown in Figures 156 to 158. The thickness of the porcelain coating on 304 decreased from 216±3 μm to 185±2 μm and 150±2 μm after exposure in the GEER for 10 and 42 days, respectively. After 10 days exposure the porcelain coating thickness decreased 31±4 μm although this sample exhibited a weight gain per area of 0.09±0.01 $mg \cdot cm^{-1}$. Note that the cross-sectional SEM images (Figs. 156 to 158) show the porcelain coating is porous and has cracks.

The elemental analyses of the porcelain-coated 304 stainless steel coupon exposed in the GEER for 10 and 42 days are shown in Figures 159 and 160, and the weight percentage of the elements are presented in Tables 39 and 40. EDS elemental analysis of the porcelain coating and of the bulk of the exposed 304 samples (Figs. 157 and 158) detected only the main constituents of these materials. For the 10-day exposure, 39.0 wt% Si, 8.3 wt% Ca, 3.1 wt% Zn, 2.3 wt% K, and 2.1 wt% Al was detected for the porcelain coating. Also, 67.3 wt% Fe, 27.8 wt% Cr, and 5.4 wt% Ni was detected for the 304 steel. For the 42-day exposure, 31.1 wt% Si, 7.9 wt% Ca, 1.3 wt% K, and 0.8 wt% Zn was detected for the porcelain coating, and 67.5 wt% Fe, 16.6 wt% Cr, and 7.5 wt% Ni was detected for the 304 steel.

Figure 161 shows the XRD patterns of the unpolished side of the 304 stainless steel samples coated with porcelain that were unexposed and exposed in the GEER for 42 days. Muscovite ($K_{0.5}Al_{2.5}Si_{3.5}O_{10}(OH)_2$, PDF card 04-013-3002), larnite ($Ca_2SiO_4$, PDF card 00-009-0351), and microcline ($KAlSi_3O_8$, PDF card 01-070-6187) crystalline phases and an amorphous phase were detected on the unexposed sample in the GEER. Silica ($SiO_2$, PDF card 01-073-3460) crystalline phase were detected on the sample exposed in the GEER for 42 days as well as those phases detected in the unexposed sample.

### 3.3.3 Ceramics

The cross-sectional SEM and BSE images of the ceramic samples $\alpha$-$Al_2O_3$, $Si_3N_4$, SiC, and amorphous $SiO_2$ that were unexposed and exposed to the Venusian atmosphere in the GEER for 10 and 42 days and their respective EDS elemental analyses, X-ray elemental mapping images, and XRD patterns are shown in Figures 162 to 185. Microstructural changes such as formation of scales or secondary phases, microcracks, flaking, and so forth were not observed for any of the ceramic materials exposed in the GEER for 10 and 42 days.

EDS elemental analyses of the ceramic samples exposed in the GEER are shown in Figures 165, 175, and 182, and the weight percentage of the elements are presented in Tables 41 and 42. EDS elemental analysis of the ceramics detected solely their constituent elements.

X-ray elemental mapping images of the ceramic samples exposed in the GEER for 10 days, which are presented in Figures 166, 167, 170, 176, 177, 184, and 185, show that the distribution of the constituent elements in the bulk is homogenous.

The XRD patterns of the alumina samples that were unexposed and exposed in the GEER for 42 days are shown in Figure 168. No additional crystalline phases were detected on the alumina sample after it was exposed in the GEER. The crystalline phases detected by XRD in both samples are $\alpha$-$Al_2O_3$ (corundum, PDF card 04-013-1687), $Al_3O_{3.76}$ ($Al_3O_{3.76}$, PDF card 04-016-0538), hibonite ($Ca(Al,Fe)_{12}O_{19}$, PDF card 00-038-0469), and magnetite ($Fe_3O_4$, PDF card 98-000-3110).

The XRD patterns of the silicon nitride samples that were unexposed and exposed in the GEER for 42 days are shown in Figure 171. Only $\alpha$-$Si_3N_4$ (PDF card 01-072-1253) crystalline phase was detected on the unexposed and exposed samples.

The XRD patterns of the silicon carbide samples that were unexposed and exposed in the GEER for 42 days are shown in Figure 178. Only SiC (PDF card 04-010-5699) crystalline phase was detected on these samples.

The XRD patterns of the silica samples that were unexposed and exposed in the GEER for 42 days are shown in Figure 185. No crystalline phases were detected on the unexposed or exposed samples.

The surfaces of the ceramic samples $\alpha$-$Al_2O_3$, $Si_3N_4$, and amorphous $SiO_2$ were also probed by SEM–EDS in order to characterize the particulate- and fiber-like materials that were found on the surfaces of the samples after exposure in the GEER for 42 days. The SEM images of the surface of the ceramic samples and their respective EDS elemental analyses are shown in Figures 186 to 193. These SEM images indicate that the particulate- and fiber-like materials are loosely collected on the surface of the ceramic samples. EDS analysis of the fiber-like material on the alumina sample (Fig. 187) detected Fe, Si, Mg, Ca, Ti, Cr, Ni, Al, S, and O as constituent elements. Ca, Mg, Al, Si, and O might be present in the fiber-like material as a calcium magnesium aluminum silicate. Ti and Fe can also be present in this silicate, or Ti can be in the form of oxides. Fe, Cr, S and O are known to form iron and chromium oxides or sulfides that are formed as scales in stainless steel 304 as previously discussed in this work. These oxides or sulfides are probably coming from the inner surface of the chamber, which is made of 304. Al and O detected by EDS analysis might be from the alumina sample since the beam size could reach the alumina sample underneath the fiber as well. EDS analysis of the particulate material on the alumina sample detected Fe, Cr, S, and O (Fig. 188). As mentioned, these elements are the constituents of iron chromium oxides and sulfides most likely coming from the inner surface of the chamber.

The particulate- and fiber-like materials found on $Si_3N_4$ (Fig. 189) that were analyzed by EDS (Figs. 190 and 191) consist of Fe, Si, Al, Ti, Na, K, Ca, S, and O. This elemental composition is similar to the fiber-like material found on the alumina samples, except that there are two additional detected elements (Na and K). As previously discussed, Fe, O, and S form iron oxides and sulfides and most probably are coming from the inner surface of the chamber. Na, K, Mg. Ti, Al, Fe, Si, and O form silicates. These elements are usually found in silicate-based materials such as the insulation wool or fibers present in the chamber. O, Fe, Mg, Si, S, Ba, Cr, and Fe were detected in the particulate-like material collected on the $Si_3N_4$ sample as well. These detected elements—including Ba—form silicates as well as oxides and sulfites as previously discussed. Si and O detected by EDS analysis might be from the $Si_3N_4$ sample since the beam size would encompass the $Si_3N_4$.

The particulate-like material found on the amorphous silica sample (Fig. 192) that was analyzed by EDS (Fig. 193) consisted of O, S, Ni, Fe, and Cr. As previously discussed, Fe, Cr, O, and S form iron and chromium oxides and/or sulfides and most probably are coming from the inner surface of the chamber. Since the size of the particulate material collected on the silica sample is small (~2 μm), the electron beam reaches the silica sample below and gives a Si signature to the EDS. Thus, Si is probably from both the particulates and the substrate.

The ceramic samples $\alpha$-$Al_2O_3$, SiC, and amorphous $SiO_2$ that showed significant amounts of debris (particulate- and fiber-like materials) on their surfaces after exposure in the GEER vessel for 42 days were analyzed by XPS, and the elemental composition of their surfaces is given in Table 43. XPS analysis

indicates that the debris covering the samples consisted of Na, Ca, Fe, Mn, Ni, S, K, F, Mg, and Cl. The elements detected by XPS corroborates with those detected by EDS. Since XPS is a high-sensitivity surface analysis technique, it detected additional elements in the debris that were not detected by EDS analysis such as Na, Ca, Mn, and K on the surface of the amorphous silica sample and Na, Mn, F, and Cl on the surface of the $\alpha$-$Al_2O_3$ sample. However, EDS analysis detected additional elements that are in the bulk of the sample such as Cr. XPS analysis was also carried out on the samples after they were sonicated in deionized water for 10 min to determine if there might be a reaction between the debris and the bulk of the samples. The XPS results are presented in Table 43. XPS analysis indicates that the amorphous $SiO_2$ sample, which has the smoothest surface, was completely unreacted. Although $\alpha$-$Al_2O_3$ and SiC did not show any reaction, elemental impurities were still detected on their surfaces. These elemental impurities are most likely present in the materials trapped in the pores of the $\alpha$-$Al_2O_3$ and SiC samples. These impurities or particulate-like materials are from the products of corrosion of the inner walls of the GEER chamber.

### 3.3.4 Sample Holders

Initially the samples were hung on a stainless steel rod coated with gold for the GEER tests. The gold coloration of the coating turned brownish after it was exposed in the GEER for 10 days. SEM and EDS analyses were used to probe the chemical and microstructural changes in this gold coating. Figure 194(a) shows that the as-fabricated gold coating consists of grains of different sizes with visible grain boundaries. These grain boundaries practically disappeared after the rod was exposed in the GEER, indicating that sintering occurred (Fig. 194(b)). The cross-sectional SEM image of the rod exposed in the GEER for 10 days is shown in Figure 195. Figure 195 shows the gold coating is dense and ~7 μm thick. Ni, Cr, and Fe were detected in the bulk of the rod and in addition to gold, Fe and Ni were also detected in the coating. The presence of Fe and Ni in the gold coating means that these species have diffused from the bulk of the rod through the grain boundaries of the gold coating.

The EDS analyses of the gold coating and of the bulk of the rod are shown in Figures 196(a) and (b).

The cross-sectional SEM and BSE images of the Inconel wire used to hang the samples exposed in the GEER for 10 days are shown in Figures 197(a) and (b). This Inconel wire did not exhibit any clear formation of scale or an oxide layer, although it did appear tarnished to the naked eye.

The EDS elemental analyses of the surface and of the bulk of the Inconel wire are shown in Figures 198(a) and (b), and the weight percentages of the elements are presented in Table 44. In addition to the main constituents of the alloy, oxygen was detected in the bulk and on the surface of the sample. Ca, Al, and Si were also detected by EDS analysis on the surface of the wire.

The X-ray elemental mappings in Figure 199 show that the distribution of the constituent elements (Ni, Cr, and Fe) in the wire is homogenous. It was also observed that the distribution of oxygen is homogenous throughout the wire, meaning that the entire wire is oxidized.

## 4.0 Discussion

The main products formed on all steels exposed in the GEER for 10 and 42 days are mainly composed of double-layered oxides containing minor amounts of sulfides and showing different chemistry, microstructure, and crystalline phases. Magnetite ($Fe_3O_4$) and nickel sulfides are the main phases formed on the base of the steels. Nickel sulfides were the main phases found in the scale formed on the nickel-based alloys. The oxide layers are formed from reaction with $CO_2$ in the supercritical fluid mixture. The oxidation of the metals in the alloys mainly occurs via conversion of $CO_2$ into CO (see Reaction (1)) since carbon was not detected by EDS and XRD analyses (only a nanometric carbon layer was detected by XPS and Auger analyses on stainless steels 304 and 316). Sulfides are formed by reactions between nickel and $SO_2$ in the supercritical mixture. Usually sulfides are formed at the base of the alloys underneath the oxide layer where the oxygen potential is too low (Ref. 15). The formation of the competing phases (e.g., $Fe_3O_4$ and NiS) in the phase assemblage (metal|metal oxide|supercritical fluid)

can be explained in terms of their thermodynamic stability. The thermodynamic stability of some preferential compounds formed, assuming that the contribution of kinetics effects are negligible here, can be calculated by computational thermochemistry tools. The FactSage free energy minimization program and associated databases (Refs. 16 and 17) was the thermochemistry computational tool used to calculate the main compounds formed at their thermodynamic equilibrium when the alloy samples are exposed to the Venusian gas mixture in the GEER. The initial amounts of the constituents in the Venus gas mixture and the initial amounts of iron, chromium, and nickel in the alloys at 467 °C (873 °F) and 92 bar (1330 psi) were the input parameters into the free energy minimizer program (Table 45).

The results of the FactSage calculations are shown in Table 46. For simplicity of the results, only the predicted thermodynamically stables compounds having activities equal to 1 are listed in Table 46, and their calculated amounts (mol) are omitted here. The compounds presented in Table 46 are listed from the highest to the lowest amounts.

## 4.1 Austenitic and Carbon Steels

The predicted thermodynamically stable compounds derived from FactSage are in good agreement with phases, elements, and compounds detected by the spectroscopic techniques used in the chemical and crystalline identification of the scales formed on the steel alloys. The only exception is for the predicted $FeS_2$ that was not detected by XRD analysis, which might be due to the detection limit of this technique. Note that for all steels, magnetite is the preferentially crystalline phase formed since it is more stable than other iron oxides (e.g., hematite, $Fe_2O_3$) in the phase assemblage of the Venus gas mixture and alloy samples. It has been observed before by Rouillard et al. (Ref. 1) that scales formed on ferritic-martensitic steel T91 (89.0% Fe, 8.6% Cr, 0.2% Ni, and 2.2% others) consist of an inner spinel oxide ($Fe_{3-x}Cr_xO_4$) layer overlaid by magnetite ($Fe_3O_4$) after 310 h exposure in supercritical $CO_2$ at 550 °C (1022 °F) and 250 bar (3626 psi). In case of stainless steel 316L (67.1% Fe, 17.4% Cr, 11.1% Ni, and 4.4% others) at the same conditions, the scale consists mainly of chromia or a mixed iron chromium oxide. The observations made by Rouillard et al. (Ref. 1) on the chemistry and morphology of the scales and their growing process on ferritic-martensitic and austenitic steels corroborates well with other results carried out in oxidizing environments (Refs. 18 to 20).

Qualitatively it is known (Ref. 5) that the oxidation behavior of Fe-Ni-Cr alloys depends on their chromium content. Alloys with less than 9% to 12% chromium form a scale consisting of an inner layer spinel oxide ($Fe_{3-x}Cr_xO_4$) layer overlaid by an iron oxide layer, and the scales on alloys with more than 20% chromium consist of an inner $Cr_2O_3$ layer overlaid by spinel oxide ($Fe_{3-x}Cr_xO_4$). In this study, magnetite was detected by XRD analysis on carbon steel 1018 containing 0.09% chromium. The detection limit of XRD analysis is approximately 1%, and any spinel phase below this limit would not be detected by this technique. Moreover, the crystalline phases detected by XRD might contain other elements in the case of solid solution formation such as in the $Fe_3O_4$-$FeCr_2O_4$ binary system. We can conclude that the oxidation behavior of carbon steel 1018 in a Venusian atmosphere is similar to that observed by alloys containing less than 9% to 12% chromium (Refs. 21 and 22), even though the limitation of XRD only allowed the detection of magnetite.

The oxidation behavior of the alloys or stainless steels 304, 310, and 316 containing 18.1%, 26%, and 16.6% of chromium, respectively, is different from that observed in other oxidizing environments as described earlier. Here magnetite ($Fe_3O_4$) is the main phase detected in the outer layer on the alloys and not spinel oxide as previously described. $Cr_2O_3$ or $Fe_{3-x}Cr_xO_4$ could be the phases formed in the inner layer of the 304 since Fe, Cr, and O were detected by XPS and Auger spectroscopies at the same depths in this sample. In 310 and 316, $Cr_2O_3$ was not detected by XRD. EDS analysis on these sample detected Cr, Fe, and O, which can be interpreted as chromium oxide and iron oxide or chromium iron oxide. Most probably the oxide interpreted from EDS is the one detected by XRD since these techniques work around the same detection limit. The preferential formation of hematite ($Fe_3O_4$) over spinel oxide ($Fe_{3-x}Cr_xO_4$) on the 304, 310, and 316 strongly depends on the reaction of Ni in the alloys with $SO_2$. The $SO_2$ from the Venus gas mixture reacts with Ni forming nickel sulfides. This reaction consumes nickel from the alloys

and decreases the Ni/Fe ratio leading to an increase in the iron activity. Thus, at higher activities the amount of iron is enough to solubilize in $Cr_2O_3$ forming spinel oxide ($Fe_{3-x}Cr_xO_4$), and the excess Fe will readily oxidize to $Fe_3O_4$. This is clearly noticed in the experimental results obtained by XRD, EDS, XPS, and Auger analyses on the 304, 310, and 316 samples.

It is well known that the oxidation resistance in the Fe-Ni-Cr alloys increases with the Ni/Fe ratio (Ref. 5). The Ni/Fe ratios of stainless steel samples 310, 304, and 316 at a fixed chromium content are 0.4, 0.11, and 0.14, respectively. Thus, the corrosion resistance of these samples is expected to increase in this order. However, in this work the corrosion resistance of the stainless steels increases in the order 316 < 310 < 304. The unexpected corrosion behavior of 316 could be explained in terms of other influential parameters on oxide growth rate rather than the chromium content such as surface finishing, grain size, cold working, silicon content, and the small addition of rare-earth elements. Here, the 316 sample with total surface roughness of 4.78 μm exhibited higher corrosion compared to the 304 sample with total surface roughness of 3.57 μm.

## 4.2 Nickel-Based Alloys

The main products of the reactions of the chromium-nickel-iron alloys G30 and 625 exposed in the GEER for 10 and 42 days are nickel sulfides in the outer layer and iron and/or chromium oxides in the inner layers of the scales. The disagreement between the predicted thermodynamic compounds and the phases detected by XRD on nickel-chromium alloys G30 and G625 can be related to either the detection limit of this technique or some of the crystalline phases formed on these alloys maybe being isotypic.

The detected phases and compounds of this study are in good agreement with those predicted by the thermodynamic calculations (Table 46). The oxidation behavior of the β-NiAl alloy sample exposed to the Venusian gas mixture suggests that alumina formed as a protective scale on this alloy. NiS was also formed in this scale, which is a product of the reaction of nickel and sulfur dioxide. The formation of the $\alpha$-$Al_2O_3$ protective scale has been noticed before (Ref. 5) as the only reaction product of β-NiAl in pure oxygen at 0.1 bar (1.5 psi), which was also noticed in this work.

## 4.3 Coatings

### 4.3.1 4YSZ

Although the high porosity and oxygen vacancies of the 4YSZ coating contribute to diffusion of the species present in the Venus gas mixture phase, leading to oxidation of the alloy, it significantly improves the corrosion resistance of the alloys by providing a $CO_2$ molecule barrier. As clearly noticed in Figures 8 and 10, the weight gain per area of the 4YSZ-coated alloys is much lower than that of the bare ones. Carbon steel coated with 4YSZ was the only sample that had an iron oxide phase form between the coating and the base of the alloy after exposure to the Venusian atmosphere in the GEER.

### 4.3.2 Porcelain

The porcelain coating was effective in protecting the stainless steel 304 substrate. Changes in the chemistry and formation of scales were not detected by SEM–EDS analysis in the interface between the coating and the base of the alloy. The thickness decrease of the porcelain coating after it was exposed in the GEER is related to the crystallization of its amorphous phase as shown in the XRD patterns of Figure 161. The decrease in the thickness of the porcelain coating is accompanied by a decrease in the weight change per area of this sample as noticed in Figure 10 for the sample exposed for 42 days.

### 4.3.3 SilcoNert® and Dursan®

SilcoNert® coating was effective in protecting the surface of the stainless steels 304 and 316 against corrosion of the Venus gas mixture in the GEER. The small decrease of 0.10±0.02 μm in the thickness of the SilcoNert® coating applied on 304 that was exposed in the GEER for 21 days (Table 6) is related to the partial reaction of silicon from the coating with iron from the base of the alloy when exposed to temperature of 467 °C (873 °F) in the GEER. These iron silicide crystalline phases were detected by XRD analysis on the samples exposed for 42 days. There was no change in the thickness of the coating applied on 316 exposed for 21 days in the GEER. The results obtained by XPS analysis corroborate well with those obtained by XRD and EDS analyses. From XPS it is concluded that there is only a slight change in the atomic concentration of elements at the interface between the SilcoNert® coating and the base of the alloy for the samples that were exposed for 21 days in the GEER. Dursan® was not effective in protecting the surface of the samples 304 and 316 against corrosion of the Venus gas mixture in the GEER. This is clearly noticed since the constituent of the Venus gas mixture permeated/diffused through the coating and reacted with the base of the alloy forming iron and chromium oxides as detected by EDS analysis in the sample exposed for 42 days. Small amount of sulfur was detected by EDS analysis on the surface of the coating, which are present in a form of rectangular grains as shown in Figure 119. This is most probably in the form of iron sulfides, which are products of the reaction between the Venus gas mixture and the iron from the base of the alloy.

## 4.4 Ceramics

All the ceramics ($\alpha$-$Al_2O_3$, $Si_3N_4$, SiC, and amorphous $SiO_2$) exposed in the GEER for 10 and 42 days were unreacted, which is evident from electron microscopy, EDS analysis, and elemental mapping. Future work in which ceramic powder exposed to the Venusian atmosphere is needed since the surface area might affect the extent of molecular interaction between the chemical species in the supercritical and solid phases.

# 5.0 Summary of Results

## 5.1 Weight Gain Per Area

The weight-gain-per-area performance of the materials exposed in the GEER are divided into three groups and are listed from the lowest to the highest weight gain per area as follows:

1. Group I—Metallic Materials:
   a. Gold did not exhibit any weight change considering the experimental uncertainties.
   b. Nickel-based alloys: β- NiAl < G30 < 625.
   c. Steels: 04 < 310 < 316 < 1018 for 10- and 42-day exposures.
2. Group II—Coatings: SilcoNert® (SilcoTek Co.) < Porcelain < Dursan® (SilcoTek Co.) < 4YSZ for 10- and 42-day exposures.
3. Group III—Ceramics: Considering the experimental uncertainties, no weight change was noticed for all ceramics of this work ($\alpha$-$Al_2O_3$, $Si_3N_4$, SiC, amorphous $SiO_2$).

## 5.2 Cross Section Characterization, XPS, AES, and XRD Analyses

1. Steels—A double layer oxide mainly in which the outer layer is magnetite and inner layer is nickel sulfide formed on the austenitic steels 304, 310, and 316 exposed in the GEER for 10 and 42 days. These oxide layers are formed due to the reaction between $CO_2$ in the supercritical fluid mixture and the metals present in the alloy. Other oxide phases were found to form on the base of the austenitic steels as well but their abundance is limited by their thermodynamic stability and kinetics.

a. 304 Stainless Steel—From XPS analysis, it was found that the major thin layers consist of iron oxide and chromium oxide with a thin layer of sulfide formed between these oxides and the alloy base. From XRD, it was noticed that magnetite ($Fe_3O_4$) and nickel sulfide ($Ni_{0.96}S$) crystalline phases were formed on the 304 stainless steel exposed for 42 days. It is possible that minor amounts of other phases such as $Cr_xO_y$, $Fe_xCr_yO_z$ $Ni_xS_y$, NiO, and $Cr_xC_y$ formed at the interface between the oxide scale and the base of the alloy as well.
b. 310 Stainless Steel—From electron microscopy, EDS analysis, and elemental mapping, the inner layer formed on 310 stainless steel sample exposed for 10 and 42 days in the GEER is rich in iron, chromium, and oxygen, which can be attributed to the formation of iron and/or chromium oxide crystalline phases. XRD analysis only detected magnetite ($Fe_3O_4$) and nickel sulfide (NiS) on the surface of this alloy. The outer layer formed on this sample is rich in nickel, iron, sulfur, and oxygen, which are related to the formation of nickel sulfide and iron oxide phases. Both layers are porous and the outer layer exhibited spallation.
c. 316 Stainless Steel—From electron microscopy, EDS, and elemental mapping, the outer layer formed on 316 stainless steel sample exposed for 10 and 42 days in the GEER is porous and is rich in iron and oxygen, which can be attributed to the formation of an iron oxide crystalline phase. The inner layer of this sample is dense and is rich in iron, chromium, and oxygen, which are related to the formation of iron and/or chromium oxide crystalline phases. XPS depth profile analysis, only detected iron oxide formed on this sample down to the depth of 1.8 μm at which point the profile was stopped. From XRD, it was noticed that magnetite ($Fe_3O_4$), chromium iron oxide (spinel) and nickel sulfides (NiS) crystalline phases were formed on the 316 exposed for 42 days.
d. 1018 Carbon Steel—From electron microscopy and EDS analysis, the inner and outer layers formed on 1018 steel sample exposed in the GEER are rich in iron, sulfur, and oxygen, which can be attributed to the formation of iron sulfide and/or oxide crystalline phases. Both layers are not well bonded to each other and to the base of the alloy, and are porous. XRD analysis has only detected magnetite formed on this alloy.

2. Nickel-based alloys—The conclusions derived here are based on electron microscopy, EDS analysis and elemental mapping of the samples exposed in the GEER. Thus, we make assumptions on the metal oxides that might have formed on these alloys based on the abundances of the elements detected by EDS and elemental mapping analyses and also based on the thermodynamic stability of the competing oxide phases. XRD analysis detected nickel sulfide phases on the nickel alloys. In addition to nickel sulfide phases, XRD analysis also detected $FeCr_2O_4$ on the alloy G30, and $FeCr_2O_4$ and $NiMoO_4$ on the alloy 625.
   a. G30—The outer layer formed on the sample consists of nickel sulfides ($Fe_{0.11}Ni_{0.86}S$ and $Ni_{0.96}S$) and the inner layer consists of chromite ($FeCr_2O_4$). Mo was detected in both layers as well, but its Kα spectral line overlaps with that of sulfur. Both layers are porous and the outer layer exhibits spallation.
   b. 625—The outer and inner layers formed are dense and free of pores. They consist of nickel sulfides (NiS, $Ni_{53}S_{54}$) and oxides ($FeCr_2O_4$ and $NiMoO_4$), respectively. Mo was detected in both layers as well.
   c. β-NiAl—Although scales or oxide layers on β-NiAl alloy were not observed by electron microscopy, XRD detected nickel sulfide. Furthermore, EDS analysis of the surface detected oxygen and fluorine in addition to the constituent elements.
3. Coatings
   a. 4YSZ—The 4YSZ coating deposited on stainless steels 304 and 316 and on carbon steel 1018 exhibited high porosity. High porosity contributes to gas/fluid diffusion of the species present in the supercritical phase, which leads to oxidation of the alloy. Its high concentration of oxygen vacancies provides a path for ionic diffusion leading to further oxidation of the alloy as well. From EDS analysis and elemental mapping, it was found that an iron oxide phase formed between the coating and the base of the 316 alloy and in the pores as well.

b. SilcoNert® and Dursan®—SilcoNert® was effective in protecting the stainless steels 304 and 316 against corrosion of the Venus atmosphere. Products of corrosion (iron and/or chromium oxide) was formed at the base of the alloy underneath of the Dursan® coating.
c. Porcelain—The porcelain coating was effective in protecting the base of the stainless steel 304 sample and was unreacted in the Venus atmosphere. Only crystallization of some of the amorphous contents took place most probably due to the heat treatment in the GEER.

4. Ceramics—All the ceramics ($\alpha$-$Al_2O_3$, $Si_3N_4$, SiC, amorphous $SiO_2$) exposed in the GEER for 10 and 42 days were unreacted within the detection limits of the spectroscopic and microscopic techniques used in this work.

# References


1. Rouillard, F.; Charton, F.; and Moine, G: Corrosion Behaviour of Different Metallic Materials in Supercritical $CO_2$ at 550 °C and 250 Bars. Proceedings of $SCCO_2$ Power Cycle Symposium, Troy, NY, 2009.
2. Kato, Yasuyoshi: Advanced High Temperature Gas-Cooled Reactor Systems. J. Eng. Gas Turbines Power, vol. 132, no. 1, 2009.
3. Venus Exploration Analysis Group (VEXAG): Venus Exploration Themes. 2014.
4. Venus Exploration Analysis Group (VEXAG): Roadmap for Venus Exploration. 2014.
5. Young, David: High Temperature Oxidation and Corrosion of Metals. First ed., Elsevier Science, New York, NY, 2008.
6. Holmes, D.R.; Hill, Rodney; and Wyatt, L.M.: Corrosion of Steels in $CO_2$. Proceedings of the British Nuclear Energy Society International Conference at Reading University, Reading, England, 1974.
7. Devereaux, Owen F.: Topics in Metallurgical Thermodynamics. Krieger Publishing Company, Malabar, FL, 1989.
8. Ellingham, H.J.T.: Reducibility of Oxides and Sulphides in Metallurgical Processes. Journal of the Society of Chemical Industry, 1944, pp. 125–133.
9. Gibbs, Jonathan Paul: Corrosion of Various Engineering Alloys in Supercritical Carbon Dioxide. MIT Thesis, Massachusetts Institute of Technology, 2010.
10. Stobbs, W.M.; Newcomb, S.B.; and Metcalfe, E.: A Microstructural Study of the Oxidation of Fe-Ni-Cr Alloys. II. 'Non-Protective' Oxide Growth. Phil. Trans. R. Soc. Lond. A, vol. 319, 1986, pp. 219–247.
11. Pritchard, A.M.; and Truswell, A.E.: Mechanistic Experiments on the Oxidation of 9% Cr Steels in $CO_2$ at 550 °C. Corrosion of Steels in $CO_2$, The British Nuclear Energy Society, London, 1974.
12. Holmes, D.R.; Mortimer, D.; and Newell, J.: Discovery and Assessment of Accelerated Corrosion in Fe-9Cr Alloys and Steels. Proceedings of the British Nuclear Energy Society International Conference on Corrosion of Steels in $CO_2$, Reading, England, 1974.
13. Smart, Neil G., et al.: Solubility of Chelating Agents and Metal-Containing Compounds in Supercritical Carbon Dioxide. Talanta, vol. 44, no. 2, 1997, pp. 137–150.
14. Warzee, M., et al.: Effect of Surface Treatment on the Corrosion of Stainless Steels in High-Temperature Water and Steam. J. Electrochem. Soc., vol. 112, 1965, pp. 670–674.
15. Jacobson, Nathan S.; and Worrel, Wayne L.: Reaction of Cobalt in $SO_2$ Atmospheres at Elevated Temperatures. J. Electrochem. Soc., vol. 131, 1984, pp. 1182–1188.
16. Bale, C.W., et al.: FactSage Thermochemical Software and Databases, 2010–2016. CALPHAD: Computer Coupling of Phase Diagrams and Thermochemistry, vol. 54, 2016, pp. 35–53.
17. Bale, C.W., et al.: FactSage Thermochemical Software and Databases. Calphad, vol. 26, no. 2, 2002, pp. 189–228.
18. Ampornrat, Pantip; and Was, Gary S.: Oxidation of Ferritic-Martensitic Alloys T91, HCM12A and HT–9 in Supercritical Water. J. Nucl. Mater., vol. 371, 2007, pp. 1–17.

19. Martinelli, L., et al.: Oxidation Mechanism of an Fe-9Cr-1Mo Steel Liquid Pb-Bi Eutectic Alloy at 470 °C (Part II). Corros. Sci., vol. 50, no. 9, 2008, pp. 2537–2548.
20. Quadakkers, W.J., et al.: Steam Oxidation of Ferritic Steels—Laboratory Test Kinetic Data. Mater. High Temp., vol. 22, nos. 1–2, 2005, pp. 47–60.
21. Ferreira, L.F.R., et al.: A Study of the Mechanism of Corrosion of Some Ferritic Steels in High-Pressure Carbon Dioxide With the Aid of Oxygen-18 as a Tracer. III. Fe-9% Cr-1% Mo-0.26% Si. Proc. R. Soc. A, vol. 422, no. 1863, 1989, pp. 279–288.
22. Allen, G.C.; Brown, I.T.; and Wild, R.K.: The Early Stages of the Oxidation of a 9% Chromium Steel in Carbon Dioxide Studied by Auger Electron Spectroscopy. J. Nucl. Mater., vol. 68, no. 2, 1977, pp. 179–185.

TABLE 1.—METALLIC MATERIALS (ALLOYS) USED IN THIS WORK

| Sample | Stainless steel | | | Carbon steel | Nickel-based alloy | |
|---|---|---|---|---|---|---|
| | 304[a] | 310 | 316[b] | 1018 | G30 | 625 |
| Manufacturer/ provider | ATI Allegheny Ludlum, Midland, PA | OnlineMetals.com, Seattle, WA | ATI Allegheny Ludlum, Midland, PA | Charter Manufacturing Co., Inc., Milwaukee, WI | Haynes International, Inc., Houston, TX | OnlineMetals.com, Seattle, WA |
| Dimensions, cm | 5.2×4.1×0.2 | 5.0×4.3×0.3 | 5.2×4.1×0.2 | 5.1×3.2×0.5 | 5.1×4.2×0.2 | 5.0×4.3×0.3 |
| Surface area, $cm^2$ | 45 | 48 | 45 | 41 | 46 | 48 |

[a]Plate hot-rolled coils annealed pickled.
[b]Cold-rolled coils annealed.

TABLE 2.—CHEMICAL COMPOSITION OF METALLIC MATERIALS (ALLOYS) USED IN THIS WORK

| Element | Composition, wt% | | | | | |
|---|---|---|---|---|---|---|
| | Stainless steel | | | Carbon steel | Nickel-based alloy | |
| | 304 | 310 | 316 | 1018 | G30[a] | 625 |
| Fe | 70.506 | 48 to 53 | 68.376 | 98.6808 | 13.0 to 17.0 | 5[b] |
| Cr | 18.14 | 26 | 16.6 | 0.09 | 28.0 to 31.5 | 20 to 23 |
| Ni | 8.07 | 19 to 22 | 10.09 | 0.05 | 43 | 68.8 to 79.3 |
| Co | ---------- | ---------- | ---------- | ---------- | 5.0[b] | ---------- |
| Mn | 1.64 | 2 | 1.87 | 0.67 | 1.5[b] | 0.5[b] |
| Mo | 0.46 | ---------- | 2.04 | 0.02 | 4.0 to 6.0 | 8 to 10 |
| Nb | ---------- | ---------- | ---------- | ---------- | ---------- | 3.15 to 4.15 |
| Ta | ---------- | ---------- | ---------- | ---------- | ---------- | 0.05[b] |
| Cu | 0.51 | ---------- | 0.52 | 0.11 | 1.0 to 2.4 | ---------- |
| Sn | ---------- | ---------- | ---------- | 0.006 | ---------- | ---------- |
| Al | ---------- | ---------- | ---------- | 0.002 | ---------- | 0.4[b] |
| Ti | ---------- | ---------- | ---------- | 0.002 | ---------- | 0.4[b] |
| V | ---------- | ---------- | ---------- | 0.002 | ---------- | ---------- |
| W | ---------- | ---------- | ---------- | ---------- | 1.5 to 4.0 | ---------- |
| Si | 0.58 | 1.5 | 0.44 | 0.19 | 0.8[b] | 0.05 |
| N | 0.07 | ---------- | 0.04 | 0.007 | ---------- | ---------- |
| C | 0.024 | 0.25 | 0.024 | 0.17 | 0.03[b] | 0.1[b] |
| B | ---------- | ---------- | ---------- | 0.0002 | ---------- | ---------- |
| P | 0.034 | 0.045[b] | 0.031 | ---------- | 0.04 | 0.015[b] |
| S | 0.001 | 0.03 | 0.005 | ---------- | 0.02 | 0.015[b] |

[a]Nb+Ta = 0.3 to 1.5 wt%.
[b]Maximum.

TABLE 3.—CERAMIC MATERIALS USED IN THIS WORK

| Sample | CVD $Si_3N_4$ | CVD β-SiC | α-$Al_2O_3$ | Amorphous $SiO_2$ |
|---|---|---|---|---|
| Manufacturer | Advanced Ceramics Corporation, ON, Canada | Rayrheon/Bomass Machine Specialties, Somerviller, MA | Graphtek LLC, Buffalo Grove, IL | QSI Quartz Scientific, Inc, Fairport Harbor, OH |
| Additives/impurities | C and O,<br>01 to 1.0 wt%<br><br>H, Al, and Fe (ppm) | Be and Cu < 100 ppm | All in wt%:<br>$SiO_2$ < 0.10<br>$Fe_2O_3$ < 0.050<br>$Na_2O$, Li, and K < 0.10 | All in ppm:<br>Al = 16, As < 0.4,<br>B < 0.1, Ca < 0.6,<br>Cd < 0.01, Cr = 0.05,<br>Cu < 0.1, Fe = 0.3,<br>K = 0.7, Li = 1,<br>Mg = 0.1, Mn = 0.1,<br>Na = 1, Ni < 0.1,<br>P = 1.5, Sb < 0.4,<br>Ti = 1.1, Zr = 1.5,<br>OH < 5 |
| Density, $g/cm^3$ | 3.18 | ---------- | 3.8 | 2.2 |
| Dimensions, cm | 2.5×0.7×0.4 | 2.5×1.3×0.3 | 4.0×2.5×0.5 | 2.5×2.5×0.3 |
| Surface area, $cm^2$ | 6.4 | 9.0 | 27.6 | 16.6 |

TABLE 4.—CHEMICAL COMPOSITION OBTAINED FROM ENERGY DISPERSIVE X-RAY SPECTROSCOPY ANALYSIS OF SURFACE AND BULK OF UNPOLISHED 304 STAINLESS STEEL SAMPLE EXPOSED TO VENUSIAN SURFACE CONDITIONS FOR 10 DAYS (FIG. 15(a))

| Element | Composition, wt% | |
|---|---|---|
| | Surface (location I) | Bulk (location II) |
| C | 20.4 | 7.1 |
| O | 27.0 | 1.5 |
| S | 1.2 | ------ |
| Cr | 10.0 | 16.1 |
| Mn | 0.7 | 1.8 |
| Fe | 38.1 | 65.9 |
| Ni | 2.6 | 7.1 |
| Si | ------ | 0.397 |

TABLE 5.—CHEMICAL COMPOSITION OBTAINED FROM ENERGY DISPERSIVE X-RAY SPECTROSCOPY ANALYSIS OF SURFACE AND BULK OF UNPOLISHED SIDE OF 304 STAINLESS STEEL SAMPLE EXPOSED TO VENUSIAN SURFACE CONDITIONS FOR 42 DAYS (FIG. 17(a))

| Element | Composition, wt% | |
|---|---|---|
| | Surface (location I) | Bulk (location II) |
| C | 3.1 | 3.0 |
| O | 27.7 | ------ |
| S | 8.0 | ------ |
| Cr | 34.1 | 17.5 |
| Fe | 27.1 | 71.4 |
| Ni | ------ | 8.1 |

TABLE 6.—CHEMICAL COMPOSITION OBTAINED FROM ENERGY DISPERSIVE SPECTROSCOPY ANALYSIS OF OUTER LAYER, INNER LAYER, AND BULK OF 316 STAINLESS STEEL SAMPLE EXPOSED TO VENUSIAN SURFACE CONDITIONS FOR 10 DAYS (FIG. 30(a))

| Element | Composition, wt% | | |
|---|---|---|---|
| | Outer layer (location I) | Inner layer (location II) | Bulk (location III) |
| C | 4.3 | 4.0 | 2.0 |
| O | 26.2 | 27.7 | 0.2 |
| Si | ------ | 0.9 | 0.2 |
| S | 1.1 | 4.1 | ------ |
| Cr | 0.6 | 34.7 | 14.9 |
| Fe | 67.9 | 21.1 | 70.0 |
| Ni | ------ | 1.0 | 11.0 |
| Mo | ------ | 6.6 | 1.7 |

TABLE 7.—CHEMICAL COMPOSITION OBTAINED FROM ENERGY DISPERSIVE SPECTROSCOPY ANALYSIS OF OUTER LAYER MAIN AND SECONDARY PHASES, INNER LAYER, AND BULK OF 316 STAINLESS STEEL SAMPLE EXPOSED TO VENUSIAN SURFACE CONDITIONS FOR 42 DAYS (FIG. 31(b))

| Element | Composition, wt% | | | |
|---|---|---|---|---|
| | Outer layer | | Inner layer (location III) | Bulk (location IV) |
| | Main phase (location I) | Secondary phase (location II) | | |
| C | ----- | ----- | ----- | ----- |
| O | 27.5 | ----- | 26.9 | ----- |
| Si | ----- | ----- | ----- | 0.5 |
| S | ----- | 37.5 | 7.3 | ----- |
| Cr | ----- | 0.4 | 34.8 | 16.3 |
| Fe | 72.5 | 10.3 | 27.7 | 70.1 |
| Ni | ----- | 51.7 | 3.3 | 10.0 |
| Mo | ----- | ----- | ----- | 3.1 |

TABLE 8.—CHEMICAL COMPOSITION OBTAINED FROM ENERGY DISPERSIVE SPECTROSCOPY ANALYSIS OF BULK, SCALE, AND INNER LAYER BETWEEN THEM OF 310 STAINLESS STEEL SAMPLE EXPOSED TO VENUSIAN SURFACE CONDITIONS FOR 10 DAYS (FIG. 40)

| Element | Composition, wt% | | |
|---|---|---|---|
| | Outer layer | Inner layer | Bulk |
| C | 6.9 | 4.6 | 3.2 |
| O | 18.0 | 22.8 | 2.1 |
| Si | 0.1 | 0.6 | 0.7 |
| S | 14.0 | 5.5 | ------ |
| Cr | 2.8 | 28.8 | 24.0 |
| Fe | 42.1 | 33.3 | 52.3 |
| Ni | 16.1 | 12.6 | 17.7 |

TABLE 9.—CHEMICAL COMPOSITION OBTAINED FROM ENERGY DISPERSIVE SPECTROSCOPY ANALYSIS OF SCALE AND BULK OF 310 STAINLESS STEEL SAMPLE EXPOSED TO VENUSIAN SURFACE CONDITIONS FOR 42 DAYS (FIG. 41)

| Element | Composition, wt% | |
|---|---|---|
| | Bulk | Scale |
| C | ----- | 2.2 |
| O | 1.2 | 16.5 |
| S | ----- | 7.7 |
| Cr | 23.8 | 1.7 |
| Fe | 54.4 | 59.3 |
| Ni | 20.6 | 12.6 |

TABLE 10.—CHEMICAL COMPOSITION OBTAINED FROM ENERGY DISPERSIVE SPECTROSCOPY ANALYSIS OF OUTER LAYER, INNER LAYER, AND BULK OF 1018 STEEL SAMPLE EXPOSED TO VENUSIAN SURFACE CONDITIONS FOR 10 DAYS (FIG. 48)

| Element | Composition, wt% | | |
|---|---|---|---|
| | Outer layer | Inner layer | Bulk |
| C | 2.9 | 3.8 | 3.1 |
| O | 25.1 | 25.7 | ----- |
| S | 1.3 | 2.7 | ----- |
| Fe | 70.8 | 67.8 | 96.9 |

TABLE 11.—CHEMICAL COMPOSITION OBTAINED FROM ENERGY DISPERSIVE SPECTROSCOPY ANALYSIS OF OUTER LAYER, INNER LAYER, AND BULK OF 1018 STEEL SAMPLE EXPOSED TO VENUSIAN SURFACE CONDITIONS FOR 42 DAYS (FIG. 49(a))

| Element | Composition, wt% | | |
|---|---|---|---|
| | Outer layer | Inner layer | Bulk |
| C | 0.5 | 3.3 | 2.8 |
| O | 27.7 | 24.4 | ------ |
| S | ------ | 5.5 | ------ |
| Fe | 71.9 | 67.7 | 97.2 |

TABLE 12.—CHEMICAL COMPOSITION OBTAINED FROM ENERGY DISPERSIVE SPECTROSCOPY ANALYSIS OF OUTER LAYER, INNER LAYER, AND BULK OF G30 ALLOY SAMPLE EXPOSED TO VENUSIAN SURFACE CONDITIONS FOR 10 DAYS (FIG. 56(a))

| Element | Composition, wt% | | |
|---|---|---|---|
| | Outer layer | Inner layer | Bulk |
| C | 11.9 | 4.8 | 4.7 |
| O | ------ | 15.6 | 3.4 |
| Al | ------ | 0.4 | ------ |
| S | 32.6 | 9.9 | ------ |
| Cr | 6.6 | 32.3 | 23.6 |
| Mn | 0.6 | 1.4 | 0.8 |
| Fe | 8.9 | 7.3 | 12.9 |
| Co | 7.2 | 1.0 | 3.3 |
| Ni | 30.5 | 11.4 | 43.4 |
| Mo | 1.7 | 11.5 | 6.8 |
| W | ------ | 4.3 | 1.2 |

TABLE 13.—CHEMICAL COMPOSITION OBTAINED FROM ENERGY DISPERSIVE SPECTROSCOPY ANALYSIS OF OUTER LAYER, INNER LAYER, AND BULK OF G30 ALLOY SAMPLE EXPOSED TO VENUSIAN SURFACE CONDITIONS FOR 42 DAYS (FIG. 57)

| Element | Composition, wt% | | |
|---|---|---|---|
| | Outer layer | Inner layer | Bulk |
| C | 7.5 | 6.2 | ------ |
| O | 3.7 | 20.6 | 7.1 |
| Al | ------ | 0.7 | 0.5 |
| S | 29.8 | 10.3 | 5.9 |
| Cr | 1.6 | 31.4 | 21.4 |
| Mn | ------ | ------ | ------ |
| Fe | 2.0 | 4.6 | 13.4 |
| Ni | 50.8 | 8.2 | 41.9 |
| Mo | 4.6 | 11.9 | 8.5 |
| W | ------ | 6.1 | 1.3 |

TABLE 14.—CHEMICAL COMPOSITION OBTAINED FROM ENERGY DISPERSIVE SPECTROSCOPY ANALYSIS OF OUTER LAYER, INNER LAYER, AND BULK OF ALLOY 625 SAMPLE EXPOSED TO VENUSIAN SURFACE CONDITIONS FOR 10 DAYS (FIG. 64)

| Element | Composition, wt% | | |
|---|---|---|---|
| | Outer layer | Inner layer | Bulk |
| C | 8.2 | 4.0 | 3.8 |
| O | 0.6 | 23.6 | ------ |
| S | 34.1 | 3.8 | ------ |
| Cr | 0.8 | 25.9 | 19.2 |
| Fe | 1.4 | 5.8 | 3.7 |
| Co | 0.003 | ------ | ------ |
| Ni | 55.0 | 2.6 | 53.2 |
| Mo | --------- | 33.7 | 14.0 |
| Ta | --------- | ------ | 6.0 |
| Al | --------- | 0.2 | ------ |
| Si | --------- | 0.4 | ------ |

TABLE 15.—CHEMICAL COMPOSITION OBTAINED FROM ENERGY DISPERSIVE SPECTROSCOPY ANALYSIS OF OUTER LAYER, INNER LAYER, AND BULK OF ALLOY 625 SAMPLE EXPOSED TO VENUSIAN SURFACE CONDITIONS FOR 42 DAYS (FIG. 65)

| Element | Composition, wt% | | |
|---|---|---|---|
| | Outer layer | Inner layer | Bulk |
| C | 5.3 | ------ | ------ |
| O | ------ | 20.8 | 2.1 |
| S | 34.5 | 6.7 | ------ |
| Cr | 0.7 | 26.7 | 20.3 |
| Fe | ------ | 4.2 | 4.3 |
| Ni | 59.5 | 10.1 | 58.9 |
| Mo | ------ | 30.7 | 14.4 |
| Ta | ------ | ------ | 6.0 |
| Si | ------ | 0.6 | ------ |

TABLE 16.—CHEMICAL COMPOSITION OBTAINED FROM ENERGY DISPERSIVE SPECTROSCOPY ANALYSIS OF SURFACE AND BULK OF β-NiAl ALLOY SAMPLE EXPOSED TO VENUSIAN SURFACE CONDITIONS FOR 10 DAYS (FIG. 72(a))

| Element | Composition, wt% | |
|---|---|---|
| | Surface (location I) | Bulk (location II) |
| C | 15.1 | 4.4 |
| O | 23.0 | ------ |
| F | 19.5 | ------ |
| Al | 27.4 | 27.9 |
| S | 3.7 | ------ |
| Ni | 11.3 | 67.7 |

TABLE 17.—CHEMICAL COMPOSITION OBTAINED FROM ENERGY DISPERSIVE SPECTROSCOPY ANALYSIS OF SURFACE AND BULK OF β-NiAl ALLOY SAMPLE EXPOSED TO VENUSIAN SURFACE CONDITIONS FOR 42 DAYS (FIG. 73(a))

| Element | Composition, wt% | |
|---|---|---|
| | Surface (location I) | Bulk (location II) |
| C | ------ | ------ |
| O | 7.9 | ------ |
| F | ------ | ------ |
| Al | 50.1 | 28.8 |
| S | ------ | ------ |
| Ni | 42.0 | 71.2 |

TABLE 18.—CHEMICAL COMPOSITION OBTAINED FROM ENERGY DISPERSIVE SPECTROSCOPY ANALYSIS OF GOLD WIRE SAMPLES NEAR SURFACE EDGE UNEXPOSED AND EXPOSED TO VENUSIAN SURFACE CONDITIONS FOR 10 AND 42 DAYS

| Element | Composition, wt% | | |
|---|---|---|---|
| | Unexposed (Fig. 79) | 10 days exposure (Fig. 80) | 42 days exposure (Fig. 81) |
| C | 3.1 | 6.7 | 12.3 |
| Au | 96.9 | 93.3 | 87.4 |

TABLE 19.—CHEMICAL COMPOSITION OBTAINED FROM X-RAY PHOTOELECTRON SPECTROSCOPY ANALYSIS OF SURFACE OF GOLD WIRE SAMPLE EXPOSED TO VENUSIAN SURFACE CONDITIONS FOR 42 DAYS (FIG. 81)

| Sample[a] | Atomic concentration, percent | | | | | | | | |
|---|---|---|---|---|---|---|---|---|---|
| | C | O | Au | Ni | Cl | Ca | S | Na | F |
| Gold wire | 44.2 | 23.6 | 20.6 | 4 | 2.6 | 2.3 | 2.2 | 0.5 | ---- |
| Gold wire, DI sonicated | 32.9 | 17.5 | 47.9 | --- | ---- | ---- | ---- | ---- | 1.7 |

[a]DI refers to deionized water.

TABLE 20.—CHEMICAL COMPOSITION OBTAINED FROM ENERGY DISPERSIVE SPECTROSCOPY ANALYSIS OF UNEXPOSED BULK 304 STAINLESS STEEL SAMPLE AND 4 MOL% YTTRIA-STABILIZED ZIRCONIA COATING (FIG. 85)

| Element | Composition, wt% | |
|---|---|---|
| | Bulk | Coating |
| C | 1.8 | 5.5 |
| O | ------ | 4.2 |
| Cr | 17.2 | 01 |
| Fe | 72.7 | 0.5 |
| Ni | 8.2 | 0.2 |
| Y | ------ | 5.7 |
| Zr | ------ | 83.9 |

TABLE 21.—CHEMICAL COMPOSITION OBTAINED FROM ENERGY DISPERSIVE SPECTROSCOPY ANALYSIS OF BULK 304 STAINLESS STEEL SAMPLE AND 4 MOL% YTTRIA-STABILIZED ZIRCONIA COATING, EXPOSED TO VENUSIAN SURFACE CONDITIONS FOR 10 DAYS (FIG. 86)

| Element | Composition, wt% | |
|---|---|---|
| | Bulk | Coating |
| C | 1.8 | 8.2 |
| O | ------ | 3.2 |
| Cr | 17.2 | ------ |
| Fe | 72.2 | ------ |
| Ni | 8.8 | ------ |
| Y | ------ | 1.8 |
| Zr | ------ | 86.2 |

TABLE 22.—CHEMICAL COMPOSITION OBTAINED FROM ENERGY DISPERSIVE SPECTROSCOPY ANALYSIS OF BULK 304 STAINLESS STEEL SAMPLE AND 4 MOL% YTTRIA-STABILIZED ZIRCONIA COATING, EXPOSED TO VENUSIAN SURFACE CONDITIONS FOR 42 DAYS (FIG. 87)

| Element | Composition, wt% | |
|---|---|---|
| | Bulk | Coating |
| O | ------ | 14.2 |
| Cr | 18.2 | ------ |
| Fe | 73.4 | ------ |
| Ni | 8.4 | ------ |
| Y | ------ | 15.6 |
| Zr | ------ | 70.2 |

TABLE 23.—CHEMICAL COMPOSITION OBTAINED FROM ENERGY DISPERSIVE SPECTROSCOPY ANALYSIS OF UNEXPOSED BULK 316 STAINLESS STEEL SAMPLE AND 4 MOL% YTTRIA-STABILIZED ZIRCONIA COATING (FIG. 95)

| Element | Composition, wt% | |
|---|---|---|
| | Bulk | Coating |
| C | 0.2 | ------ |
| O | ------ | 0.4 |
| Si | 0.2 | ------ |
| P | 0.03 | ------ |
| Cr | 5.6 | ------ |
| Fe | 20.5 | ------ |
| Ni | 3.2 | ------ |
| Mn | 0.5 | ------ |
| Mo | 0.8 | ------ |
| Y | ------ | 1.8 |
| Zr | ------ | 33.2 |
| Au | 68.9 | 64.6 |

TABLE 24.—CHEMICAL COMPOSITION OBTAINED FROM ENERGY DISPERSIVE SPECTROSCOPY ANALYSIS OF BULK 316 STAINLESS STEEL SAMPLE AND 4 MOL% YTTRIA-STABILIZED ZIRCONIA COATING, EXPOSED TO VENUSIAN SURFACE CONDITIONS FOR 10 DAYS (FIG. 96)

| Element | Composition, wt% | |
|---|---|---|
| | Bulk | Coating |
| C | 0.2 | ------ |
| O | ------ | 0.9 |
| Cr | 6.2 | ------ |
| Fe | 22.8 | ------ |
| Ni | 3.3 | ------ |
| Mn | 0.7 | ------ |
| Mo | 0.8 | ------ |
| Y | ------ | 1.8 |
| Zr | ------ | 35.7 |
| Au | 66.0 | 61.6 |

TABLE 25.—CHEMICAL COMPOSITION OBTAINED FROM ENERGY DISPERSIVE SPECTROSCOPY ANALYSIS OF BULK 316 STAINLESS STEEL SAMPLE AND 4 MOL% YTTRIA-STABILIZED ZIRCONIA COATING, EXPOSED TO VENUSIAN SURFACE CONDITIONS FOR 42 DAYS (FIG. 97)

| Element | Composition, wt% | |
|---|---|---|
| | Bulk | Coating |
| O | ------ | 15.0 |
| Cr | 16.3 | ------ |
| Fe | 69.3 | ------ |
| Ni | 10.7 | ------ |
| Mo | 1.9 | ------ |
| Y | ------ | 65.7 |
| Zr | ------ | 78.5 |

TABLE 26.—CHEMICAL COMPOSITION OBTAINED FROM ENERGY DISPERSIVE SPECTROSCOPY ANALYSIS OF UNEXPOSED BULK 1018 STEEL SAMPLE AND 4 MOL% YTTRIA-STABILIZED ZIRCONIA COATING (FIG. 105)

| Element | Composition, wt% | |
|---|---|---|
| | Bulk | Coating |
| C | 7.4 | 3.0 |
| O | ------ | 2.8 |
| Fe | 92.6 | 0.5 |
| Y | ------ | 25.4 |
| Zr | ------ | 68.3 |

TABLE 27.—CHEMICAL COMPOSITION OBTAINED FROM ENERGY DISPERSIVE SPECTROSCOPY ANALYSIS OF BULK 1018 STEEL SAMPLE, 4 MOL% YTTRIA-STABILIZED ZIRCONIA COATING, AND INNER LAYER FORMED BETWEEN THEM, EXPOSED TO VENUSIAN SURFACE CONDITIONS FOR 10 DAYS (FIG. 106)

| Element | Composition, wt% | | |
|---|---|---|---|
| | Bulk | Coating | Inner layer |
| C | 1.9 | ------ | 2.1 |
| O | ------ | 0.9 | 7.2 |
| Fe | 98.1 | ------ | 90.7 |
| Y | ------ | 1.8 | ------ |
| Zr | ------ | 35.7 | ------ |

TABLE 28.—CHEMICAL COMPOSITION OBTAINED FROM ENERGY DISPERSIVE SPECTROSCOPY ANALYSIS OF 1018 STEEL SAMPLE AND INNER LAYER FORMED WITH 4 MOL% YTTRIA-STABILIZED ZIRCONIA COATING, EXPOSED TO VENUSIAN SURFACE CONDITIONS FOR 42 DAYS (FIG. 107)

| Element | Composition, wt% | |
|---|---|---|
| | Bulk | Inner layer |
| C | 9.6 | ------ |
| O | ------ | 17.1 |
| S | ------ | 13.4 |
| Fe | 90.4 | 67.4 |
| Y | ------ | ------ |
| Zr | ------ | ------ |
| Al | ------ | 2.1 |

TABLE 29.—THICKNESS OF COMMERCIAL SilcoNert® AND Dursan® COATINGS ON STAINLESS STEEL 304 AND 316 SAMPLES, UNEXPOSED AND EXPOSED TO VENUSIAN SURFACE CONDITIONS FOR 10 AND 42 DAYS

| Coating[a] | Stainless steel | Exposure, days | Thickness, μm | Error, ± |
|---|---|---|---|---|
| Dursan® | 304 | 0 | 0.38 | 0.02 |
| | | 10 | 0.48 | 0.03 |
| | | 42 | 0.85 | 0.04 |
| | 316 | 0 | 1.49 | 0.04 |
| | | 10 | 0.97 | 0.02 |
| | | 42 | 1.07 | 0.04 |
| SilcoNert® | 304 | 0 | 0.53 | 0.05 |
| | | 10 | 0.72 | 0.02 |
| | | 42 | 0.77 | 0.08 |
| | 316 | 0 | 1.4 | 0.1 |
| | | 10 | 2.3 | 0.2 |
| | | 42 | 1.54 | 0.08 |

[a]From SilcoTek Co.

TABLE 30.—THICKNESS OF COMMERCIAL SilcoNert® AND Dursan® COATINGS ON STAINLESS STEELS 304 AND 316 SAMPLES, BEFORE AND AFTER EXPOSURE TO VENUSIAN SURFACE CONDITIONS FOR 21 DAYS

| Stainless steel | Coating[a] | Thickness, μm | | | |
|---|---|---|---|---|---|
| | | Before exposure | Error, ± | 21 days exposure | Error, ± |
| 304 | SilcoNert® | 1.38 | 0.01 | 1.28 | 0.02 |
| | Dursan® | 1.72 | 0.03 | 1.16 | 0.03 |
| 316 | SilcoNert® | 1.4 | 0.1 | 1.36 | 0.02 |
| | Dursan® | 1.3 | 0.1 | 1.08 | 0.04 |

[a]From SilcoTek Co.

TABLE 31.—CHEMICAL COMPOSITION OBTAINED FROM ENERGY DISPERSIVE SPECTROSCOPY ANALYSIS OF BULK 304 STAINLESS STEEL SAMPLE AND Dursan® COATING,[a] EXPOSED TO VENUSIAN SURFACE CONDITIONS FOR 10 DAYS

| Element | Composition, wt% | |
|---|---|---|
| | Bulk | Coating |
| C | 34.7 | 31.5 |
| O | 0.6 | 0.2 |
| Si | 4.0 | 21.6 |
| Cr | 11.0 | 8.4 |
| Mn | 1.0 | 1.0 |
| Fe | 44.0 | 25.3 |
| Ni | 4.8 | ------ |
| Nb | ------ | 12.0 |

[a]From SilcoTek Co.

TABLE 32.—CHEMICAL COMPOSITION OBTAINED FROM ENERGY DISPERSIVE SPECTROSCOPY ANALYSIS OF BULK 304 STAINLESS STEEL SAMPLE AND Dursan® COATING,[a] EXPOSED TO VENUSIAN SURFACE CONDITIONS FOR 42 DAYS

| Element | Composition, wt% | |
|---|---|---|
| | Bulk | Coating |
| C | ------ | 21.5 |
| O | 0.1 | 41.0 |
| Si | ------ | 28.2 |
| Cr | 17.4 | 2.5 |
| Fe | 74.2 | 6.1 |
| Ni | 8.4 | 0.7 |

[a]From SilcoTek Co.

TABLE 33.—CHEMICAL COMPOSITION OBTAINED FROM ENERGY DISPERSIVE SPECTROSCOPY ANALYSIS OF BULK 316 STAINLESS STEEL AND Dursan® COATING,[a] EXPOSED TO VENUSIAN SURFACE CONDITIONS FOR 10 DAYS

| Element | Composition, wt% | |
|---|---|---|
| | Bulk | Coating |
| C | 6.6 | 23.7 |
| O | ------ | 22.3 |
| Si | ------ | 19.1 |
| Cr | 14.6 | 1.7 |
| Fe | 58.7 | 19.9 |
| Ni | 8.9 | ------ |
| Mo | 11.3 | 13.3 |

[a]From SilcoTek Co.

TABLE 34.—CHEMICAL COMPOSITION OBTAINED FROM ENERGY DISPERSIVE SPECTROSCOPY ANALYSIS OF BULK 316 STAINLESS STEEL AND Dursan® COATING,[a] EXPOSED TO VENUSIAN SURFACE CONDITIONS FOR 42 DAYS

| Element | Composition, wt% | | |
|---|---|---|---|
| | Bulk | Coating | Inner layer |
| C | 3.0 | 3.6 | ------ |
| O | ------ | 37.2 | 29.7 |
| S | ------ | 4.5 | ------ |
| Si | 0.5 | 19.8 | ------ |
| Cr | 16.2 | 3.4 | 23.0 |
| Fe | 67.8 | 29.9 | 36.9 |
| Ni | 9.6 | 0.8 | 5.7 |
| Mo | 2.8 | 0.8 | 4.7 |

[a]From SilcoTek Co.

TABLE 35.—CHEMICAL COMPOSITION OBTAINED FROM ENERGY DISPERSIVE SPECTROSCOPY ANALYSIS OF BULK 304 STAINLESS STEEL AND SilcoNert® 1040 COATING,[a] EXPOSED TO VENUSIAN SURFACE CONDITIONS FOR 10 DAYS

| Element | Composition, wt% | |
|---|---|---|
| | Bulk | Coating |
| C | 9.3 | 31.9 |
| Si | ------ | 49.3 |
| Cr | 16.4 | 3.5 |
| Fe | 66.9 | 13.3 |
| Ni | 7.4 | 1.9 |

[a]From SilcoTek Co.

TABLE 36.—CHEMICAL COMPOSITION OBTAINED FROM ENERGY DISPERSIVE SPECTROSCOPY ANALYSIS OF BULK 304 STAINLESS STEEL AND SilcoNert® 1040 COATING,[a] EXPOSED TO VENUSIAN SURFACE CONDITIONS FOR 42 DAYS

| Element | Composition, wt% | |
|---|---|---|
| | Bulk | Coating |
| C | ------ | 28.3 |
| O | ------ | 5.0 |
| Si | ------ | 57.2 |
| Cr | 17.8 | 3.2 |
| Fe | 74.1 | 4.9 |
| Ni | 8.2 | 1.5 |

[a]From SilcoTek Co.

TABLE 37.—CHEMICAL COMPOSITION OBTAINED FROM ENERGY DISPERSIVE SPECTROSCOPY ANALYSIS OF BULK 316 STAINLESS STEEL AND SilcoNert® 1040 COATING,[a] EXPOSED TO VENUSIAN SURFACE CONDITIONS FOR 10 DAYS

| Element | Composition, wt% | |
|---|---|---|
| | Bulk | Coating |
| C | 4.4 | 36.9 |
| O | ------ | 1.8 |
| Si | 0.5 | 58.8 |
| Cr | 15.4 | ------ |
| Fe | 66.7 | 2.5 |
| Ni | 10.0 | ------ |
| Mo | 3.0 | ------ |

[a]From SilcoTek Co.

TABLE 38.—CHEMICAL COMPOSITION OBTAINED FROM ENERGY DISPERSIVE SPECTROSCOPY ANALYSIS OF BULK 316 STAINLESS STEEL AND SilcoNert® 1040 COATING,[a] EXPOSED TO VENUSIAN SURFACE CONDITIONS FOR 42 DAYS

| Element | Composition, wt% | |
|---|---|---|
| | Bulk | Coating |
| O | ------ | 4.9 |
| Si | ------ | 85.5 |
| Cr | 17.0 | ------ |
| Fe | 72.1 | 5.1 |
| Ni | 9.8 | 4.5 |

[a]From SilcoTek Co.

TABLE 39.—CHEMICAL COMPOSITION OBTAINED FROM ENERGY DISPERSIVE SPECTROSCOPY ANALYSIS OF BULK 304 STAINLESS STEEL AND PORCELAIN COATING, EXPOSED TO VENUSIAN SURFACE CONDITIONS FOR 10 DAYS

| Element | Composition, wt% | |
|---|---|---|
| | Bulk | Coating |
| C | 3.2 | 19.1 |
| O | ------ | 26.1 |
| Al | ------ | 2.1 |
| Si | ------ | 39.0 |
| K | ------ | 2.3 |
| Ca | ------ | 8.3 |
| Zn | ------ | 3.1 |
| Cr | 27.8 | ------ |
| Fe | 67.3 | ------ |
| Ni | 5.4 | ------ |

TABLE 40.—CHEMICAL COMPOSITION OBTAINED FROM ENERGY DISPERSIVE SPECTROSCOPY ANALYSIS OF BULK 304 STAINLESS STEEL AND PORCELAIN COATING, EXPOSED TO VENUSIAN SURFACE CONDITIONS FOR 42 DAYS

| Element | Composition, wt% | |
|---|---|---|
| | Bulk | Coating |
| C | 8.4 | 9.4 |
| O | ------ | 47.6 |
| Ti | ------ | 1.8 |
| Si | ------ | 31.1 |
| K | ------ | 1.3 |
| Ca | ------ | 7.9 |
| Zn | ------ | 0.8 |
| Cr | 16.6 | 0.2 |
| Fe | 67.5 | ------ |
| Ni | 7.5 | ------ |

TABLE 41.—CHEMICAL COMPOSITION OBTAINED FROM ENERGY DISPERSIVE SPECTROSCOPY ANALYSIS OF SILICON CARBIDE SAMPLES NEAR SURFACE EDGE, UNEXPOSED AND EXPOSED TO VENUSIAN SURFACE CONDITIONS FOR 10 AND 42 DAYS

| Element | Composition, wt% | | |
|---|---|---|---|
| | Unexposed | 10 days exposure | 42 days exposure |
| C | 20.0 | 19.1 | 53.8 |
| Si | 80.0 | 80.9 | 46.2 |

TABLE 42.—CHEMICAL COMPOSITION OBTAINED FROM ENERGY DISPERSIVE SPECTROSCOPY ANALYSIS OF SILICON CARBIDE SAMPLES NEAR SURFACE EDGE, UNEXPOSED AND EXPOSED TO VENUSIAN SURFACE CONDITIONS FOR 10 AND 42 DAYS

| Element | Composition, wt% | | |
|---|---|---|---|
| | Unexposed | 10 days exposure | 42 days exposure |
| C | 12.1 | 10.7 | ------ |
| Si | 29.2 | 27.2 | 57.5 |
| O | 58.7 | 62.1 | 42.5 |

TABLE 43.—CHEMICAL COMPOSITION OBTAINED FROM X-RAY PHOTOELECTRON SPECTROSCOPY ANALYSIS OF SURFACE OF CERAMIC SAMPLES EXPOSED TO VENUSIAN SURFACE CONDITIONS FOR 42 DAYS

| Sample (area, treatment) | Atomic concentration, percent | | | | | | | | | | | | | |
|---|---|---|---|---|---|---|---|---|---|---|---|---|---|---|
| | C | O | Si | Al | Na | Ca | Fe | Mn | S | Ni | K | F | Mg | Cl |
| $SiO_2$ | | | | | | | | | | | | | | |
| (area 1) | 3.1 | 67.5 | 25.7 | ---- | 0.7 | 1.2 | 0.5 | 0.1 | 1.2 | 0.1 | 0.1 | ---- | ---- | ---- |
| (area 2) | 3.1 | 66.5 | 27.1 | ---- | 0.9 | 0.9 | 0.2 | 0.1 | 1.1 | 0.1 | 0.1 | ---- | ---- | ---- |
| (DI sonicated [a]) | 2.3 | 68.2 | 29.4 | ---- | ---- | ---- | ---- | ---- | ---- | ---- | ---- | ---- | ---- | ---- |
| $Al_2O_3$ | | | | | | | | | | | | | | |
| (area 1) | 4.3 | 61.5 | 1.7 | 25.5 | 2 | 0.8 | 0.4 | 0.1 | 1.2 | ---- | ---- | 1.1 | 0.9 | 0.4 |
| (area 2) | 4 | 62 | 1.6 | 26.3 | 2.3 | 0.6 | 0.3 | 0.1 | 0.7 | ---- | ---- | 1 | 0.8 | 0.3 |
| (DI sonicated [a]) | 4.3 | 64.2 | 1.8 | 27.5 | 0.3 | 0.1 | 0.3 | 0.1 | ---- | ---- | ---- | 1 | 0.3 | ---- |
| SiC | | | | | | | | | | | | | | |
| (area 1) | 25.7 | 40.5 | 29.9 | ---- | 0.6 | 1.1 | 0.8 | 0.6 | 0.9 | ---- | ---- | ---- | ---- | ---- |
| (area 2) | 26.8 | 39.5 | 29.4 | ---- | 0.8 | 1.4 | 0.6 | 0.5 | 1.1 | ---- | ---- | ---- | ---- | ---- |
| (DI sonicated,[a] area 1) | 26.3 | 39.5 | 33.1 | ---- | ---- | ---- | 0.6 | 0.4 | ---- | 0.1 | ---- | ---- | ---- | ---- |
| (DI sonicated,[a] area 2) | 25.9 | 40.2 | 32 | ---- | ---- | ---- | 1.3 | 0.3 | ---- | 0.1 | ---- | 0.2 | ---- | ---- |

[a]Sonicated in deionized (DI) water.

TABLE 44.—CHEMICAL COMPOSITION OBTAINED FROM ENERGY DISPERSIVE SPECTROSCOPY ANALYSIS OF SURFACE AND BULK OF INCONEL WIRE USED TO HANG SAMPLES IN GLENN EXTREME ENVIRONMENTS RIG, EXPOSED TO VENUSIAN SURFACE CONDITIONS FOR 10 DAYS (FIG. 197)

| Element | Composition, wt% | |
|---|---|---|
| | Surface | Bulk |
| C | 21.2 | 11.0 |
| O | 1.0 | 1.6 |
| Ca | 0.4 | ------ |
| Al | 0.4 | ------ |
| Cr | 11.6 | 12.6 |
| Ni | 59.5 | 69.0 |
| Fe | 5.2 | 5.8 |
| Si | 0.8 | ------ |

TABLE 45.—AMOUNT OF CHEMICAL SPECIES USED AS INPUT PARAMETERS IN THERMODYNAMIC CALCULATIONS[a] OF COMPOUNDS FORMED ON SAMPLES EXPOSED TO VENUS SURFACE CONDITIONS

| Sample | Amount (mol)[b] | | | | | | | | |
|---|---|---|---|---|---|---|---|---|---|
| | Fe | | Cr | | Ni | | Al | Mo | Co |
| 304 | $3.2\times10^{-1}$ | | $8.7\times10^{-2}$ | | $3.4\times10^{-2}$ | | ---------- | ---------- | ---------- |
| 310 | $2.2\times10^{-1}$ | | $1.3\times10^{-1}$ | | $8.7\times10^{-2}$ | | ---------- | ---------- | ---------- |
| 316 | $3.1\times10^{-1}$ | | $8.0\times10^{-2}$ | | $4.3\times10^{-2}$ | | ---------- | ---------- | ---------- |
| 1018 | $4.4\times10^{-1}$ | | $4.3\times10^{-4}$ | | $2.1\times10^{-4}$ | | ---------- | ---------- | ---------- |
| β-NiAl | ---------- | | ---------- | | $3.0\times10^{-1}$ | | $2.7\times10^{-1}$ | ---------- | ---------- |
| G30 | $6.7\times10^{-2}$ | | $1.4\times10^{-1}$ | | $1.8\times10^{-1}$ | | ---------- | $1.0\times10^{-2}$ | $1.8\times10^{-2}$ |
| 625 | $2.2\times10^{-2}$ | | $1.0\times10^{-1}$ | | $3.2\times10^{-1}$ | | ---------- | $2.3\times10^{-2}$ | ---------- |
| GEER | $CO_2$ | $N_2$ | $SO_2$ | HCl | HF | $H_2S$ | OCS | CO | $H_2O$ |
| | 1247.5 | 45.2 | $2.3\times10^{-1}$ | $6.5\cdot10^{-4}$ | $3.2\times10^{-6}$ | $2.6\times10^{-3}$ | $2.3\times10^{-1}$ | $1.6\times10^{-2}$ | $3.9\times10^{-2}$ |

[a]Computations were done using FactSage program (Refs. 16 and 17).

[b]The amount of elements was calculated assuming 25 g as the average weight of the samples and the amount of the molecular species in the GEER was assumed to be that injected in the chamber for the 42-day experiment.

TABLE 46.—COMPARISON OF PREDICTED THERMODYNAMICALLY STABLE COMPOUNDS AND THOSE COMPOUNDS, PHASES, AND ELEMENTS DETECTED BY SPECTROSCOPIC TECHNIQUES

| Alloy | Phases detected by XRD | Elements detected by EDS | Compounds (oxides and sulfides) from XPS and Auger spectroscopies[a] | Predicted thermodynamically stable compounds[b] |
|---|---|---|---|---|
| 304 | $Fe_3O_4$<br>$Ni_{0.96}S$ | Fe, Cr, O, and S | Graphite, $Fe_xO_y$, $Cr_xO_y$, $Fe_xCr_yO_z$ $Ni_xS_y$, NiO, and $Cr_xC_y$ | $FeS_2$<br>$Fe_3O_4$<br>$FeCr_2O_4$<br>$Ni_3S_4$ |
| 310 | $Fe_3O_4$<br>NiS | Outer layer: main phase Fe and O with minor amounts of localized Ni and S<br>Inner layer: Fe, Cr, and O with small amounts of S | ---------- | $FeCr_2O_4$<br>$FeS_2$<br>$Fe_3O_4$<br>$Ni_3S_4$ |
| 316 | $Fe_3O_4$<br>$Fe_{1.3}Cr_{1.7}O_4NiS$[c] | Outer layer: main phase Fe and O and secondary phase Ni, Fe, and S<br>Inner layer: Fe, Cr, and O with small amounts of Ni and S | $Fe_xO_y$ | $FeS_2$<br>$Fe_3O_4$<br>$FeCr_2O_4$<br>$Ni_3S_4$ |
| 1018 | $Fe_3O_4$ | Outer layer: Fe and O<br>Inner layer: Fe, O, and S | ---------- | $FeS_2$<br>$Fe_3O_4$<br>$FeCr_2O_4$<br>$Ni_3S_4$ |
| G30 | $FeCr_2O_4$<br>$Fe_{0.11}Ni_{0.86}SNi_{0.96}S$ | Outer and inner layers: Fe, Ni, Cr, Mo, S, and O | ---------- | $FeCr_2O_4$<br>$Ni_3S_4$<br>$(CoO)Cr_2O_3$<br>$CoS_2$<br>$Ni_9S_8$<br>$MoS_2$ |
| 625 | $FeCr_2O_4$<br>NiS<br>$Ni_{53}S_{54}$<br>$NiMoO_4$ | Outer layer: Ni and S[d]<br>Inner layer: Fe, Ni, Cr, Mo, O, and S | ---------- | NiO<br>$Ni_9S_8$<br>$(NiO)(Cr_2O_3)$<br>$MoO_2$<br>$FeCr_2O_4$ |
| β-NiAl | NiS | Surface: Al, Ni , F, and O | ---------- | $Al_2O_3$<br>$Ni_9S_8$<br>$Ni_3S_4$ |

[a]In fact XPS and Auger analyses give the depth elemental composition in the samples and the oxides and sulfide compounds are interpreted based on their amounts.
[b]Predictions were done using FactSage program (Refs. 16 and 17).
[c]Hexagonal and rhombohedral symmetries.
[d]Elements with weight percent less than 2 percent are omitted here. We also omitted the Mo element since its EDS spectrum overlaps with the S spectrum.

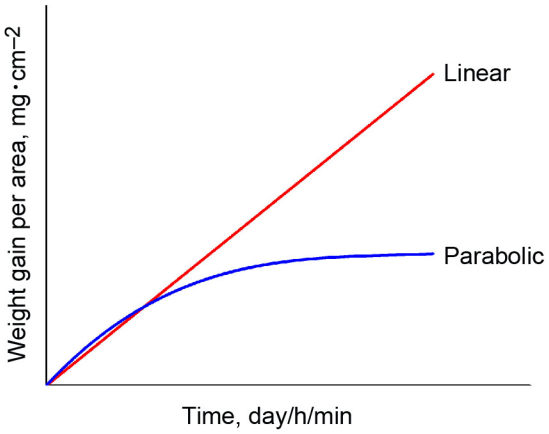


Figure 1.—Linear and parabolic kinetics of oxidation of an alloy.

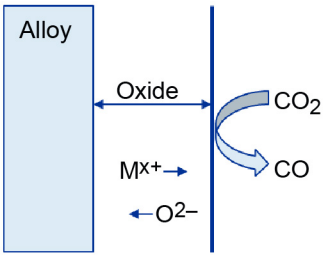


Figure 2.—Alloy undergoing high-temperature oxidation in pure supercritical $CO_2$.

(a)

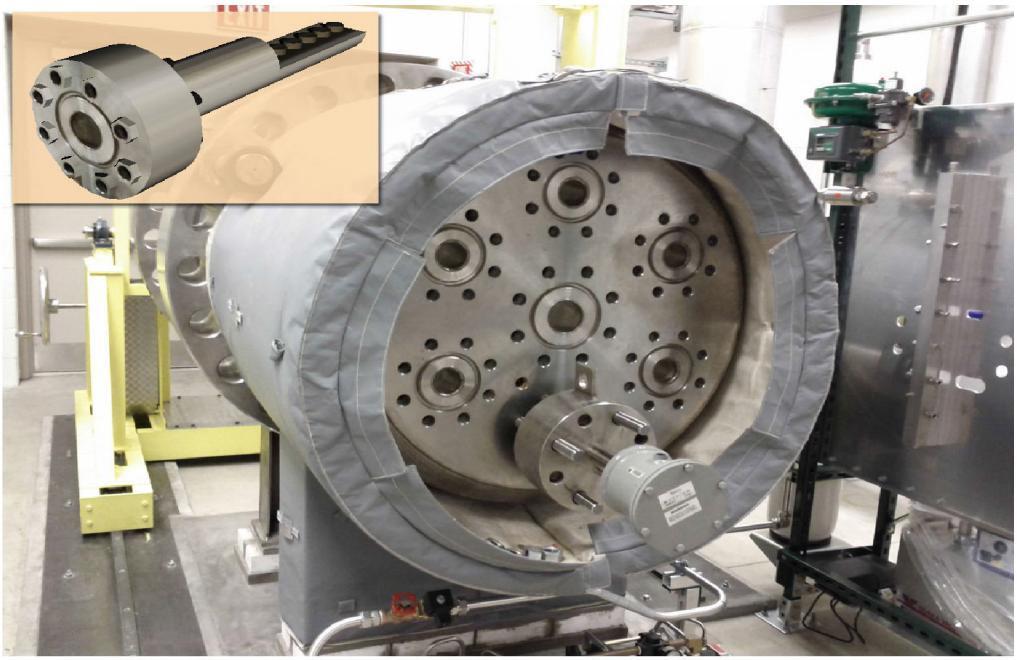

(b)

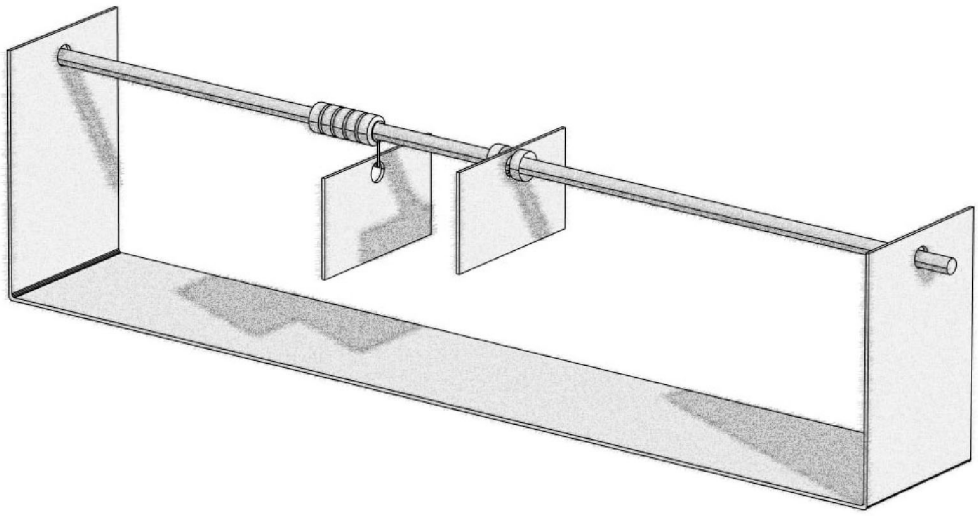

Figure 3.—Testing apparatus. (a) End view of Glenn Extreme Environments Rig chamber. Inset shows rail system that attaches to one of seven ports, allowing exposure to high-fidelity Venus surface conditions. (b) Sample holder with alumina rod used to accommodate sample coupons.

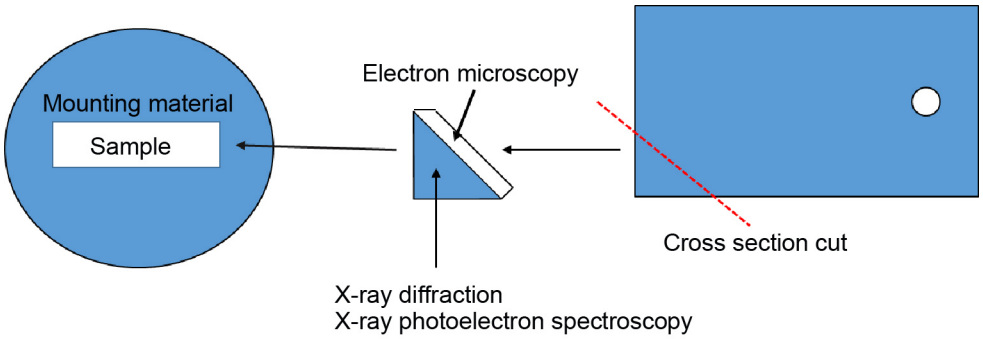


Figure 4.—Sample preparation process for scanning electron microscopy, X-ray diffraction, and X-ray photoelectron spectroscopy analyses.

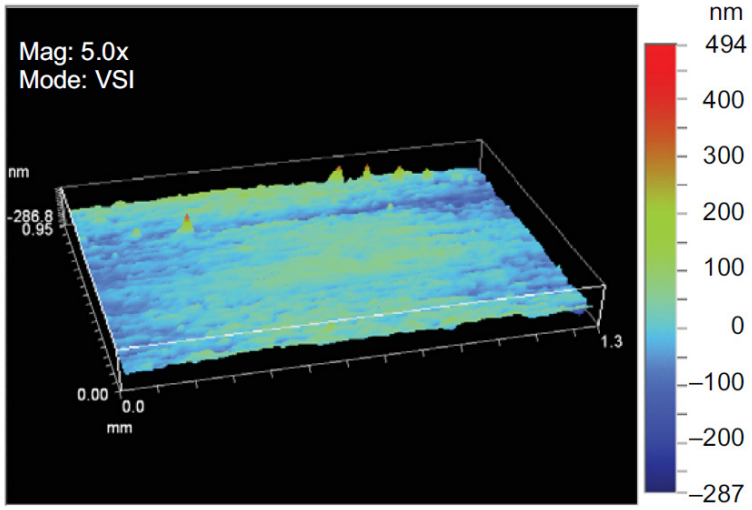


Figure 5.—Three-dimensional optical image of polished surface of 304 stainless steel coupon.

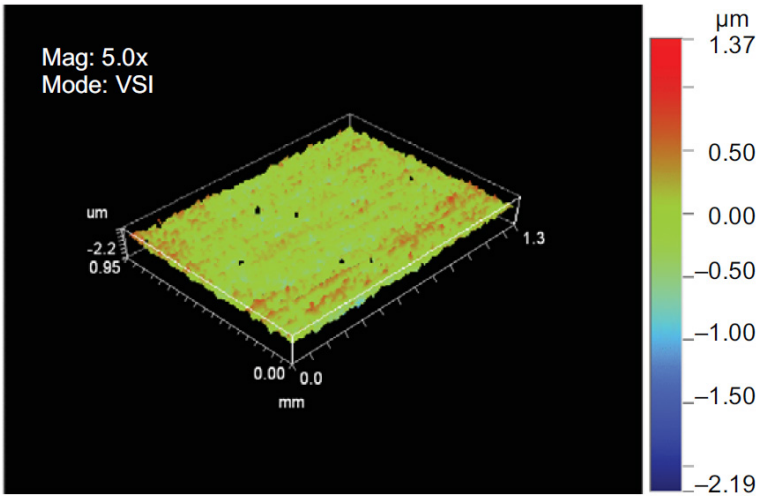


Figure 6.—Three-dimensional optical image of unpolished surface of 304 stainless steel coupon.

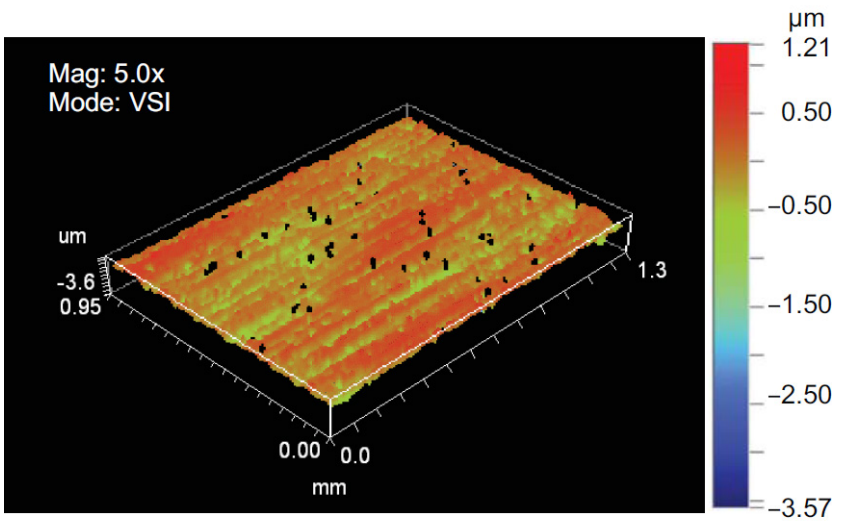


Figure 7.—Three-dimensional optical image of surface of 316 stainless steel coupon. Neither side of coupon was polished.

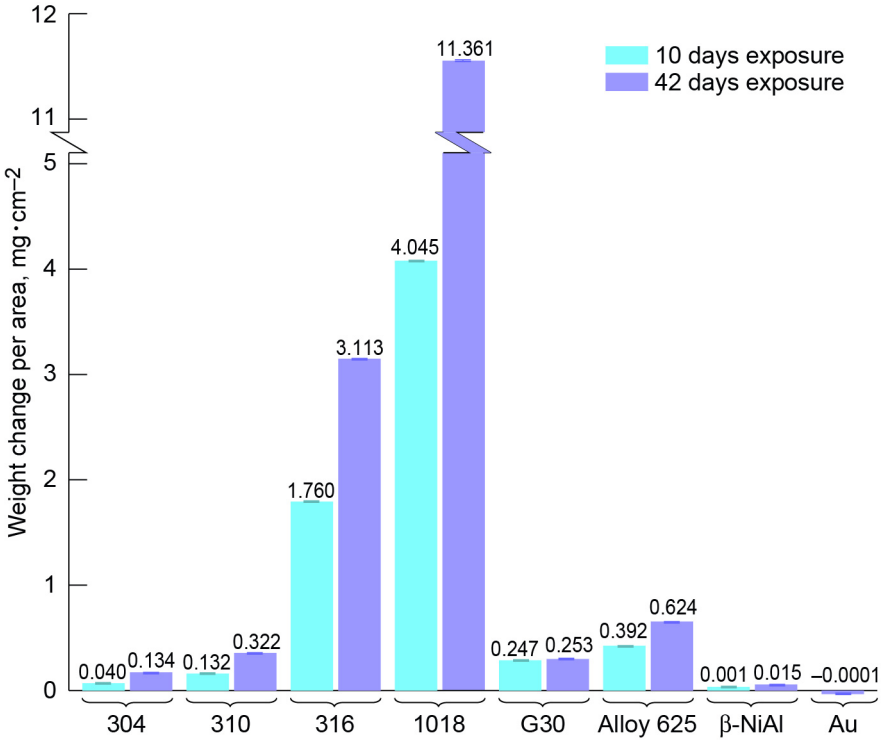


Figure 8.—Weight change per area of different metallic materials exposed to Venusian surface conditions for 10 and 42 days. Materials are stainless steels 304 and 316; carbon steel 1018; nickel-based alloys G30, 625, and β-NiAl; and gold. Error bars are orders of magnitude smaller than weight-gain-per-area values and are not noticed in graph.

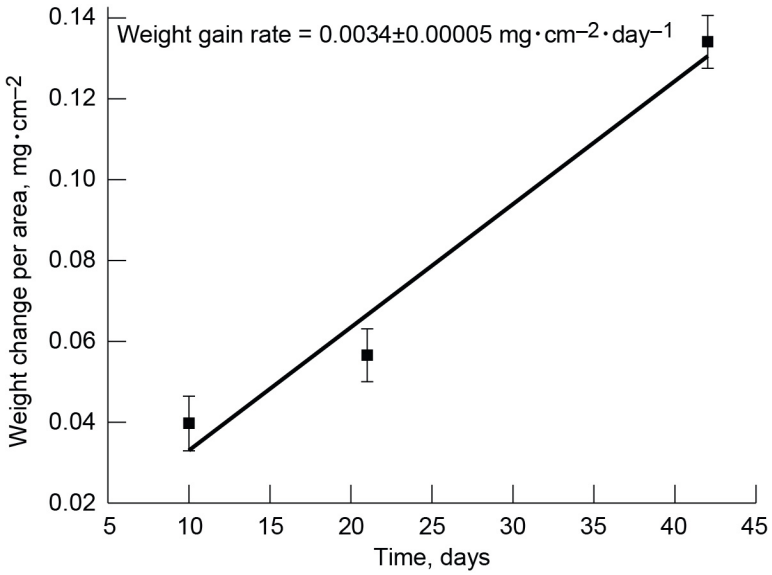


Figure 9.—Weight change per area versus time for stainless steel 304 exposed in Glenn Extreme Environments Rig.

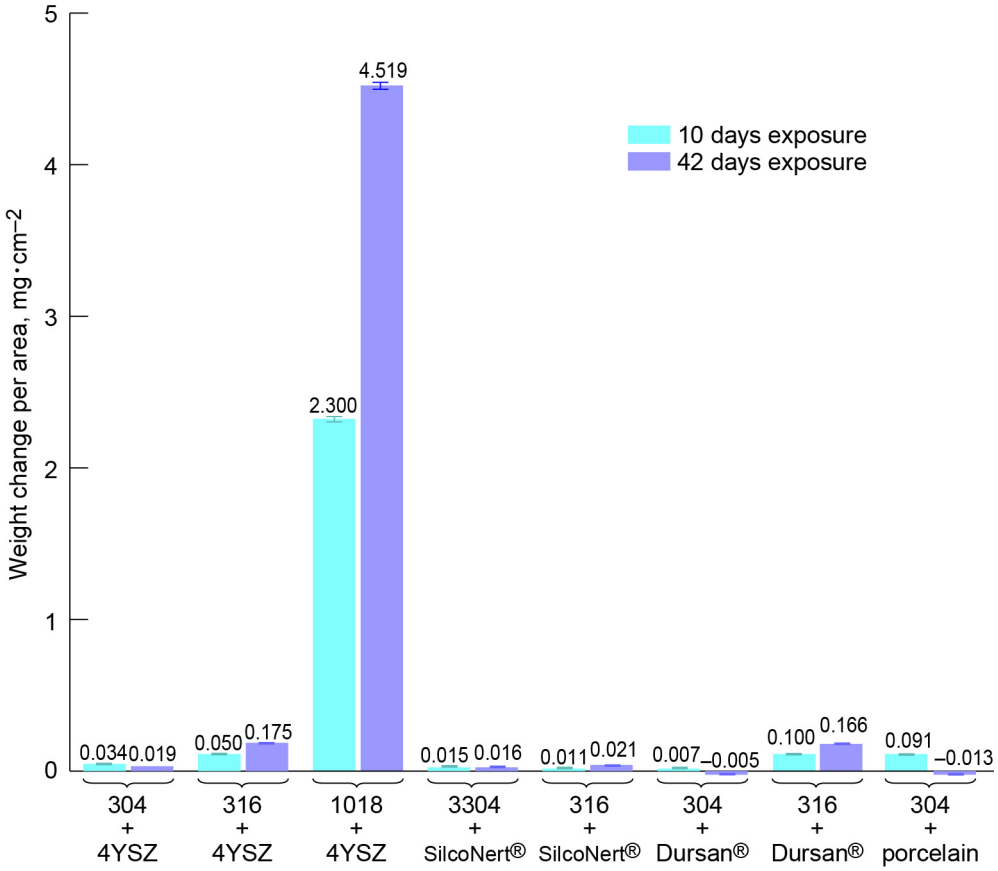


Figure 10.—Weight change per area of different coated metallic materials exposed to Venusian surface conditions for 10 and 42 days. Metallic materials are stainless steels 304 and 316 and carbon steel 1018; coatings are 4 mol% yttria-stabilized zirconia (4YSZ), SilcoNert® and Dursan® (SilcoTek Co.), and porcelain. Error bars are orders of magnitude smaller than weight-gain-per-area values and are not noticed in graph.

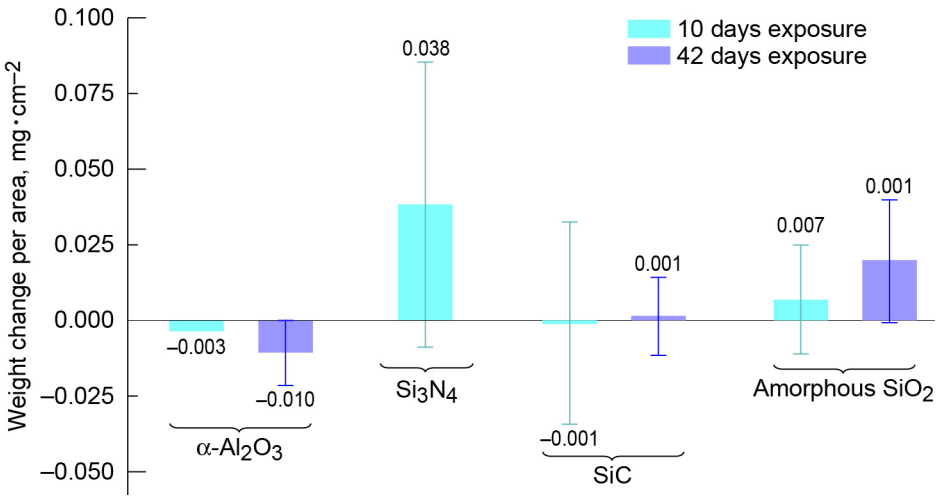


Figure 11.—Weight change per area of different ceramic materials exposed to Venusian surface conditions for 10 and 42 days.

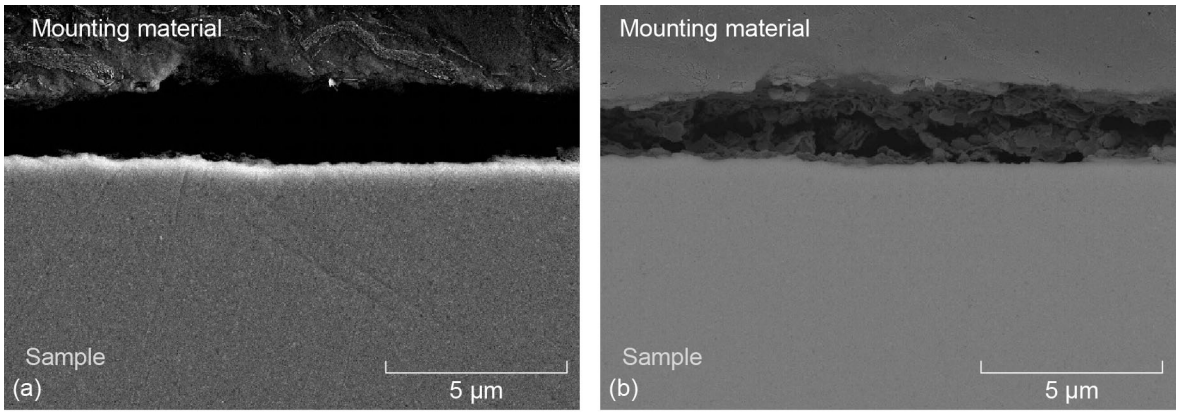


Figure 12.—Cross-sectional images of polished side of unexposed 304 stainless steel. (a) Scanning electron microscopy image. (b) Backscattered-electron image.

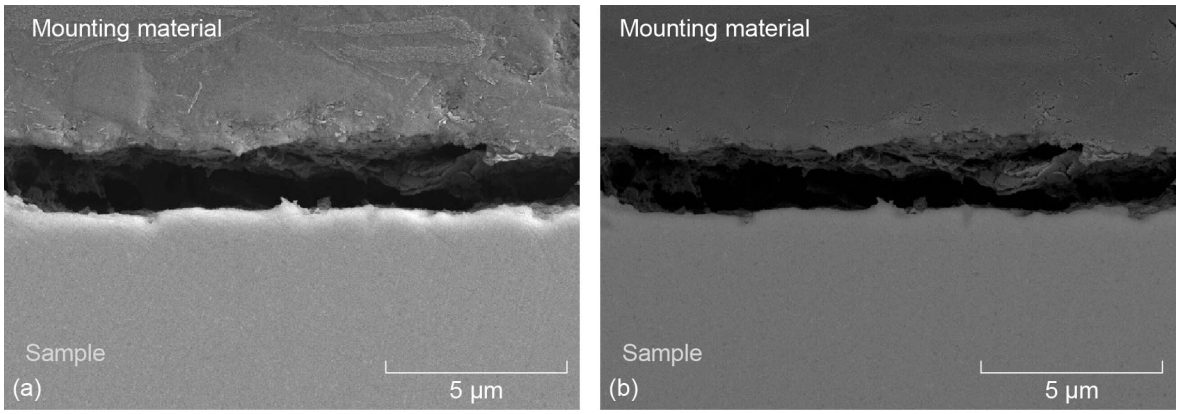


Figure 13.—Cross-sectional images of unpolished side of unexposed 304 stainless steel. (a) Scanning electron microscopy image. (b) Backscattered-electron image.

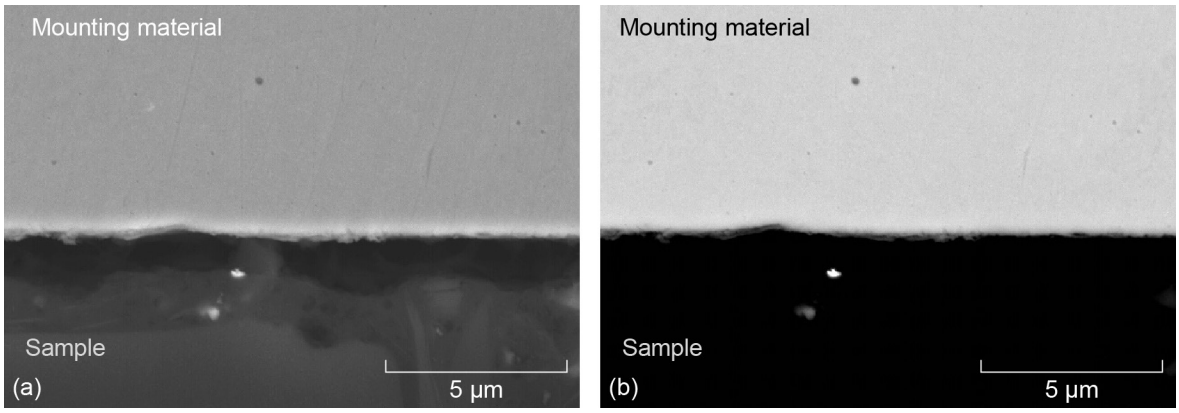


Figure 14.—Cross-sectional images of polished side of 304 stainless steel sample exposed to Venusian surface conditions for 10 days. (a) Scanning electron microscopy image. (b) Backscattered-electron image.

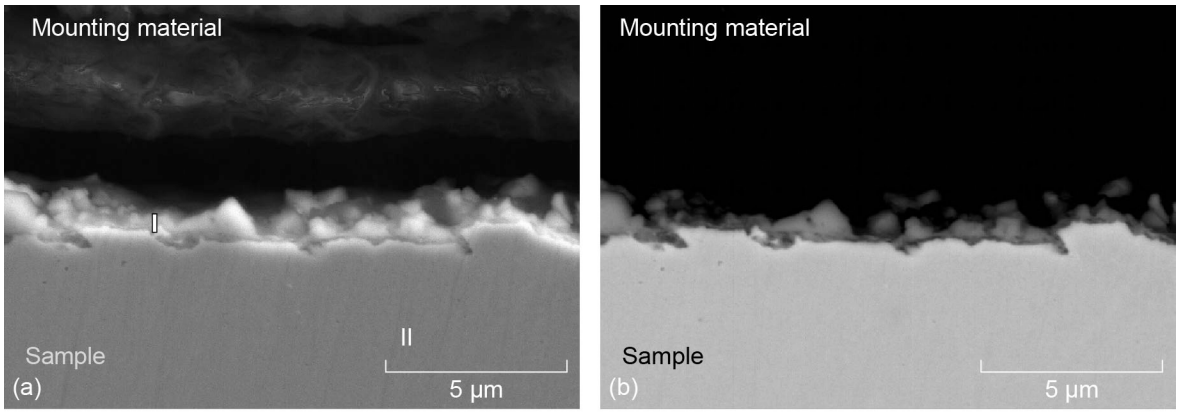


Figure 15.—Cross-sectional images of unpolished side of 304 stainless steel sample exposed to Venusian surface conditions for 10 days. (a) Scanning electron microscopy image showing surface (location I) and bulk (location II). (b) Backscattered-electron image.

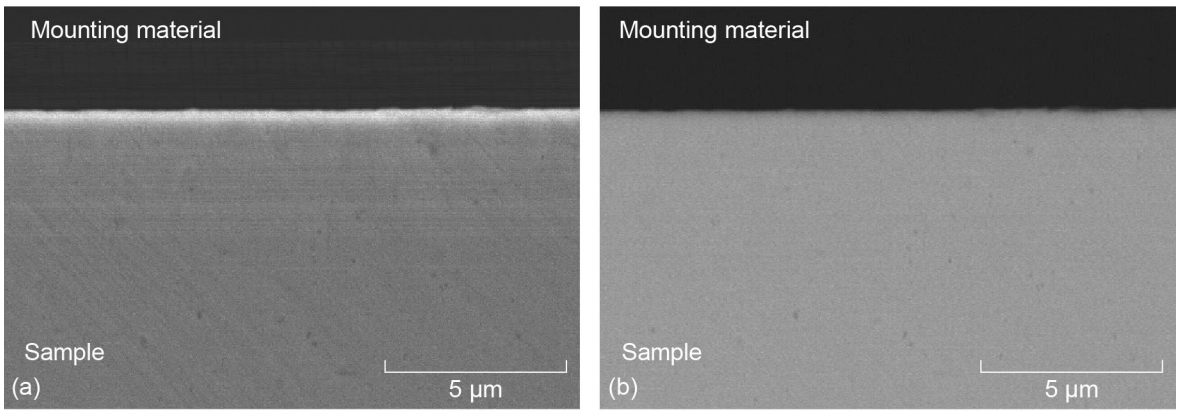


Figure 16.—Cross-sectional images of polished side of 304 stainless steel sample exposed to Venusian surface conditions for 42 days. (a) Scanning electron microscopy image. (b) Backscattered-electron image.

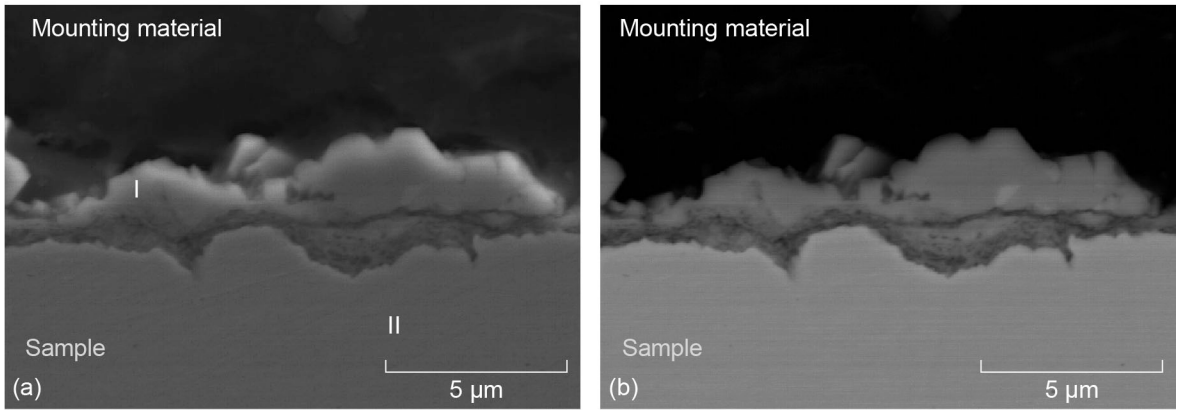


Figure 17.—Cross-sectional images of unpolished side of 304 stainless steel sample exposed to Venusian surface conditions for 42 days. (a) Scanning electron microscopy image, showing surface (location I) and bulk (location II). (b) Backscattered-electron image.

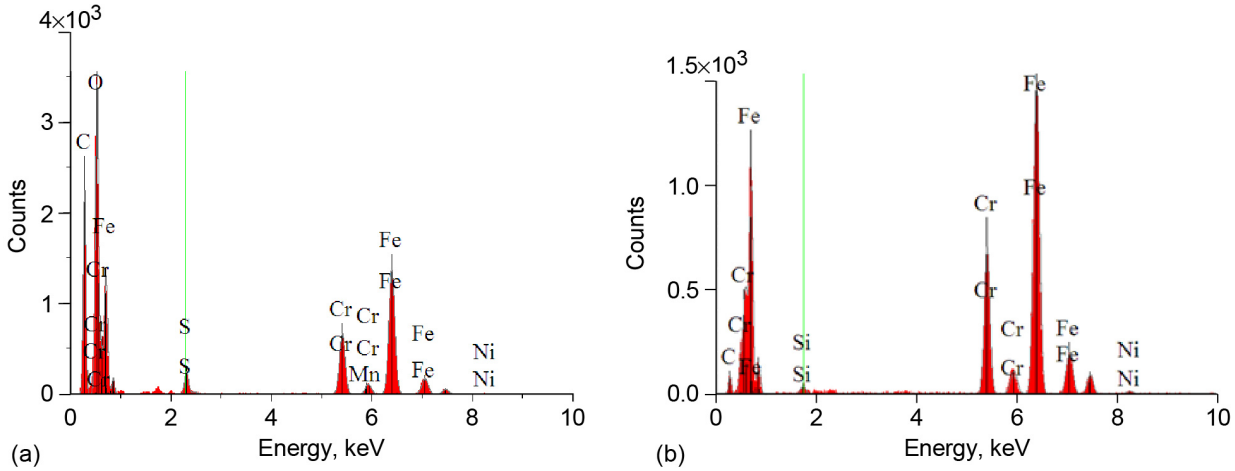


Figure 18.—Energy dispersive X-ray spectroscopy analysis of unpolished side of 304 stainless steel exposed to Venusian surface conditions for 10 days (Fig. 15(a)). (a) Surface (location I). (b) Bulk (location II).

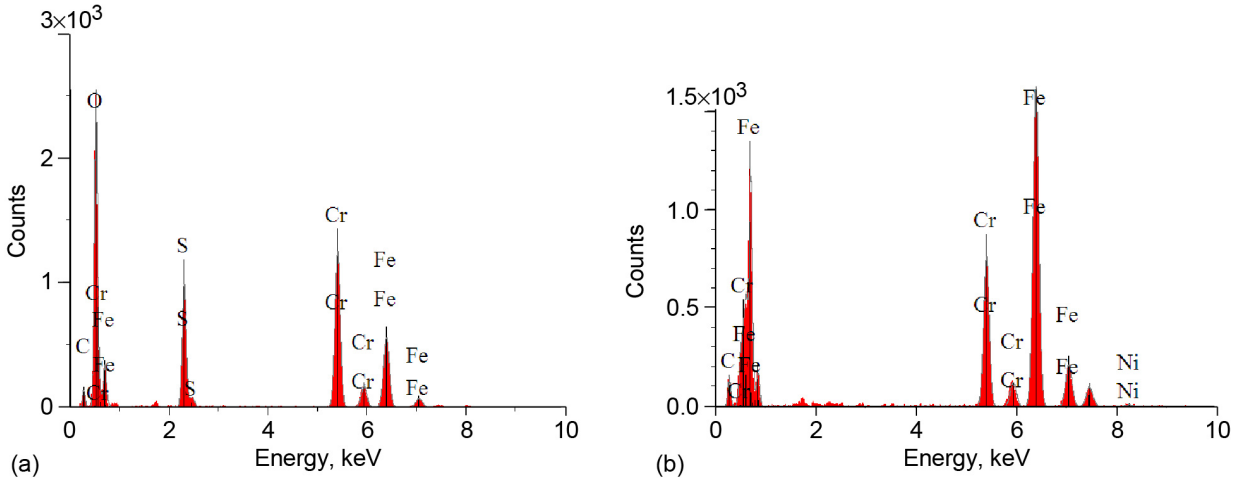


Figure 19.—Energy dispersive X-ray spectroscopy analysis of unpolished side of 304 stainless steel sample exposed to Venusian surface conditions for 42 days (Fig. 17(a)). (a) Scale (location I). (b) Bulk (location II).

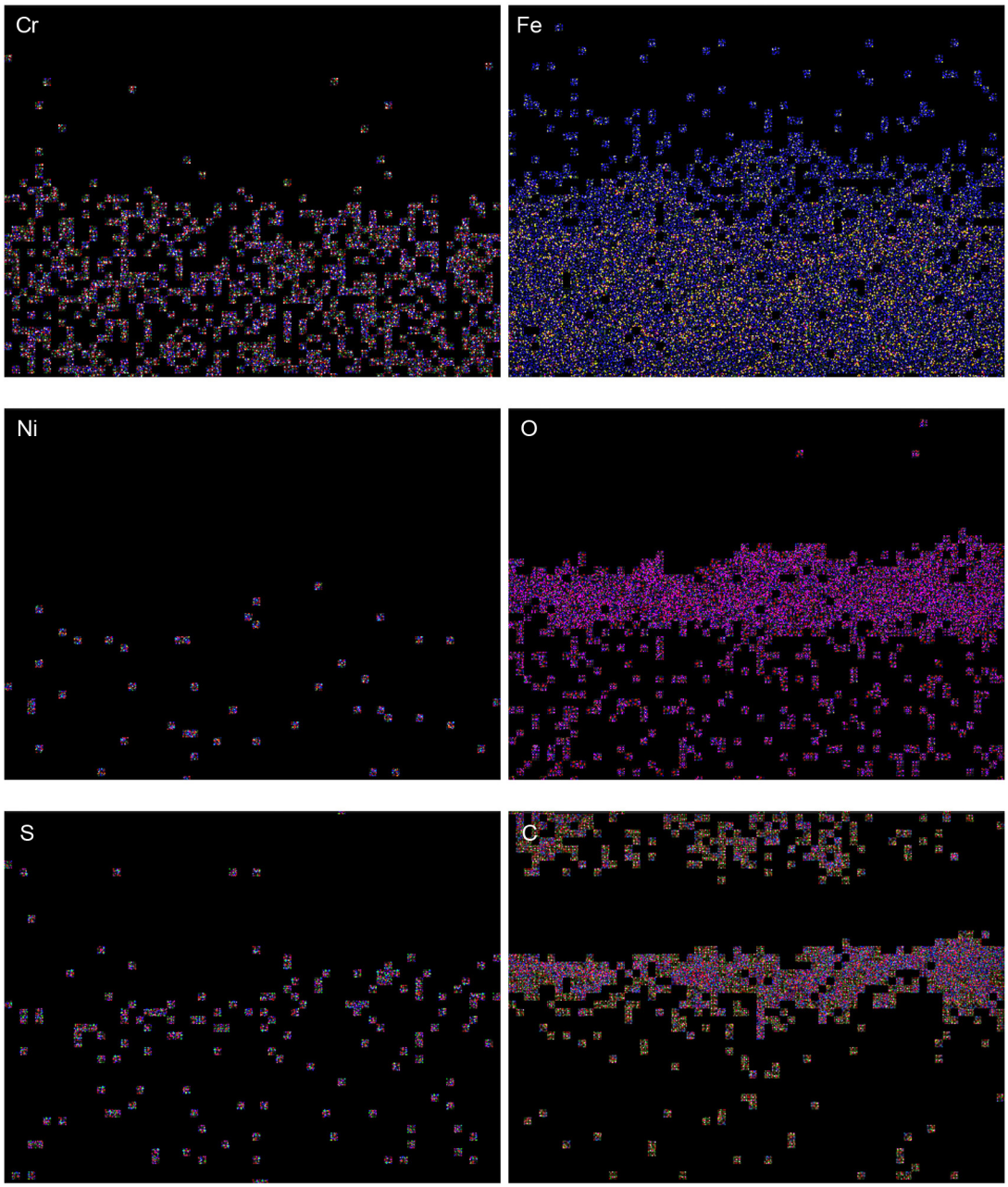


Figure 20.—X-ray elemental images of unpolished side 304 stainless steel sample exposed to Venusian surface conditions for 10 days (area mapped is that of Fig. 15(a)). Each pixel represents information gathered by spectrometer at Cr, Fe, Ni, O, C, and S Kα line.

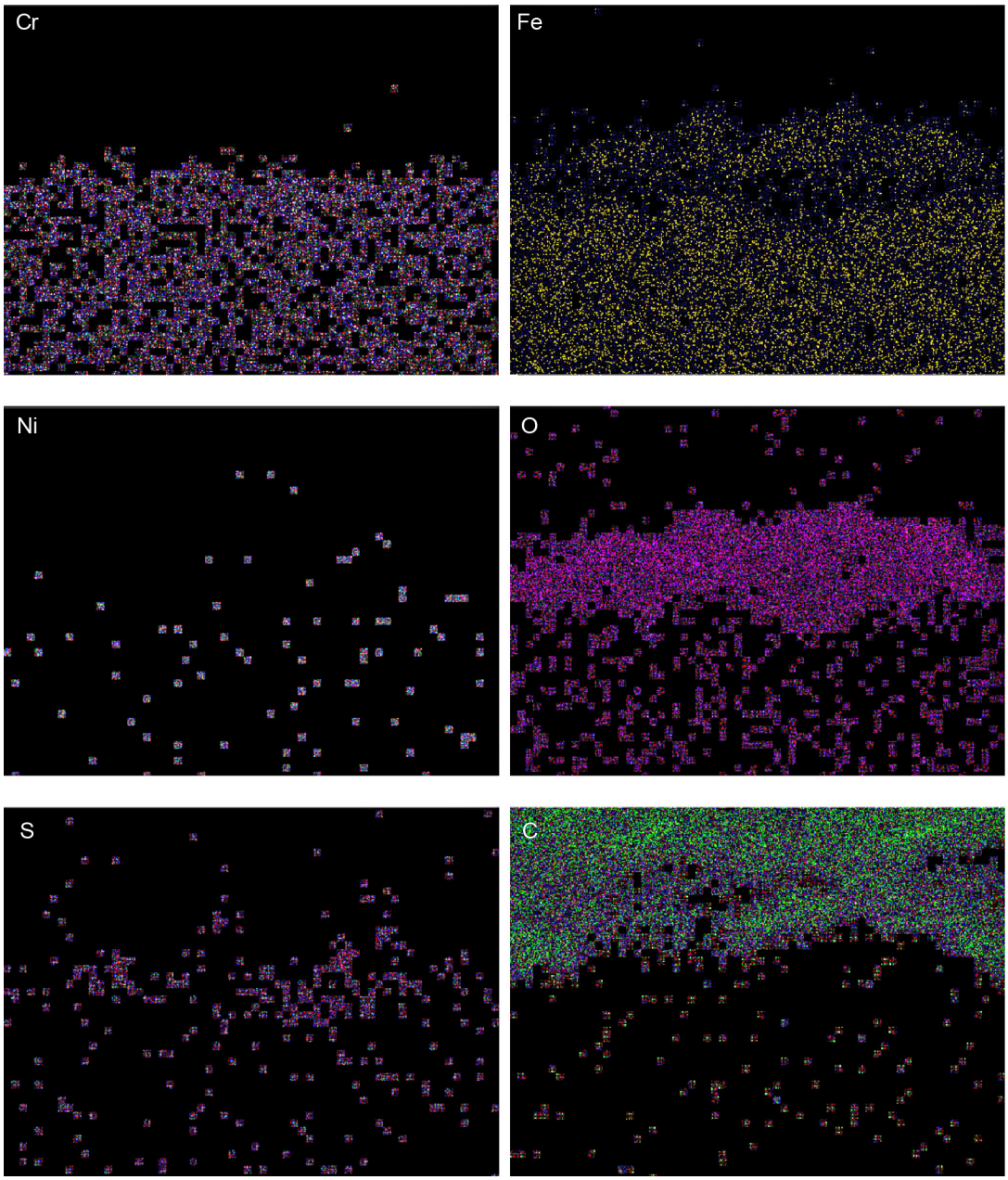


Figure 21.—X-ray elemental images of unpolished side of 304 stainless steel sample exposed to Venusian surface conditions for 42 days (area mapped is that of Fig. 17(a)). Each pixel represents information gathered by spectrometer at Cr, Fe, Ni, O, C, and S Kα line.

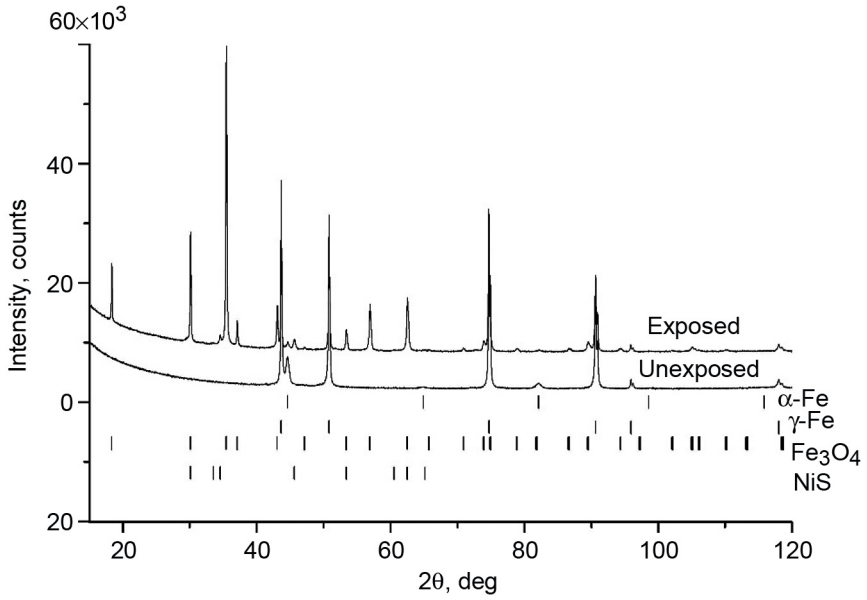


Figure 22.—X-ray diffraction patterns of unpolished side of 304 stainless steel samples, unexposed and exposed to Venusian surface conditions for 42 days.

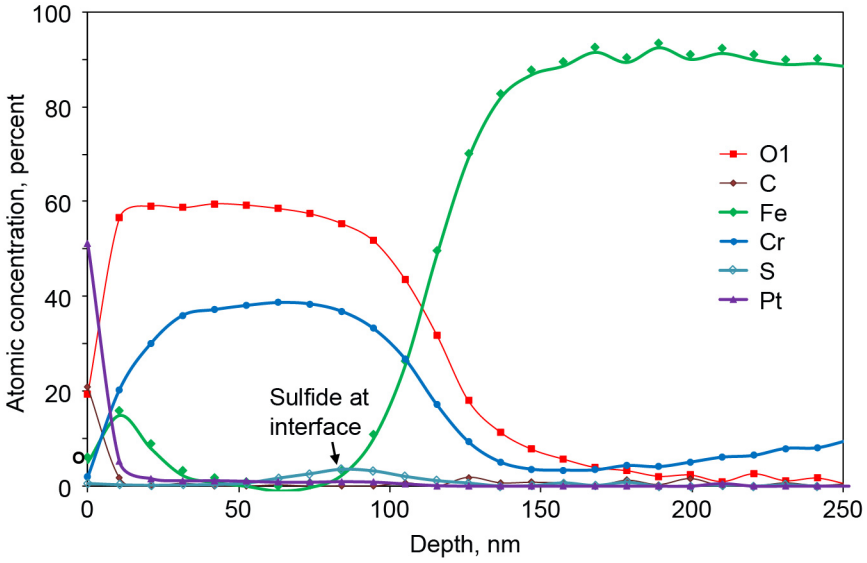


Figure 23.—X-ray photoelectron spectroscopy depth profile using high-resolution regions of polished side of stainless steel 304 sample exposed to Venusian surface conditions for 10 days.

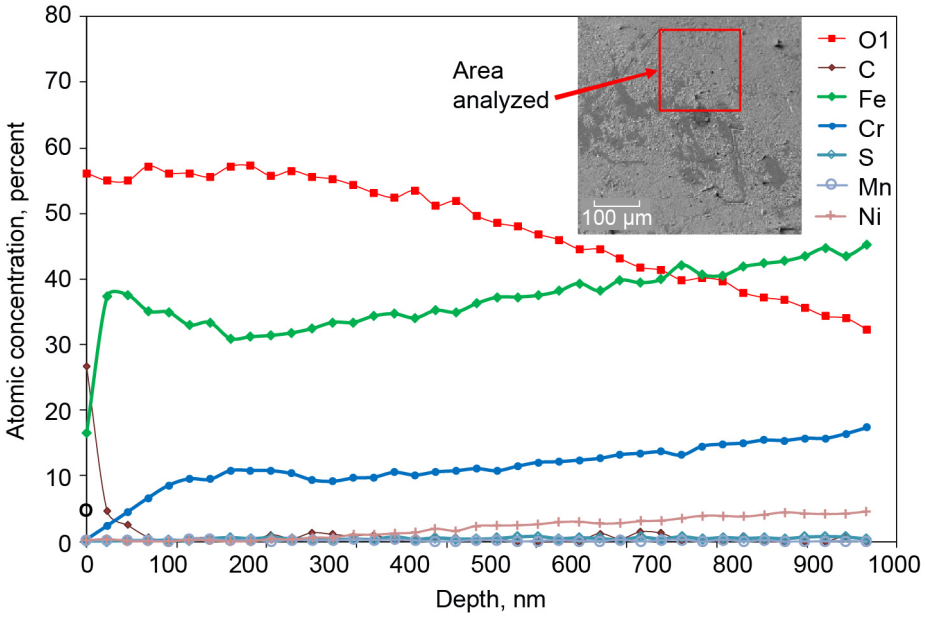


Figure 24.—X-ray photoelectron spectroscopy depth profile using high-resolution regions of polished side of stainless steel 304 sample exposed to Venusian surface conditions for 42 days.

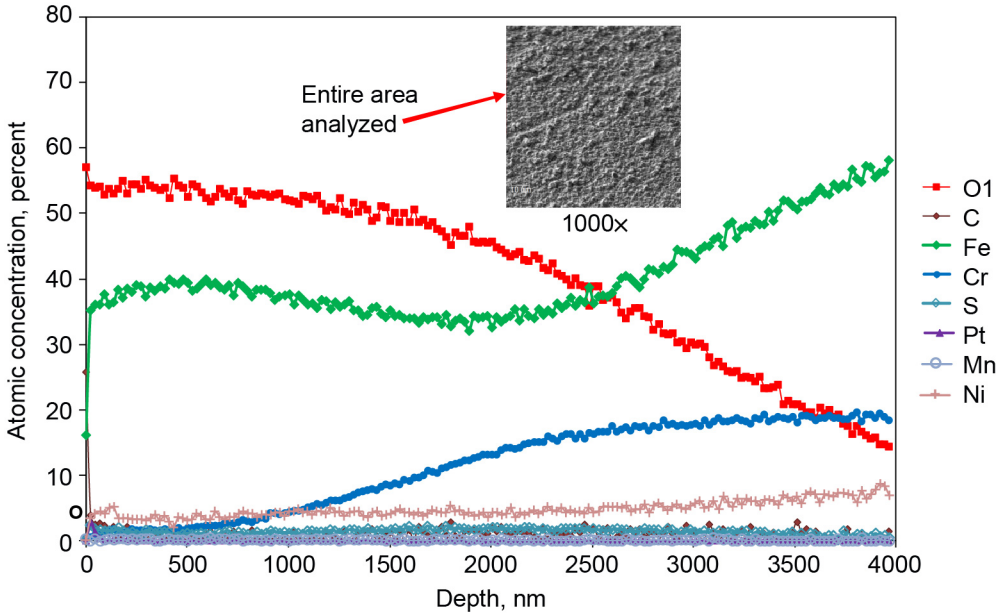


Figure 25.—X-ray photoelectron spectroscopy depth profile using high-resolution regions of unpolished side of stainless steel 304 sample exposed to Venusian surface conditions for 42 days.

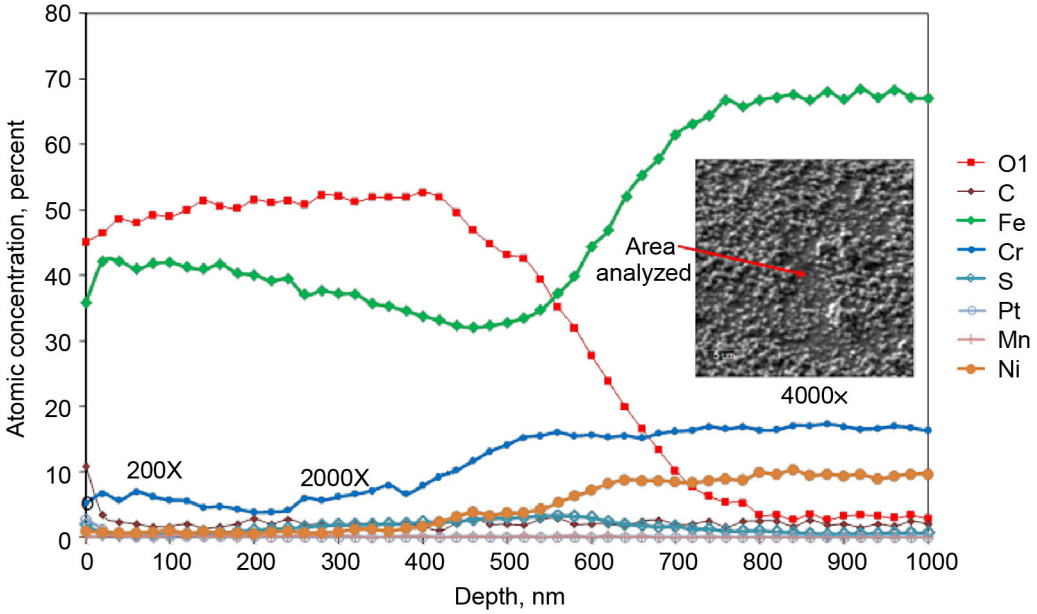


Figure 26.—Auger depth profile of polished side of stainless steel 304 sample exposed to Venusian surface conditions for 42 days. Data were collected in point area as shown in image inset.

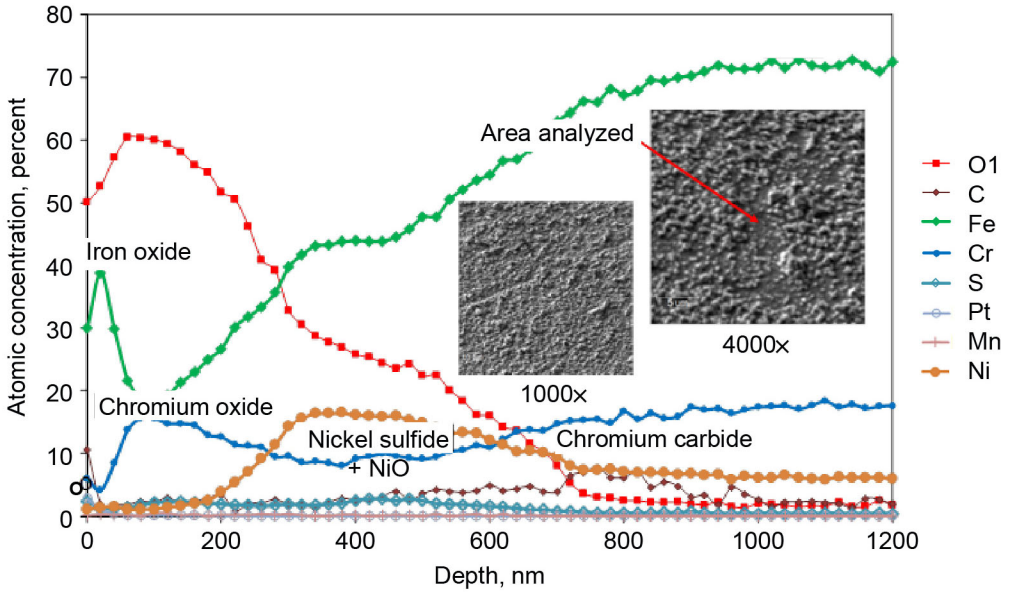


Figure 27.—Auger depth profile of unpolished side of stainless steel 304 sample exposed to Venusian surface conditions for 42 days. Data were collected in point area in which particles were not observed as shown in image inset.

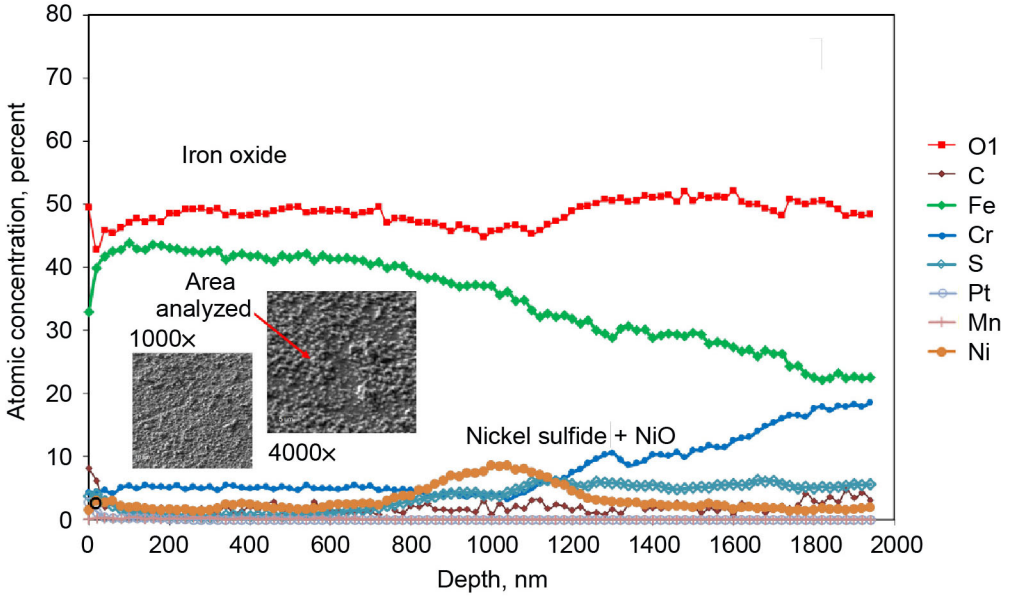


Figure 28.—Auger depth profile of unpolished side of stainless steel 304 sample exposed to Venusian surface conditions for 42 days. Data were collected in point area in which particles were observed as shown in image inset.

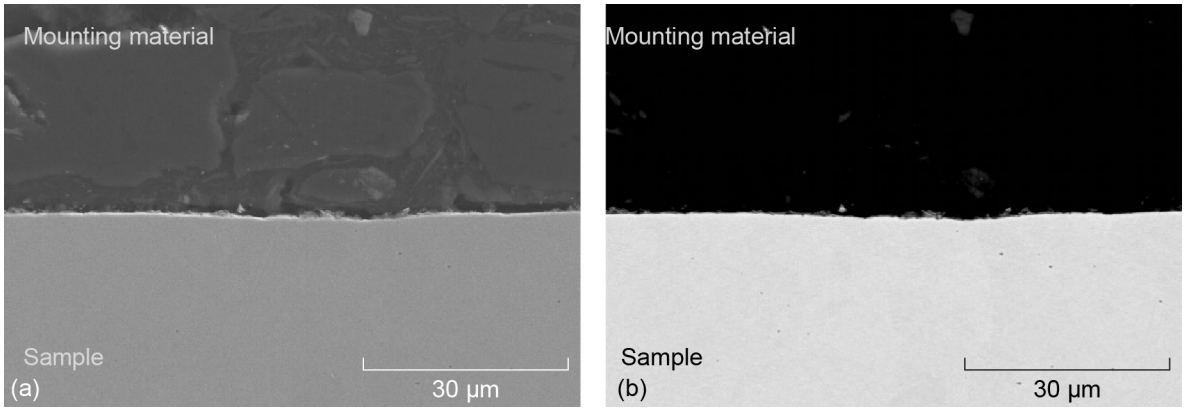


Figure 29.—Cross-sectional images of unexposed 316 stainless steel sample. (a) Scanning electron microscopy image. (b) Backscattered-electron image.

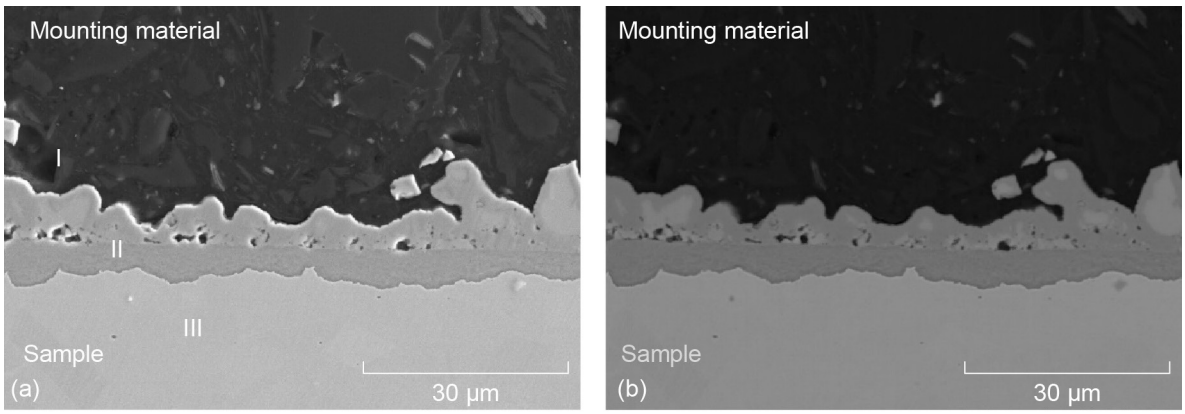


Figure 30.—Cross-sectional images of 316 stainless steel sample exposed to Venusian surface conditions for 10 days. (a) Scanning electron microscopy image. (b) Backscattered-electron image.

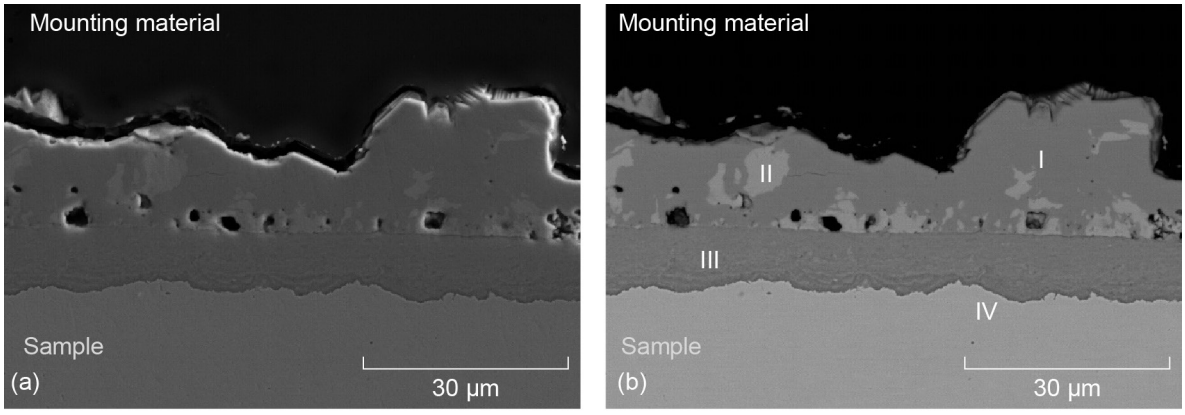


Figure 31.—Cross section images of 316 stainless steel sample exposed to Venusian surface conditions for 42 days. (a) Scanning electron microscopy image. (b) Backscattered-electron image.

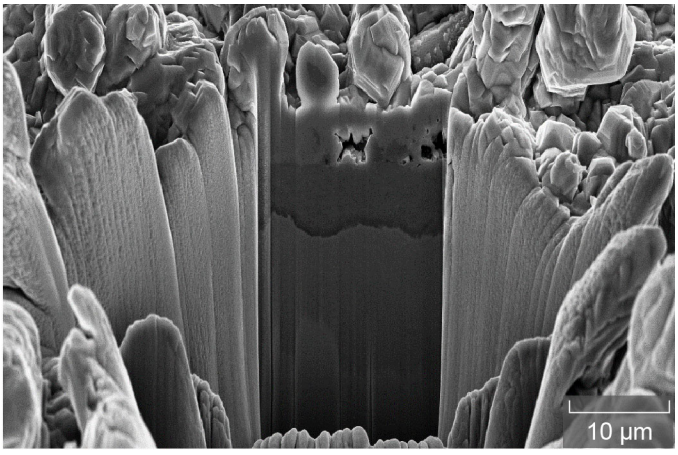


Figure 32.—Cross-sectional focused ion beam image of 316 stainless steel sample exposed to Venusian surface conditions for 10 days.

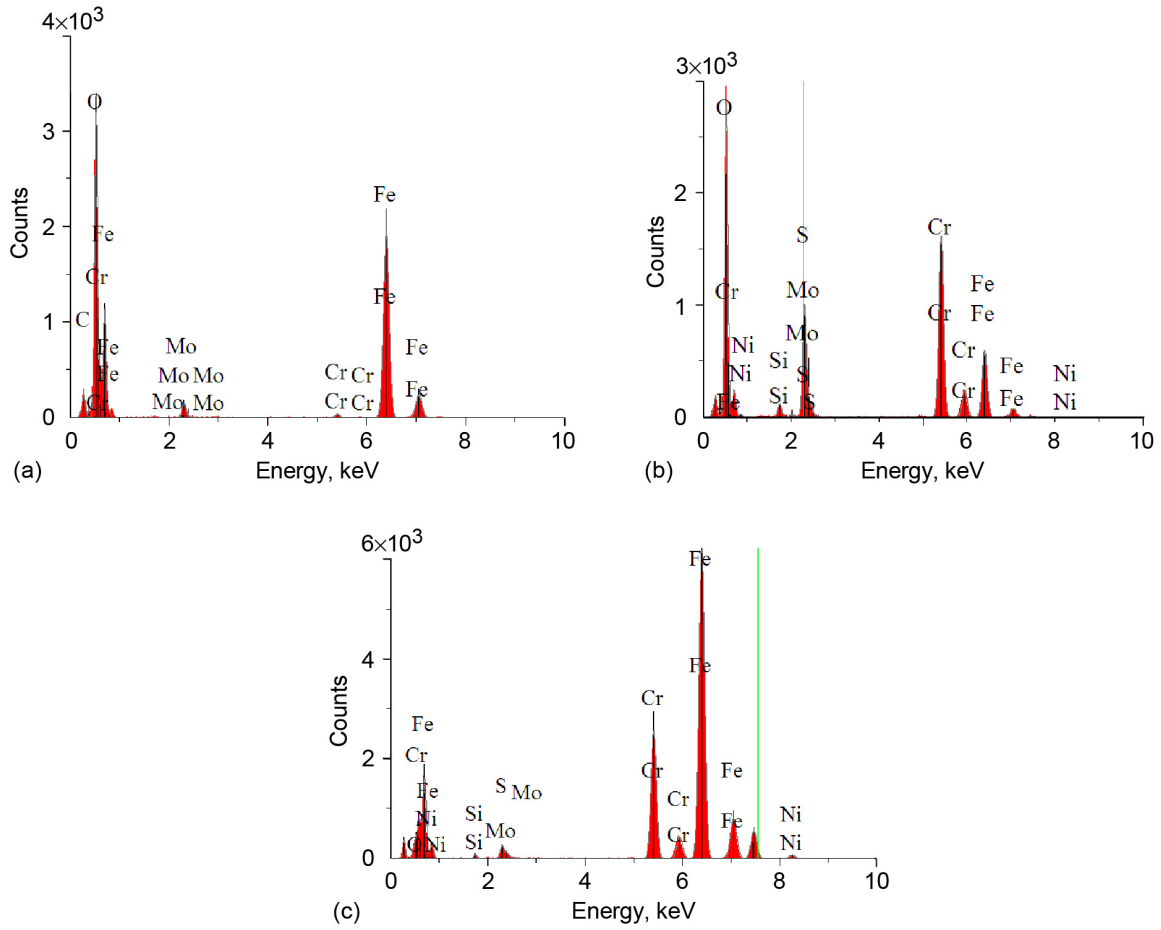


Figure 33.—Energy dispersive X-ray spectroscopy analysis of 316 stainless steel sample exposed to Venusian surface conditions for 10 days (Fig. 30(a)). (a) Outer layer (location I). (b) Inner layer (location II). (c) Bulk (location III).

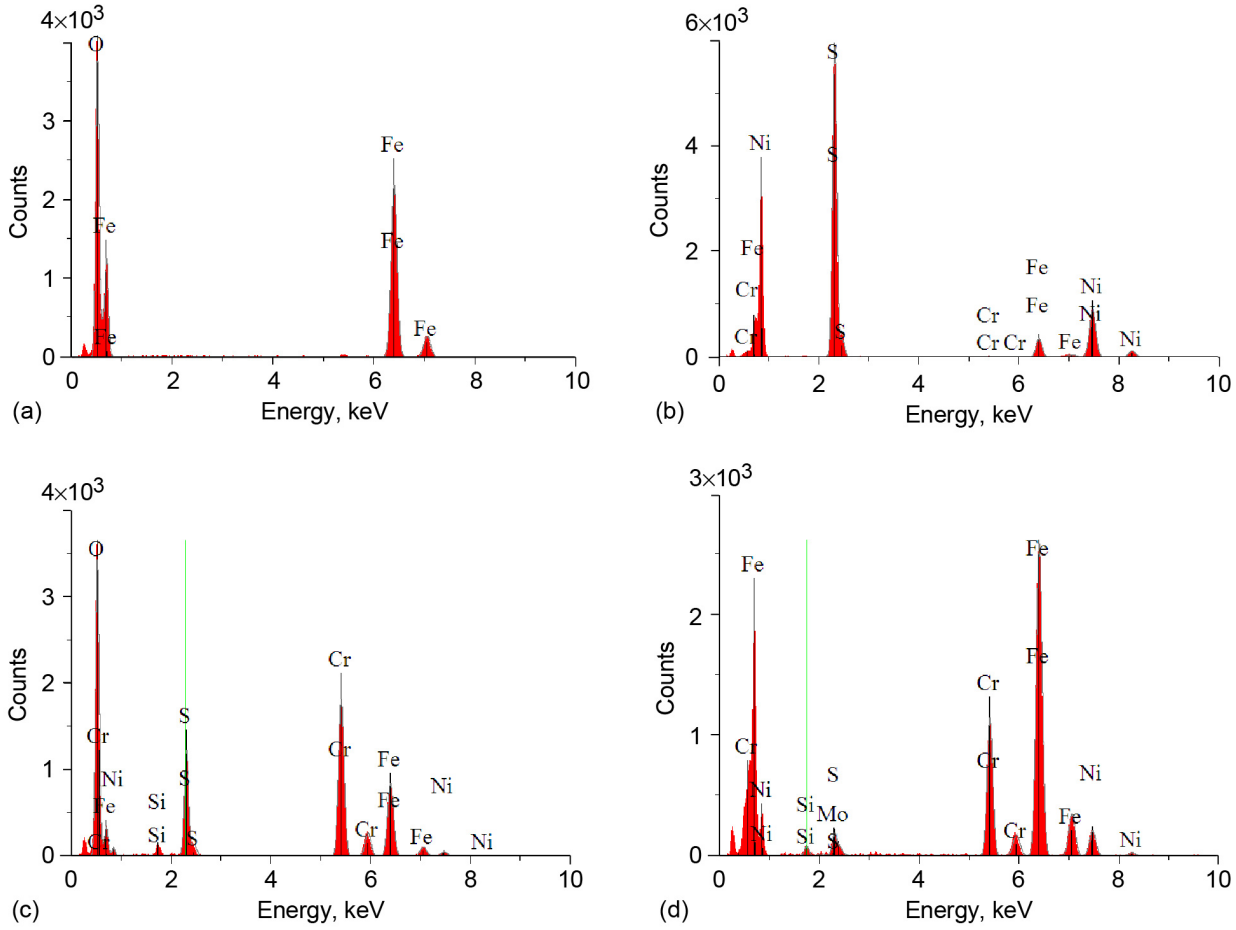


Figure 34.—Energy dispersive X-ray spectroscopy analysis of 316 stainless steel sample exposed to Venusian surface conditions for 42 days (Fig. 31(b)). (a) Main phase in outer layer (location I). (b) Secondary phase in outer layer (location II). (c) Inner layer (location III). (d) Bulk (location IV).

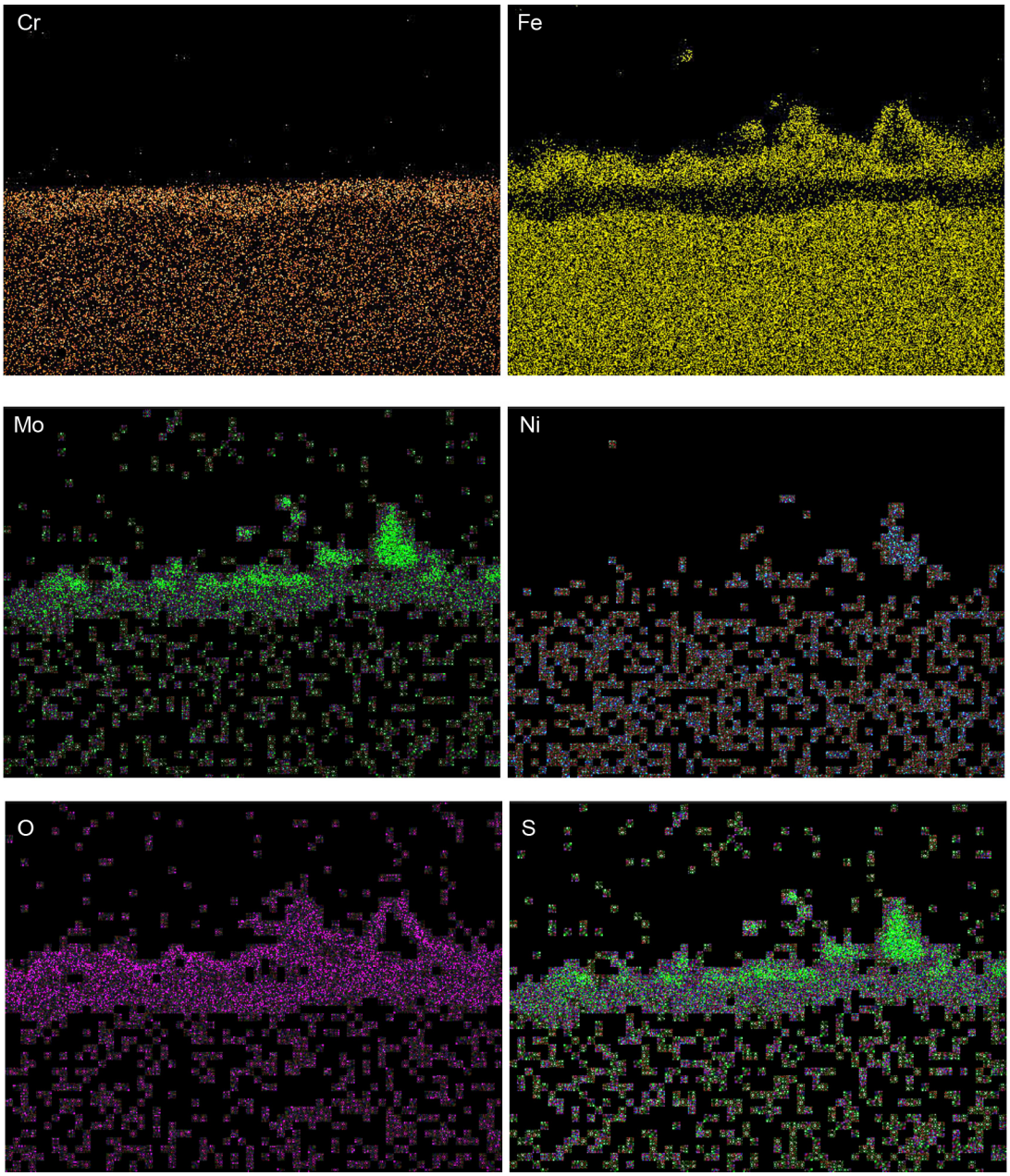


Figure 35.—X-ray elemental images of 316 stainless steel sample exposed to Venusian surface conditions for 10 days (area mapped is that of Fig. 30). Each pixel represents information gathered by spectrometer at Cr, Fe, Ni, O, and S K$\alpha$ line and at Mo L$\alpha$ line.

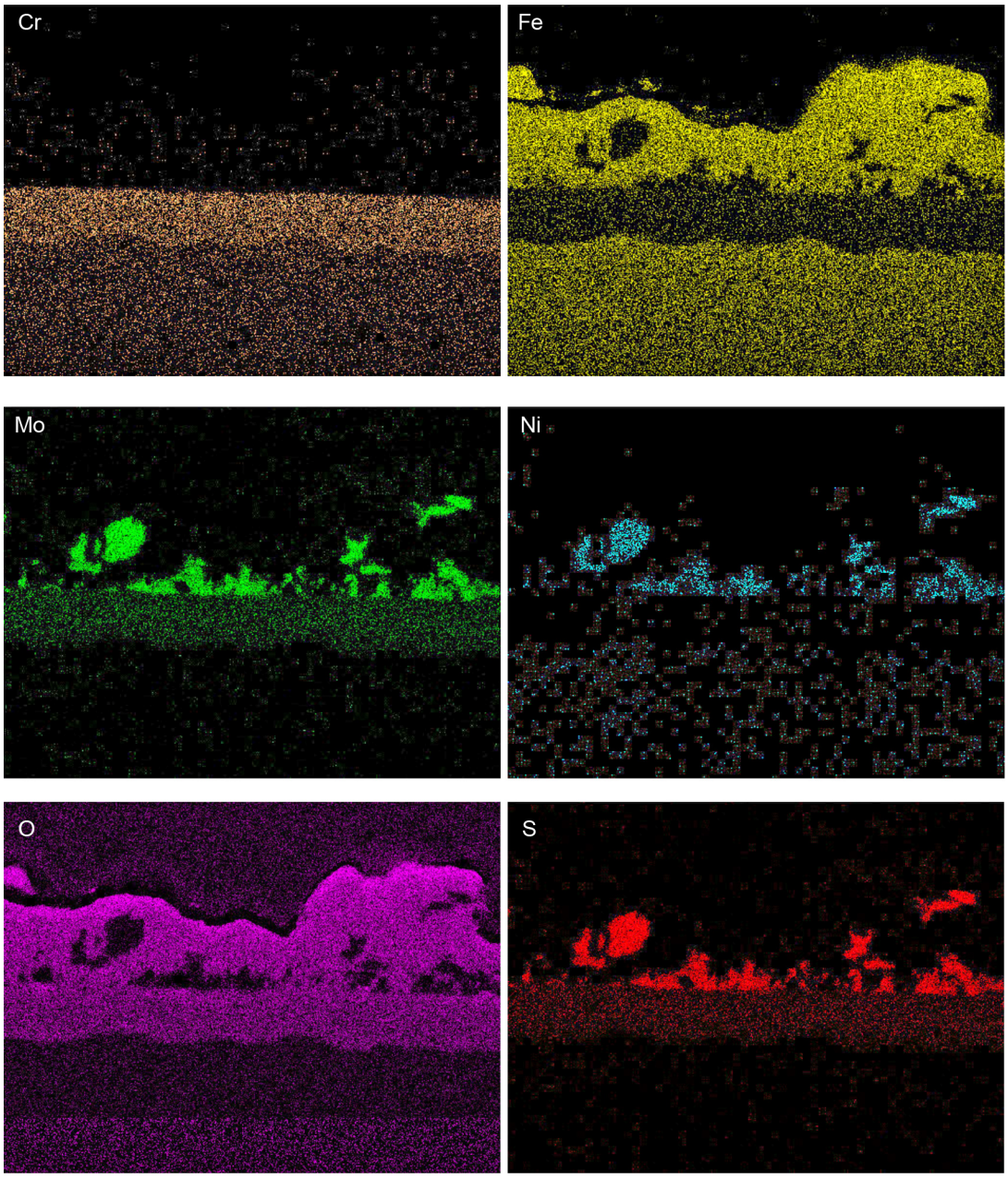


Figure 36.—X-ray elemental images of 316 stainless steel sample exposed to Venusian surface conditions for 42 days (area mapped is that of Fig. 31). Each pixel represents information gathered by spectrometer at Cr, Fe, Ni, O, and S K$\alpha$ line and at Mo L$\alpha$ line.

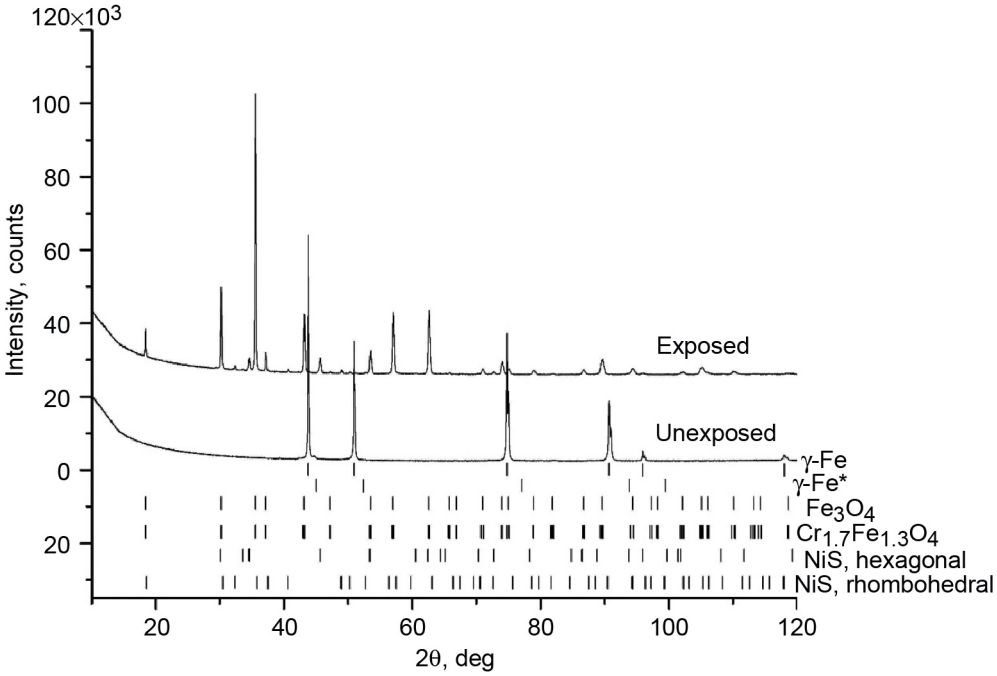


Figure 37.—X-ray diffraction patterns of 316 stainless steel samples, unexposed and exposed to Venusian surface conditions for 42 days.

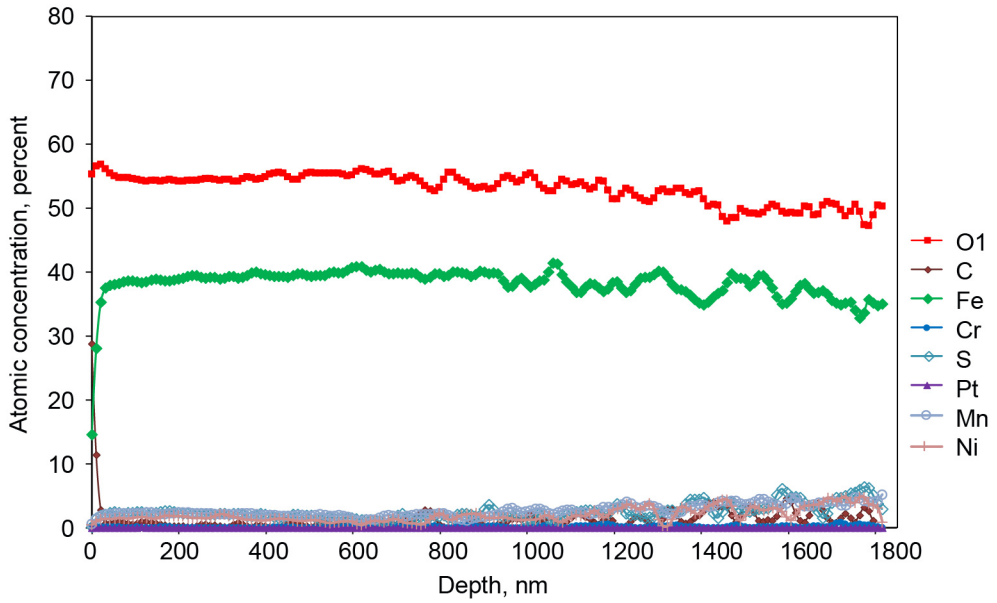


Figure 38.—X-ray photoelectron spectroscopy depth profile using high-resolution regions of unpolished stainless steel 316 sample exposed to Venusian surface conditions for 10 days.

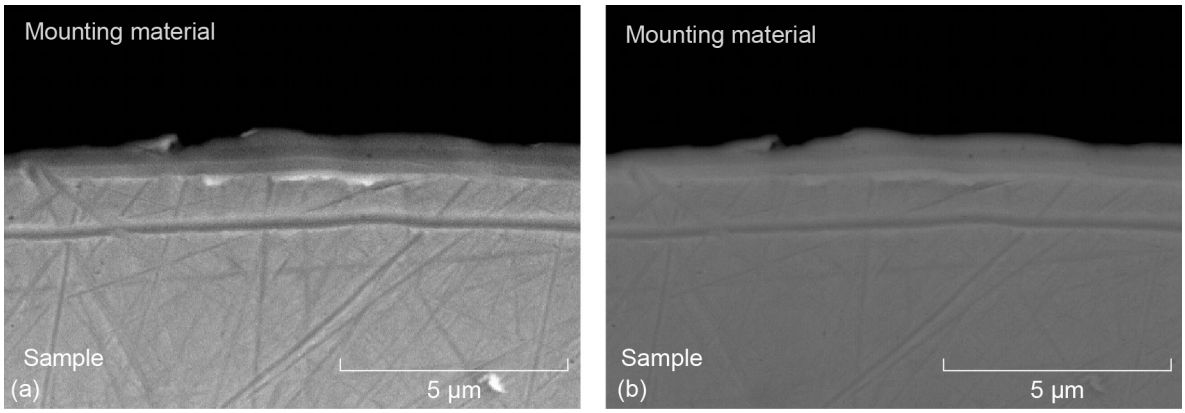


Figure 39.—Cross-sectional images of unexposed 310 stainless steel sample. (a) Scanning electron microscopy image. (b) Backscattered-electron image.

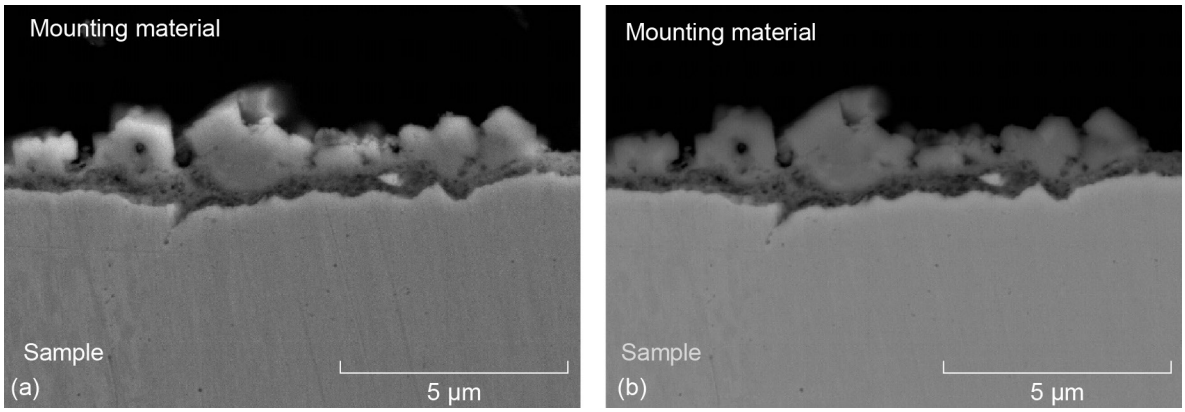


Figure 40.—Cross-sectional images of 310 stainless steel sample exposed to Venusian surface conditions for 10 days. (a) Scanning electron microscopy image. (b) Backscattered-electron image.

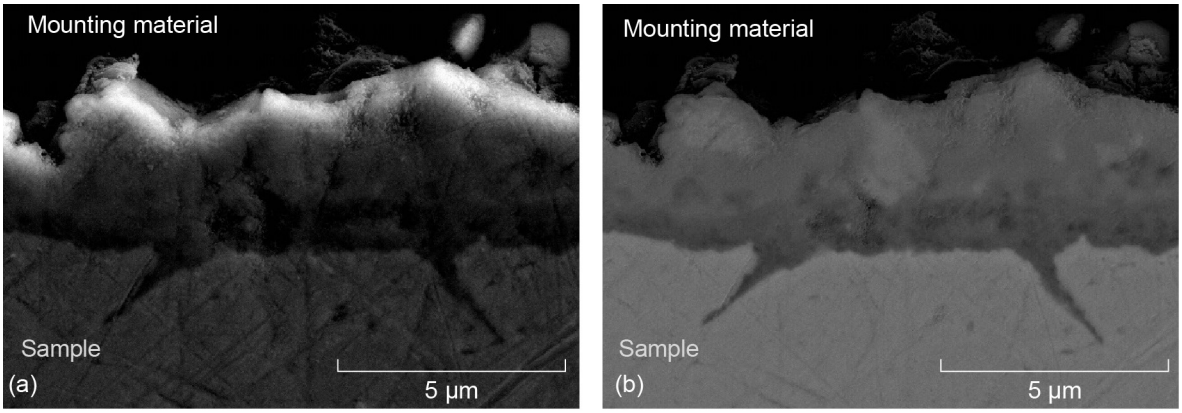


Figure 41.—Cross-sectional images of 310 stainless steel sample exposed to Venusian surface conditions for 42 days. (a) Scanning electron microscopy image. (b) Backscattered-electron image.

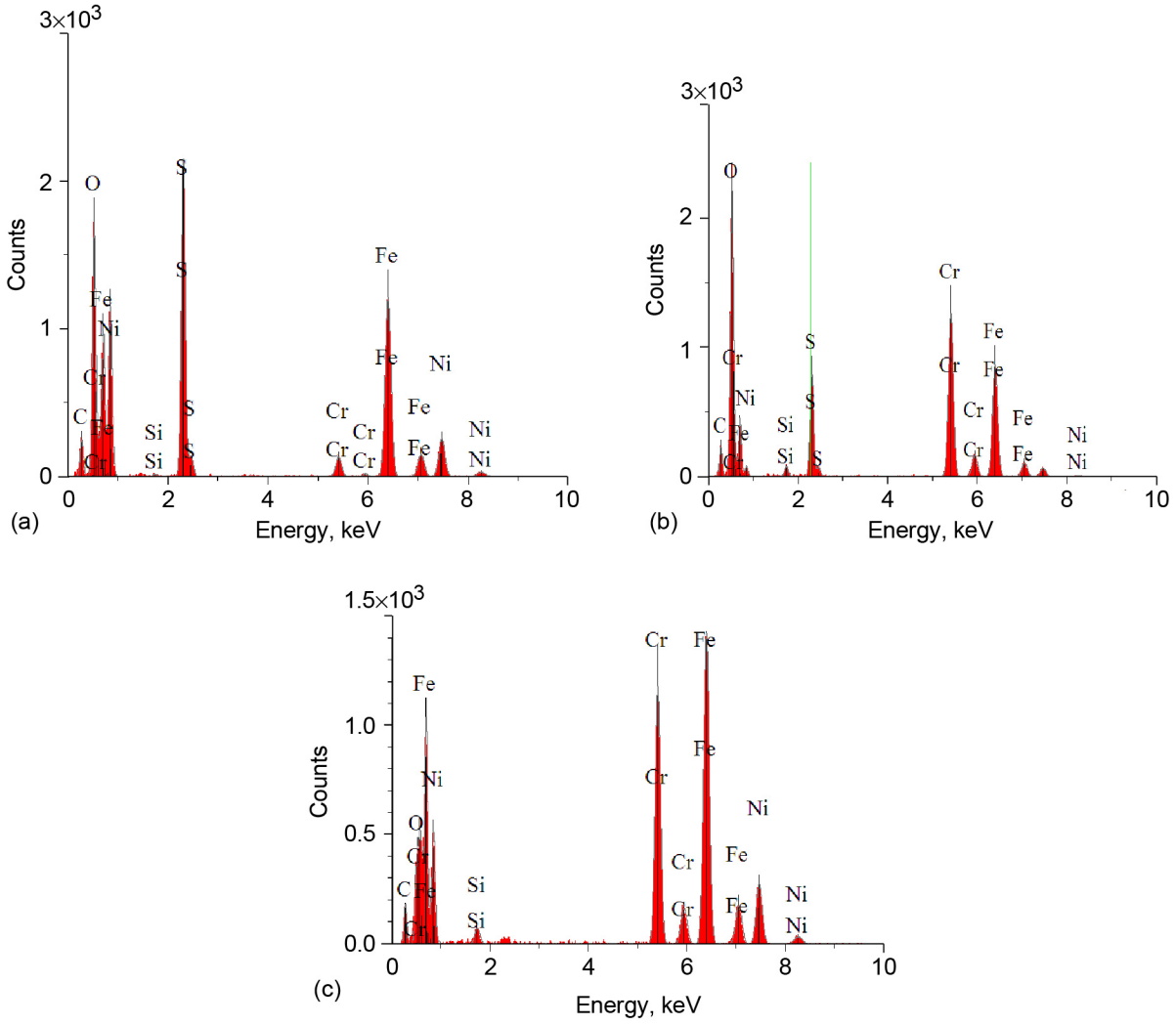


Figure 42.—Energy dispersive spectroscopy analysis of 310 stainless steel sample exposed to Venusian surface conditions for 10 days (Fig. 40). (a) Outer layer. (b) Inner layer. (c) Bulk.

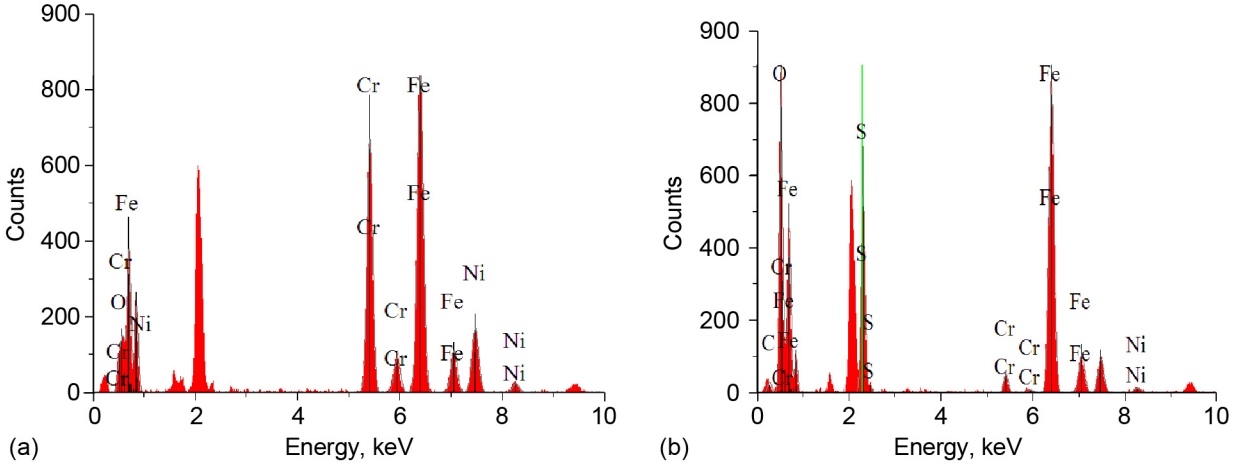


Figure 43.—Energy dispersive spectroscopy analysis of 310 stainless steel sample exposed to Venusian surface conditions for 42 days (Fig. 41). Unlabeled peak corresponds to Pt coating. (a) Bulk. (b) Scale.

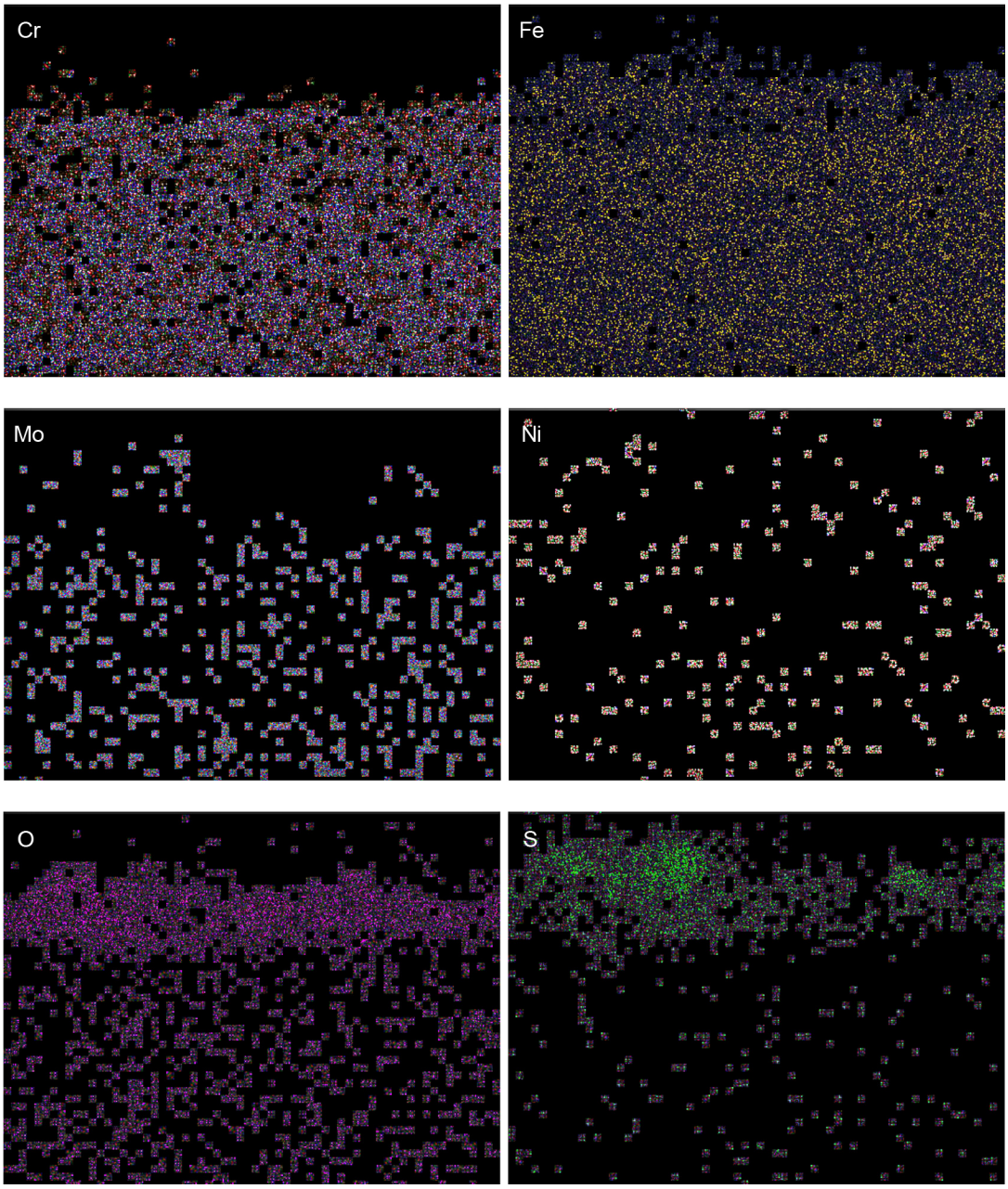


Figure 44.—X-ray elemental images of 310 stainless steel sample exposed to Venusian surface conditions for 10 days (area mapped is that of Fig. 40). Each pixel represents information gathered by spectrometer at Cr, Fe, Ni, O, and S Kα line.

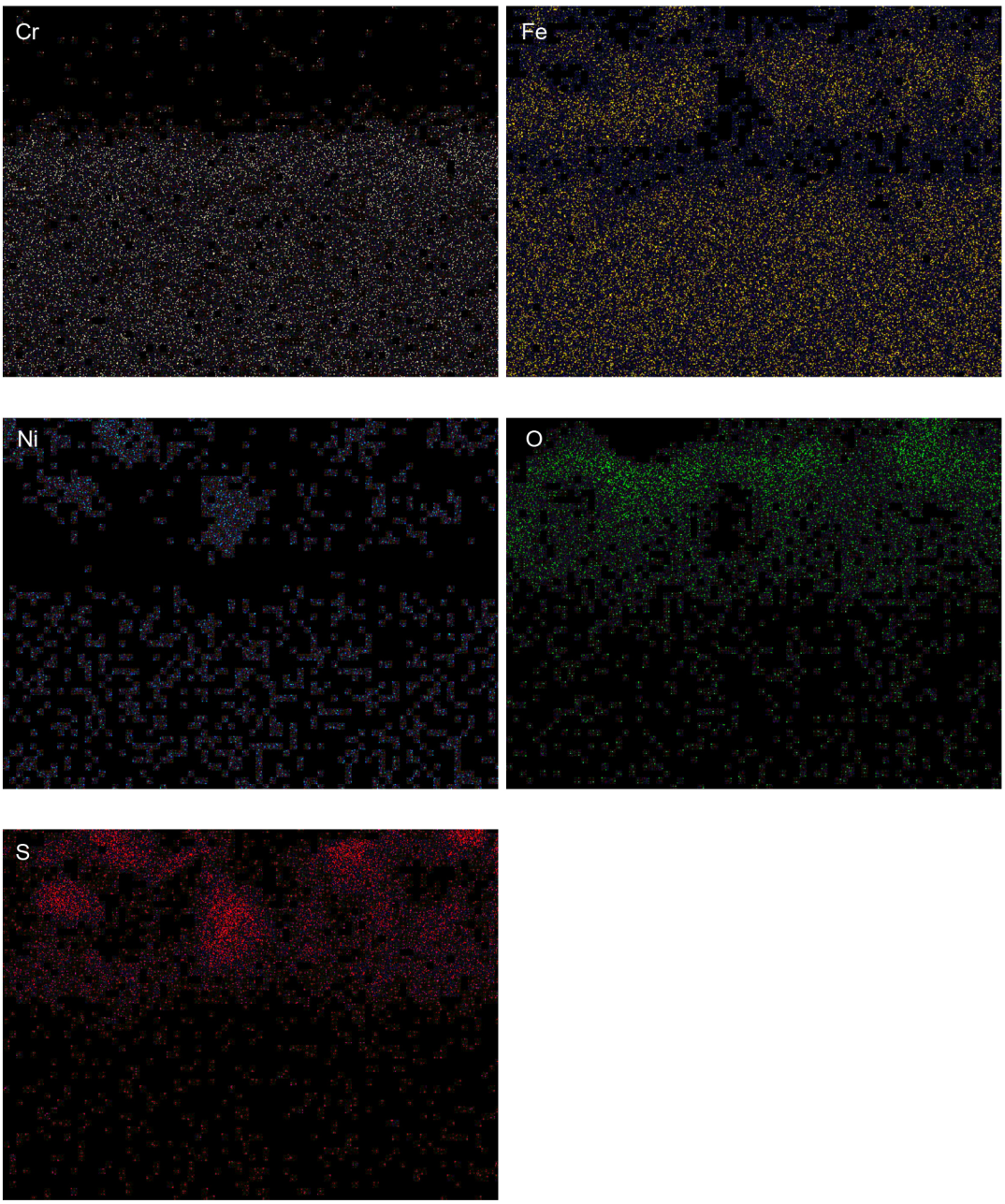


Figure 45.—X-ray elemental images of 310 stainless steel sample exposed to Venusian surface conditions for 42 days (area mapped is that of Fig. 41(a)). Each pixel represents information gathered by spectrometer at Cr, Fe, Ni, O, and S Kα line.

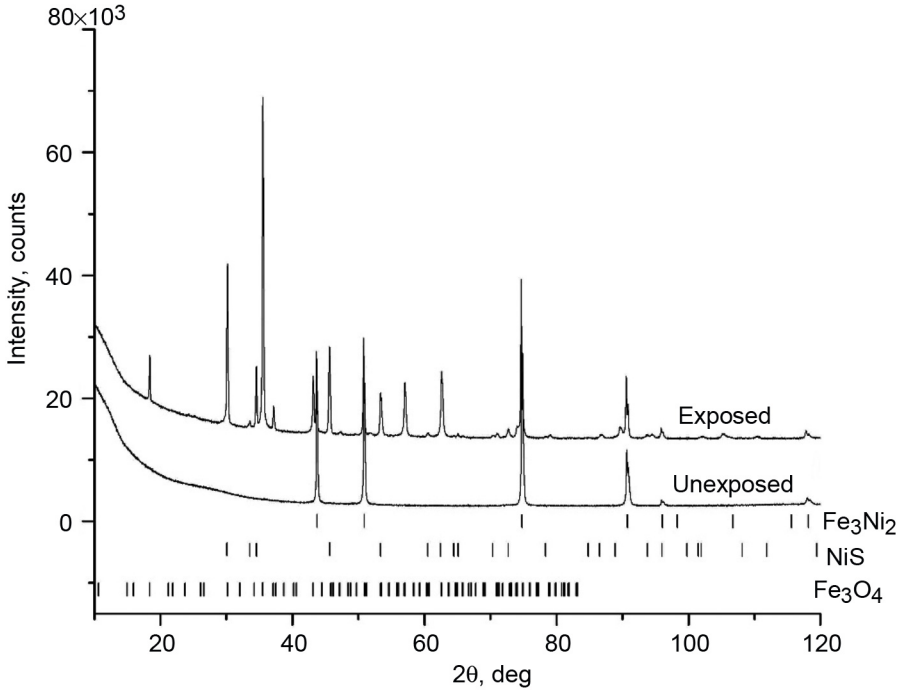


Figure 46.—X-ray diffraction patterns of 310 stainless steel samples, unexposed and exposed to Venusian surface conditions for 42 days.

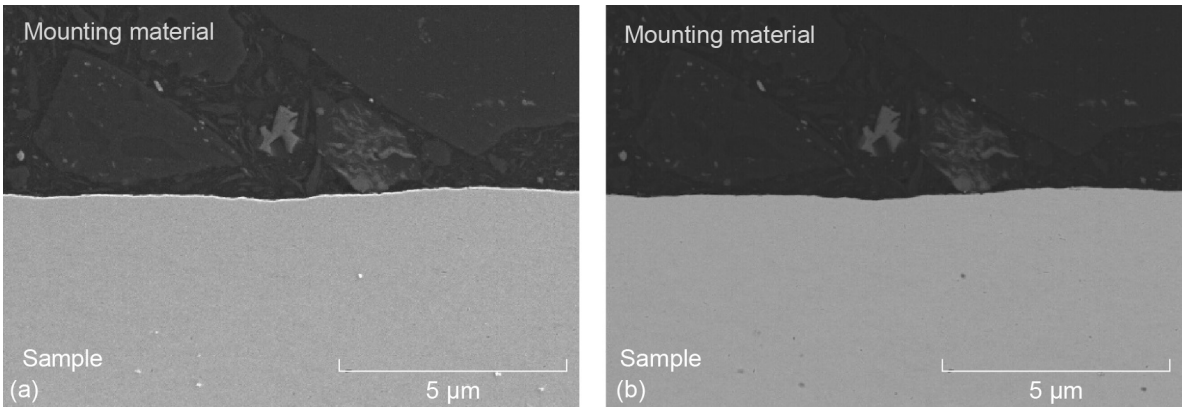


Figure 47.—Cross-sectional images of unexposed 1018 steel sample. (a) Scanning electron microscopy image. (b) Backscattered-electron image.

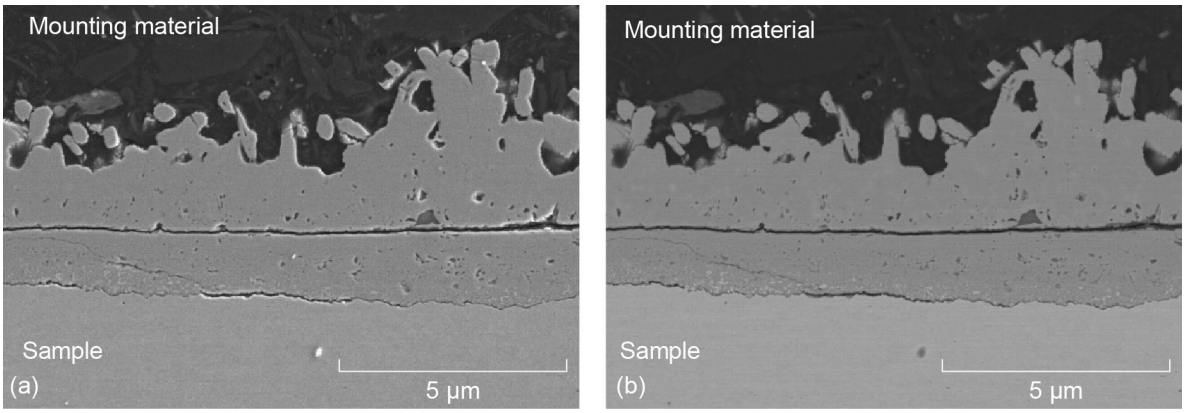


Figure 48.—Cross-sectional images of 1018 steel sample exposed to Venusian surface conditions for 10 days. (a) Scanning electron microscopy image. (b) Backscattered-electron image.

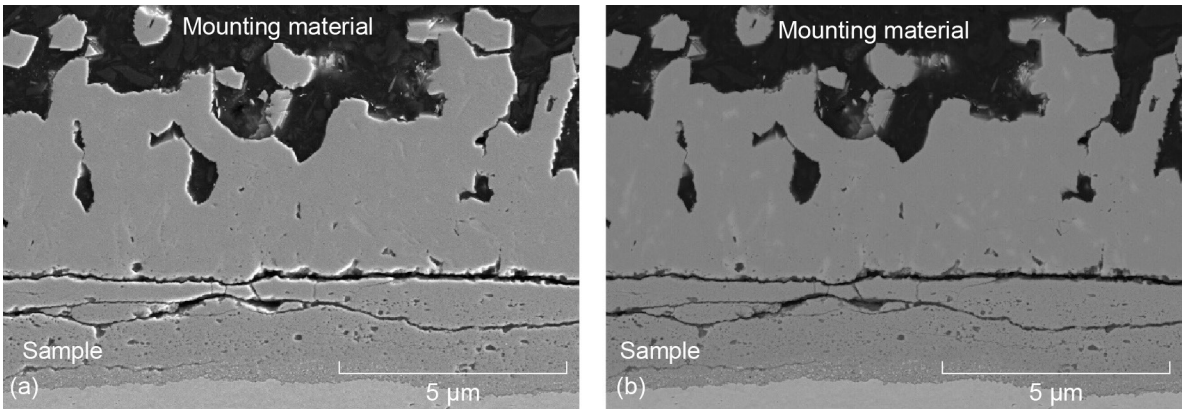


Figure 49.—Cross-sectional images of 1018 steel sample exposed to Venusian surface conditions for 42 days. (a) Scanning electron microscopy image. (b) Backscattered-electron image.

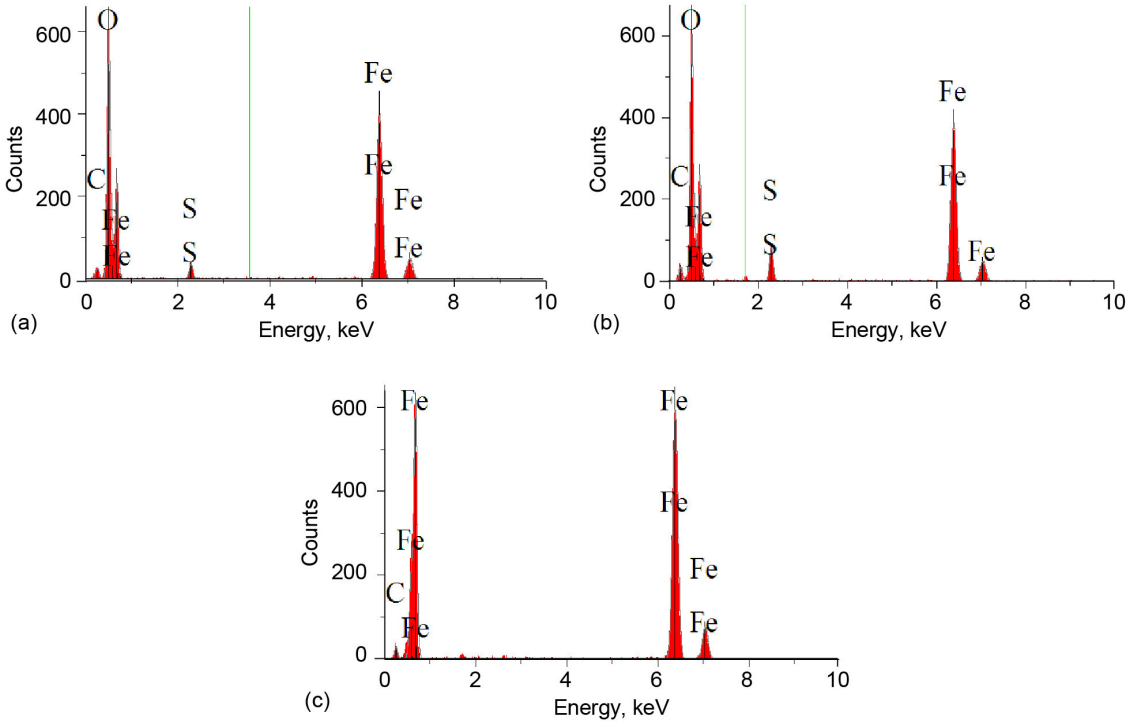


Figure 50.—Energy dispersive spectroscopy analysis of 1018 steel sample exposed to Venusian surface conditions for 10 days (Fig. 48). (a) Outer layer. (b) Inner layer. (c) Bulk.

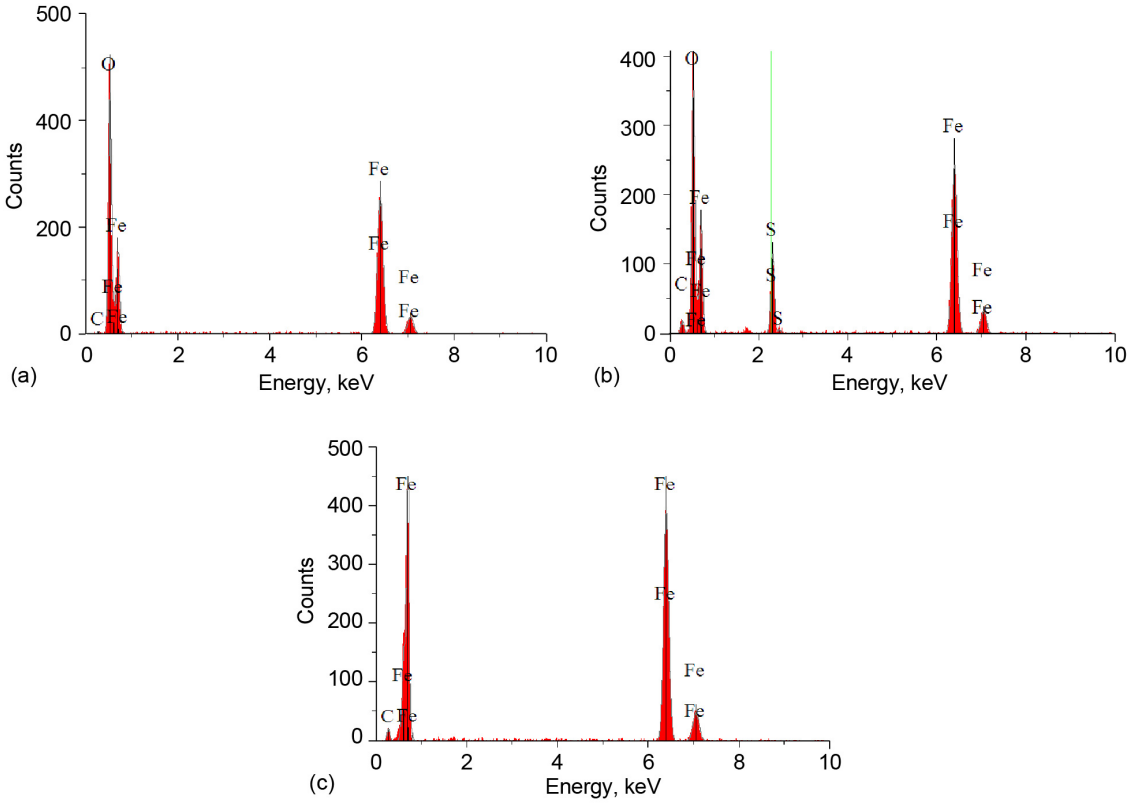


Figure 51.—Energy dispersive spectroscopy analysis of 1018 steel sample exposed to Venusian surface conditions for 42 days (Fig. 49). (a) Outer layer. (b) Inner layer. (c) Bulk.

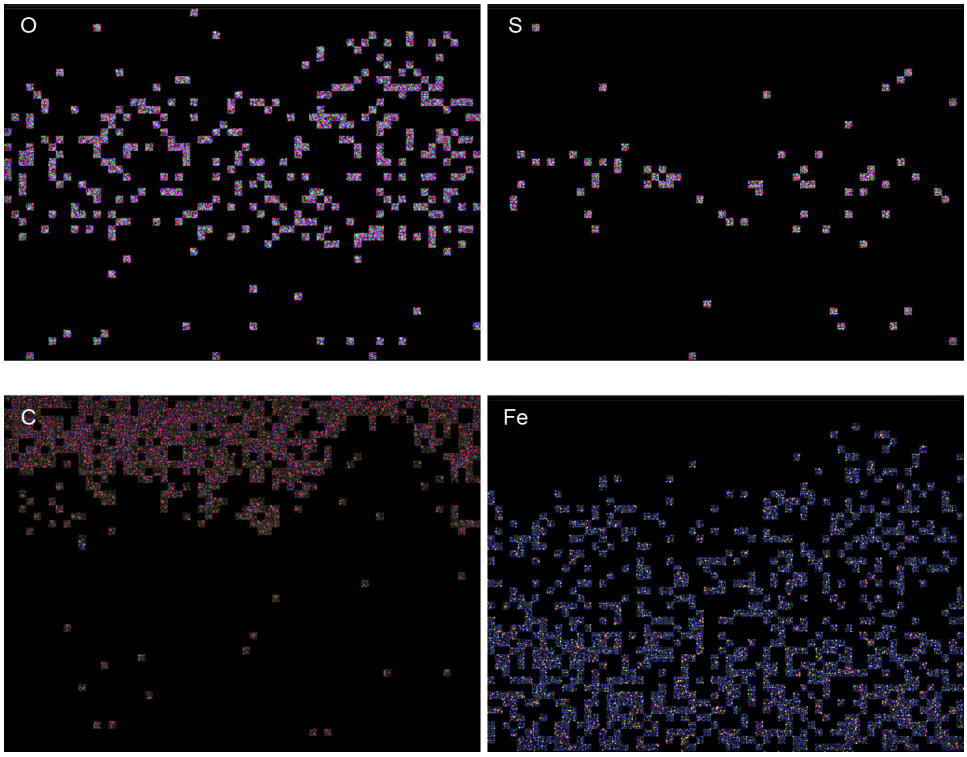


Figure 52.—X-ray elemental images of 1018 steel sample exposed to Venusian surface conditions for 10 days (area mapped is that of Fig. 48). Each pixel represents information gathered by spectrometer at C, Fe, O, and S Kα line.

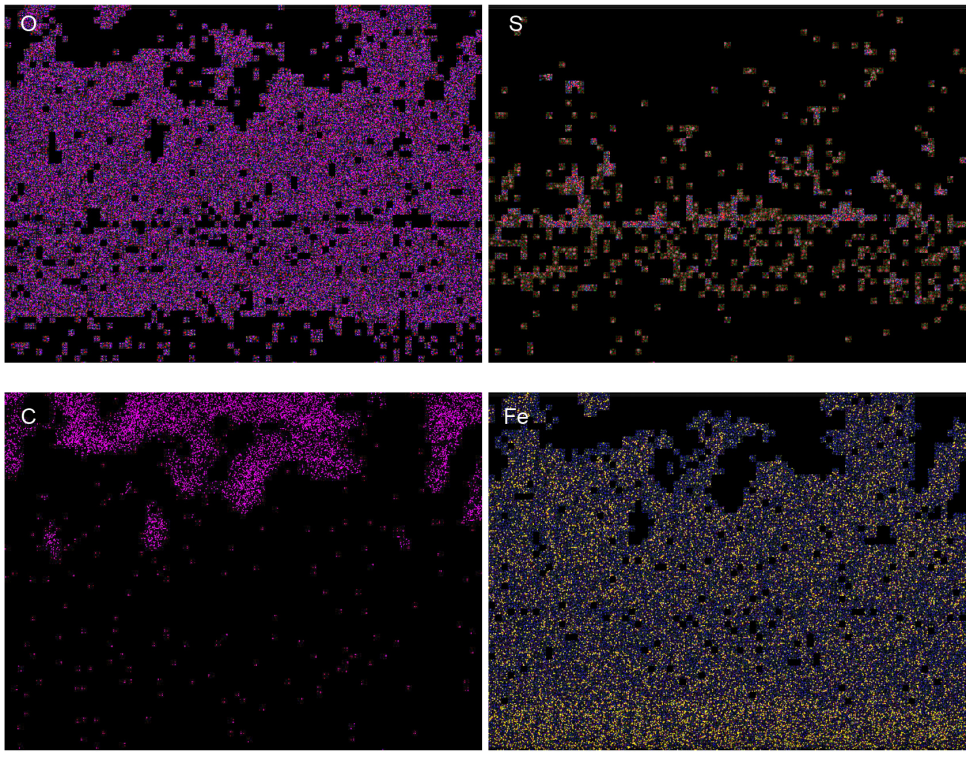


Figure 53.—X-ray elemental images of 1018 steel sample exposed to Venusian surface conditions for 42 days (area mapped is that of Fig. 49). Each pixel represents information gathered by spectrometer at C, Fe, O, and S Kα line.

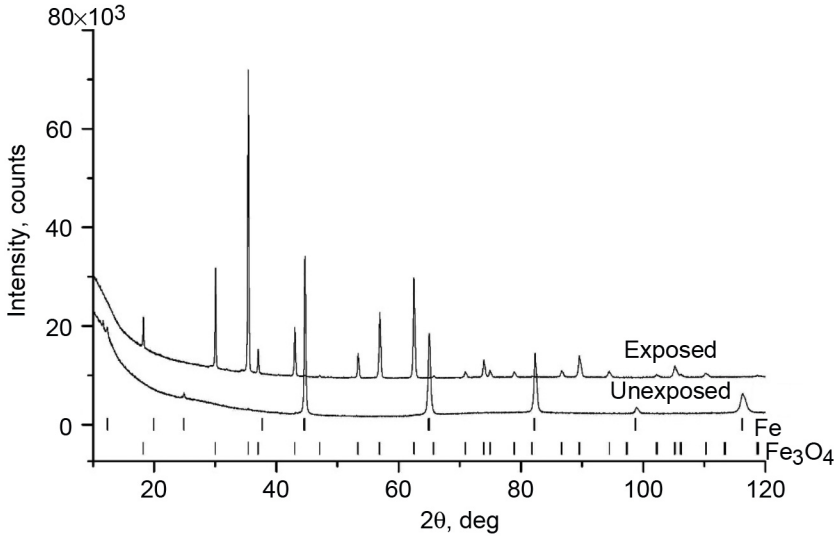


Figure 54.—X-ray diffraction patterns of 1018 steel samples, unexposed and exposed to Venusian surface conditions for 42 days.

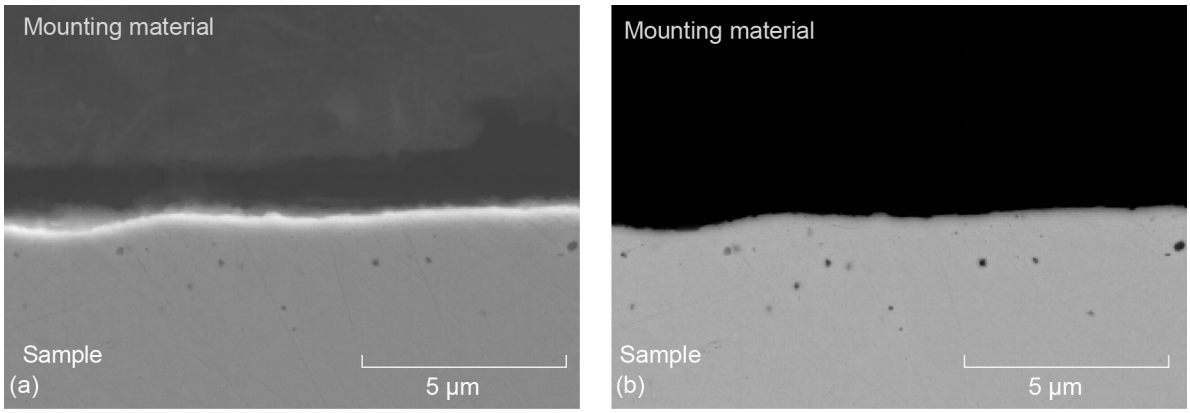


Figure 55.—Cross-sectional images of unexposed G30 alloy sample. (a) Scanning electron microscopy image. (b) Backscattered-electron image.

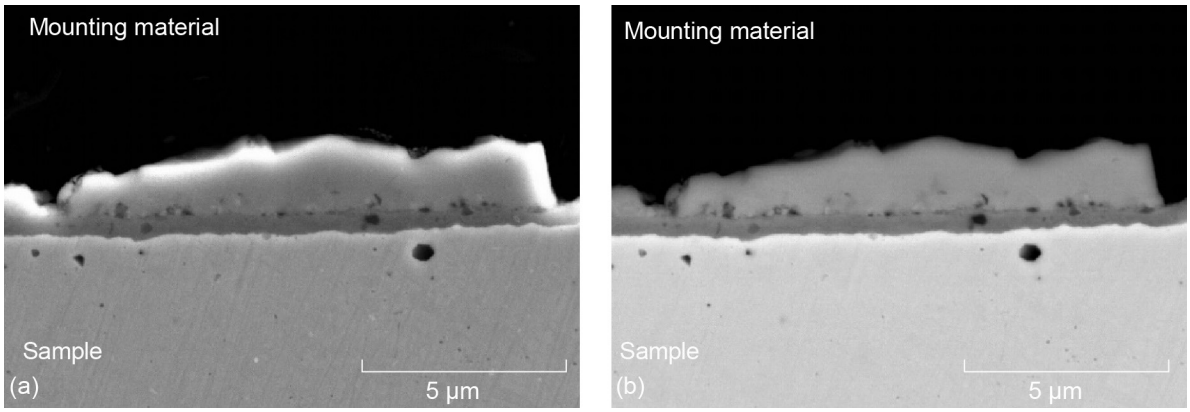


Figure 56.—Cross-sectional images of G30 alloy sample exposed to Venusian surface conditions for 10 days. (a) Scanning electron microscopy image. (b) Backscattered-electron image.

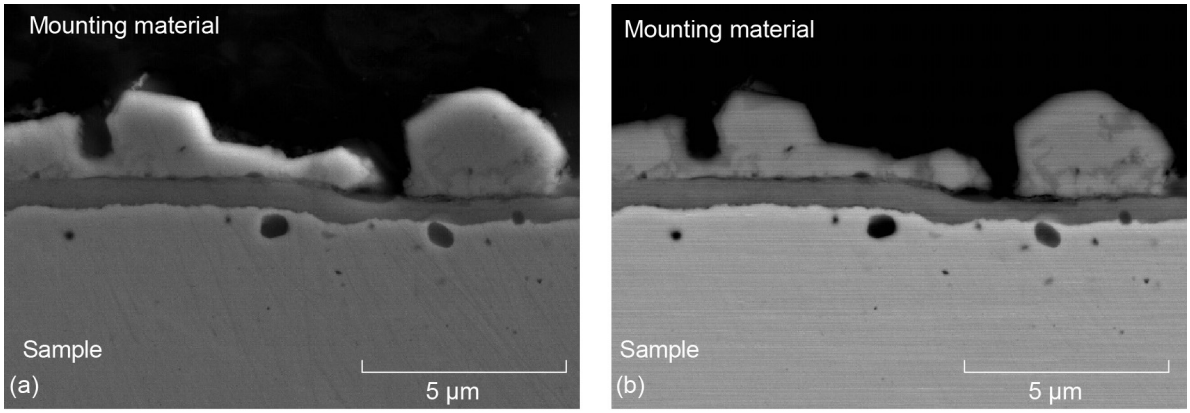


Figure 57.—Cross-sectional images of G30 alloy sample exposed to Venusian surface conditions for 42 days. (a) Scanning electron microscopy image. (b) Backscattered-electron image.

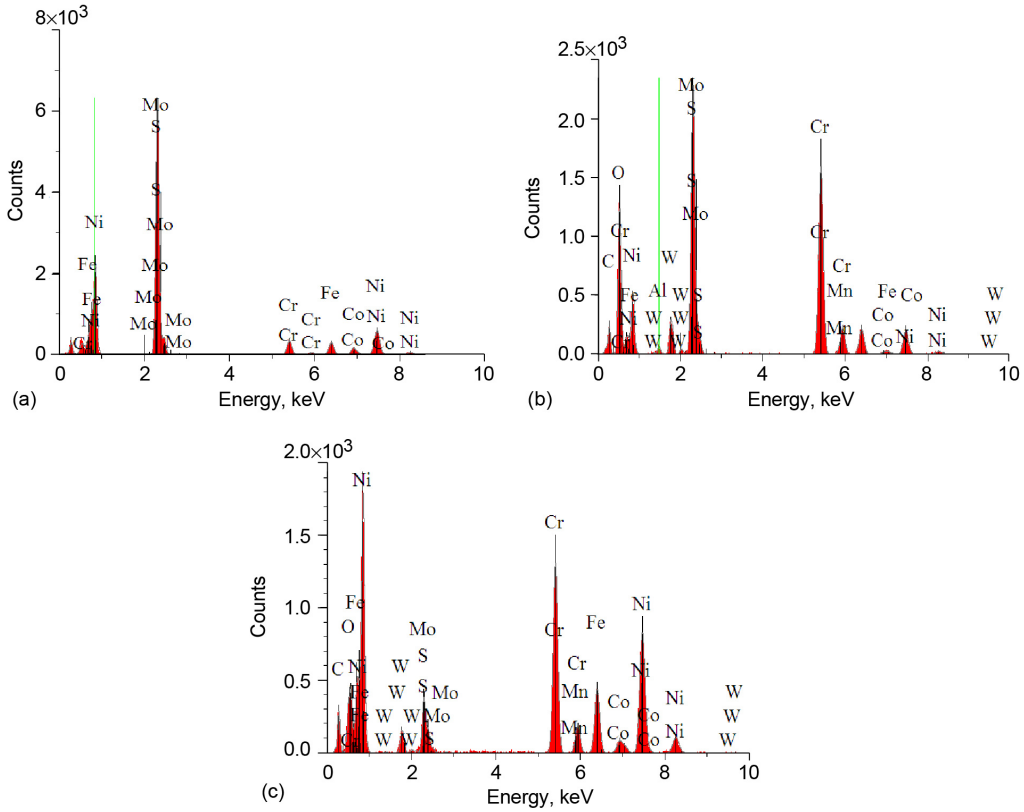


Figure 58.—Energy dispersive spectroscopy analysis of G30 alloy sample exposed to Venusian surface conditions for 10 days (Fig. 56). (a) Outer layer. (b) Inner layer. (c) Bulk.

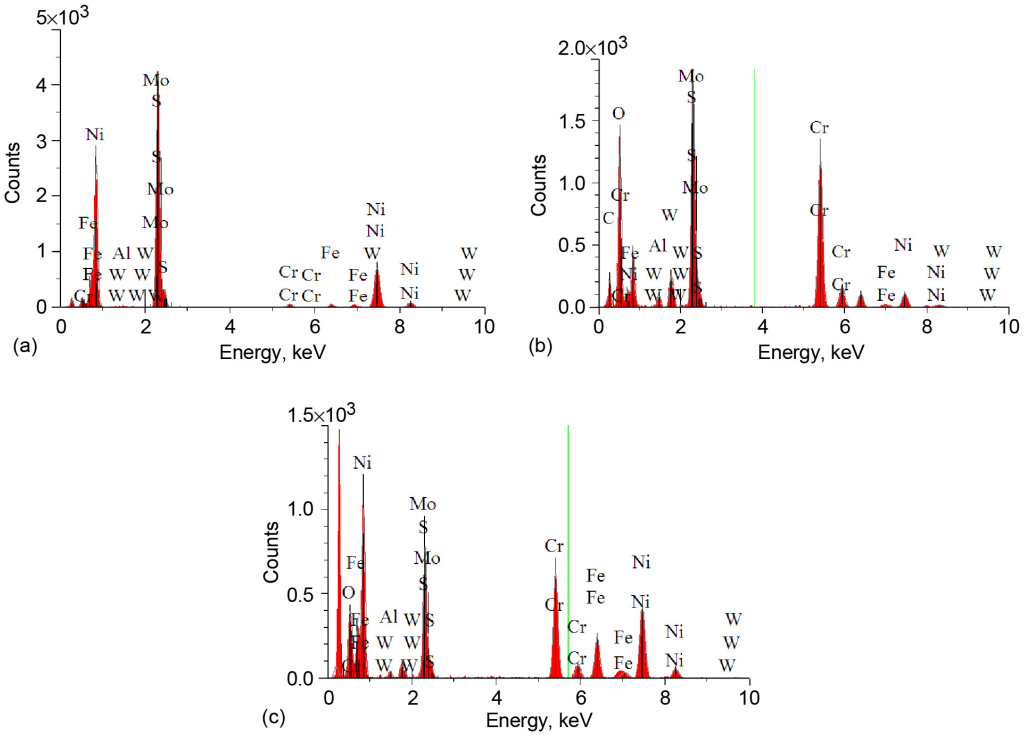


Figure 59.—Energy dispersive spectroscopy analysis of G30 alloy sample exposed to Venusian surface conditions for 42 days (Fig. 57). (a) Outer layer. (b) Inner layer. (c) Bulk.

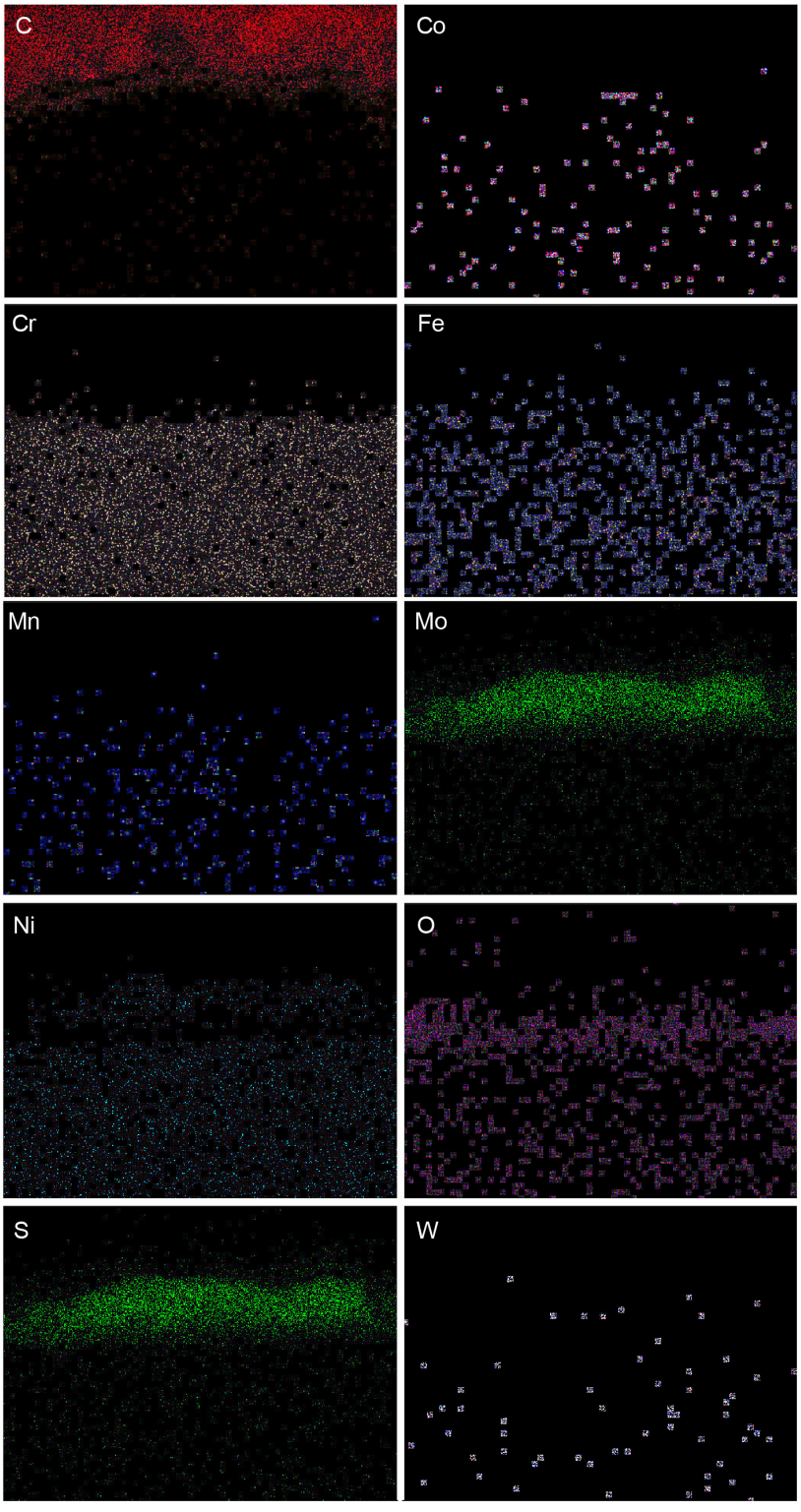


Figure 60.—X-ray elemental images of G30 alloy sample exposed to Venusian surface conditions for 10 days (area mapped is that of Fig. 56). Each pixel represents information gathered by spectrometer at C, Co, Cr, Fe, Mn, Ni, O, and S K$\alpha$ line and at Mo and W L$\alpha$ line.

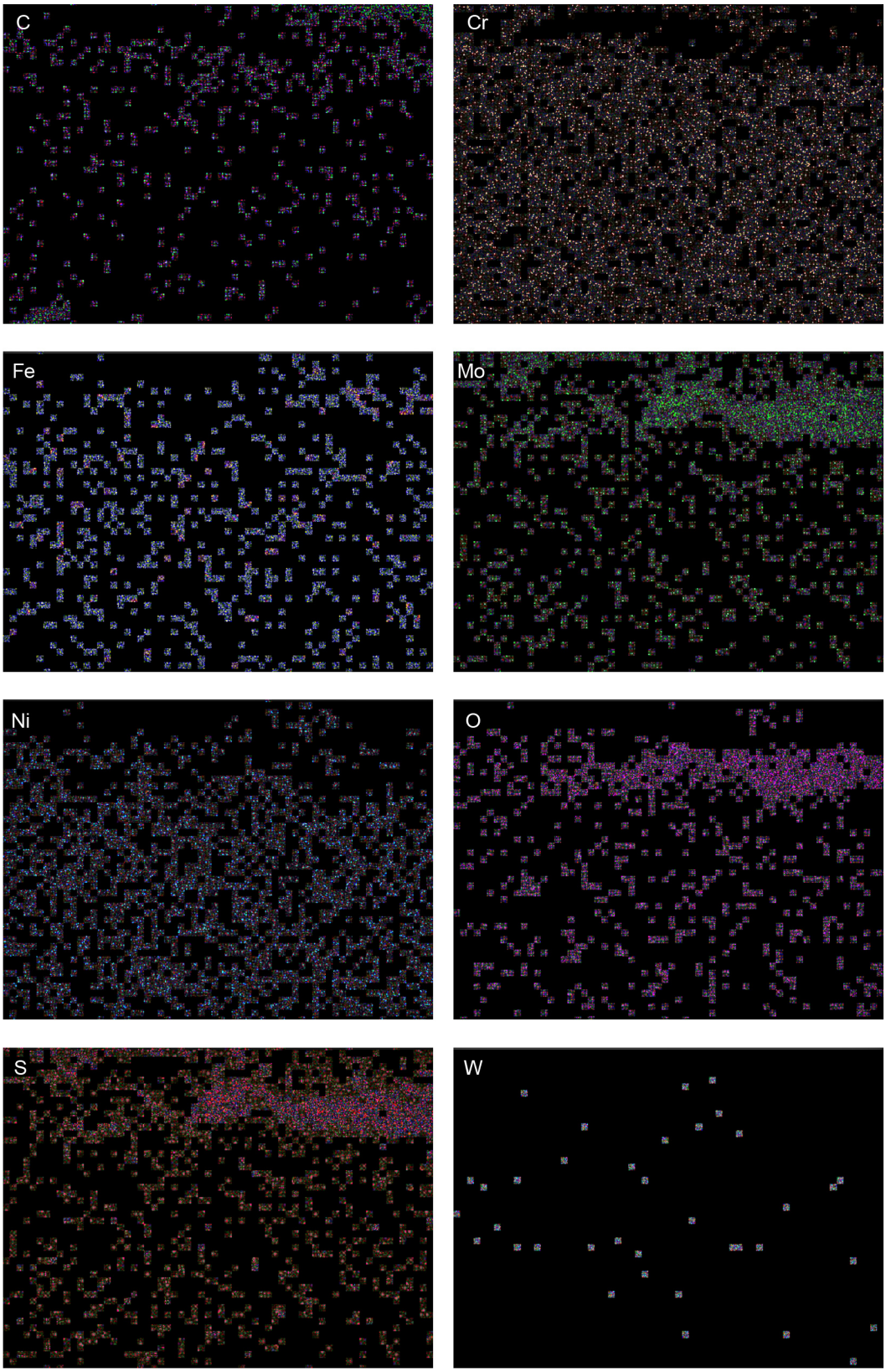


Figure 61.—X-ray elemental images of G30 alloy sample exposed to Venusian surface conditions for 42 days (area mapped is that of Fig. 57). Each pixel represents information gathered by spectrometer at C, Cr, Fe, Ni, O, and S Kα line and at Mo and W Lα line.

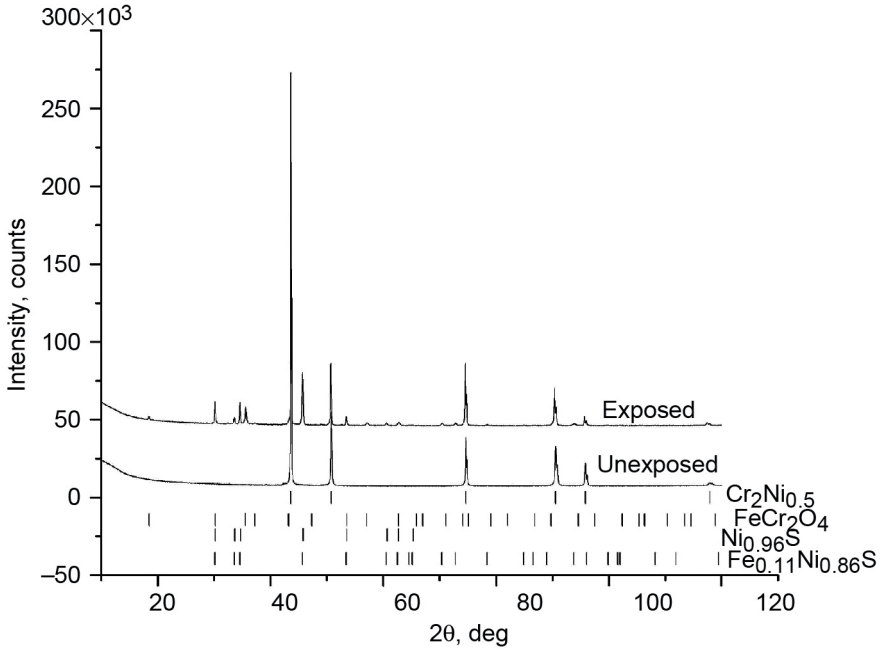


Figure 62.—X-ray diffraction patterns of G30 alloy samples, unexposed and exposed to Venusian surface conditions for 42 days.

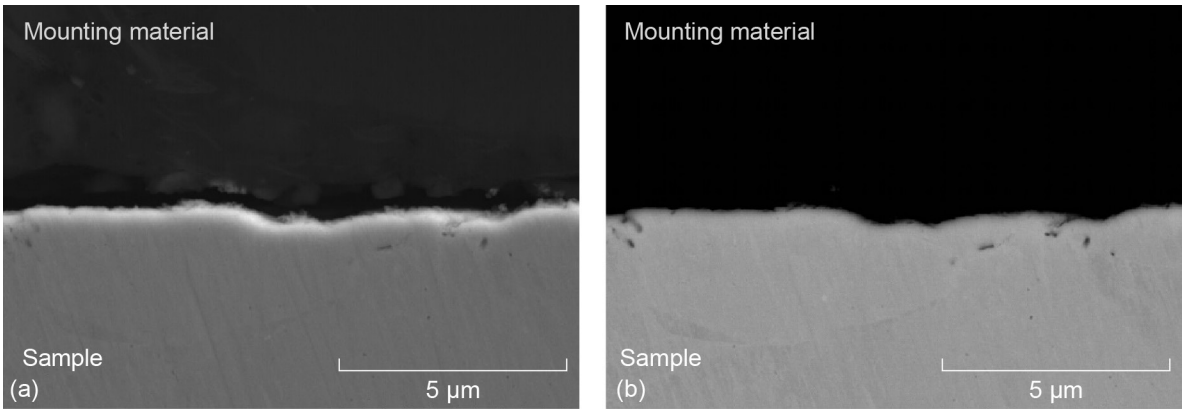


Figure 63.—Cross-sectional images of unexposed alloy 625 sample. (a) Scanning electron microscopy image. (b) Backscattered-electron image.

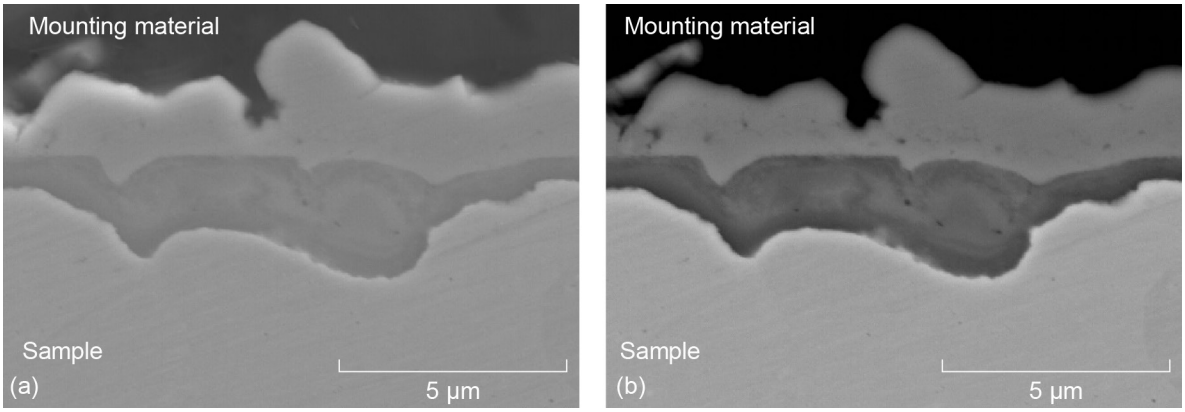


Figure 64.—Cross-sectional images of alloy 625 sample exposed to Venusian surface conditions for 10 days. (a) Scanning electron microscopy image. (b) Backscattered-electron image.

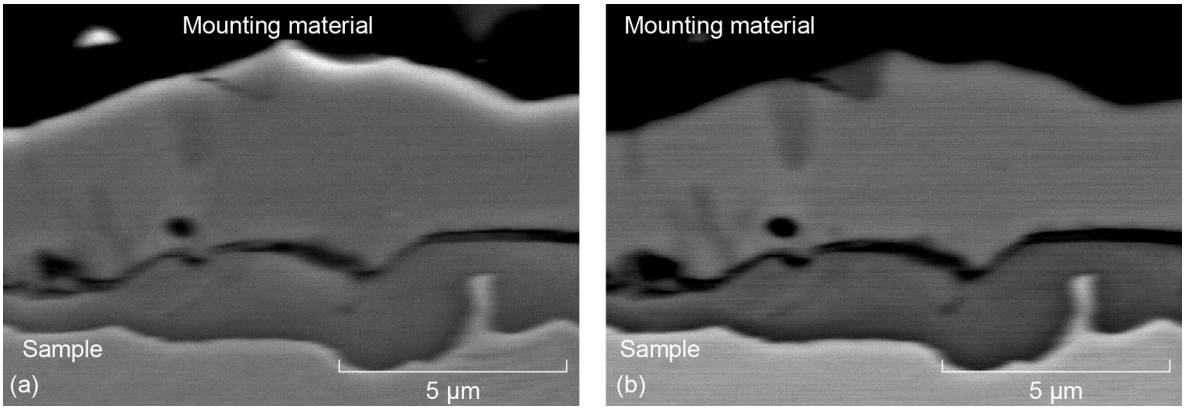


Figure 65.—Cross-sectional images of alloy 625 sample exposed to Venusian surface conditions for 42 days. (a) Scanning electron microscopy image. (b) Backscattered-electron image.

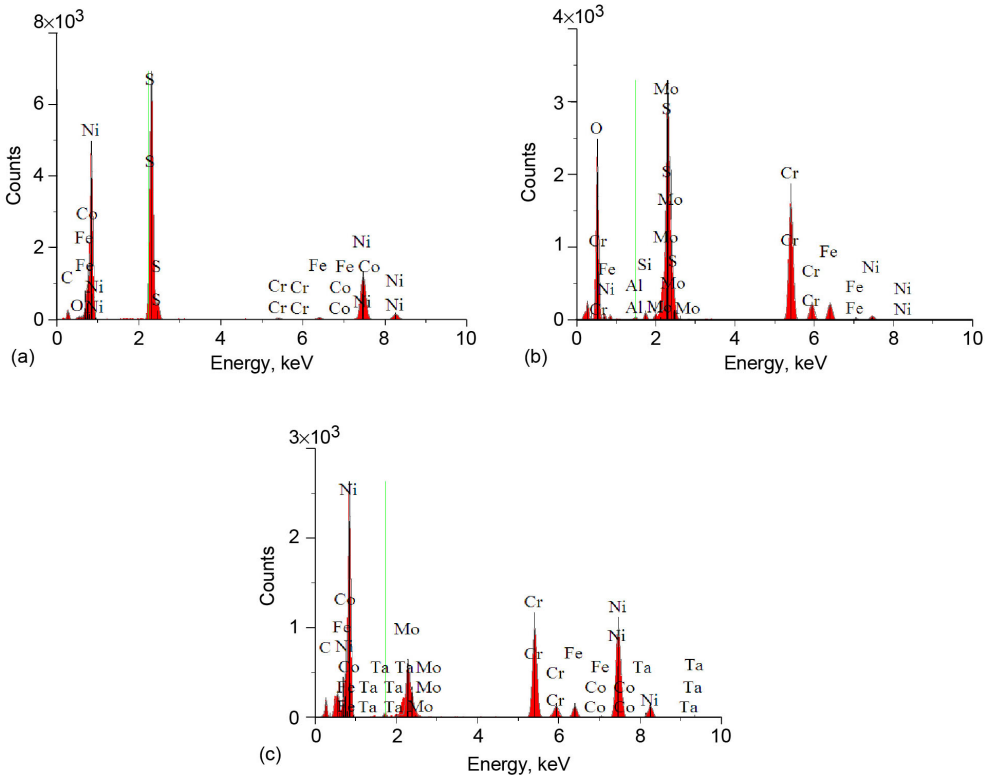


Figure 66.—Energy dispersive spectroscopy analysis of alloy 625 sample exposed to Venusian surface conditions for 10 days (Fig. 64). (a) Outer layer. (b) Inner layer. (c) Bulk.

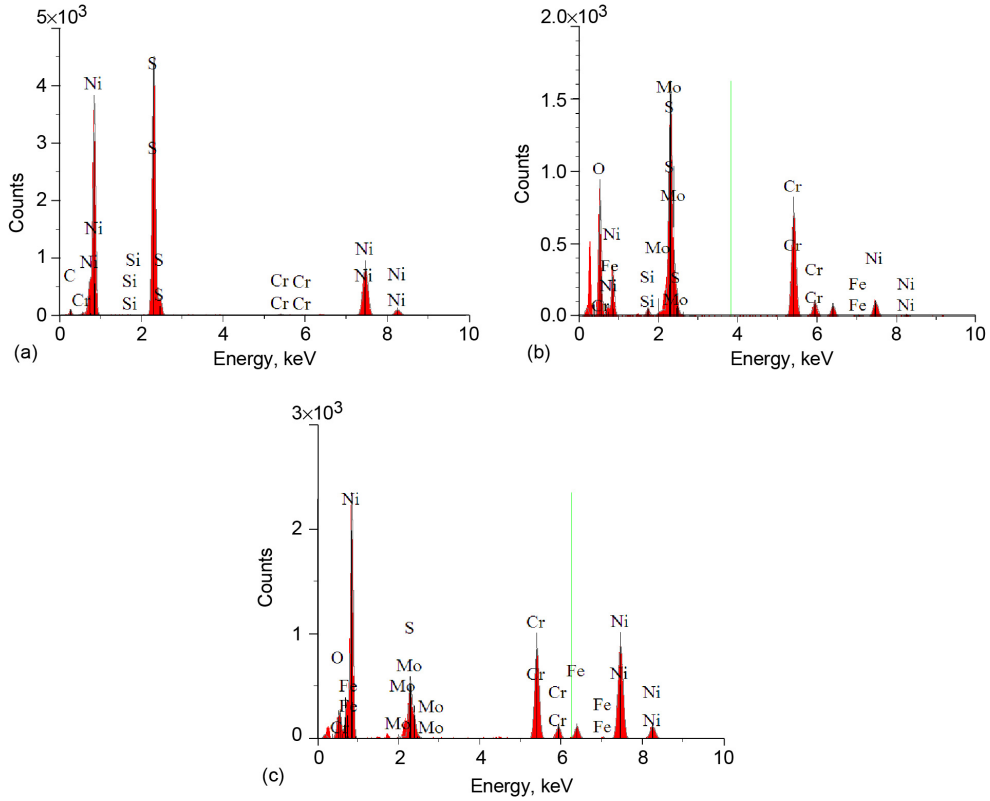


Figure 67.—Energy dispersive spectroscopy analysis of alloy 625 sample exposed to Venusian surface conditions for 42 days (Fig. 65). (a) Outer layer. (b) Inner layer. (c) Bulk.

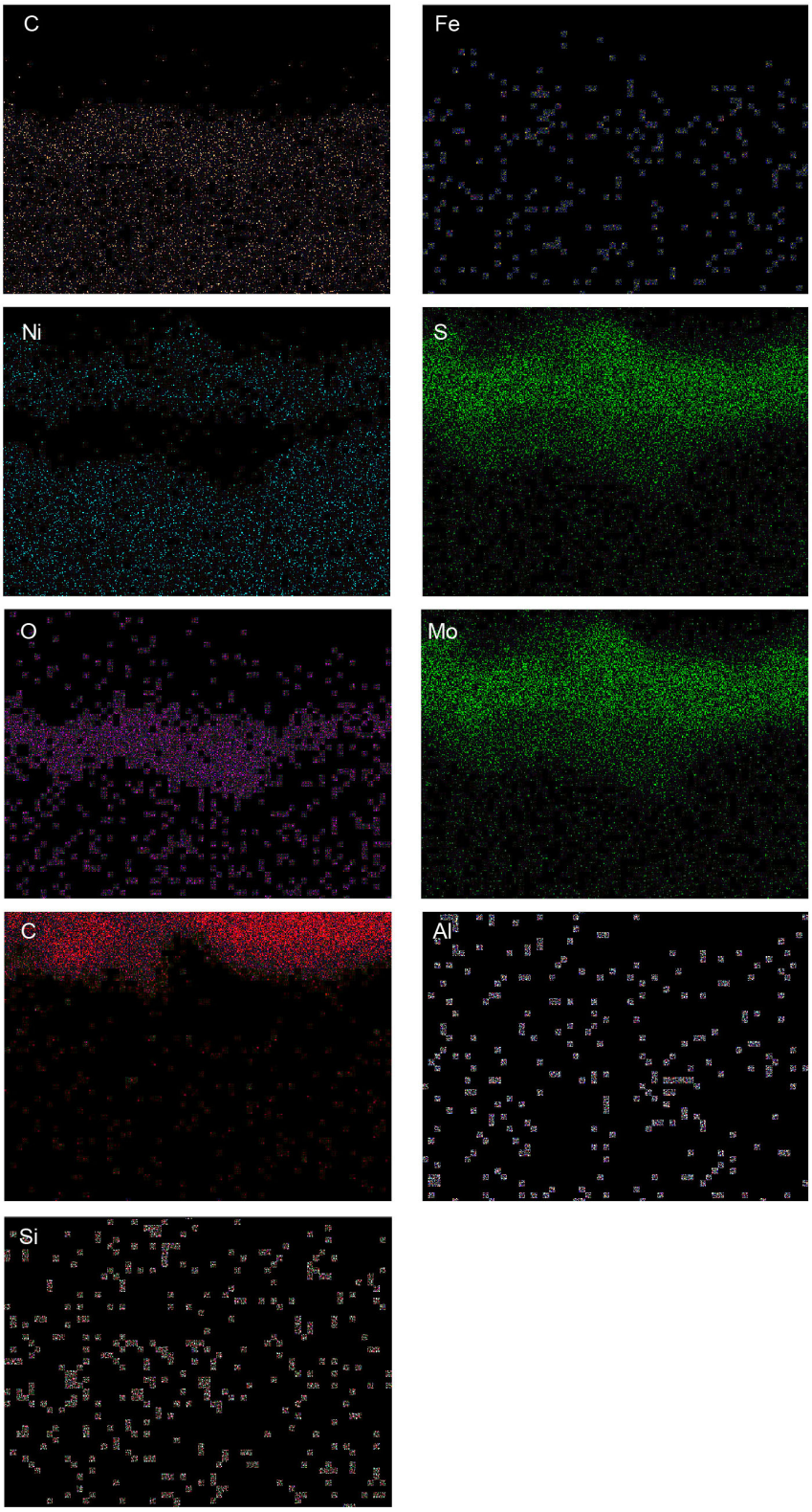


Figure 68.—X-ray elemental images of alloy 625 sample exposed to Venusian surface conditions for 10 days (area mapped is that of Fig. 64). Each pixel represents information gathered by spectrometer at C, Cr, Fe, Al, Ni, Si, Co, O, and S Kα line and at Mo and Ta Lα line.

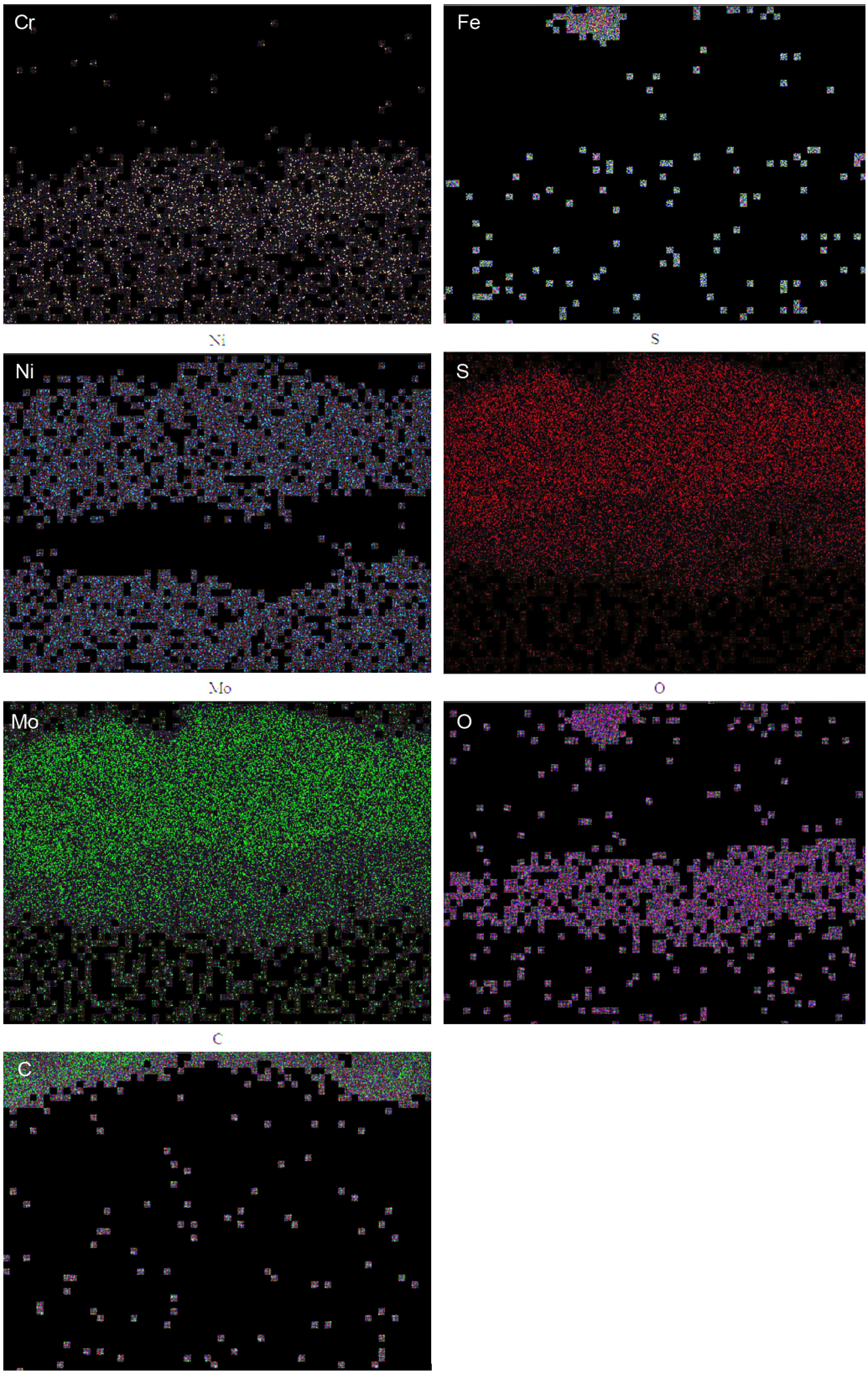


Figure 69.—X-ray elemental images of alloy 625 sample exposed to Venusian surface conditions for 42 days (area mapped is that of Fig. 65). Each pixel represents information gathered by spectrometer at C, Cr, Fe, Al, Ni, Si, Co, O, and S Kα line and at Mo and Ta Lα line.

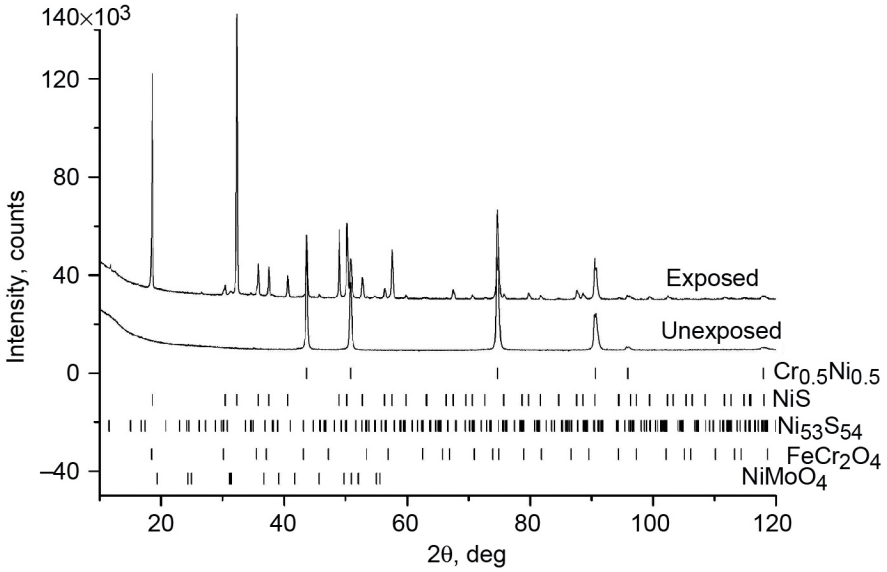


Figure 70.—X-ray diffraction patterns of alloy 625 sample, unexposed and exposed to Venusian surface conditions for 42 days.

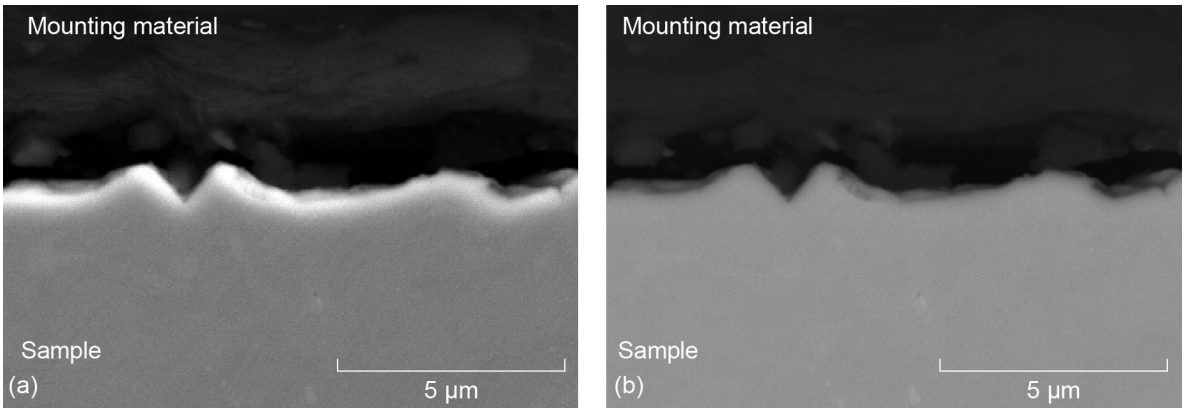


Figure 71.—Cross-sectional images of unexposed β-NiAl alloy sample. (a) Scanning electron microscopy image. (b) Backscattered-electron image.

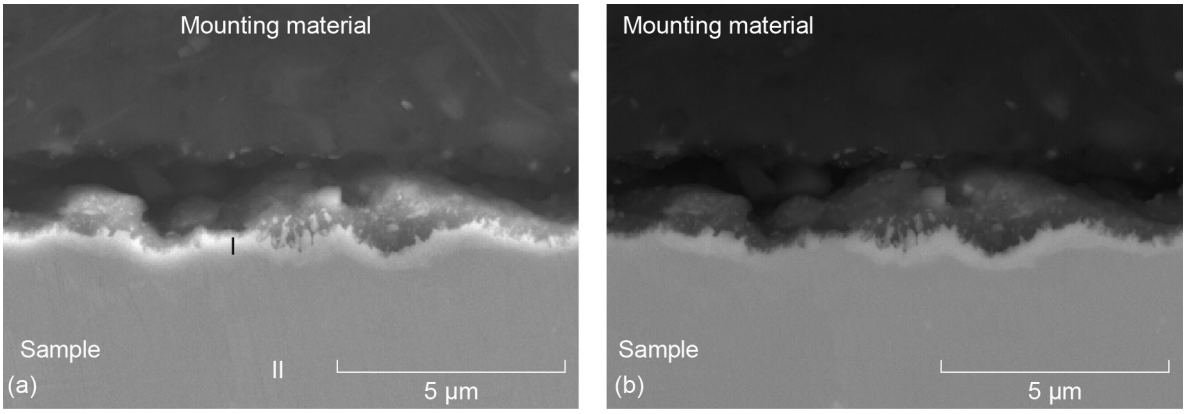


Figure 72.—Cross-sectional images of β-NiAl alloy sample exposed to Venusian surface conditions for 10 days. (a) Scanning electron microscopy image. (b) Backscattered-electron image.

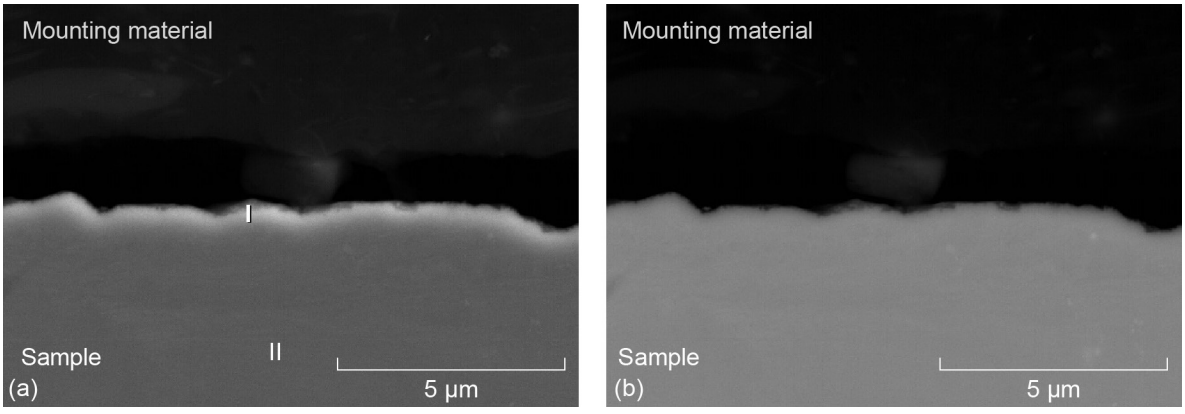


Figure 73.—Cross-sectional images of β-NiAl alloy sample exposed to Venusian surface conditions for 42 days. (a) Scanning electron microscopy image. (b) Backscattered-electron image.

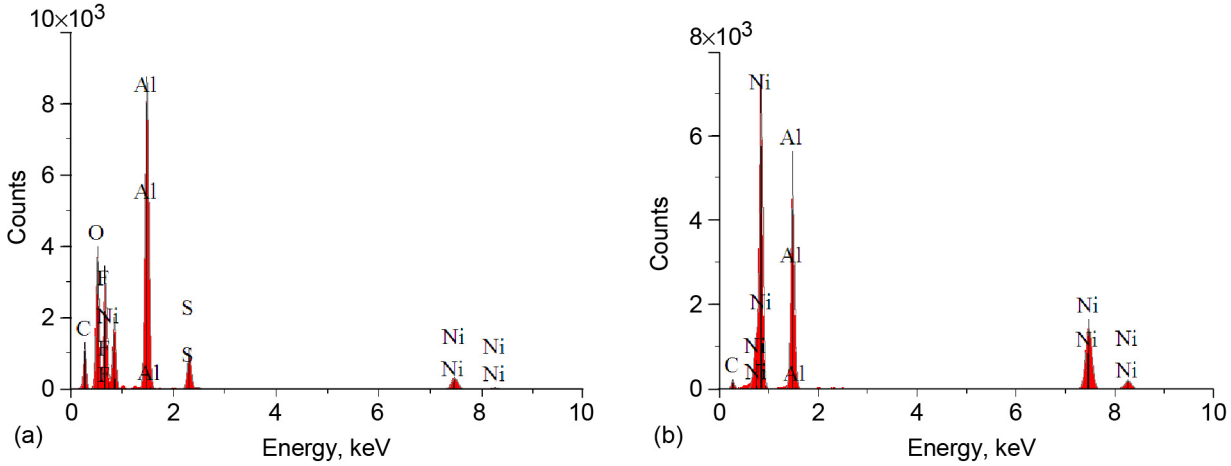


Figure 74.—Energy dispersive spectroscopy analysis of β-NiAl alloy sample exposed to Venusian surface conditions for 10 days (Fig. 72(a)). (a) Surface (location I). (b) Bulk (location II).

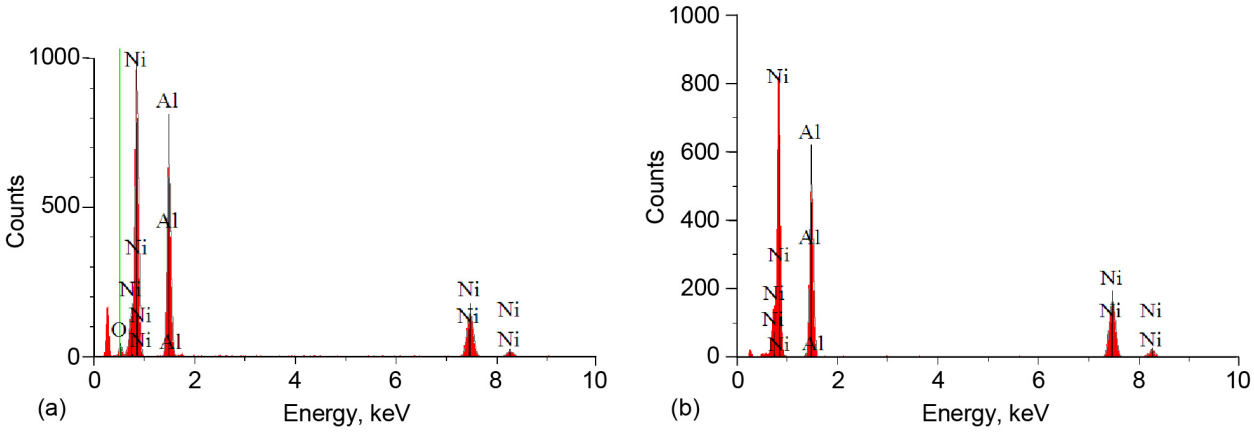


Figure 75.—Energy dispersive spectroscopy analysis of β-NiAl alloy sample exposed to Venusian surface conditions for 42 days (Fig. 73(a)). (a) Surface (location I). (b) Bulk (location II).

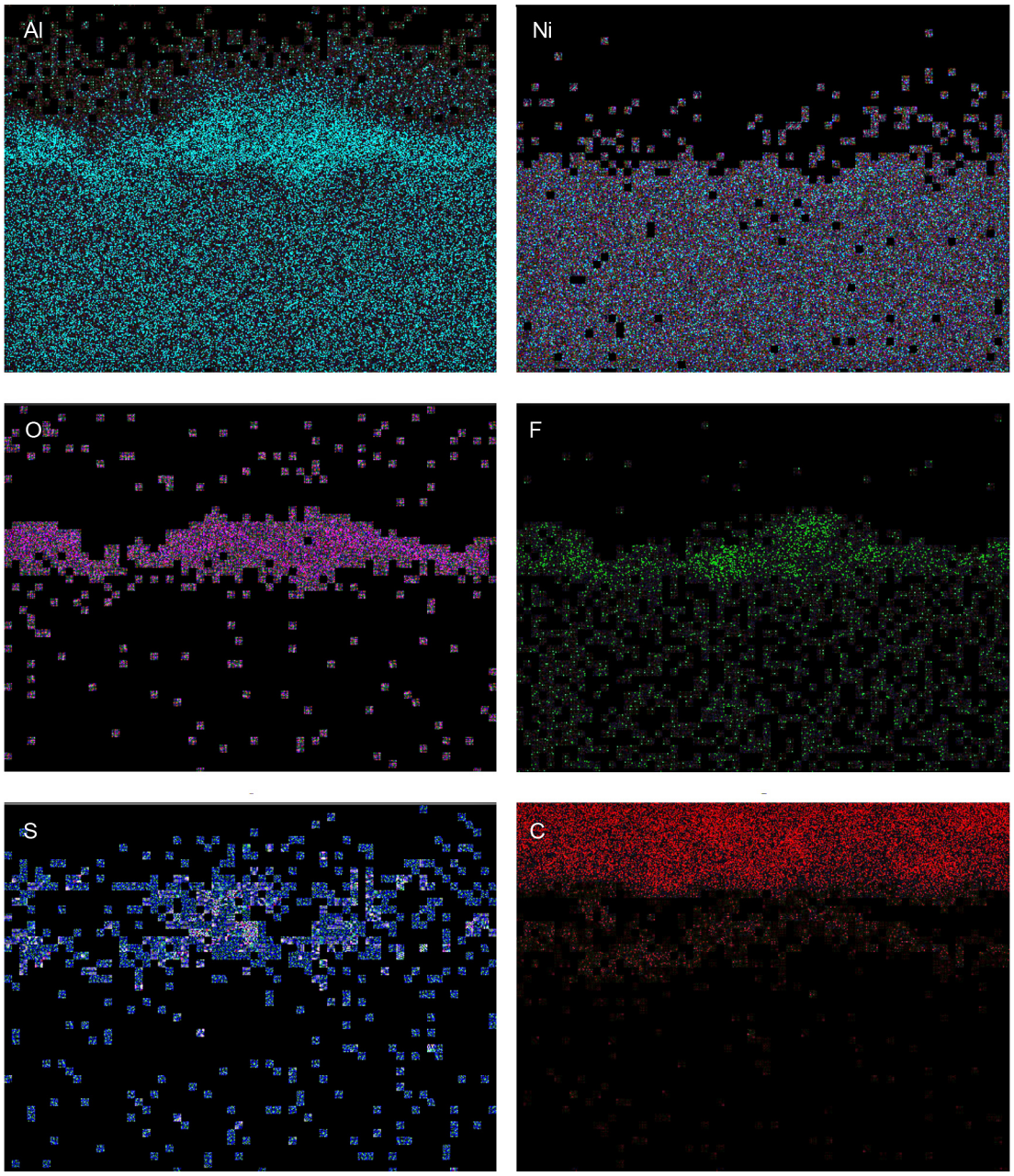


Figure 76.—X-ray elemental images of β-NiAl alloy sample exposed to Venusian surface conditions for 10 days (area mapped is that of Fig. 72). Each pixel represents information gathered by spectrometer at C, O, F, Al, Ni, and S Kα line.

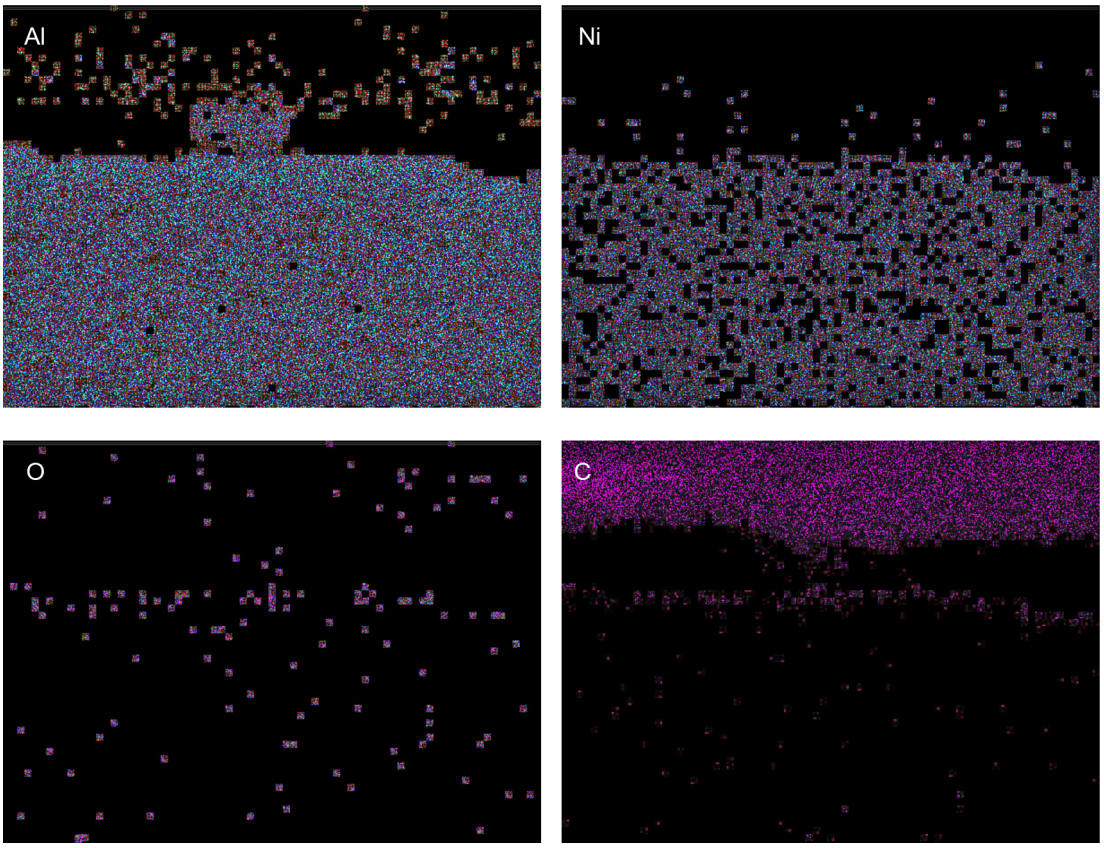


Figure 77.—X-ray elemental images of β-NiAl alloy sample exposed to Venusian surface conditions for 42 days (area mapped is that of Fig. 73). Each pixel represents information gathered by spectrometer at C, O, Al, and Ni Kα line.

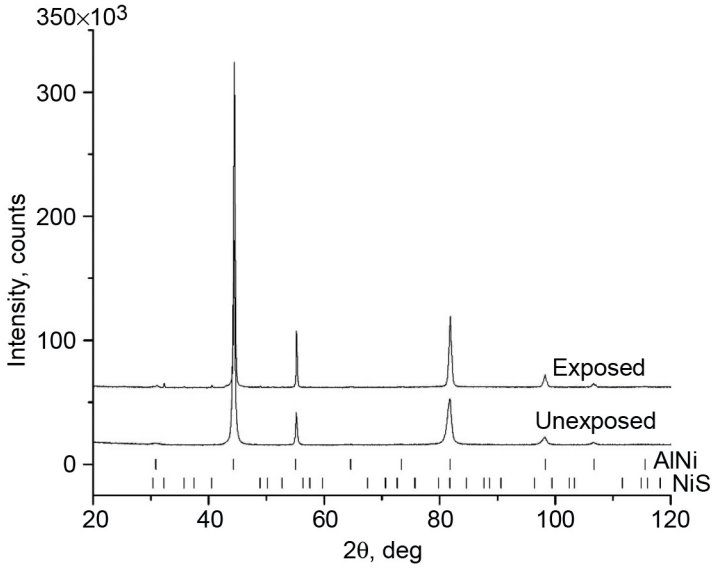


Figure 78.—X-ray diffraction patterns of β-NiAl alloy samples, unexposed and exposed to Venusian surface conditions for 42 days.

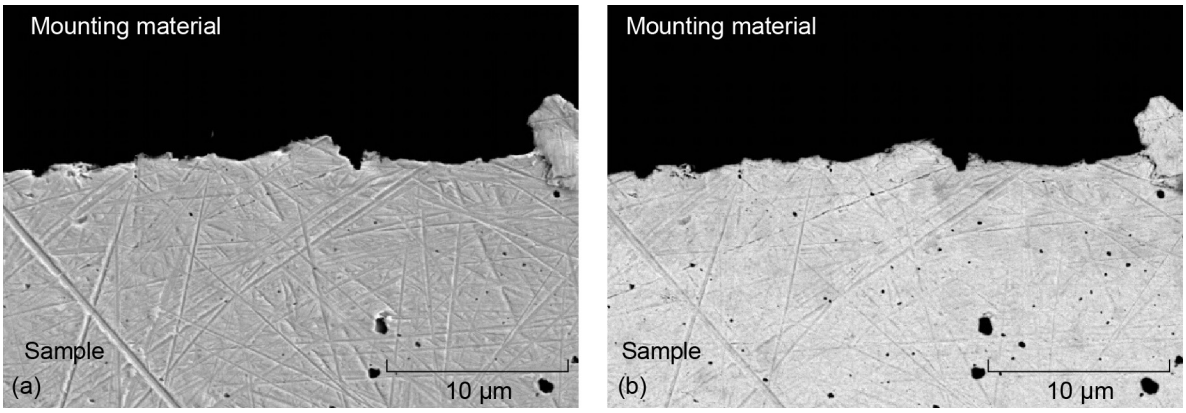


Figure 79.—Cross-sectional images of unexposed gold wire sample. (a) Scanning electron microscopy image. (b) Backscattered-electron image.

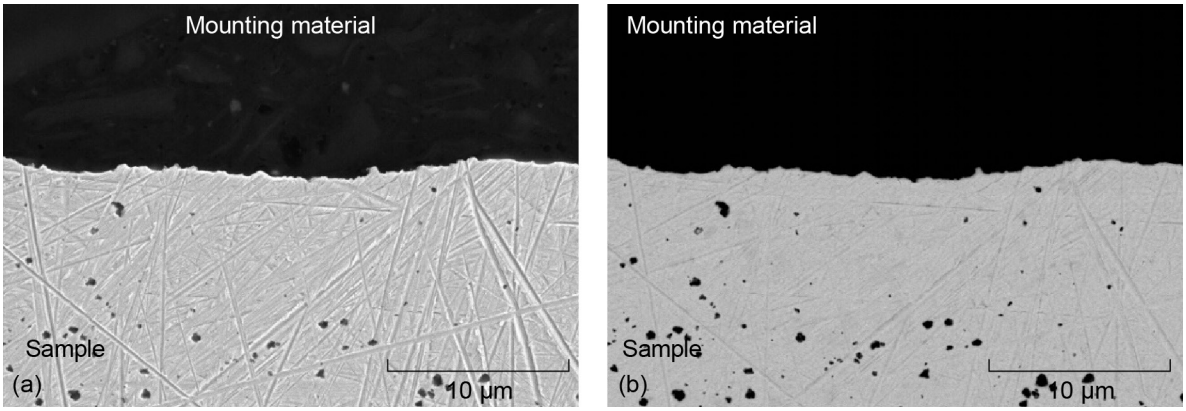


Figure 80.—Cross-sectional images of gold wire sample exposed to Venusian surface conditions for 10 days. (a) Scanning electron microscopy image. (b) Backscattered-electron image.

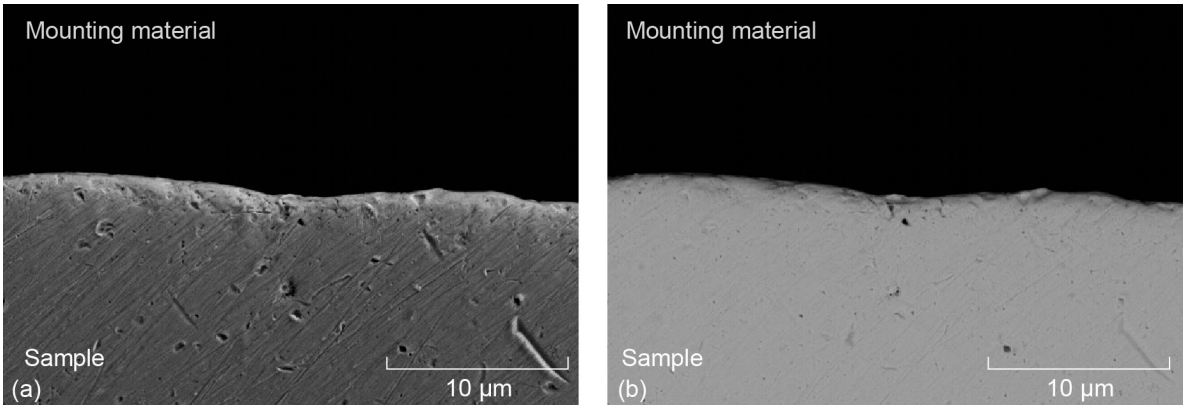


Figure 81.—Cross-sectional images of gold wire sample exposed to Venusian surface conditions for 42 days. (a) Scanning electron microscopy image. (b) Backscattered-electron image.

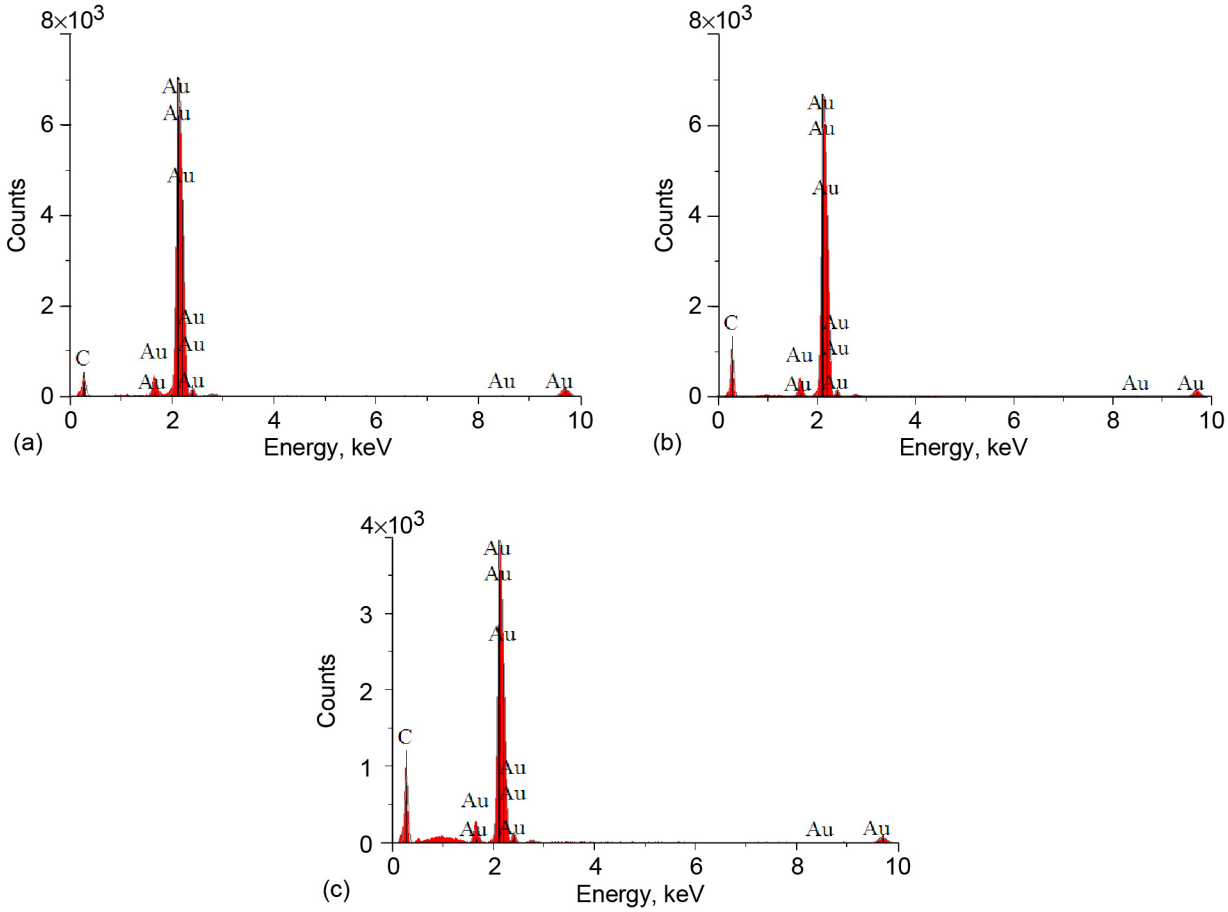


Figure 82.—Energy dispersive spectroscopy analysis (of bulk, near edge of surface) of gold wire samples, unexposed and exposed to Venusian surface conditions. (a) Unexposed (Fig. 79). (b) Exposed for 10 days (Fig. 80). (c) Exposed for 42 days (Fig. 81).

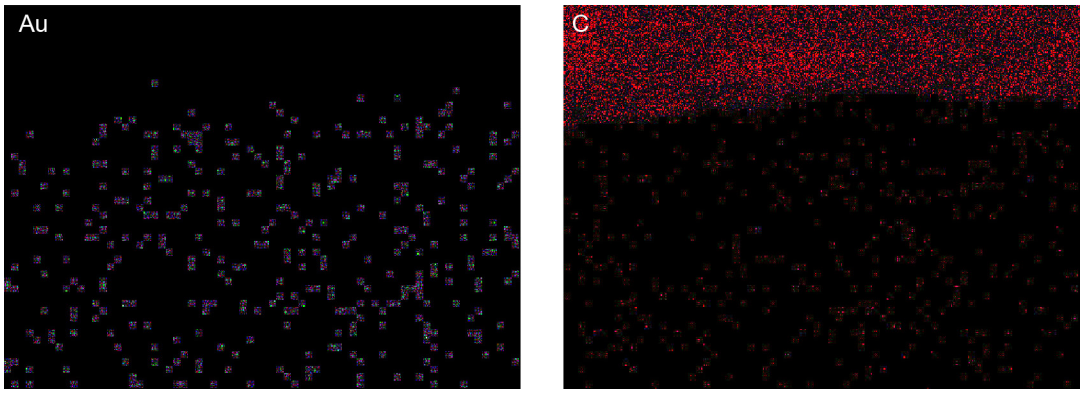


Figure 83.—X-ray elemental images of gold wire sample exposed to Venusian surface conditions for 10 days (area mapped is that of Fig. 80). Each pixel represents information gathered by spectrometer at Au and C Kα line.

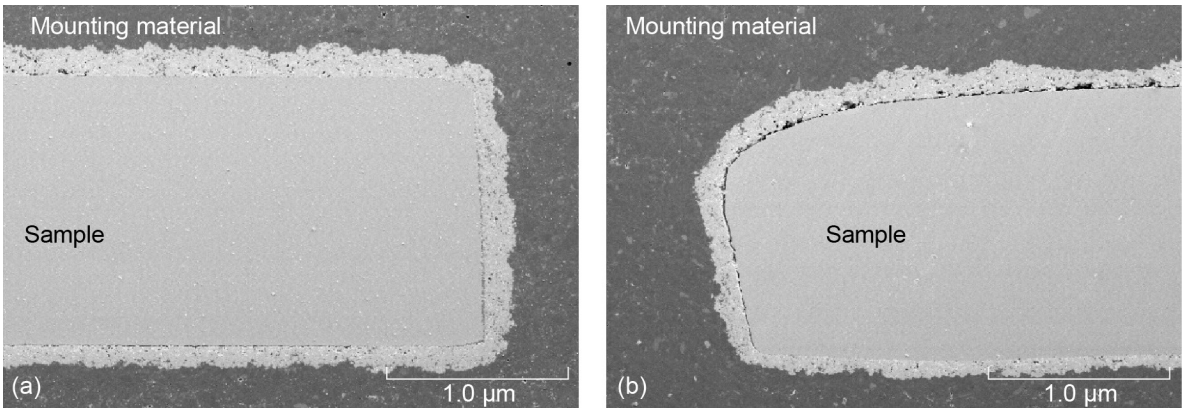


Figure 84.—Cross-sectional scanning electron microscopy images of 304 stainless steel samples coated with 4 mol% yttria-stabilized zirconia. (a) Unexposed. (b) Exposed to Venusian surface conditions for 10 days.

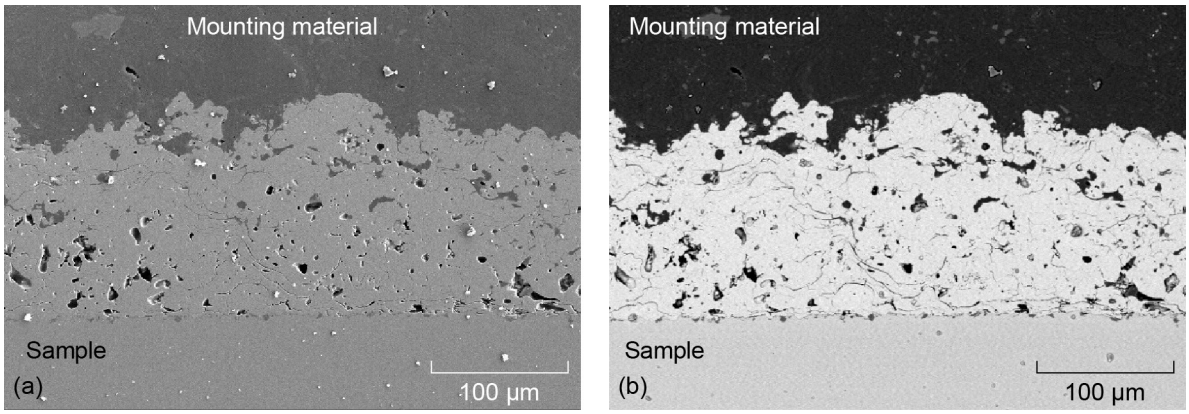


Figure 85.—Cross-sectional images of unexposed 304 stainless steel sample coated with 4 mol% yttria-stabilized zirconia. (a) Scanning electron microscopy image. (b) Backscattered-electron image.

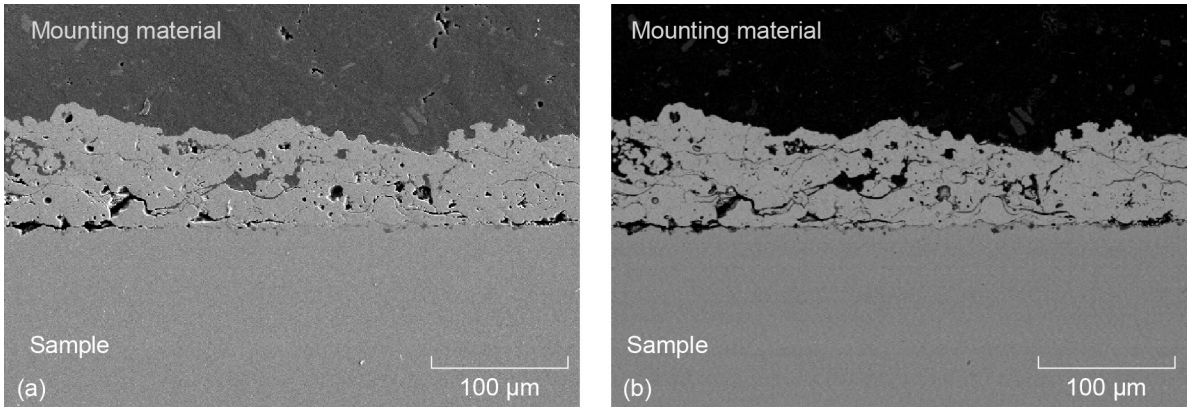


Figure 86.—Cross-sectional images of 304 stainless steel sample coated with 4 mol% yttria-stabilized zirconia, exposed to Venusian surface conditions for 10 days. (a) Scanning electron microscopy image. (b) Backscattered-electron image.

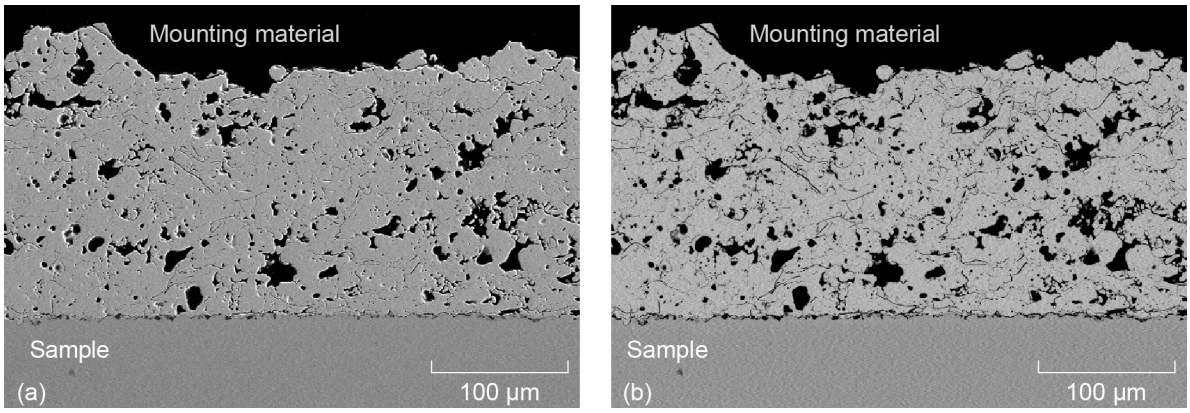


Figure 87.—Cross-sectional of 304 stainless steel sample coated with 4 mol% yttria-stabilized zirconia, exposed to Venusian surface conditions for 42 days. (a) Scanning electron microscopy image. (b) Backscattered-electron image.

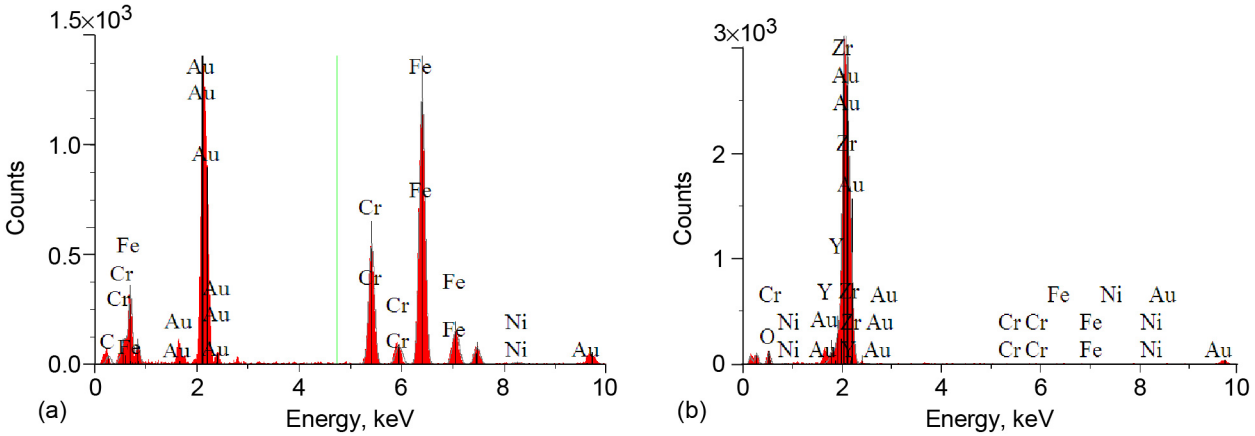


Figure 88.—Energy dispersive spectroscopy analysis of unexposed 304 stainless steel sample coated with 4 mol% yttria-stabilized zirconia (Fig. 85). (a) Bulk. (b) Coating.

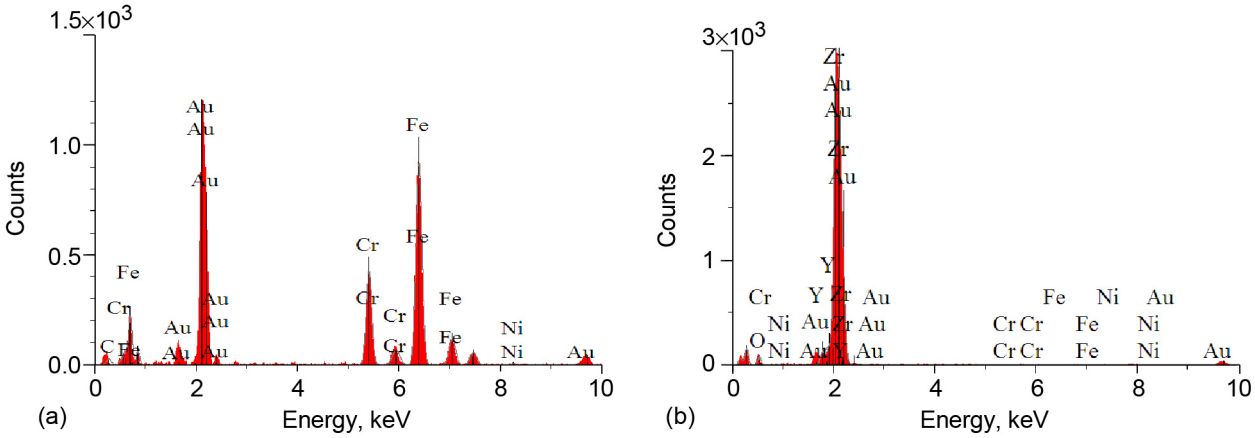


Figure 89.—Energy dispersive spectroscopy analysis of 304 stainless steel sample coated with 4 mol% yttria-stabilized zirconia, exposed to Venusian surface conditions for 10 days (Fig. 86). (a) Bulk. (b) Coating.

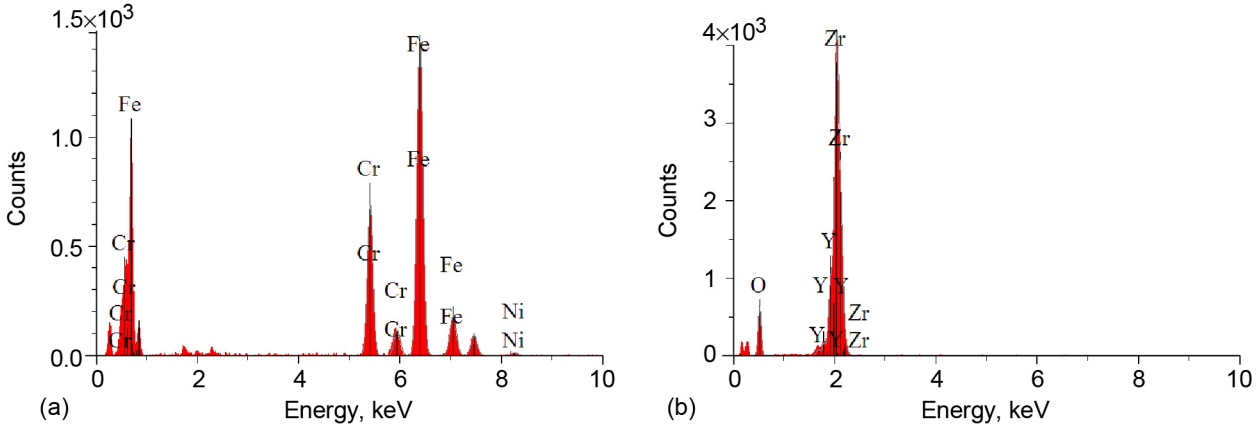


Figure 90.—Energy dispersive spectroscopy analysis of 304 stainless steel sample coated with 4 mol% yttria-stabilized zirconia, exposed to Venusian surface conditions for 42 days (Fig. 87). (a) Bulk. (b) Coating.

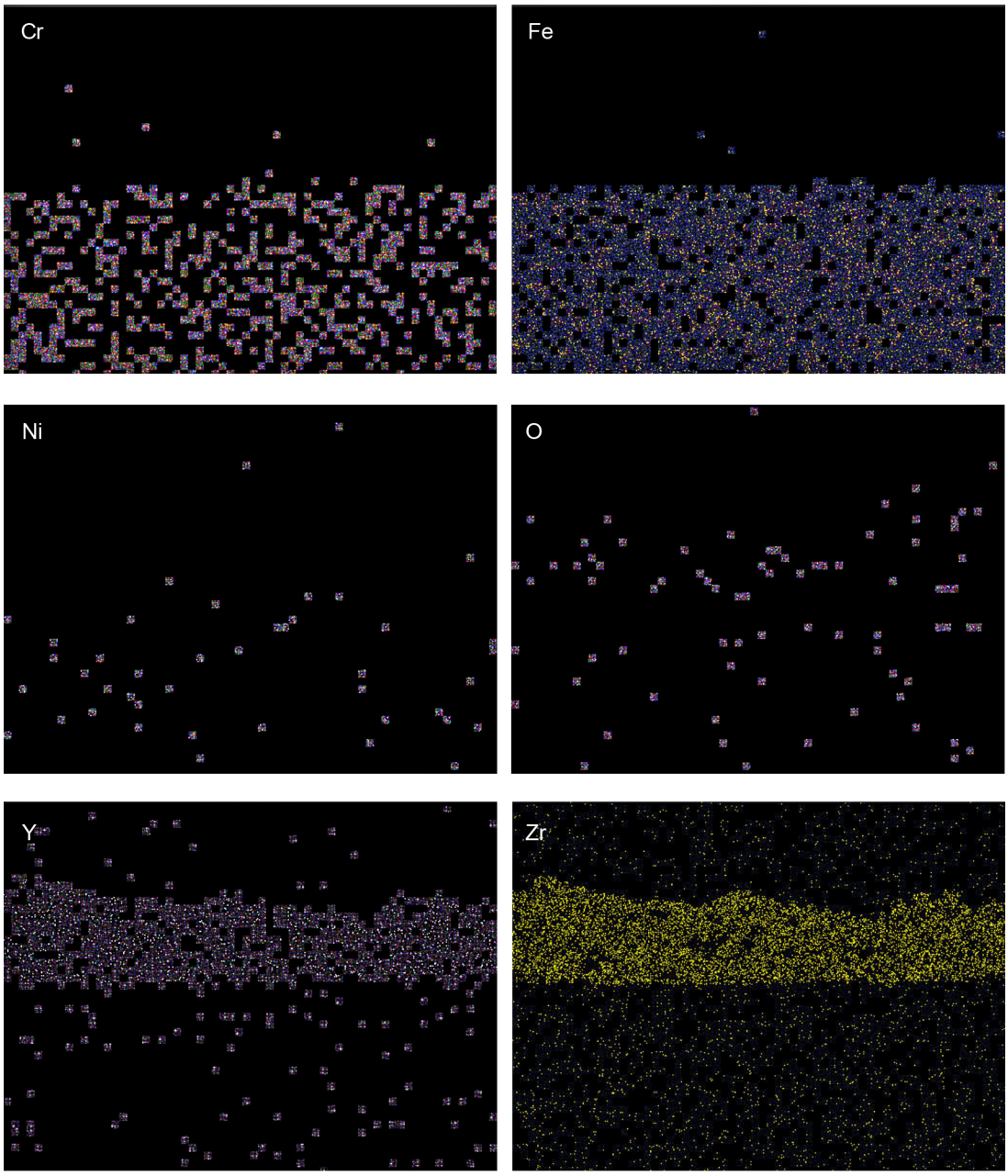


Figure 91.—X-ray elemental images of 304 stainless steel sample coated with 4 mol% yttria-stabilized zirconia, exposed to Venusian surface conditions for 10 days (area mapped is that of Fig. 86(a)). Each pixel represents information gathered by spectrometer at O, Cr, Fe, and Ni Kα line and at Y and Zr Lα line.

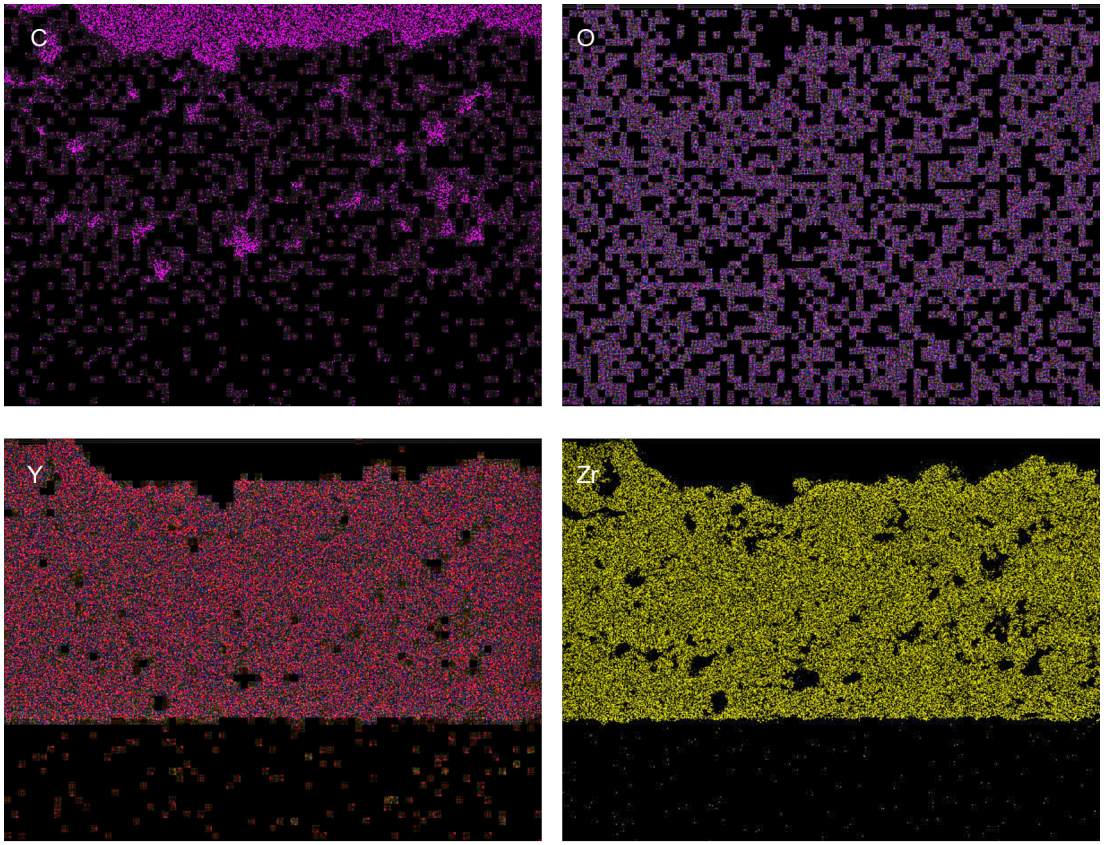


Figure 92.—X-ray elemental images of 304 stainless steel sample coated with 4 mol% yttria-stabilized zirconia, exposed to Venusian surface conditions for 42 days (area mapped is that of Fig. 87). Each pixel represents information gathered by spectrometer at C and O Kα line and at Y and Zr Lα line.

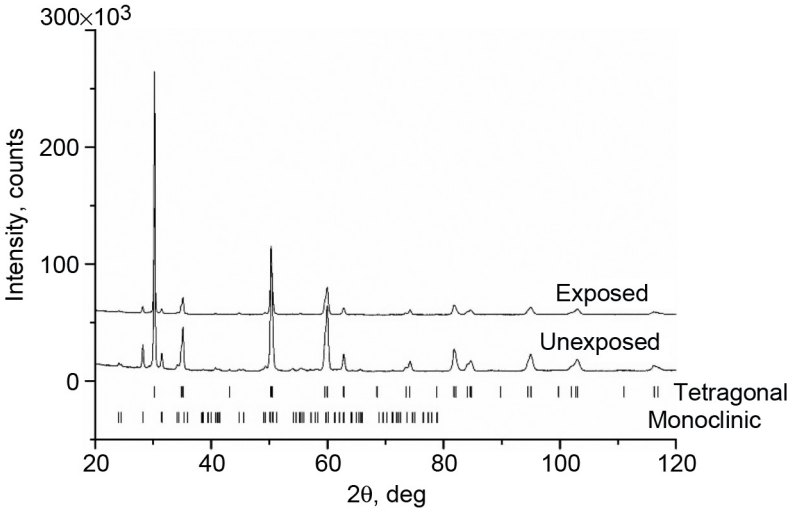


Figure 93.—X-ray diffraction patterns of unpolished side of 304 stainless steel samples coated with 4 mol% yttria-stabilized zirconia, unexposed and exposed to Venusian surface conditions for 42 days.

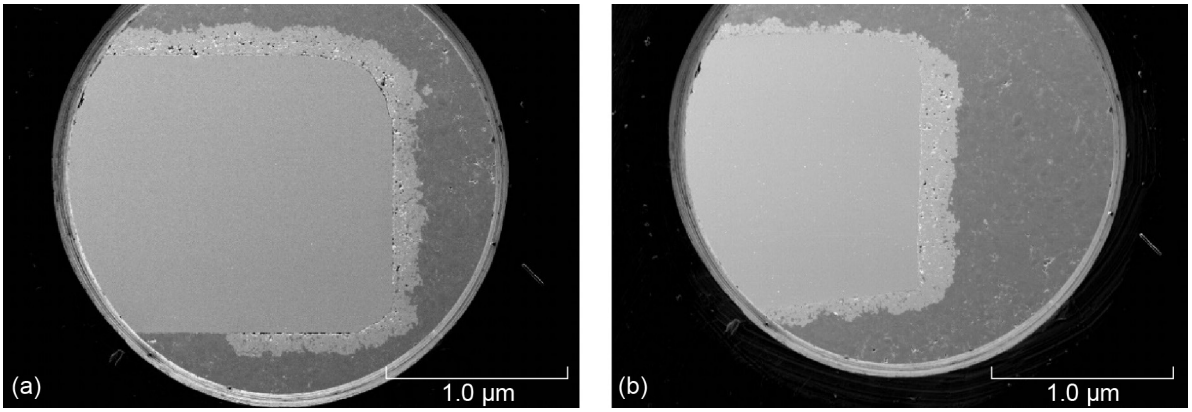


Figure 94.—Cross-sectional scanning electron microscopy images of 316 stainless steel samples coated with 4 mol% yttria-stabilized zirconia. (a) Unexposed. (b) Exposed to Venusian surface conditions for 10 days.

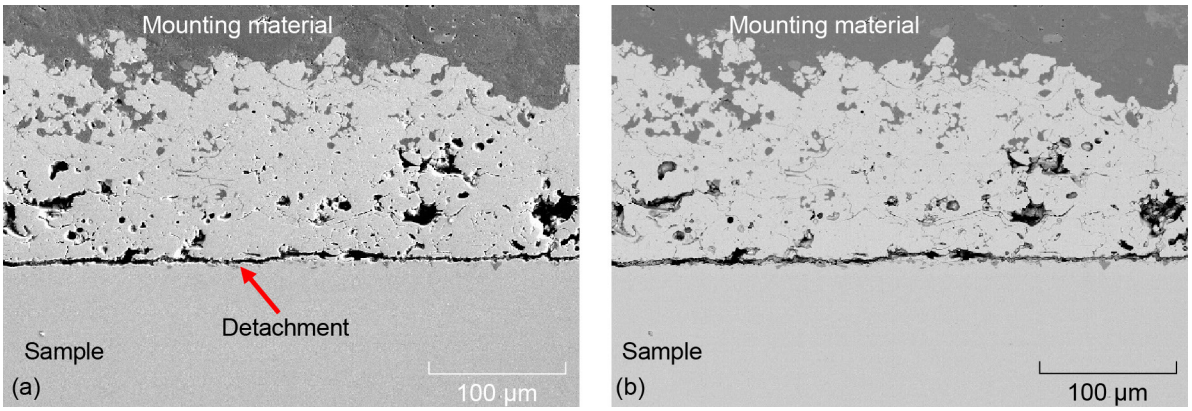


Figure 95.–Cross-sectional images of unexposed 316 stainless steel samples coated with 4 mol% yttria-stabilized zirconia. (a) Scanning electron microscopy image. (b) Backscattered-electron image.

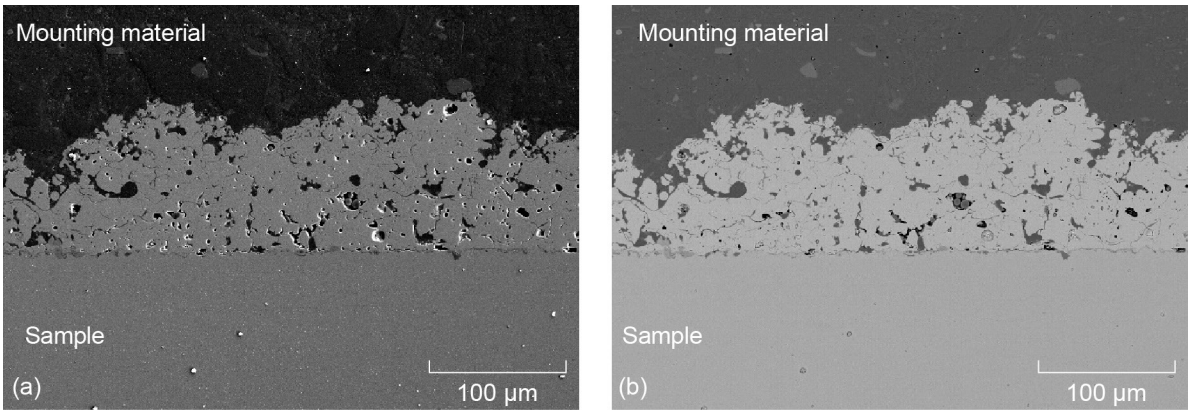


Figure 96.—Cross-sectional images of 316 stainless steel samples coated with 4 mol% yttria-stabilized zirconia, exposed to Venusian surface conditions for 10 days. (a) Scanning electron microscopy image. (b) Backscattered-electron image.

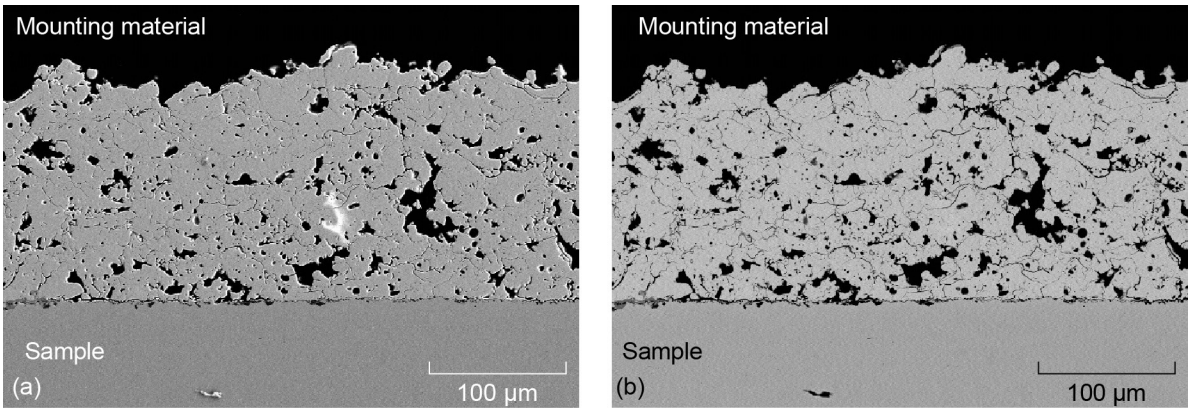


Figure 97.—Cross-sectional images of 316 stainless steel samples coated with 4 mol% yttria-stabilized zirconia, exposed to Venusian surface conditions for 42 days. (a) Scanning electron microscopy image. (b) Backscattered-electron image.

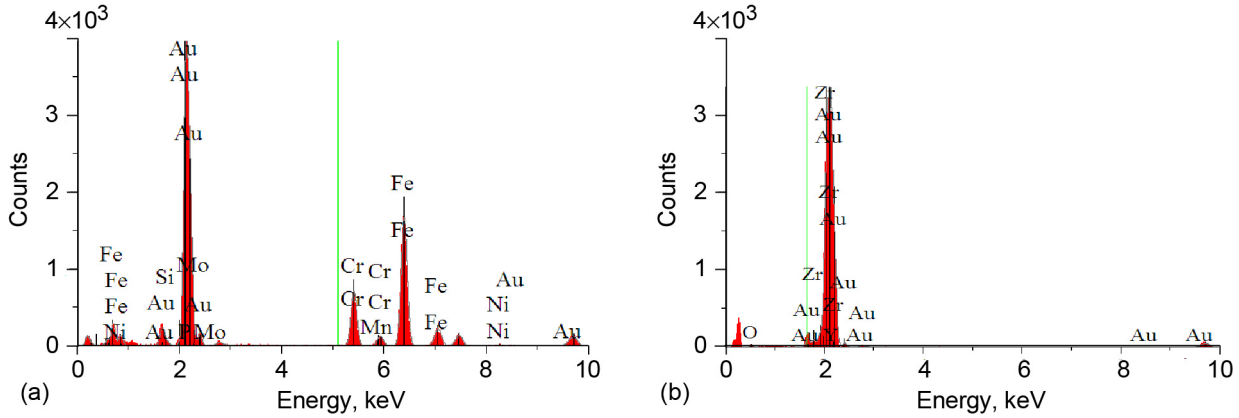


Figure 98.—Energy dispersive spectroscopy analysis of unexposed 316 stainless steel sample coated with 4 mol% yttria-stabilized zirconia (Fig. 95). (a) Bulk. (b) Coating.

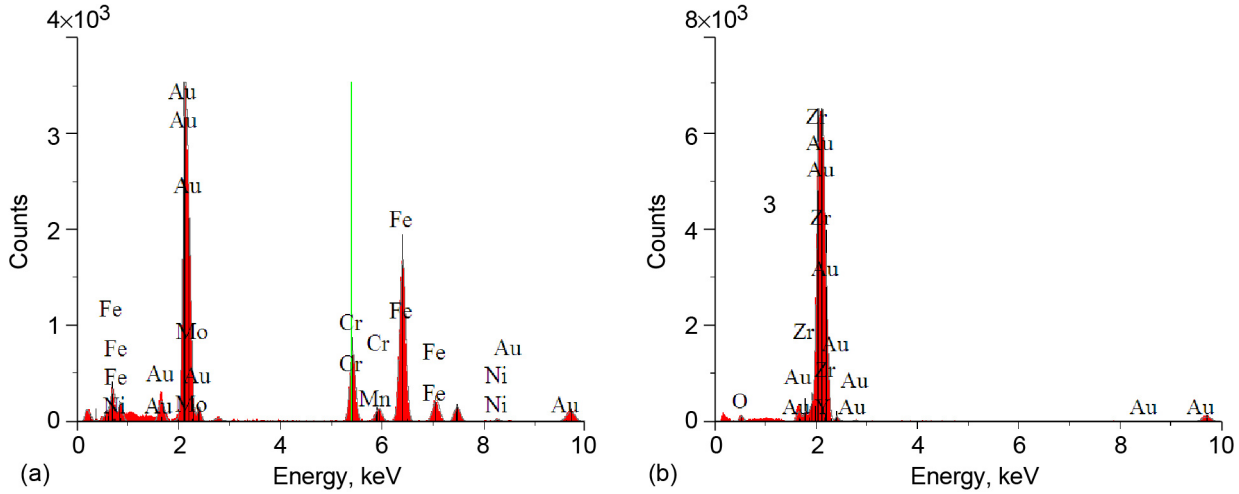


Figure 99.—Energy dispersive spectroscopy analysis of 316 stainless steel sample coated with 4 mol% yttria-stabilized zirconia, exposed to Venusian surface conditions for 10 days (Fig. 96). (a) Bulk. (b) Coating.

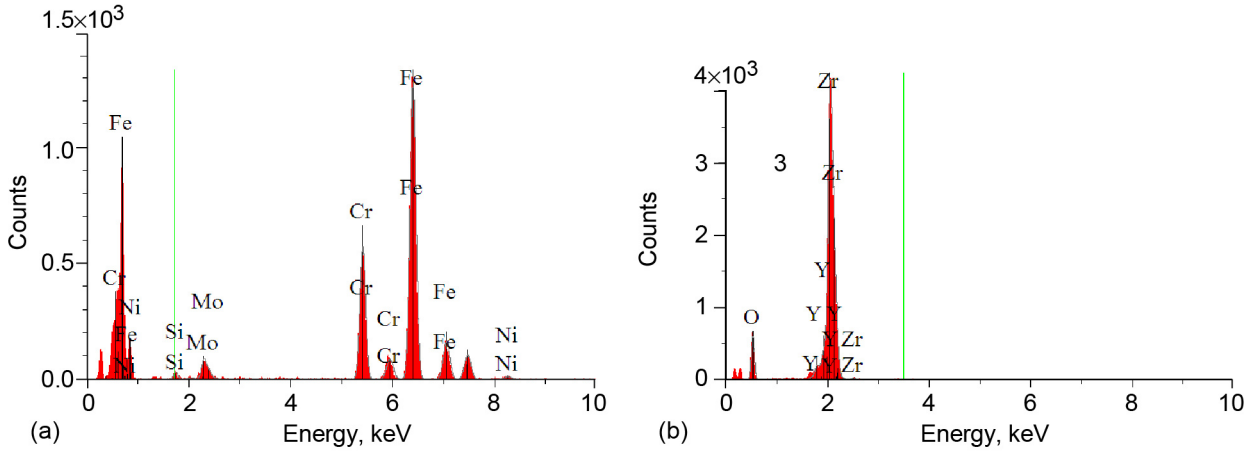


Figure 100.—Energy dispersive spectroscopy analysis of 316 stainless steel sample coated with 4 mol% yttria-stabilized zirconia, exposed to Venusian surface conditions for 42 days (Fig. 97). (a) Bulk. (b) Coating.

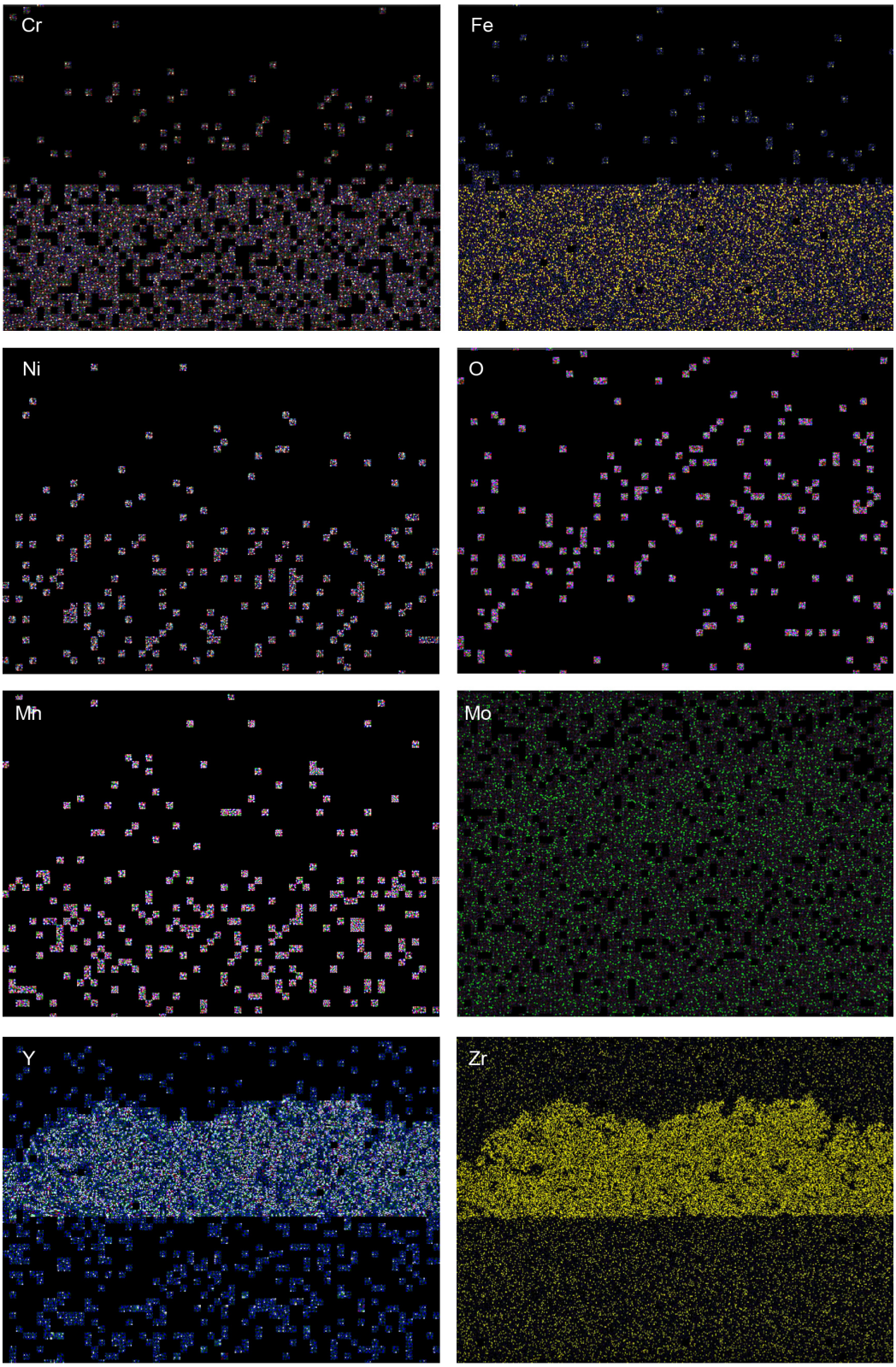


Figure 101.—X-ray elemental images of 316 stainless steel sample coated with 4 mol% yttria-stabilized zirconia, exposed to Venusian surface conditions for 10 days (area mapped is that of Fig. 96). Each pixel represents information gathered by spectrometer at O, Cr, Fe, Ni, and Mn Kα line and at Mo, Y, and Zr Lα line.

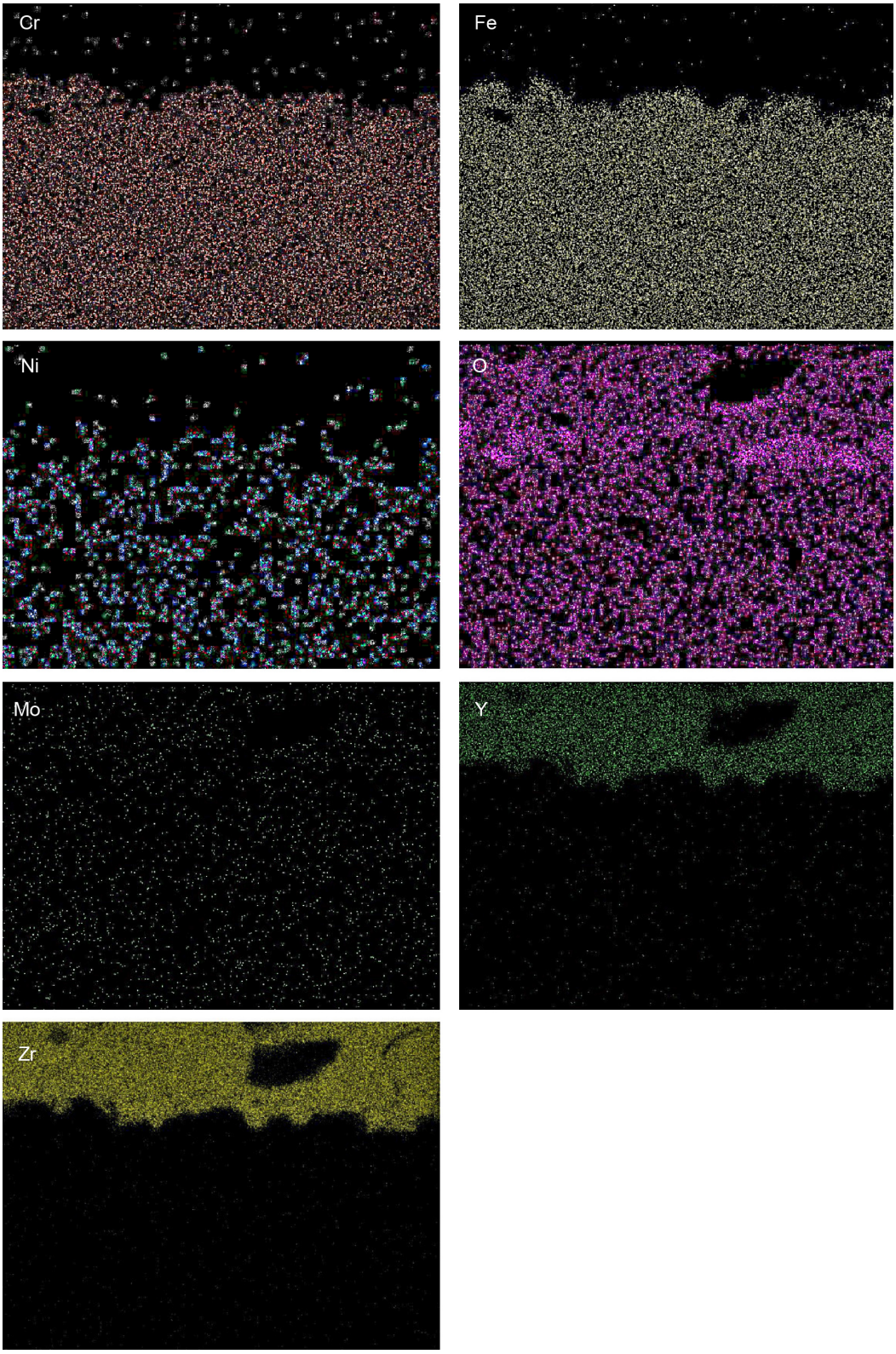


Figure 102.—X-ray elemental images of 316 stainless steel sample coated with 4 mol% yttria-stabilized zirconia, exposed to Venusian surface conditions for 42 days (area mapped is that of Fig. 97). Each pixel represents information gathered by spectrometer at O, Cr, Fe, and Ni Kα line and at Mo, Y, and Zr Lα line.

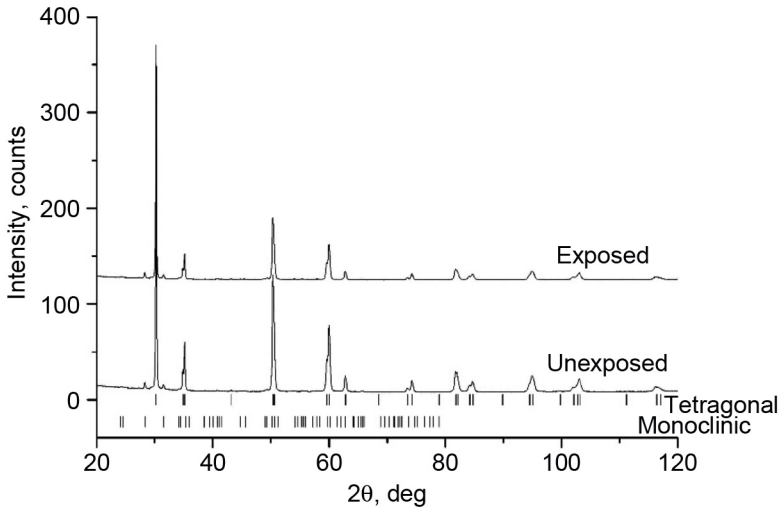


Figure 103.—X-ray diffraction patterns of unpolished side of 316 stainless steel samples coated with 4 mol% yttria-stabilized zirconia, unexposed and exposed to Venusian surface conditions for 42 days.

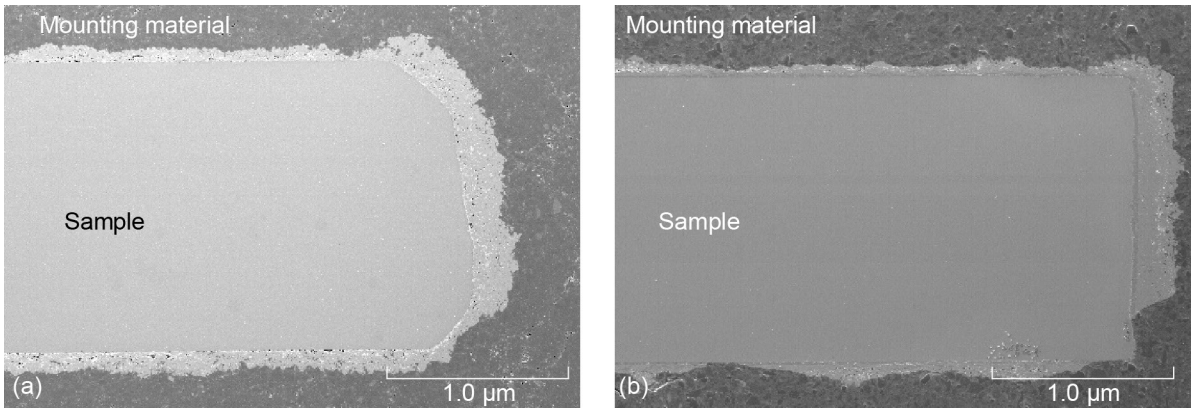


Figure 104.—Cross-sectional scanning electron microscopy images of 1018 steel samples coated with 4 mol% yttria-stabilized zirconia. (a) Unexposed. (b) Exposed to Venusian surface conditions for 10 days.

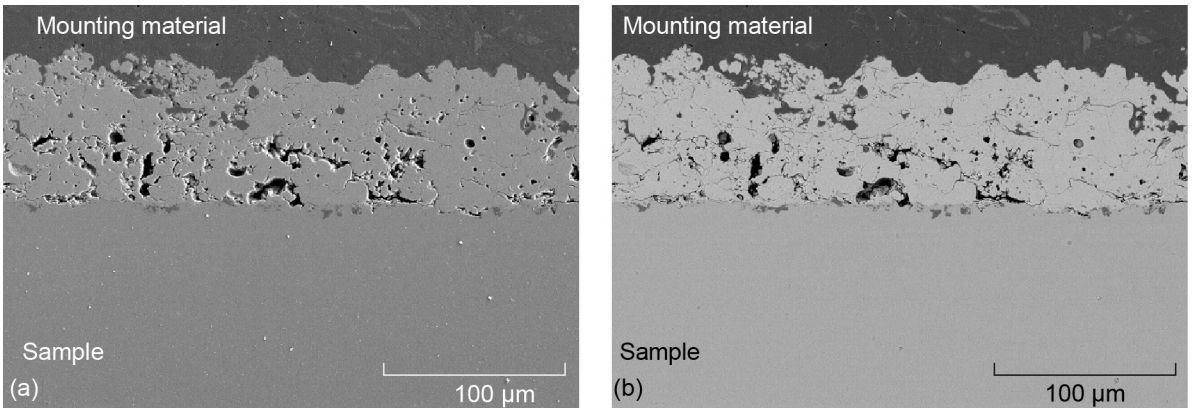


Figure 105.—Cross-sectional images of unexposed 1018 steel sample coated with 4 mol% yttria-stabilized zirconia. (a) Scanning electron microscopy image. (b) Backscattered-electron image.

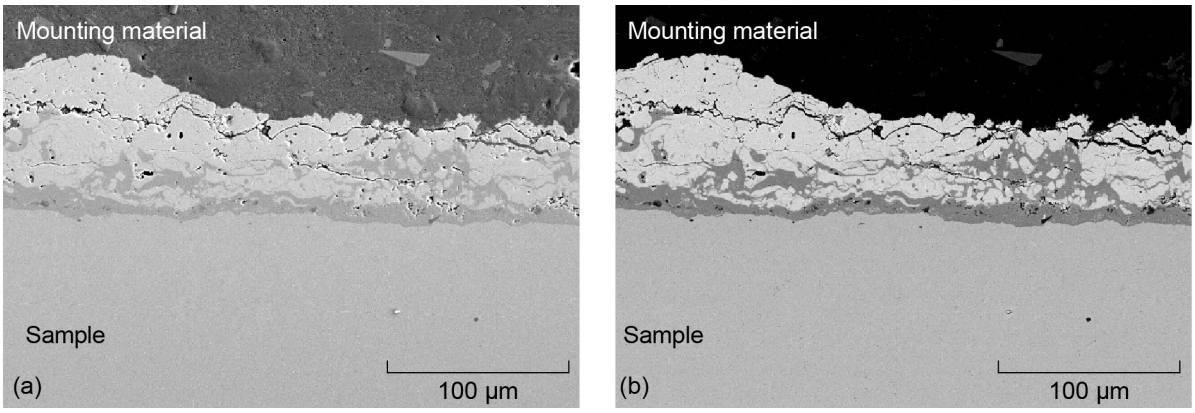


Figure 106.—Cross-sectional images of 1018 steel sample coated with 4 mol% yttria-stabilized zirconia, exposed to Venusian surface conditions for 10 days. (a) Scanning electron microscopy image. (b) Backscattered-electron image.

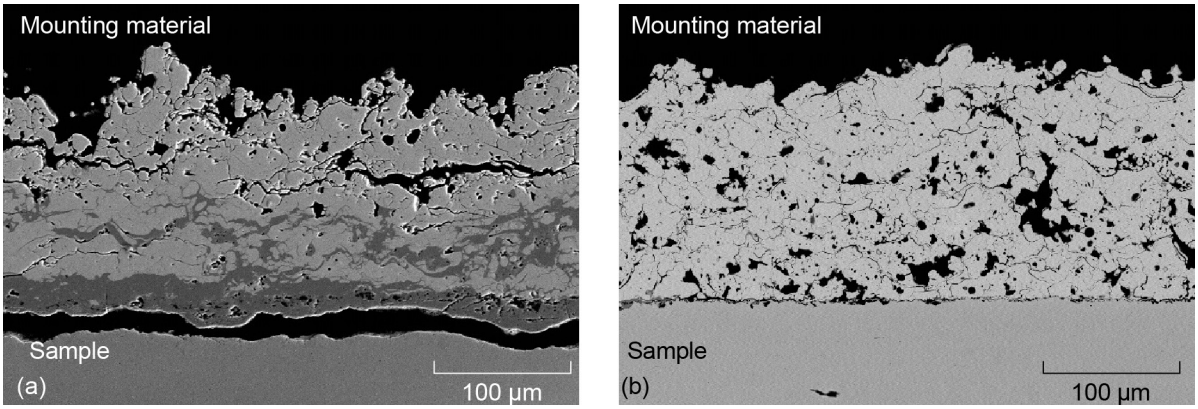


Figure 107.—Cross-sectional images of 1018 steel sample coated with 4 mol% yttria-stabilized zirconia, exposed to Venusian surface conditions for 42 days. (a) Scanning electron microscopy image. (b) Backscattered electron image.

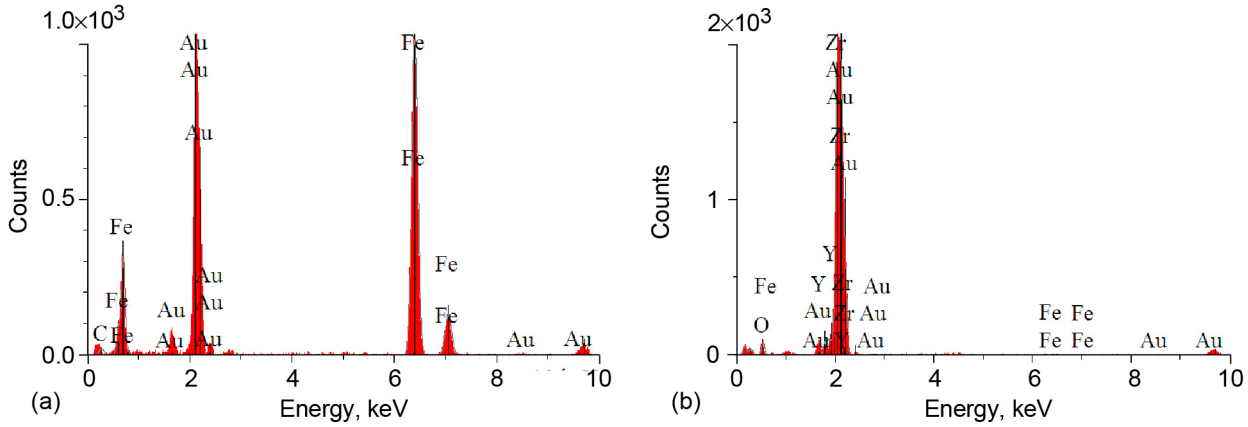


Figure 108.—Energy dispersive spectroscopy analysis of unexposed 1018 stainless steel sample coated with 4 mol% yttria-stabilized zirconia (Fig. 105). (a) Bulk. (b) Coating.

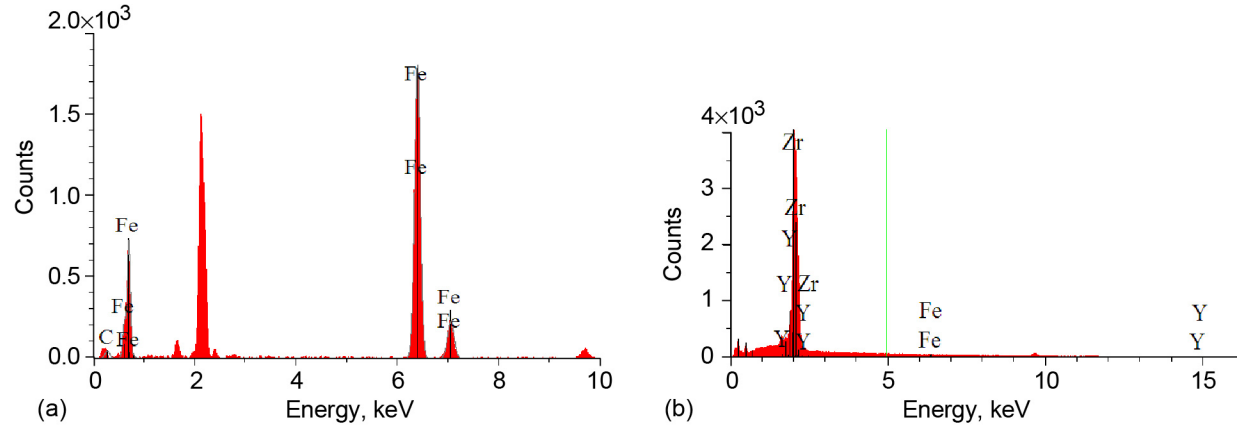


Figure 109.—Energy dispersive spectroscopy analysis of 1018 stainless steel sample coated with 4 mol% yttria-stabilized zirconia exposed to Venusian surface conditions for 10 days (Fig. 106). (a) Bulk. (b) Coating.

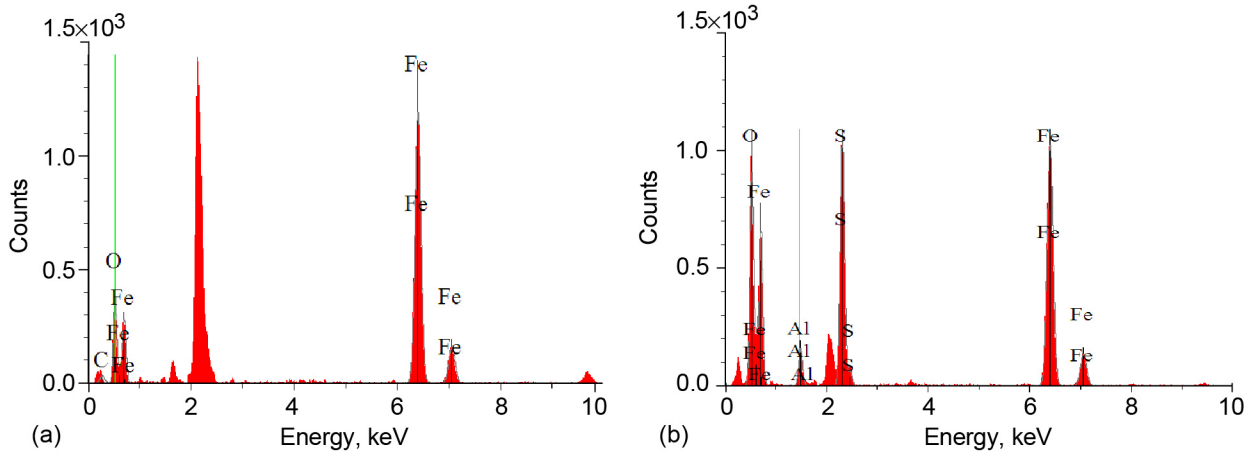


Figure 110.—Energy dispersive spectroscopy analysis of inner layer formed between bulk and coating of 1018 stainless steel sample coated with 4 mol% yttria-stabilized zirconia, exposed to Venusian surface conditions. (a) 10 days exposure (Fig. 106). (b) 42 days exposure (Fig. 107).

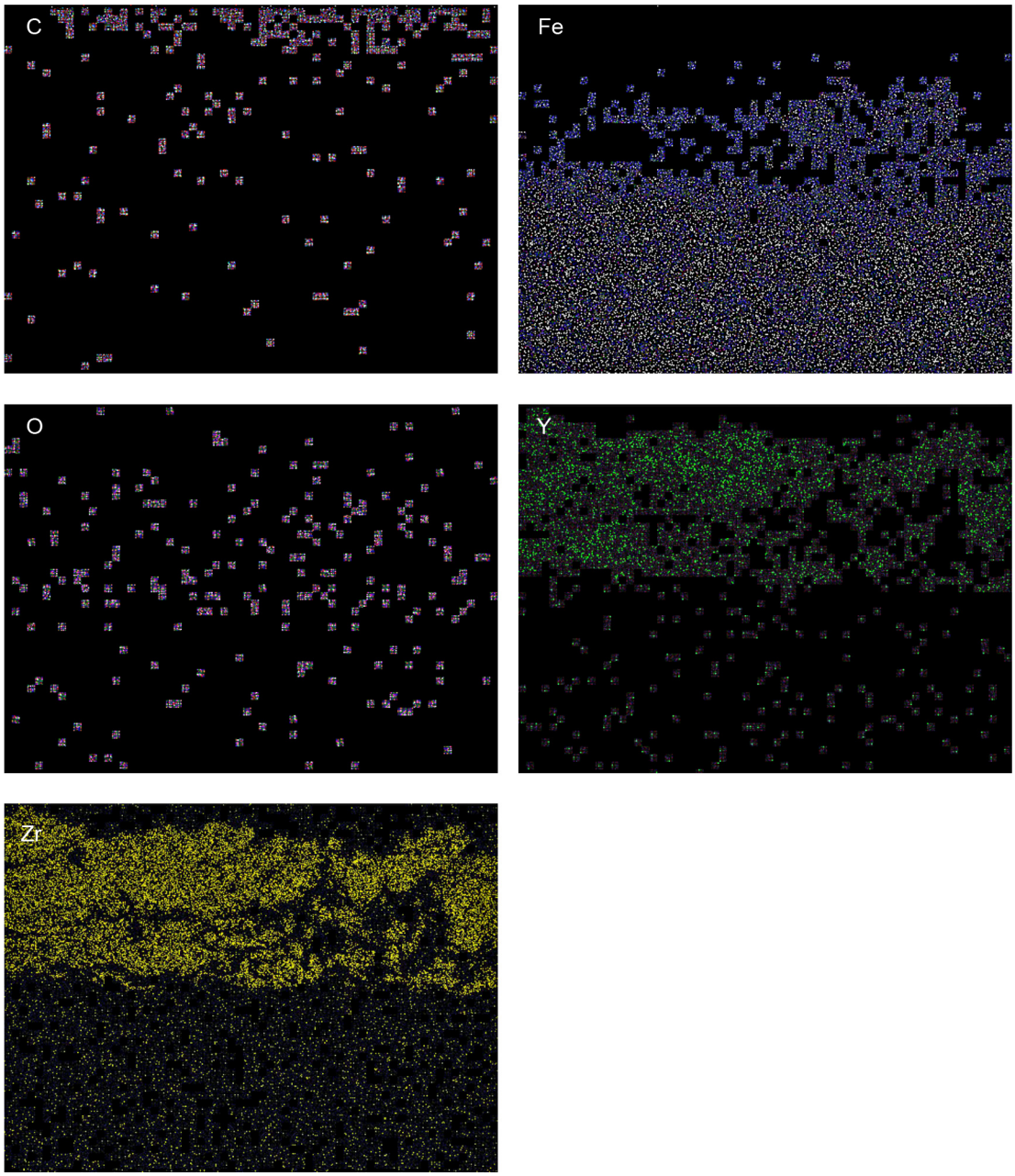


Figure 111.—X-ray elemental images of 1018 steel sample coated with 4 mol% yttria-stabilized zirconia, exposed to Venusian surface conditions for 10 days (area mapped is that of Fig. 106). Each pixel represents information gathered by spectrometer at C, Fe, O, Y, and Zr Kα line.

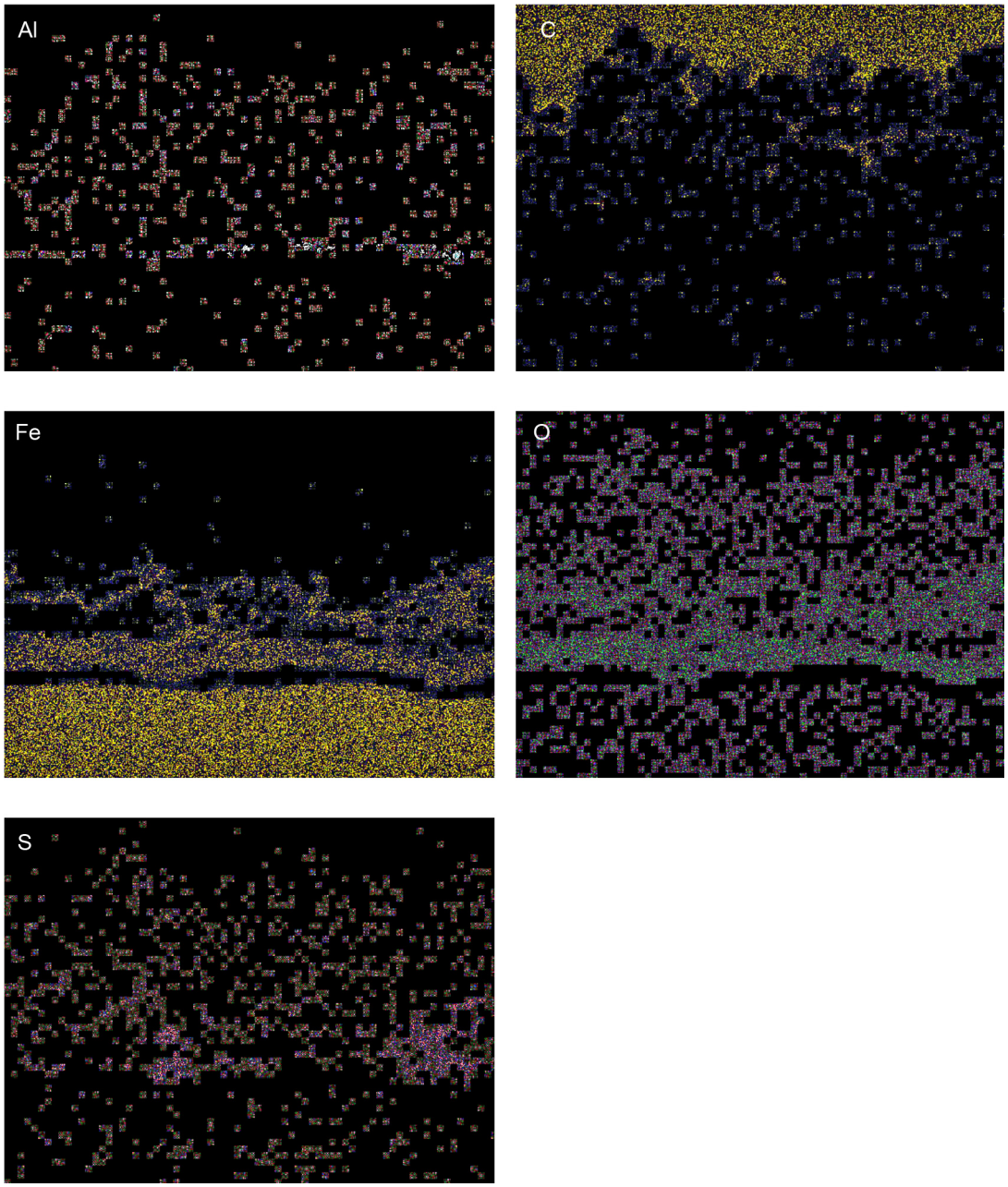


Figure 112.—X-ray elemental images of 1018 steel sample coated with 4 mol% yttria-stabilized zirconia, exposed to Venusian surface conditions for 42 days (area mapped is that of Fig. 107(a)). Each pixel represents information gathered by spectrometer at C, Fe, O, Y, and Zr K$\alpha$ line.

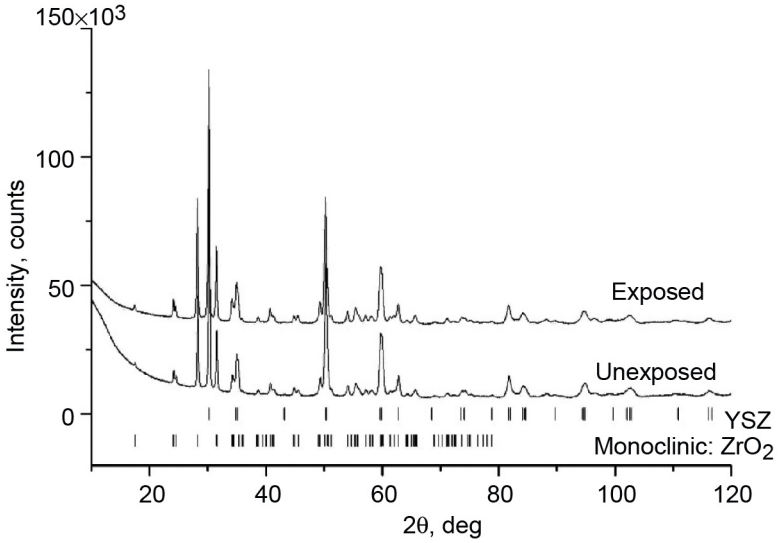


Figure 113.—X-ray diffraction patterns of unpolished side of 1018 steel samples coated with 4 mol% yttria-stabilized zirconia, unexposed and exposed to Venusian surface conditions for 42 days.

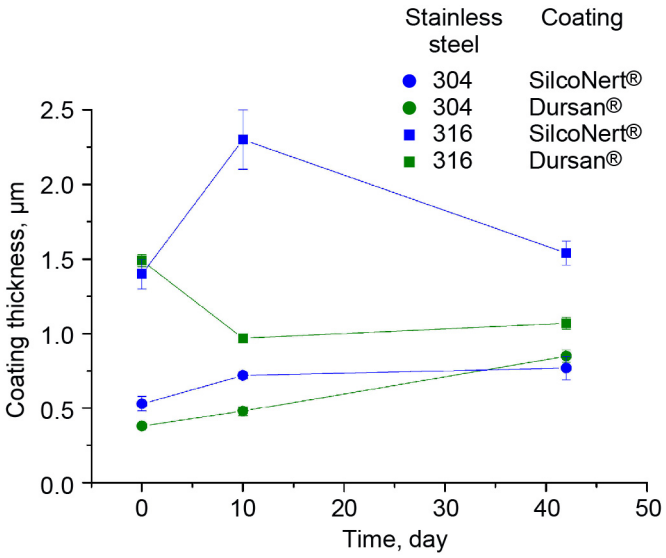


Figure 114.—Thicknesses of coatings on stainless steels 304 and 316 versus time exposed to Venusian surface conditions. Lines were added to data points to serve as a guide to the eyes.

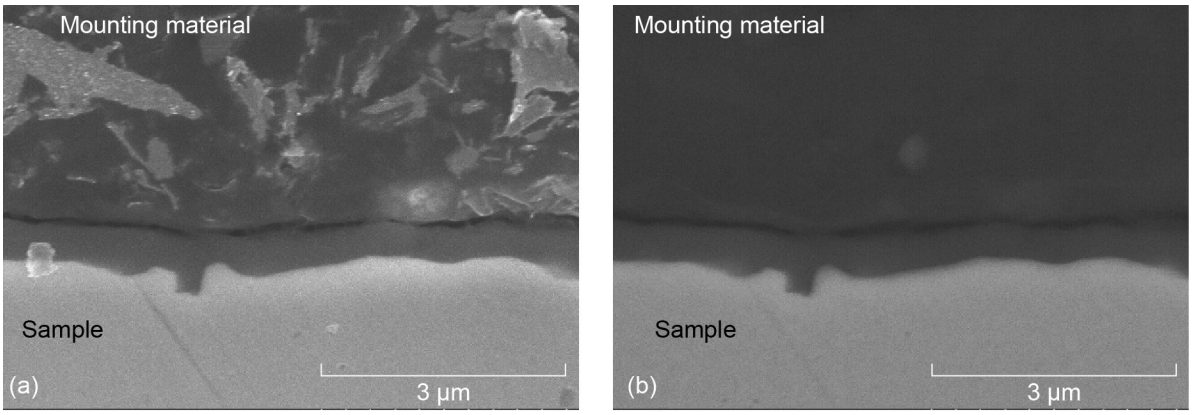


Figure 115.—Cross-sectional images of unexposed 304 stainless steel sample coated with Dursan® (SilcoTek Co.). (a) Scanning electron microscopy image. (b) Backscattered-electron image.

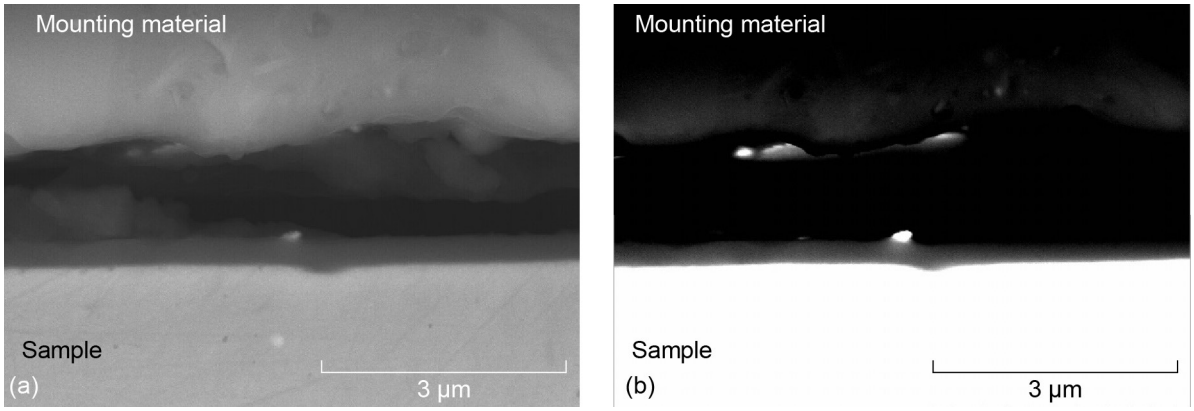


Figure 116.—Cross-sectional images of 304 stainless steel sample coated with Dursan® (SilcoTek Co.), exposed to Venusian surface conditions for 10 days. (a) Scanning electron microscopy image. (b) Backscattered-electron image.

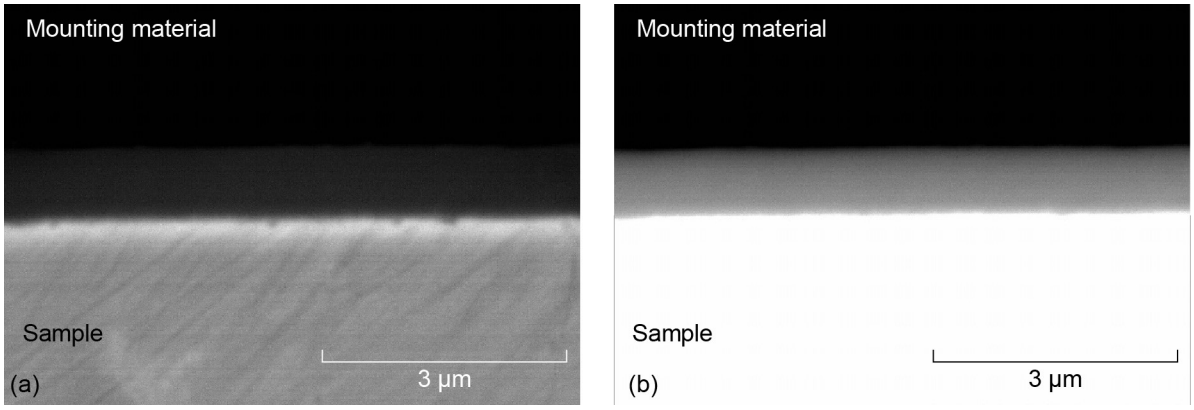


Figure 117.—Cross-sectional images of 304 stainless steel sample coated with Dursan® (SilcoTek Co.), exposed to Venusian surface conditions for 42 days. (a) Scanning electron microscopy image. (b) Backscattered-electron image.

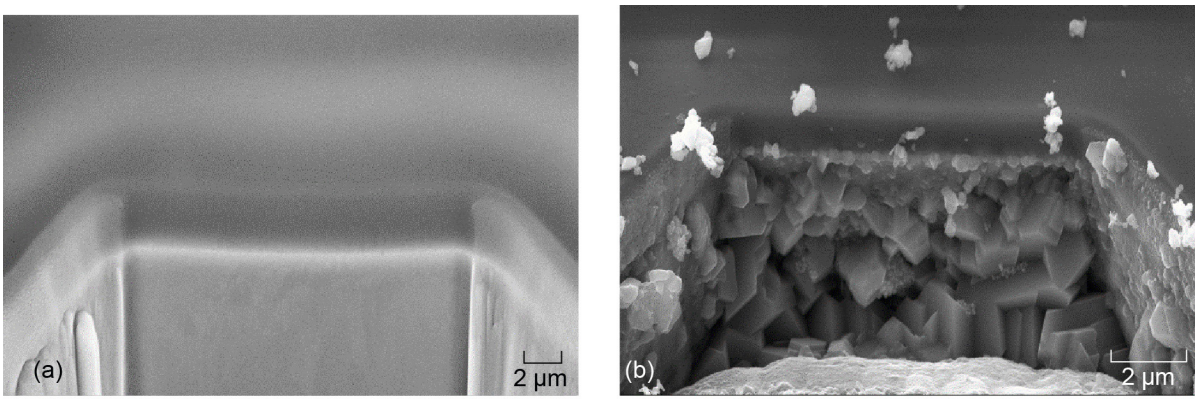


Figure 118.—Cross-sectional focused ion beam images of 304 stainless steel sample coated with Dursan® (SilcoTek Co.), before and after exposure to Venusian surface conditions for 21 days. (a) Before. (b) After.

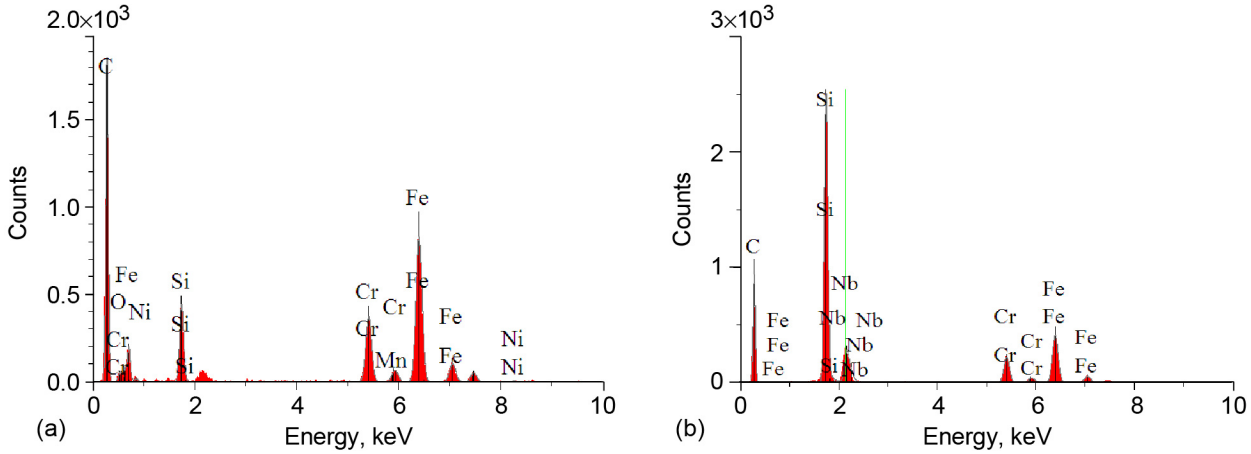


Figure 119.—Energy dispersive spectroscopy analysis of 304 stainless steel sample coated with Dursan® (SilcoTek Co.), exposed to Venusian surface conditions for 10 days (Fig. 116). (a) Bulk. (b) Coating.

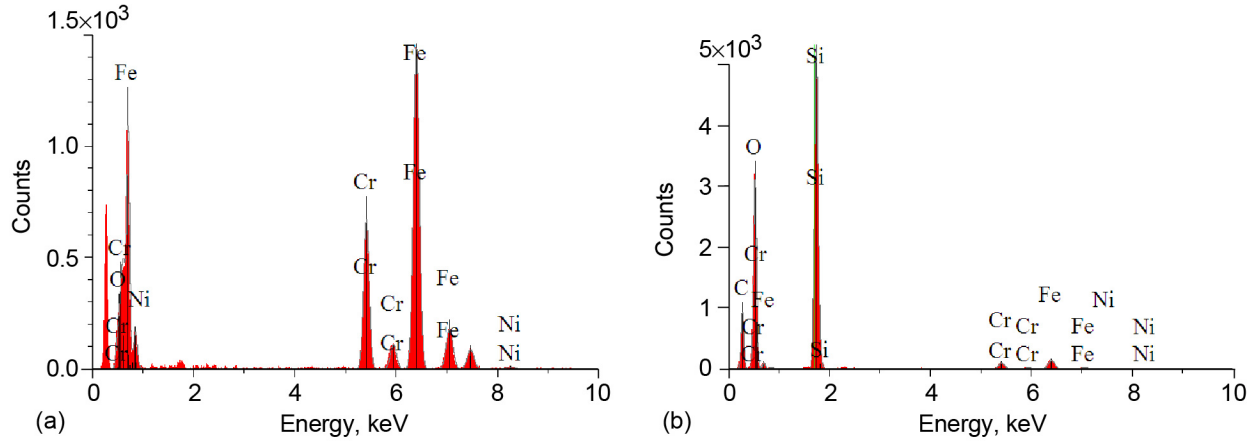


Figure 120.—Energy dispersive spectroscopy analysis of 304 stainless steel sample coated with Dursan®, exposed to Venusian surface conditions for 42 days (Fig. 117). (a) Bulk. (b) Coating.

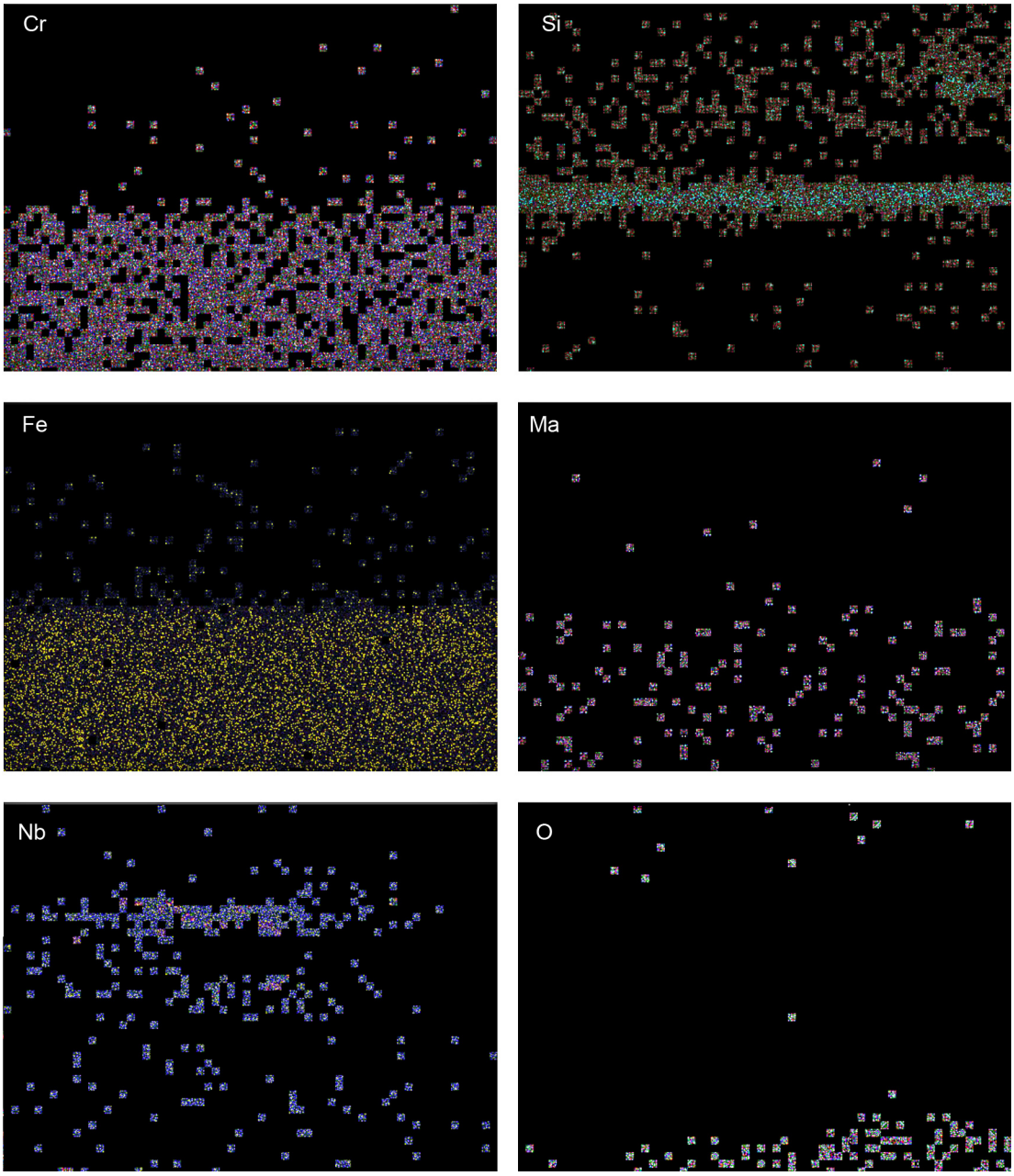


Figure 121.—X-ray elemental images of 304 stainless steel sample coated with Dursan® (SilcoTek Co.), exposed to Venusian surface conditions for 10 days (area mapped is that of Fig. 116). Each pixel represents information gathered by spectrometer at O, Si, Cr, Mn, Fe, and Ni Kα line and at Nb Lα line.

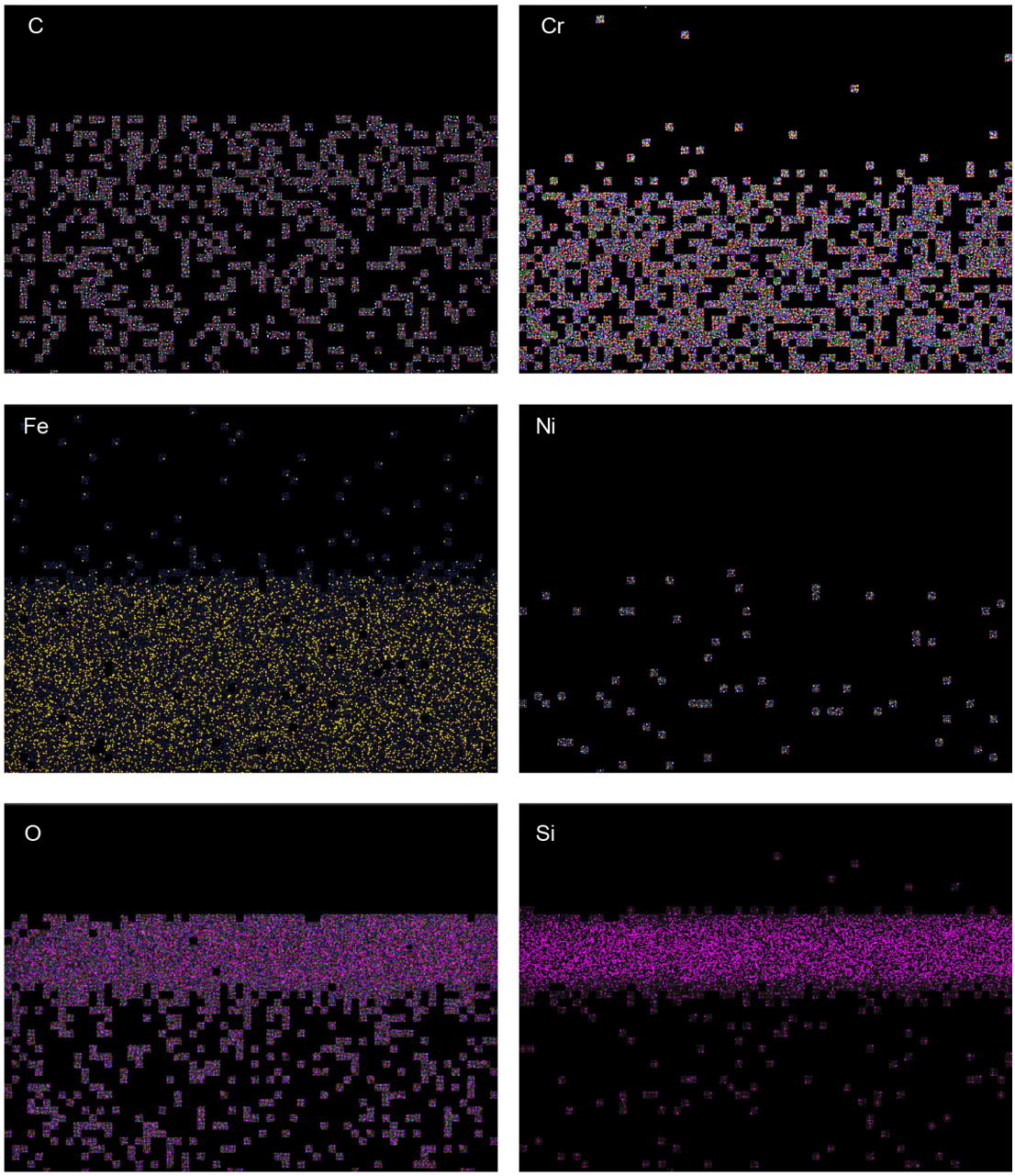


Figure 122.—X-ray elemental images of 304 stainless steel sample coated with Dursan® (SilcoTek Co.), exposed to Venusian surface conditions for 42 days (area mapped is that of Fig. 117). Each pixel represents information gathered by spectrometer at C, O, Si, Cr, Mn, Fe, and Ni Kα line and at Nb Lα line.

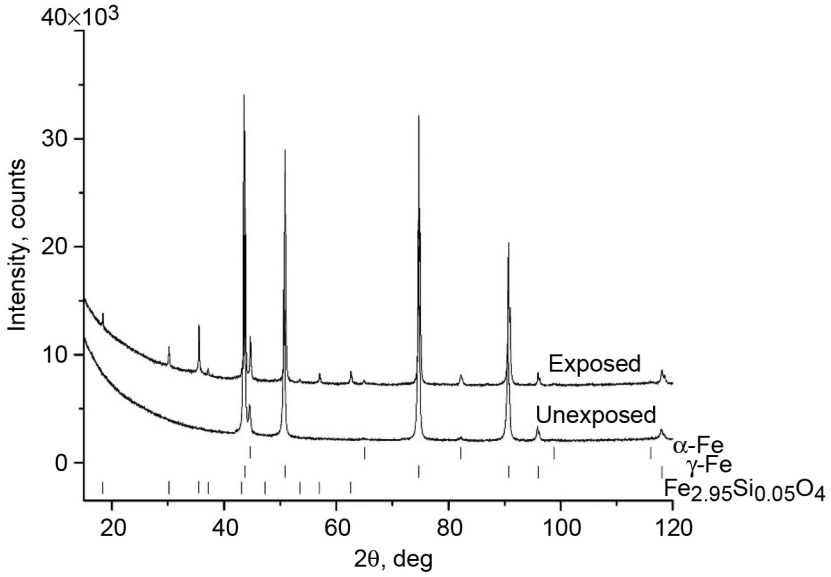


Figure 123.—X-ray diffraction patterns of unpolished side of 304 stainless steel samples coated with Dursan® (SilcoTek Co.), unexposed and exposed to Venusian surface conditions for 42 days.

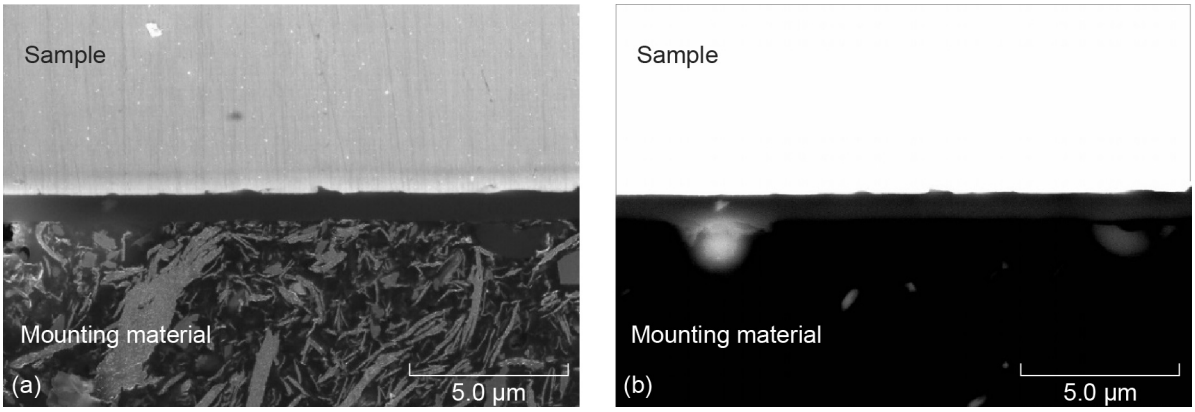


Figure 124.—Cross-sectional images of unexposed 316 stainless steel sample coated with Dursan® (SilcoTek Co.). (a) Scanning electron microscopy image. (b) Backscattered-electron image.

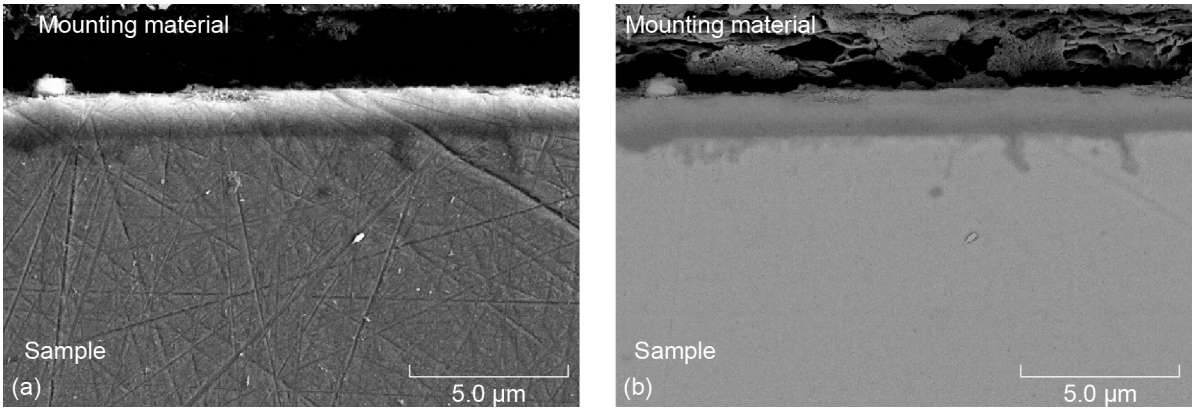


Figure 125.—Cross-sectional images of 316 stainless steel sample coated with Dursan® (SilcoTek Co.), exposed to Venusian surface conditions for 10 days. (a) Scanning electron microscopy image. (b) Backscattered-electron image.

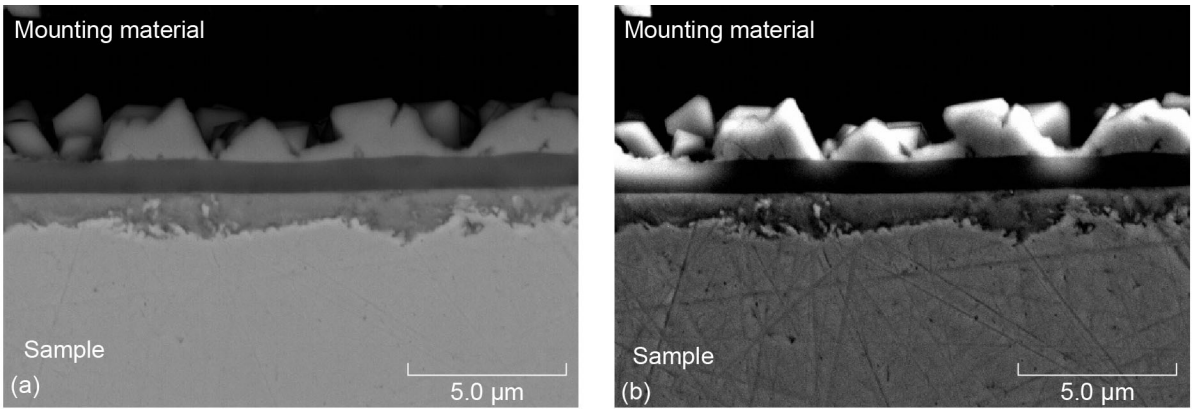


Figure 126.—Cross-sectional images of 316 stainless steel sample coated with Dursan® (SilcoTek Co.), exposed to Venusian surface conditions for 42 days. (a) Scanning electron microscopy image. (b) Backscattered-electron image.

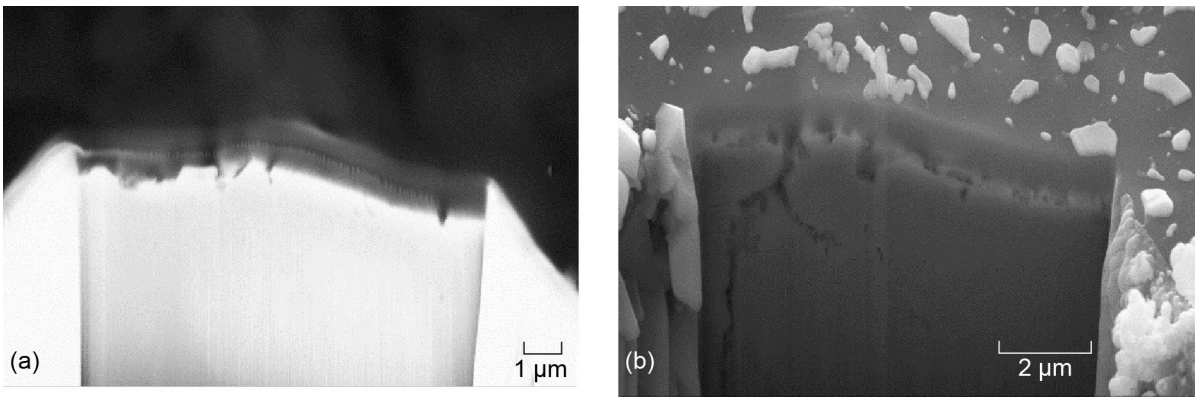


Figure 127.—Cross-sectional focused ion beam images of 316 stainless steel sample coated with Dursan® (SilcoTek Co.), before and after exposure to Venusian surface conditions for 21 days. (a) Before. (b) After.

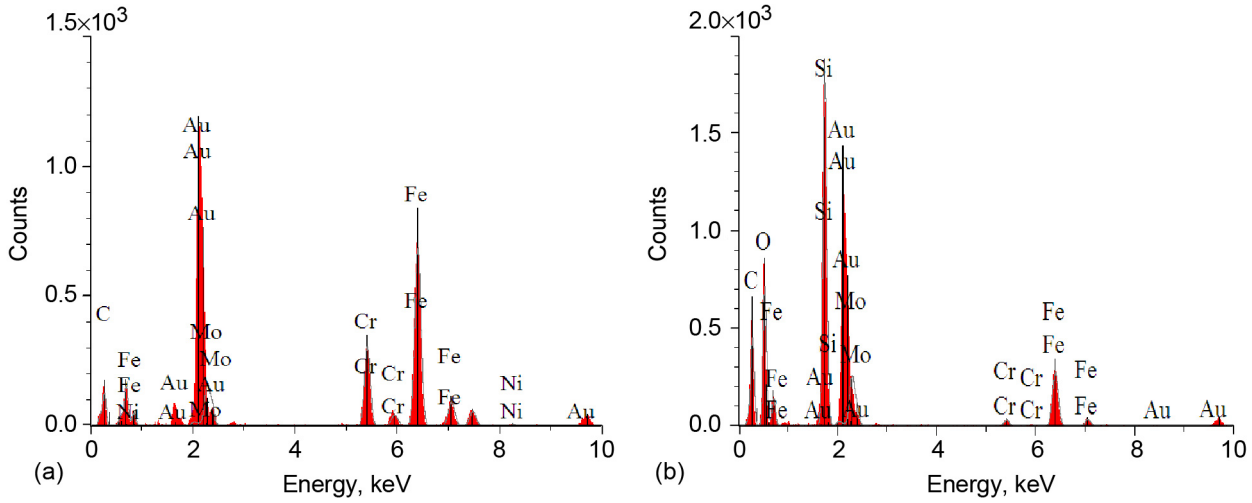


Figure 128.—Energy dispersive spectroscopy analysis of 316 stainless steel sample coated with Dursan® (SilcoTek Co.), exposed to Venusian surface conditions for 10 days (Fig. 125). (a) Bulk. (b) Coating.

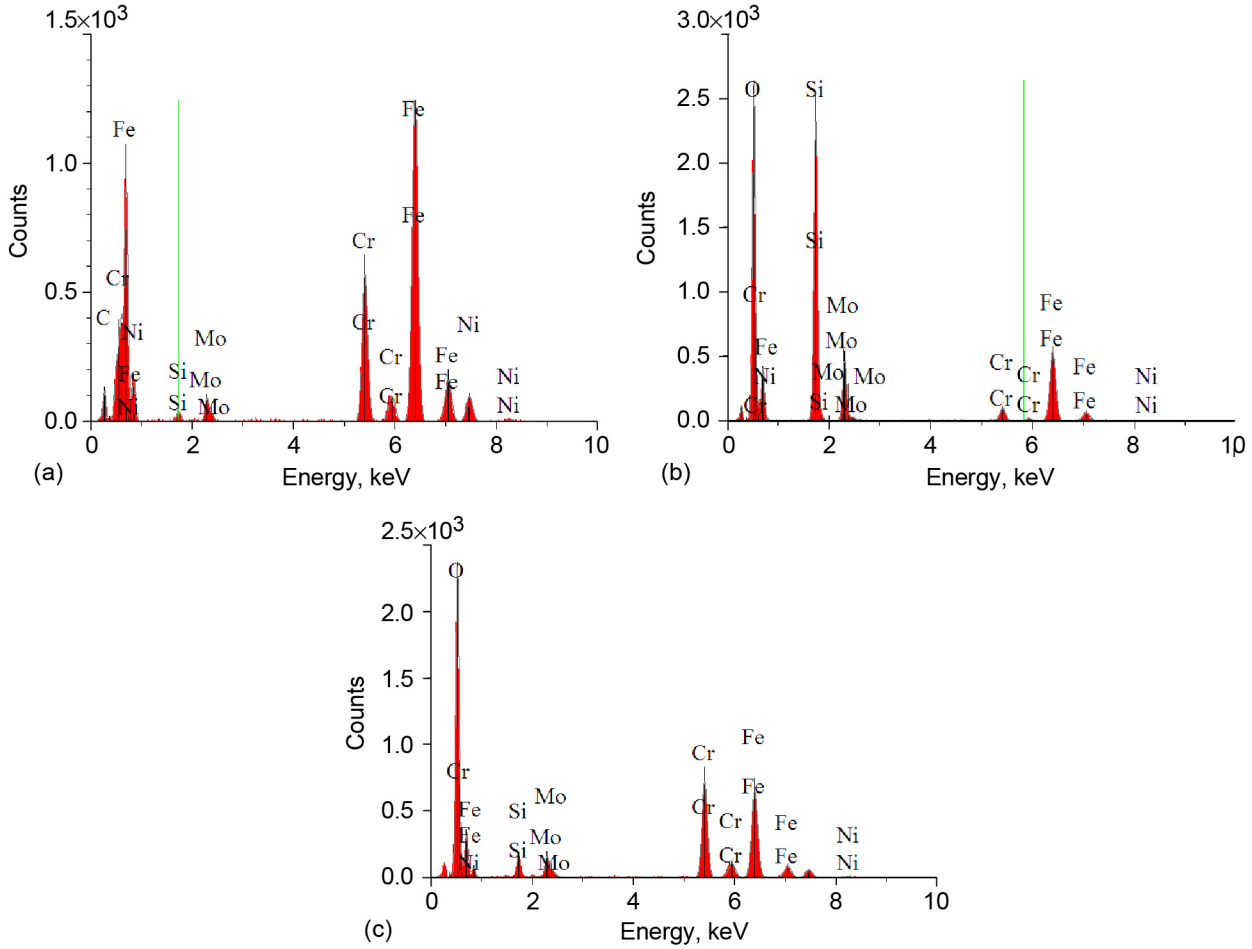


Figure 129.—Energy dispersive spectroscopy analysis of 316 stainless steel sample coated with Dursan® (SilcoTek Co.), exposed to Venusian surface conditions for 42 days (Fig. 126). (a) Bulk. (b) Coating. (c) Inner layer between them.

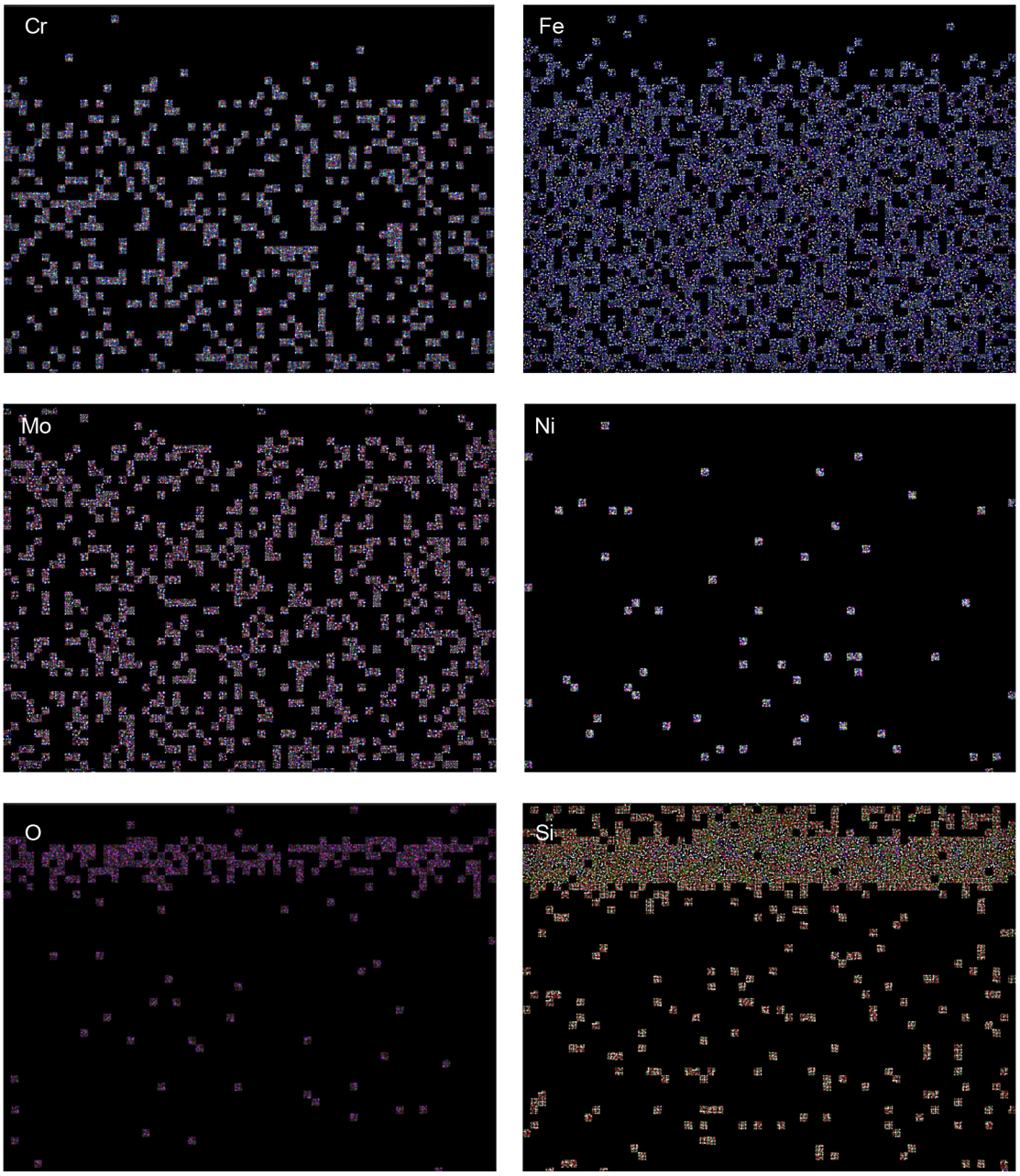


Figure 130.—X-ray elemental images of 316 stainless steel sample coated with Dursan® (SilcoTek Co.), exposed to Venusian surface conditions for 10 days (area mapped is that of Fig. 125). Each pixel represents information gathered by spectrometer at O, Si, Cr, Fe, and Ni Kα line and at Mo Lα line.

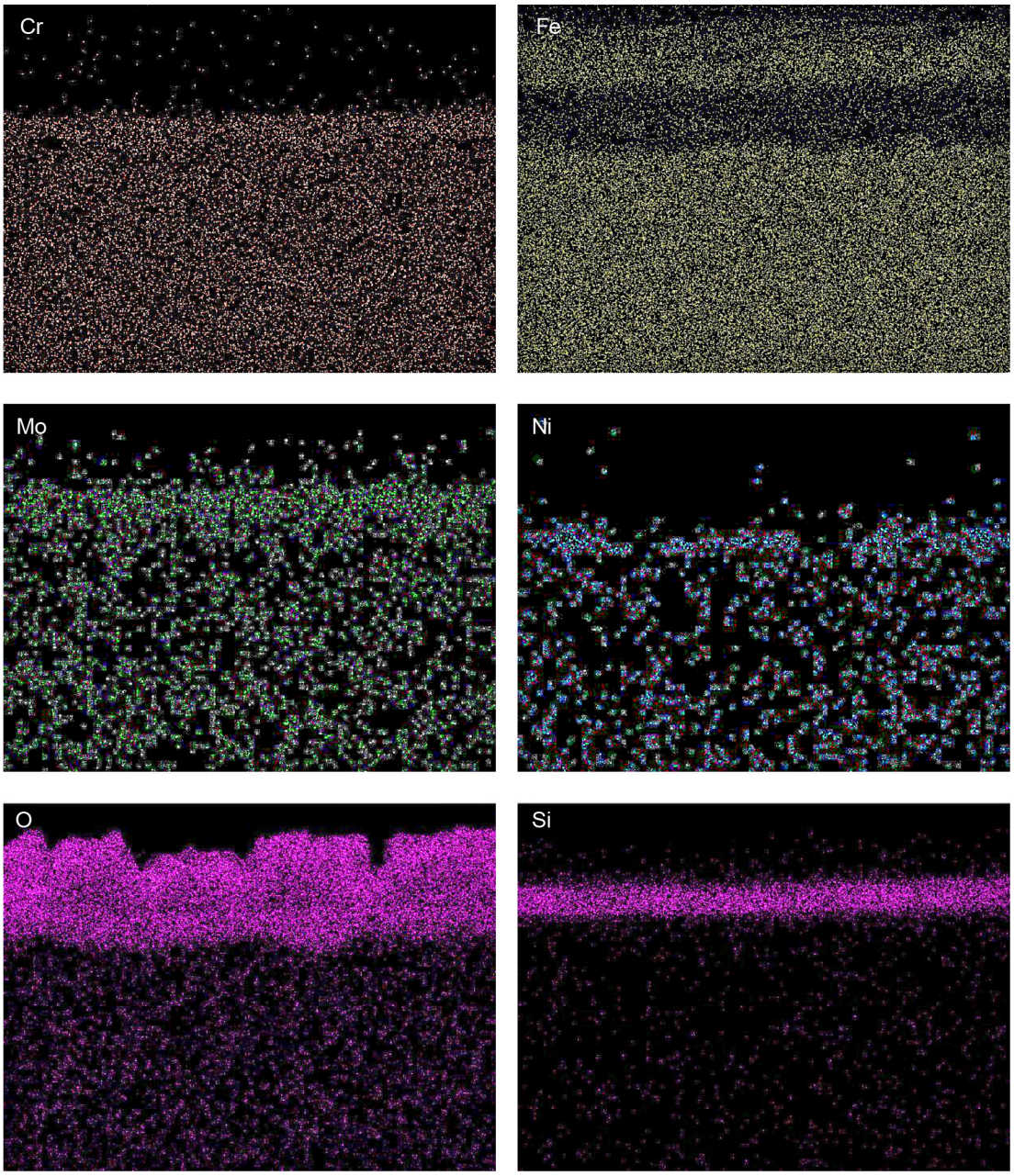


Figure 131.—X-ray elemental images of 316 stainless steel sample coated with Dursan® (SilcoTek Co.), exposed to Venusian surface conditions for 42 days (area mapped is that of Fig. 126). Each pixel represents information gathered by spectrometer at O, Si, Cr, Fe, and Ni Kα line and at Mo Lα line.

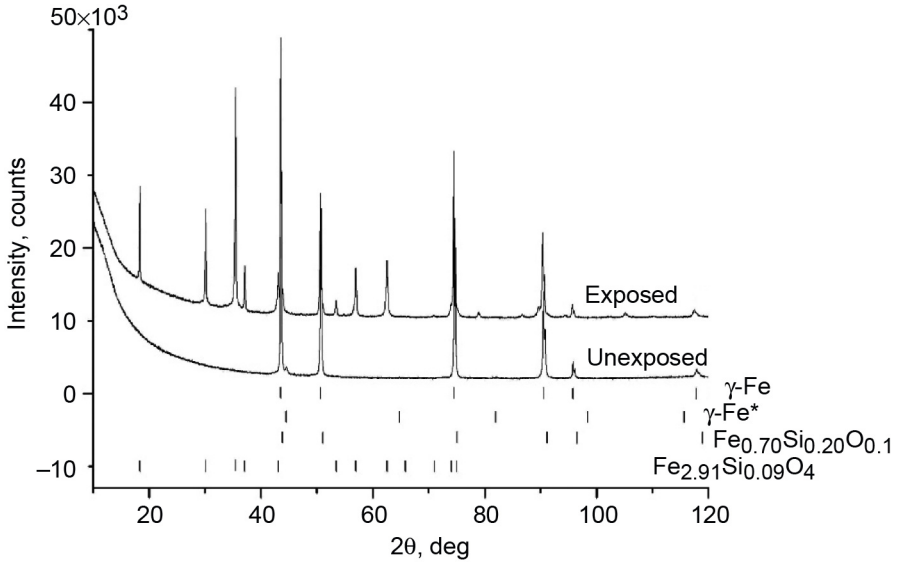


Figure 132.—X-ray diffraction patterns of the 316 stainless steel samples coated with Dursan® (SilcoTek Co.), unexposed and exposed to Venusian surface conditions for 42 days.

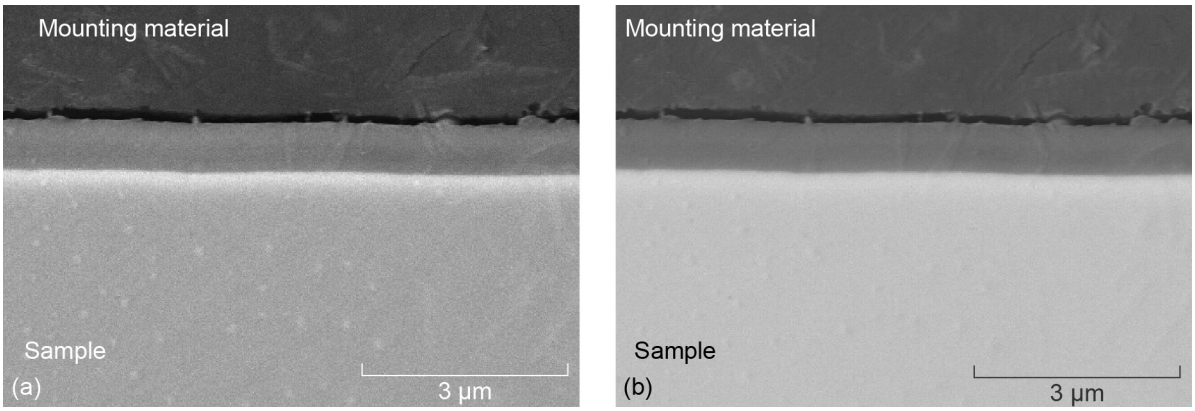


Figure 133.—Cross-sectional images of unexposed 304 stainless steel sample coated with SilcoNert® 1040 (SilcoTek Co.). (a) Scanning electron microscopy image. (b) Backscattered-electron image.

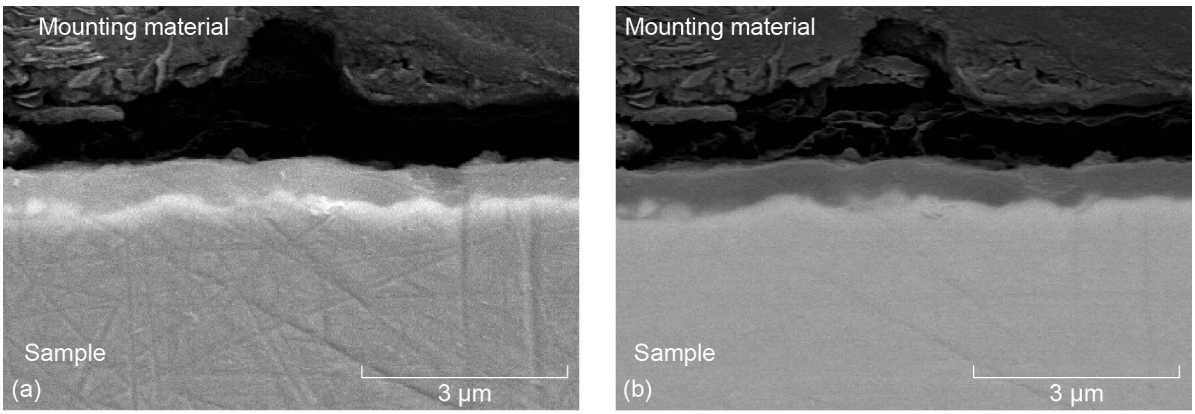


Figure 134.—Cross-sectional images of 304 stainless steel sample coated with SilcoNert® 1040 (SilcoTek Co.), exposed to Venusian surface conditions for 10 days. (a) Scanning electron microscopy image. (b) Backscattered-electron image.

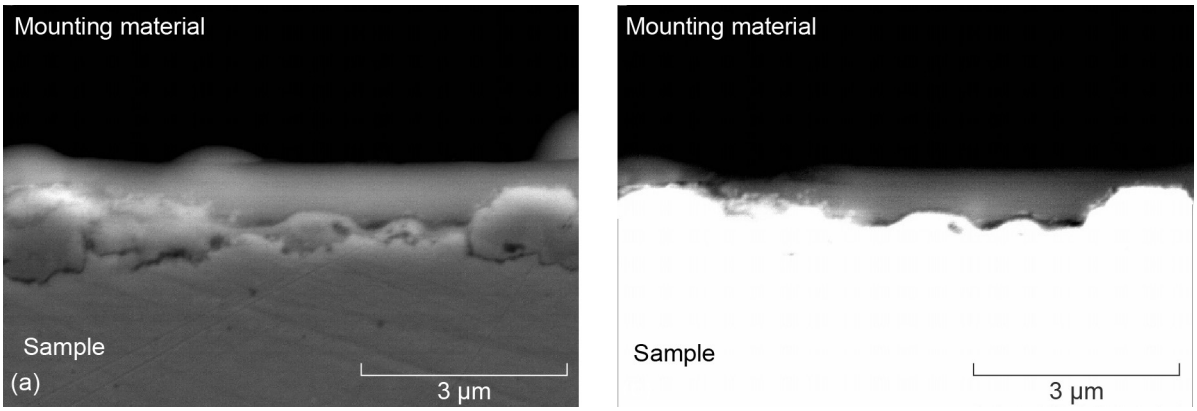


Figure 135.—Cross-sectional images of 304 stainless steel sample coated with SilcoNert® 1040 (SilcoTek Co.), exposed to Venusian surface conditions for 42 days. (a) Scanning electron microscopy image. (b) Backscattered-electron image.

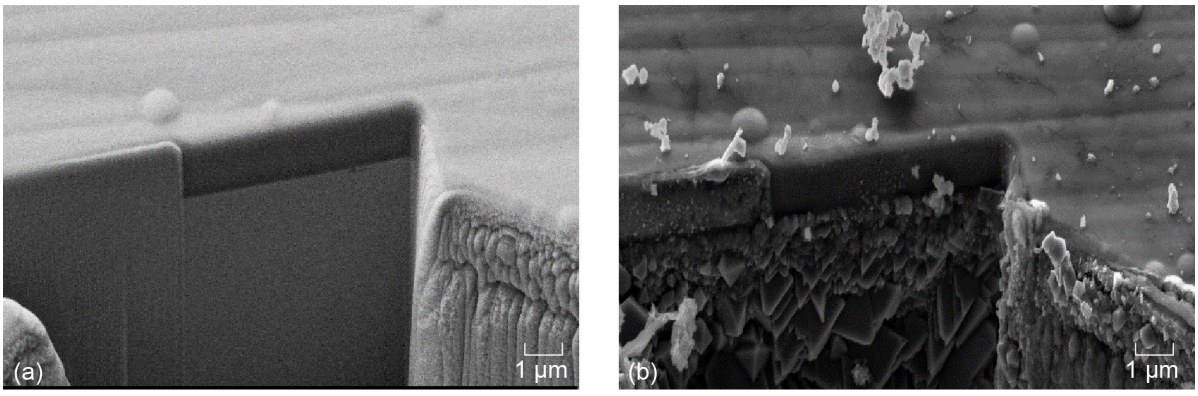


Figure 136.—Cross-sectional focused ion beam images of 304 stainless steel sample coated with SilcoNert® 1040 (SilcoTek Co.), before and after exposure to Venusian surface conditions for 21 days. (a) Before. (b) After.

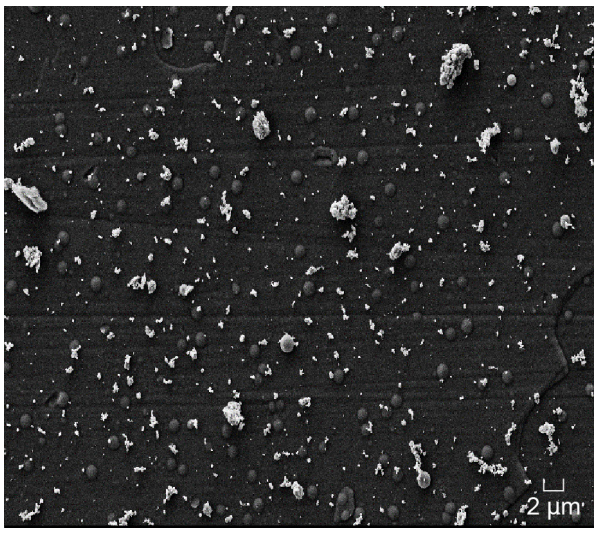


Figure 137.—Scanning electron microscopy image of surface of 304 stainless steel coated with SilcoNert® 1040 (SilcoTek Co.), exposed to Venusian surface conditions for 21 days.

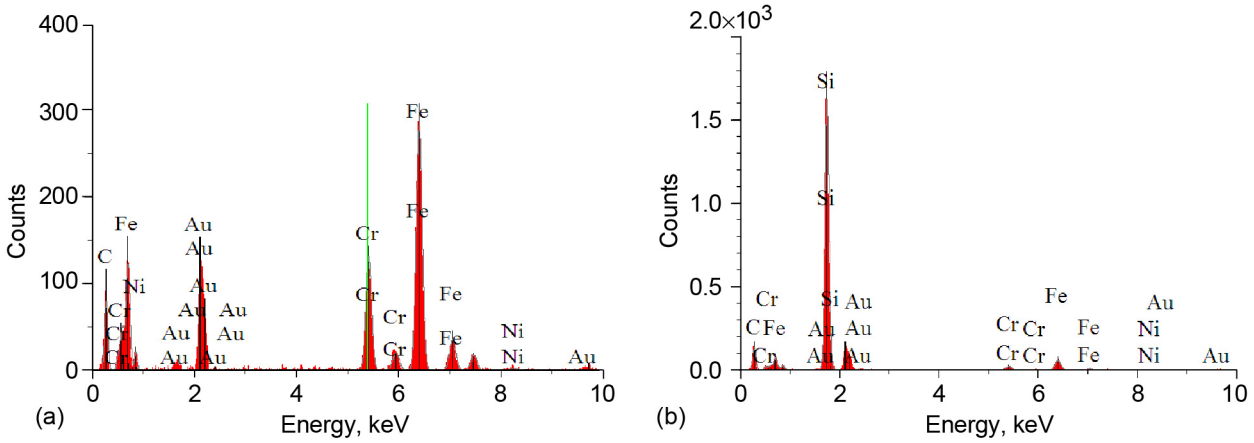


Figure 138.—Energy dispersive spectroscopy analysis of 304 stainless steel coated with SilcoNert® 1040 (SilcoTek Co.), exposed to Venusian surface conditions for 10 days (Fig. 134). (a) Bulk. (b) Coating.

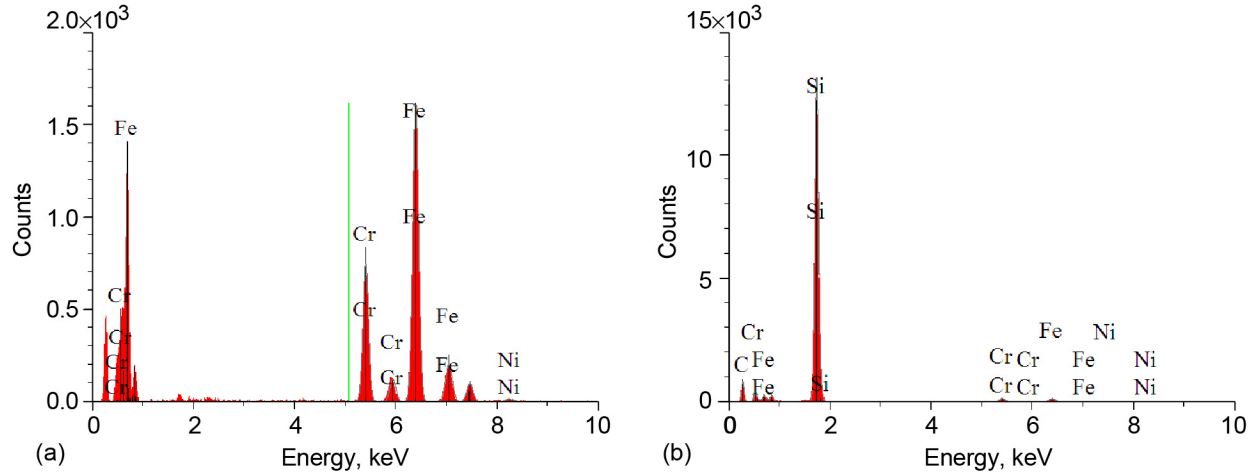


Figure 139.—Energy dispersive spectroscopy analysis of 304 stainless steel coated with SilcoNert® 1040 (SilcoTek Co.), exposed to Venusian surface conditions for 42 days (Fig. 135). (a) Bulk. (b) Coating.

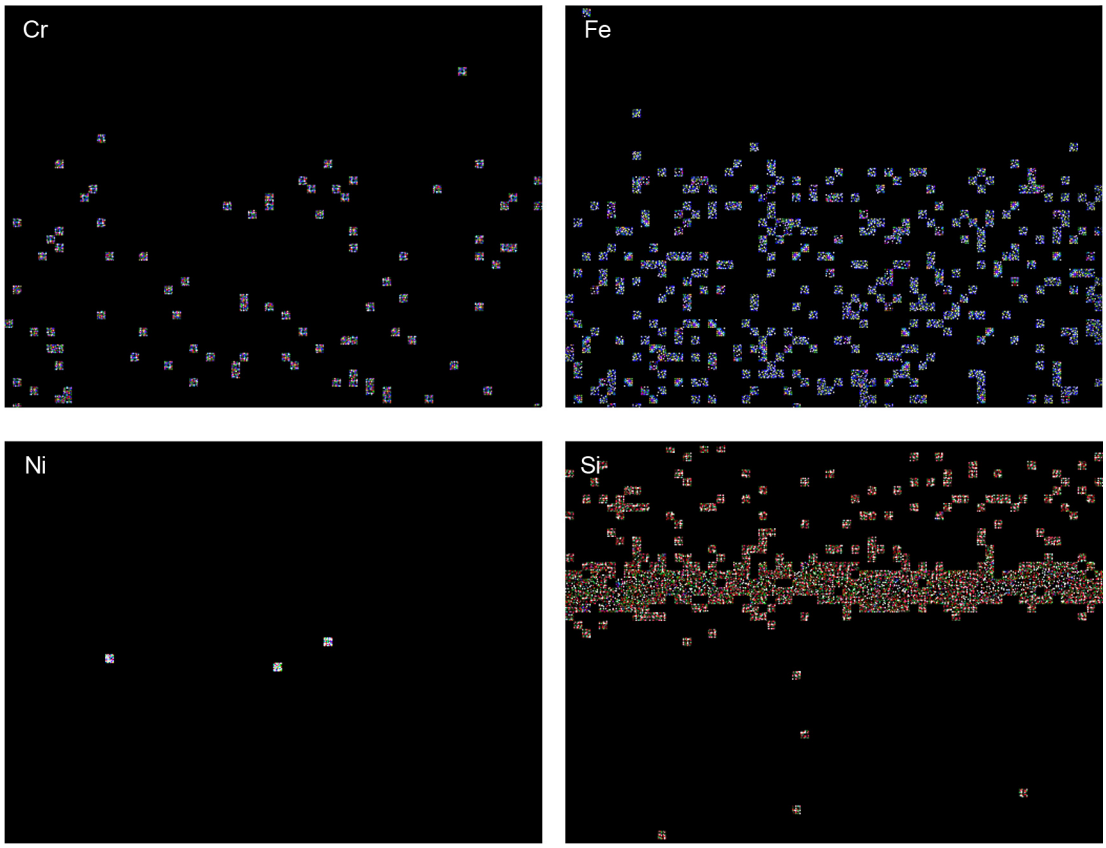


Figure 140.—X-ray elemental images of 304 stainless steel coated with SilcoNert® 1040 (SilcoTek Co.), exposed to Venusian surface conditions for 10 days (area mapped is that of Fig. 134). Each pixel represents information gathered by spectrometer at C, Si, Cr, Fe, and Ni Kα line.

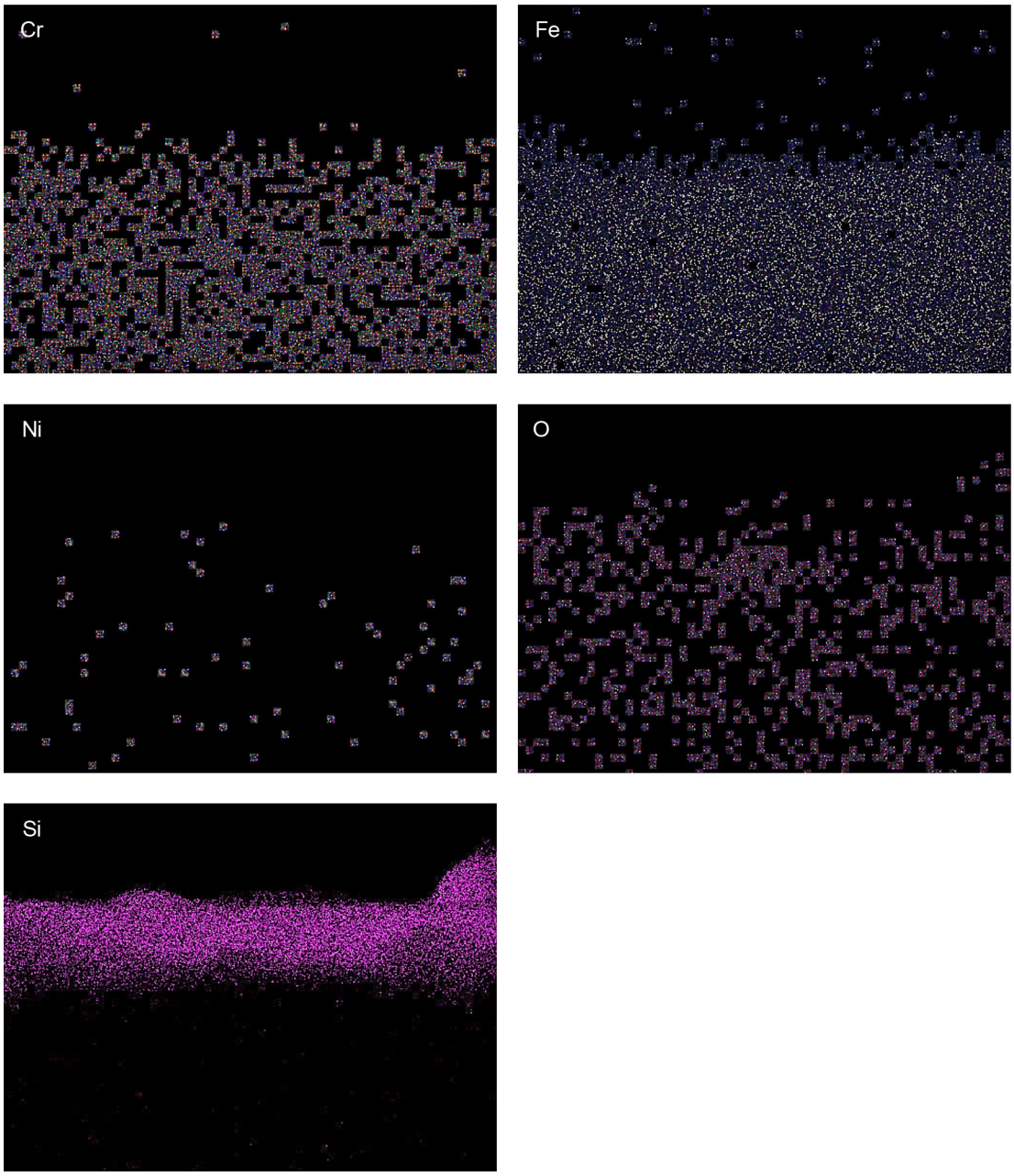


Figure 141.—X-ray elemental images of 304 stainless steel coated with SilcoNert® 1040 (SilcoTek Co.), exposed to Venusian surface conditions for 42 days (area mapped is that of Fig. 135). Each pixel represents information gathered by spectrometer at O, C, Si, Cr, Fe, and Ni Kα line.

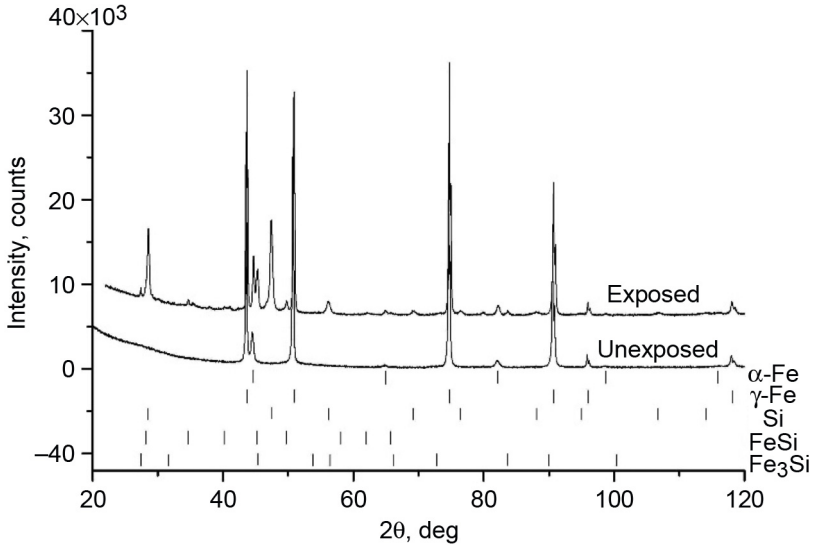


Figure 142.—X-ray diffraction patterns of unpolished side of 304 stainless steel coated with SilcoNert® 1040 (SilcoTek Co.), unexposed and exposed to Venusian surface conditions for 42 days.

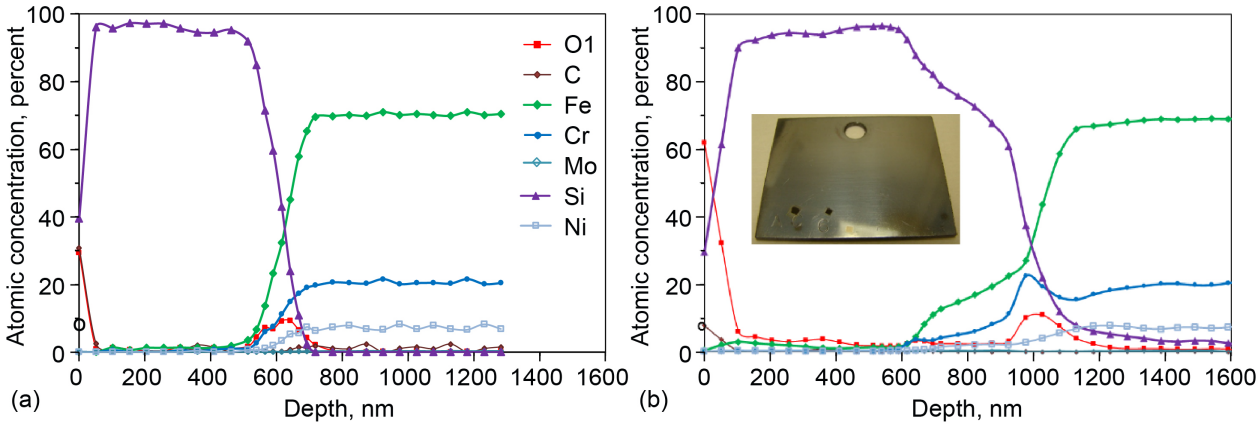


Figure 143.—X-ray photoelectron spectroscopy depth profile using high-resolution regions of stainless steel 304 sample polished side coated with SilcoNert® 1040 (SilcoTek Co.), before and after exposure to Venusian surface conditions for 21 days. (a) Before. (b) After.

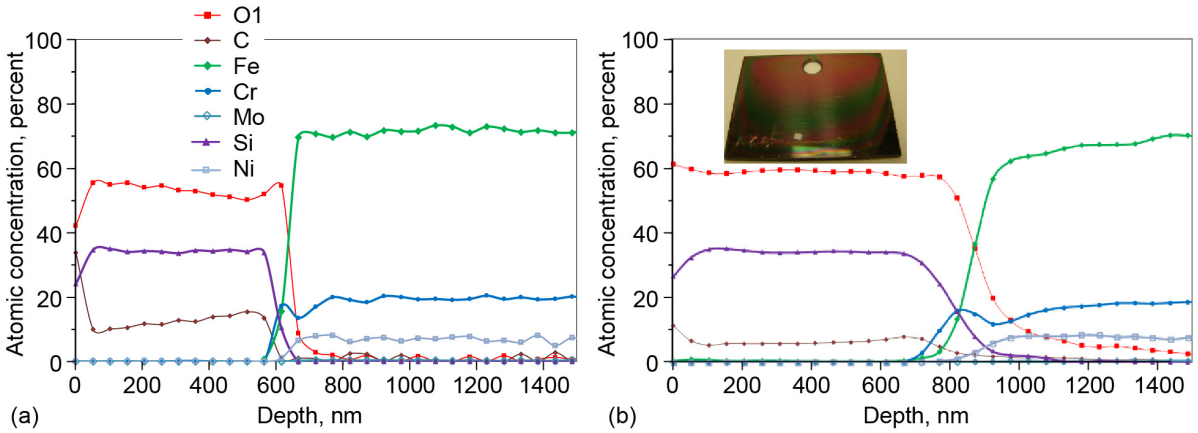


Figure 144.—X-ray photoelectron spectroscopy depth profile using high-resolution regions of stainless steel 304 sample polished side coated with Dursan® (SilcoTek Co.), before and after exposure to Venusian surface conditions for 21 days. (a) Before. (b) After.

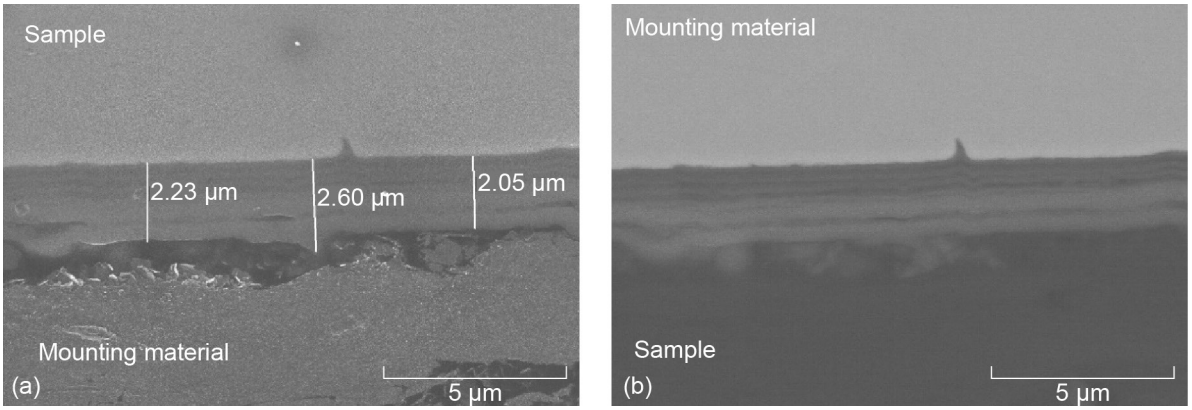


Figure 145.—Cross-sectional images of unexposed 316 stainless steel coated with SilcoNert® 1040 (SilcoTek Co.). (a) Scanning electron microscopy image. (b) Backscattered-electron image.

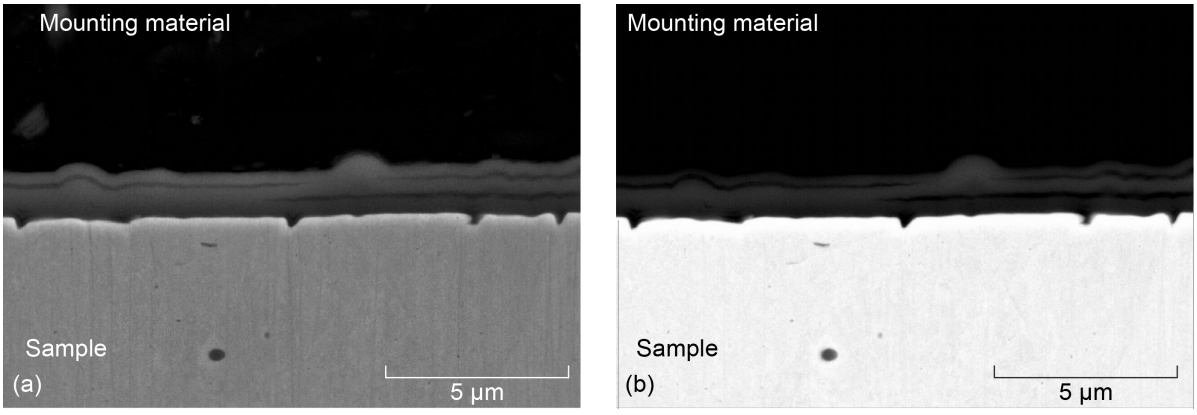


Figure 146.—Cross-sectional images of 316 stainless steel coated with SilcoNert® 1040 (SilcoTek Co.), exposed to Venusian surface conditions for 10 days. (a) Scanning electron microscopy image. (b) Backscattered-electron image.

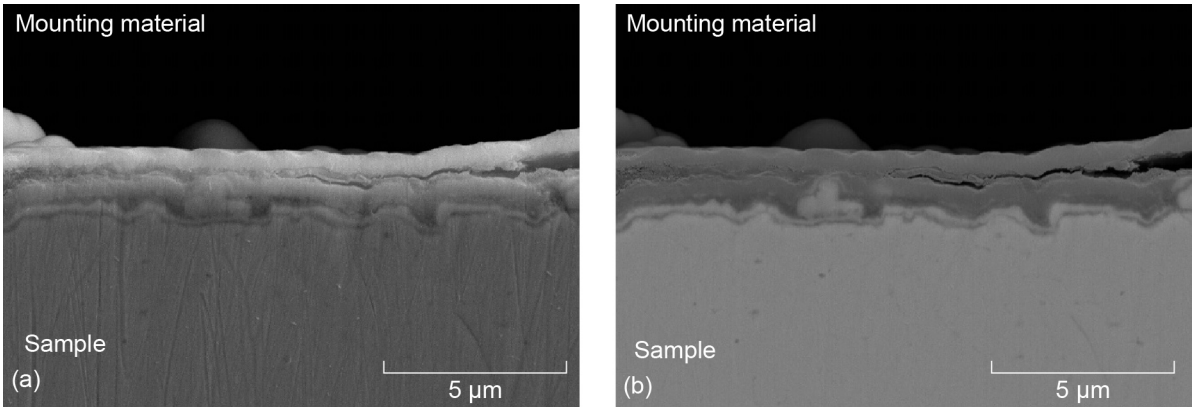


Figure 147.—Cross-sectional images of 316 stainless steel coated with SilcoNert® 1040 (SilcoTek Co.), exposed to Venusian surface conditions for 42 days. (a) Scanning electron microscopy image. (b) Backscattered-electron image.

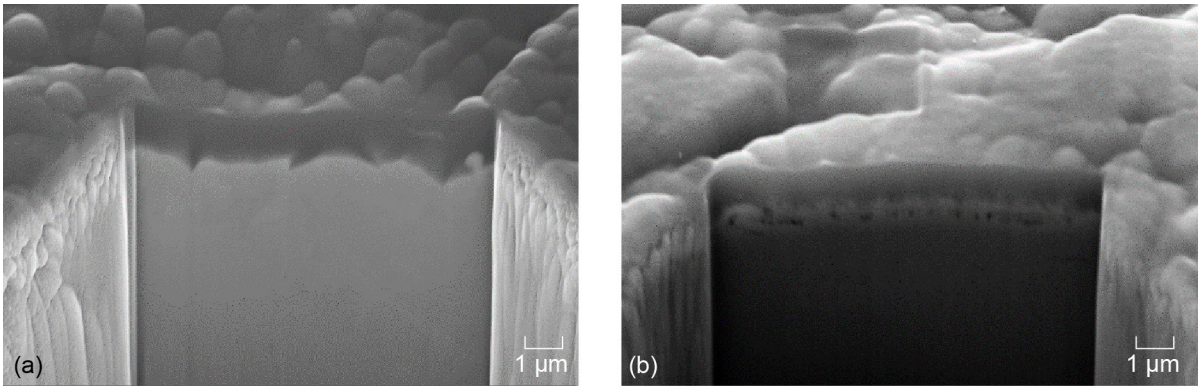


Figure 148.—Cross-sectional focused ion beam images of 316 stainless steel coated with SilcoNert® 1040 (SilcoTek Co.), before and after exposure to Venusian surface conditions for 21 days. (a) Before. (b) After.

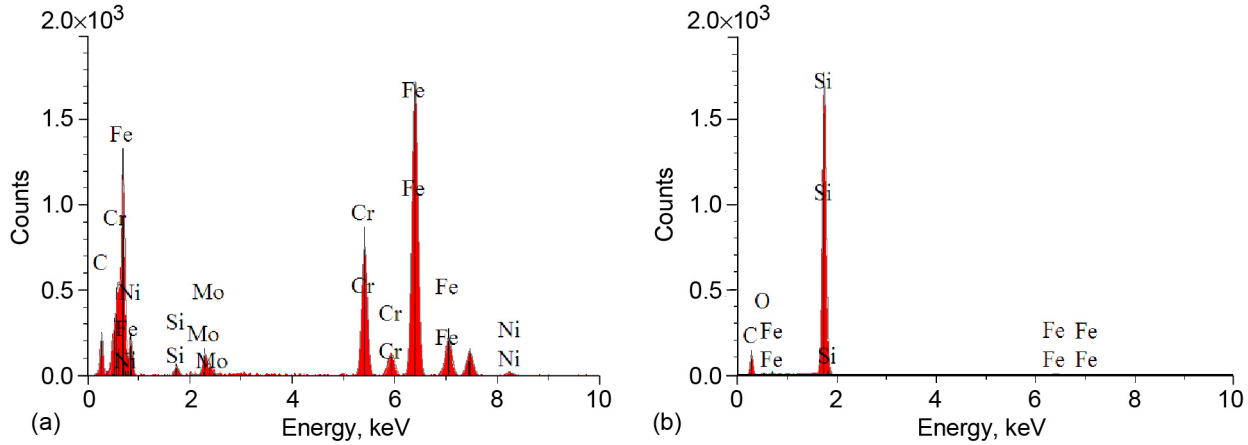


Figure 149.—Energy dispersive spectroscopy analysis of 316 stainless steel coated with SilcoNert® 1040 (SilcoTek Co.), exposed to Venusian surface conditions for 10 days (Fig. 146). (a) Bulk. (b) Coating.

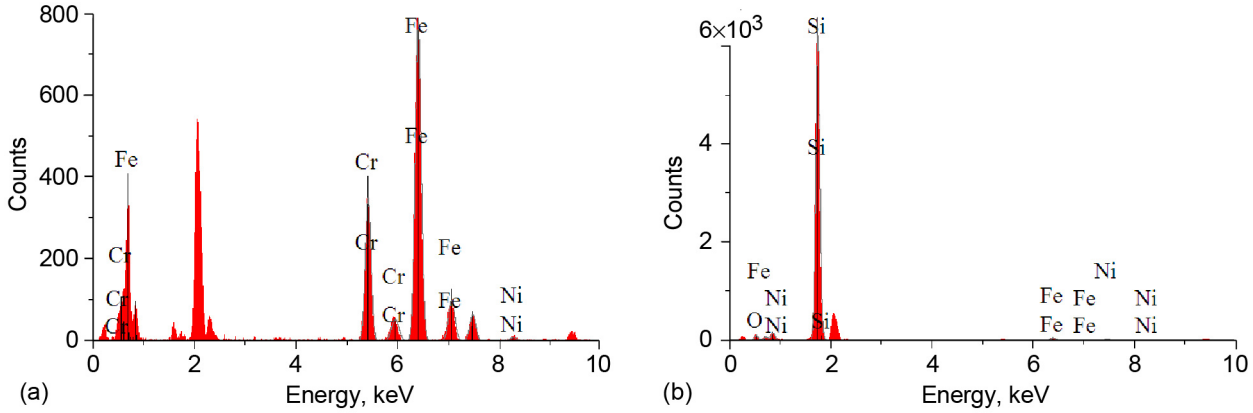


Figure 150.—Energy dispersive spectroscopy analysis of 316 stainless steel coated with SilcoNert® 1040 (SilcoTek Co.), exposed to Venusian surface conditions for 42 days (Fig. 147(a)). (a) Bulk. (b) Coating.

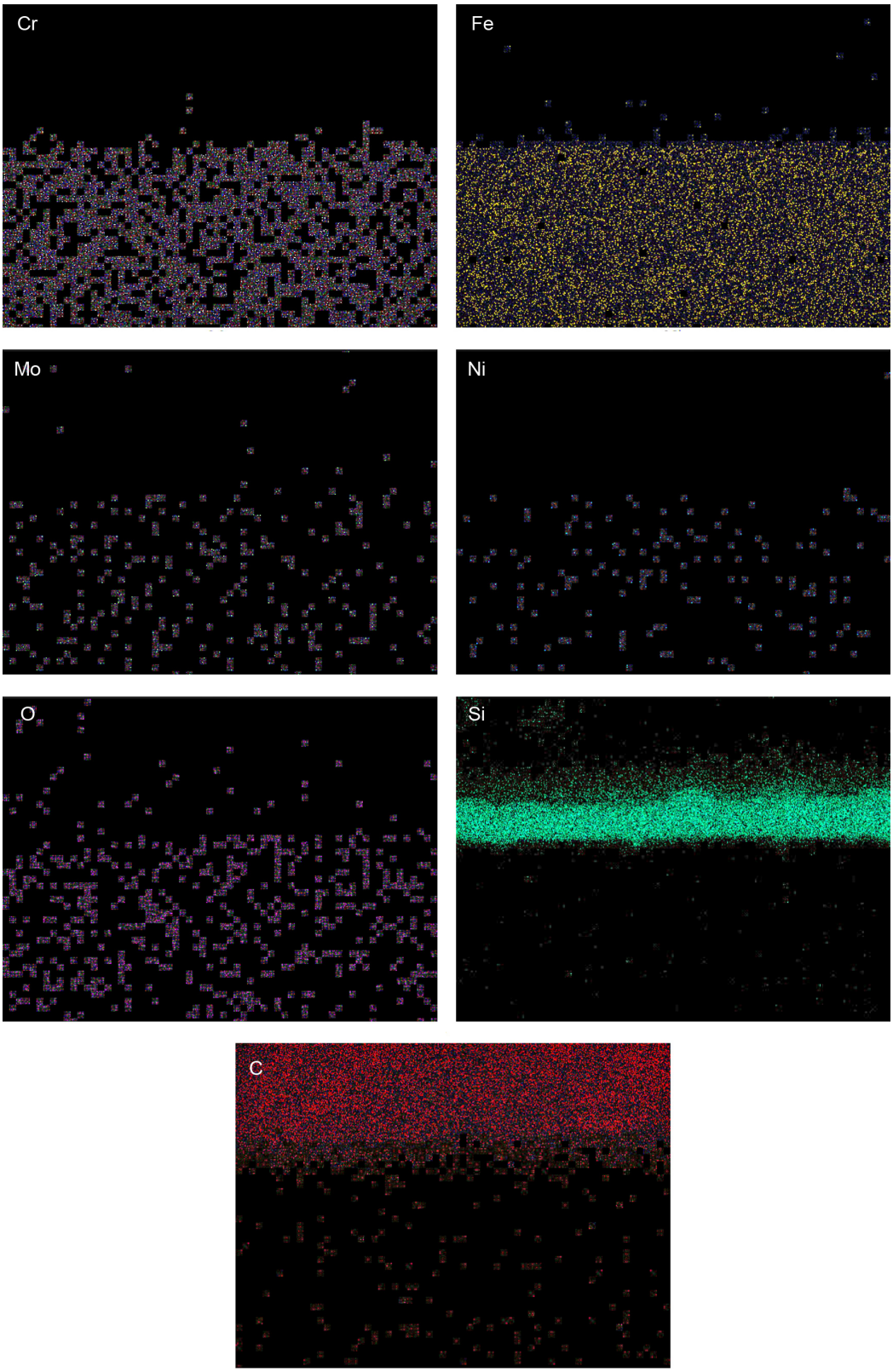


Figure 151.—X-ray elemental images of 316 stainless steel coated with SilcoNert® 1040 (SilcoTek Co.), exposed to Venusian surface conditions for 10 days (area mapped is that of Fig. 146). Each pixel represents information gathered by spectrometer at C, O, Si, Cr, Fe, and Ni Kα line and at Mo Lα line.

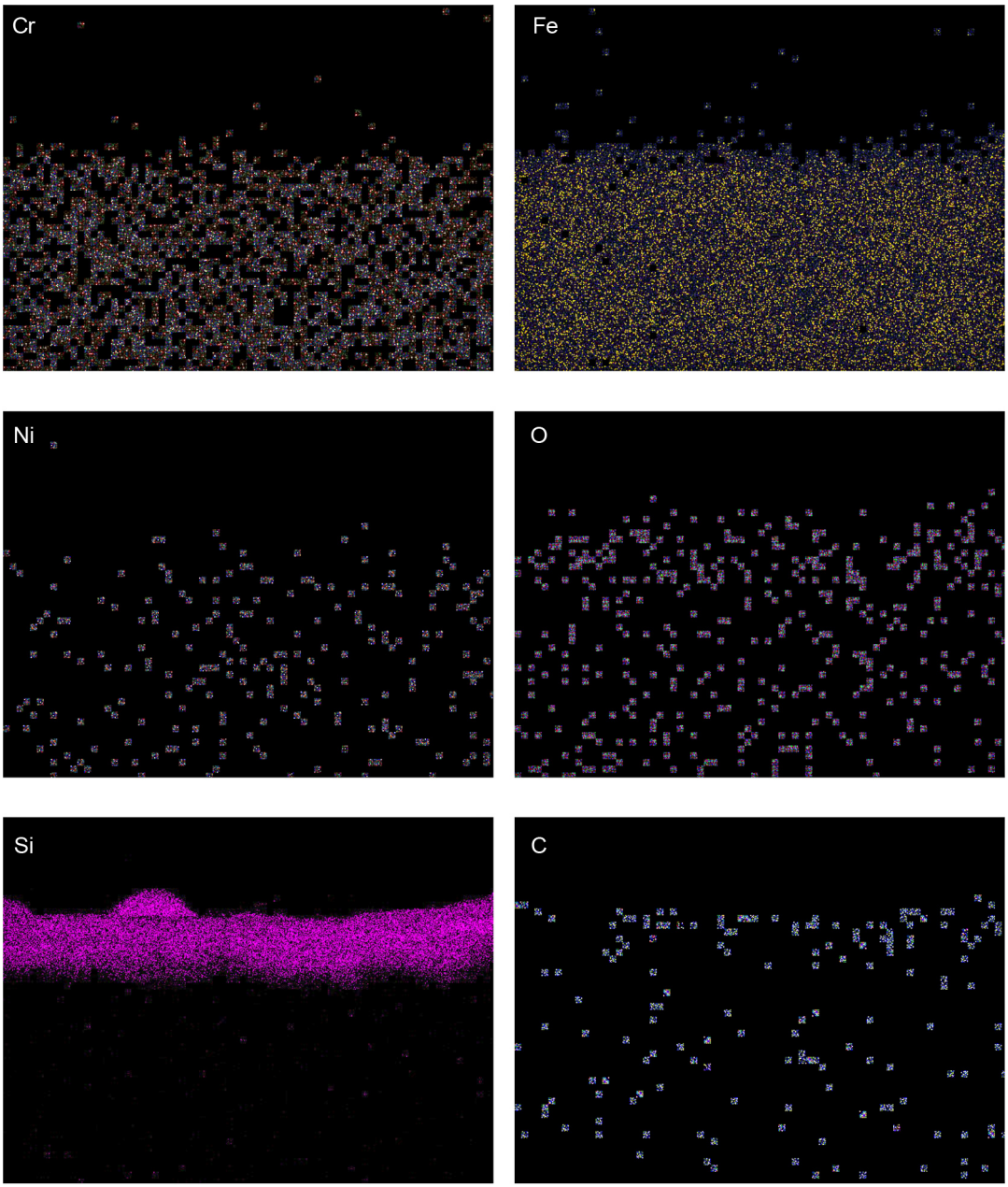


Figure 152.—X-ray elemental images of 316 stainless steel coated with SilcoNert® 1040 (SilcoTek Co.), exposed to Venusian surface conditions for 42 days (area mapped is that of Fig. 147). Each pixel represents information gathered by spectrometer at C, O, Si, Cr, Fe, and Ni Kα line.

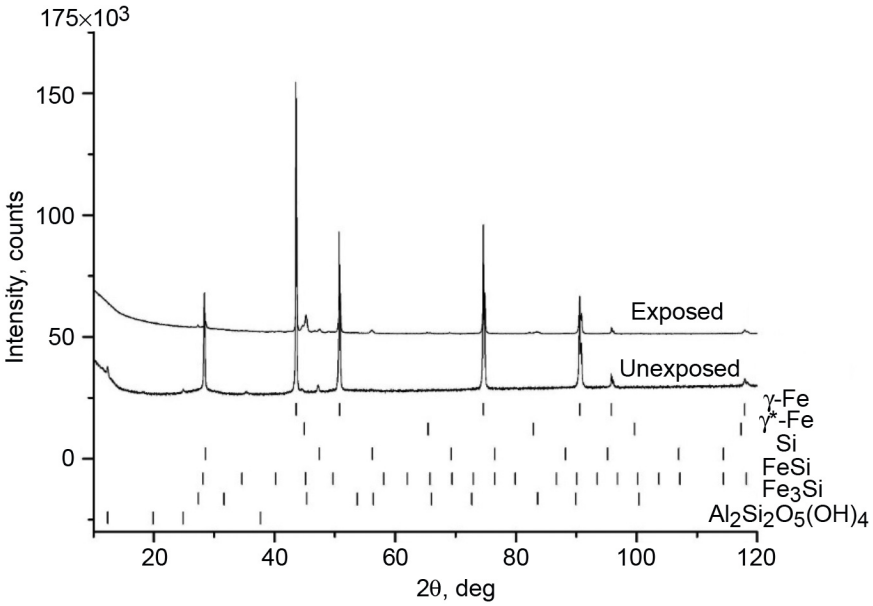


Figure 153.—X-ray diffraction patterns of unpolished side of 316 stainless steel samples coated with SilcoNert® 1040 (SilcoTek Co.), unexposed and exposed to Venusian surface conditions for 42 days.

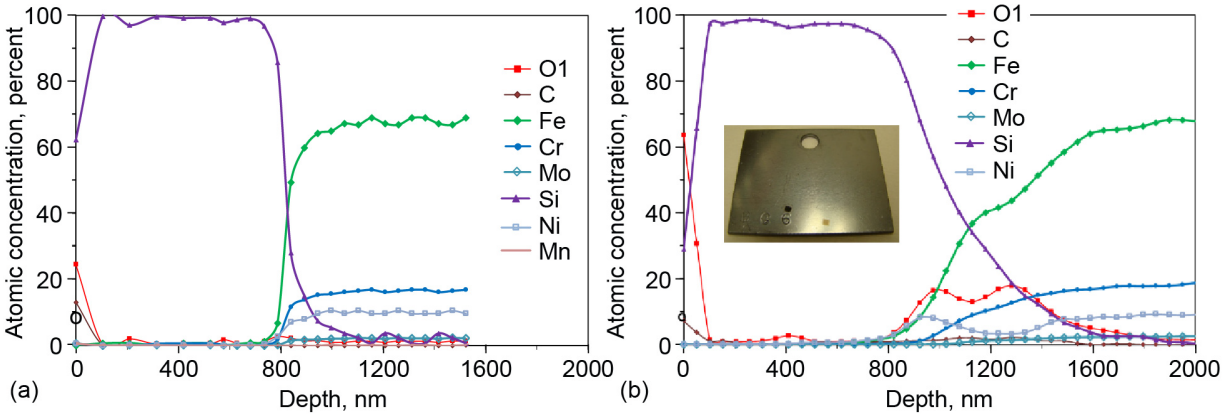


Figure 154.—X-ray photoelectron spectroscopy depth profile using high-resolution regions of stainless steel 316 sample coated with SilcoNert® 1040 (SilcoTek Co.), before and after exposure to Venusian surface conditions for 21 days. (a) Before. (b) After.

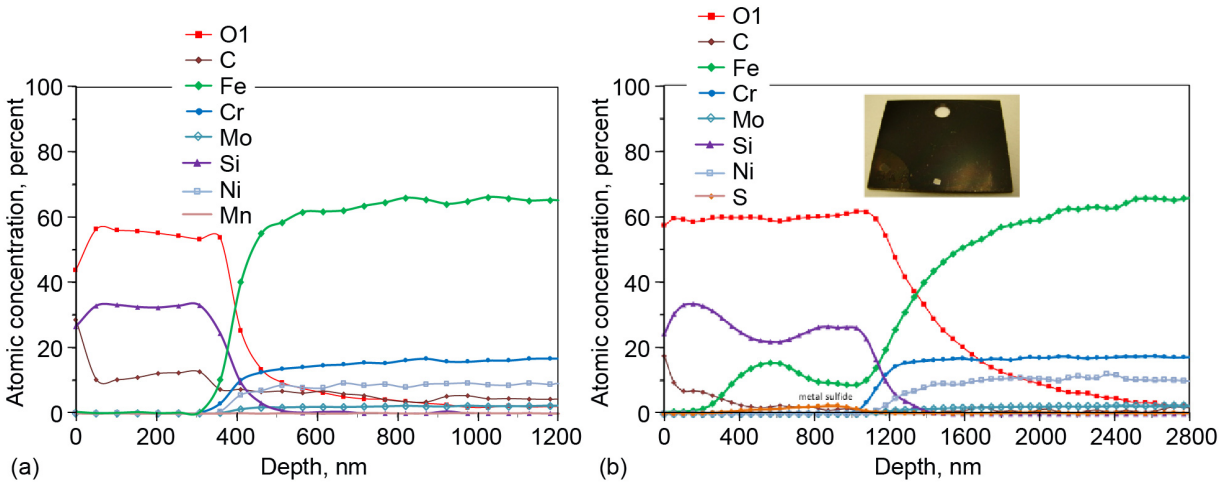


Figure 155.—X-ray photoelectron spectroscopy depth profile using high-resolution regions of stainless steel 316 sample coated with Dursan® (SilcoTek Co.), before and after exposure to Venusian surface conditions for 21 days. (a) Before. (b) After.

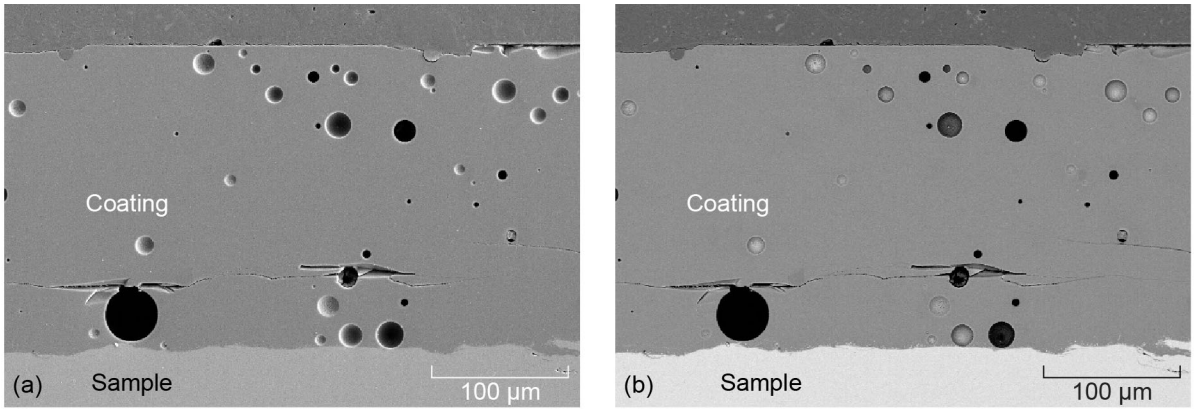


Figure 156.—Cross-sectional images of unexposed 304 stainless steel coated with porcelain. (a) Scanning electron microscopy image. (b) Backscattered-electron image.

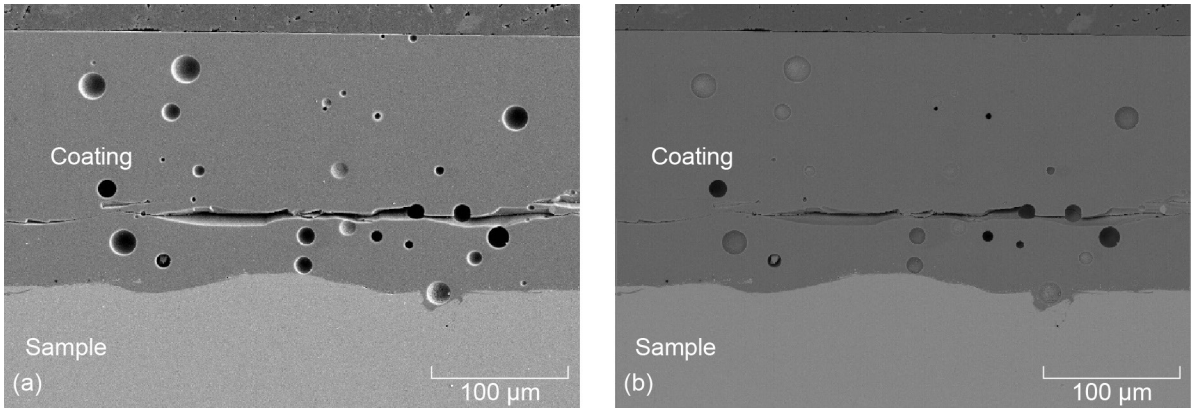


Figure 157.—Cross-sectional images of 304 stainless steel coated with porcelain, exposed to Venusian surface conditions for 10 days. (a) Scanning electron microscopy image. (b) Backscattered-electron image.

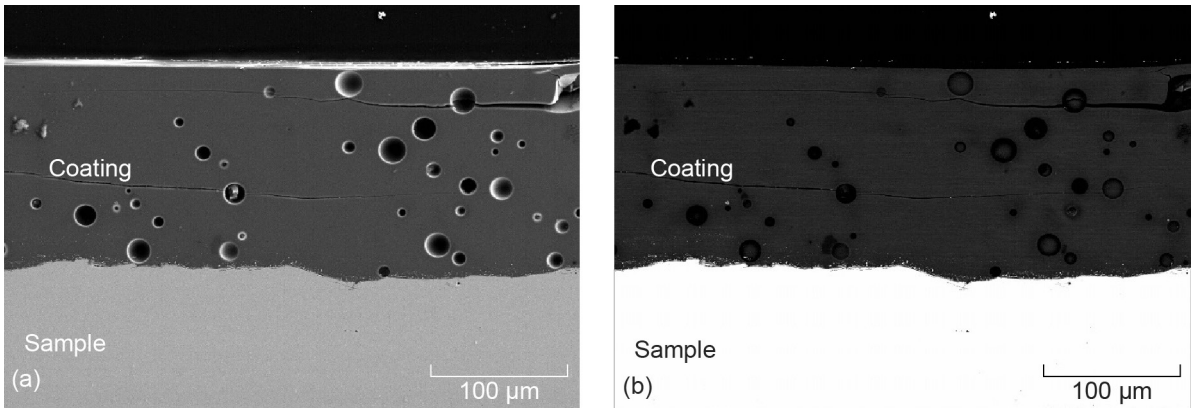


Figure 158.—Cross-sectional images of 304 stainless steel coated with porcelain, exposed to Venusian surface conditions for 42 days. (a) Scanning electron microscopy image. (b) Backscattered-electron image.

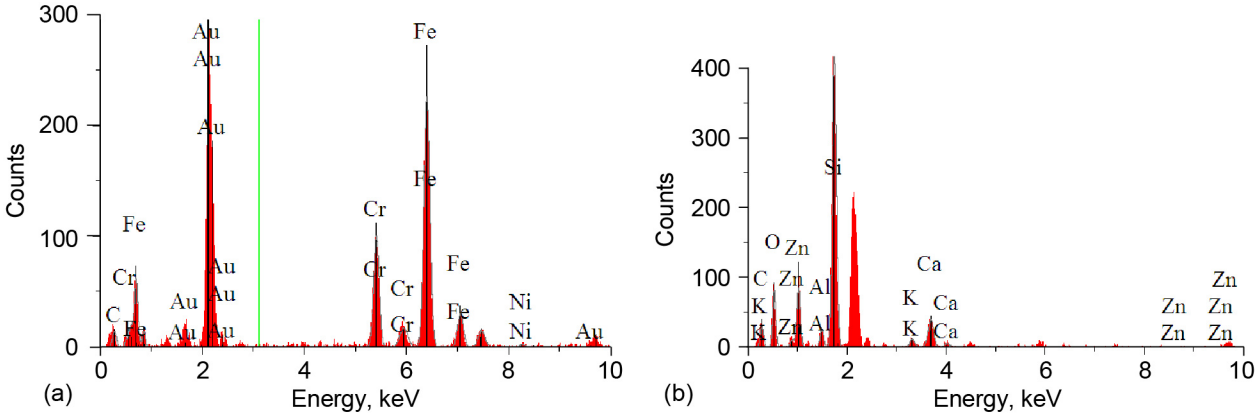


Figure 159.—Energy dispersive spectroscopy analysis of bulk 316 stainless steel and porcelain coating, exposed to Venusian surface conditions for 10 days (Fig. 157). (a) Bulk. (b) Coating.

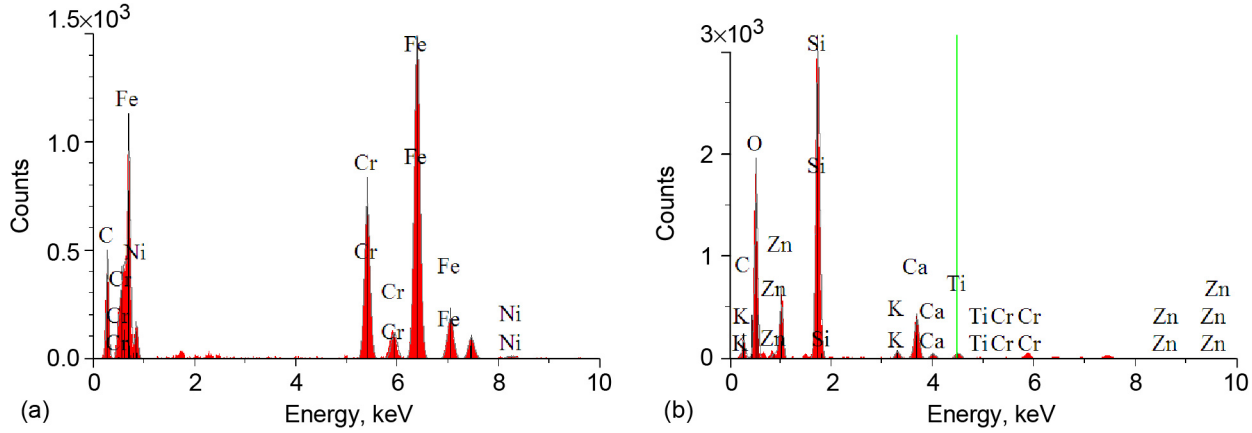


Figure 160.—Energy dispersive spectroscopy analysis of bulk 316 stainless steel and porcelain coating, exposed to Venusian surface conditions for 42 days (Fig. 158). (a) Bulk. (b) Coating.

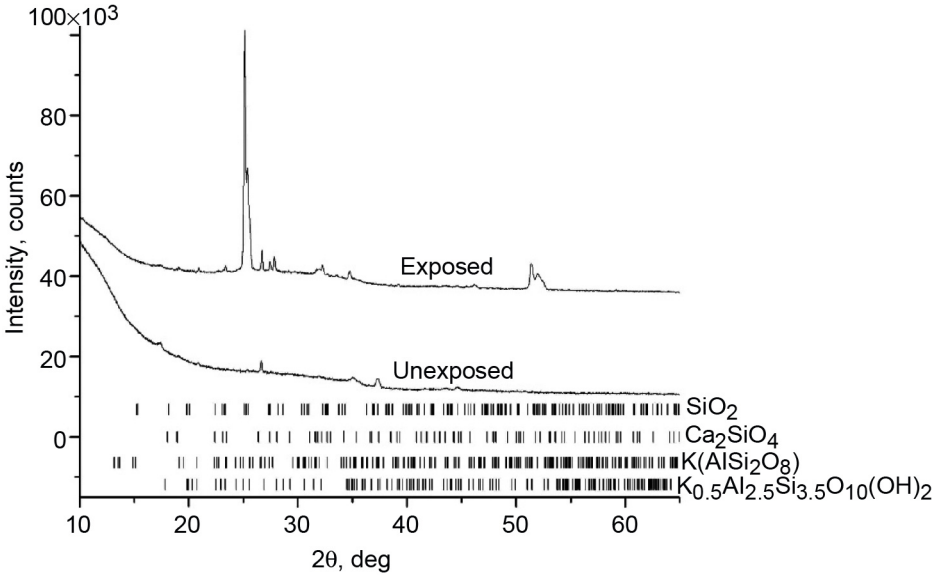


Figure 161.—X-ray diffraction patterns of 304 stainless steel samples coated with porcelain, unexposed and exposed to Venusian surface conditions for 42 days.

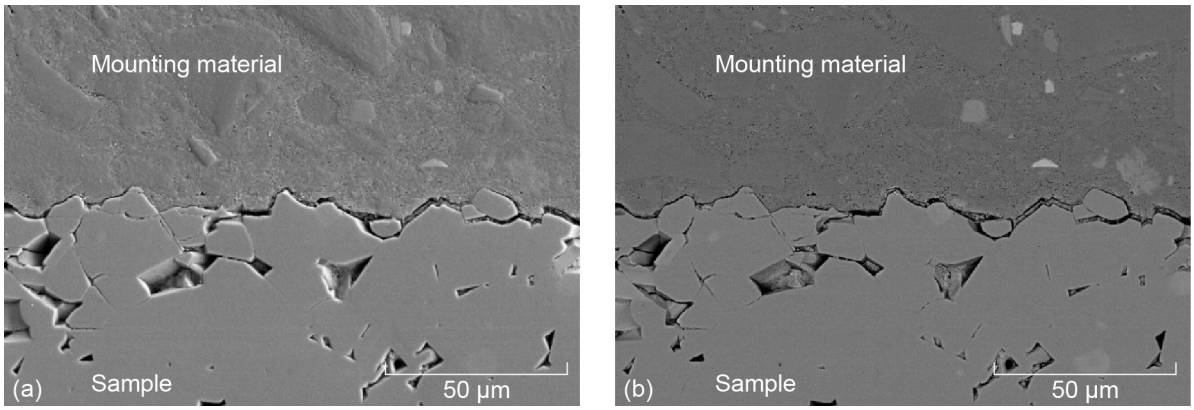


Figure 162.—Cross-sectional images of unexposed alumina. (a) Scanning electron microscopy image. (b) Backscattered-electron image.

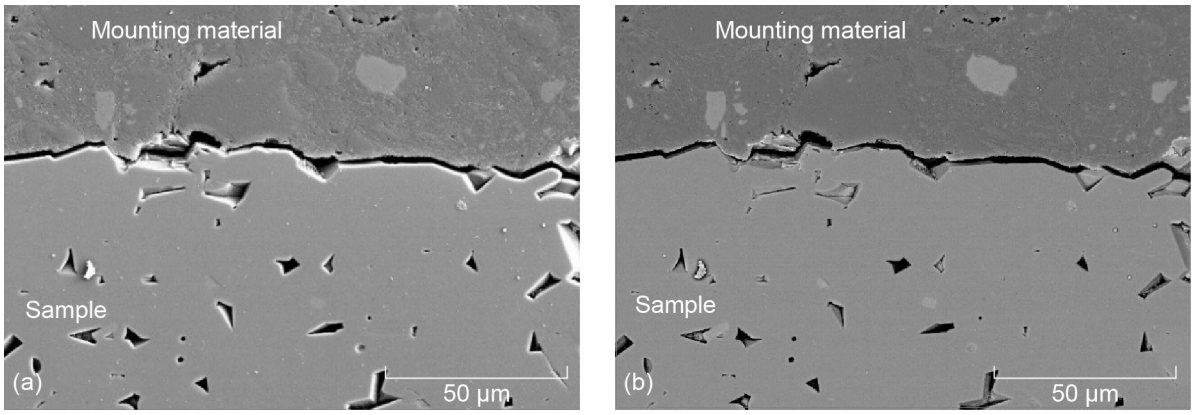


Figure 163.—Cross-sectional images of alumina sample exposed to Venusian surface conditions for 10 days. (a) Scanning electron microscopy image. (b) Backscattered-electron image.

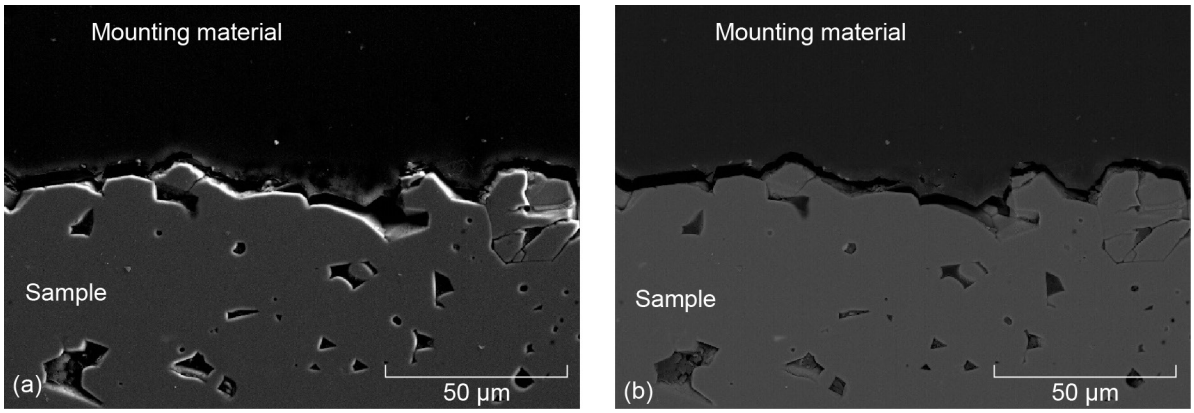


Figure 164.—Cross-sectional images of alumina sample exposed to Venusian surface conditions for 42 days. (a) Scanning electron microscopy image. (b) Backscattered-electron image.

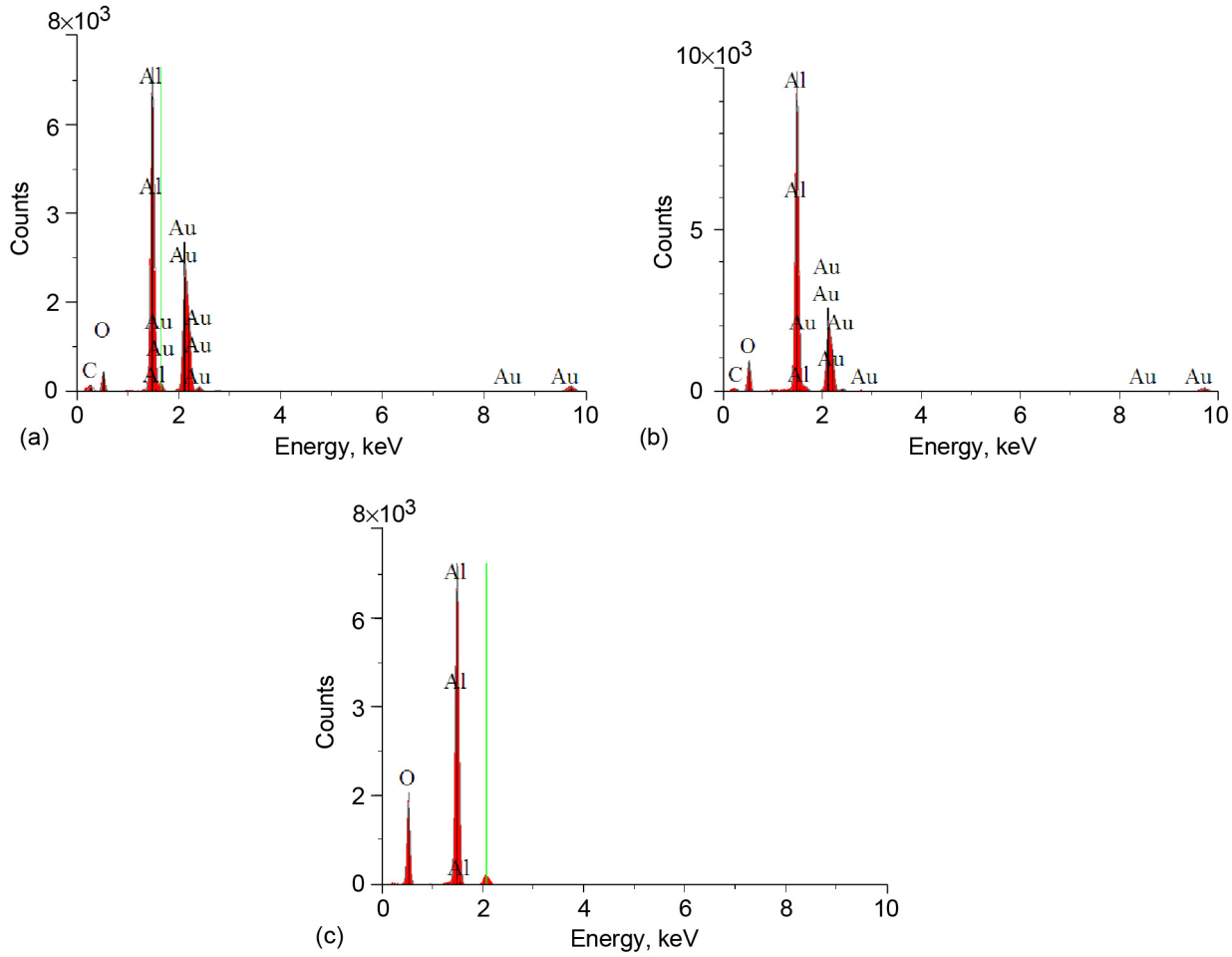


Figure 165.—Energy dispersive spectroscopy analysis of alumina. (a) Unexposed (Fig. 162). (b) Exposed to Venusian surface conditions for 10 days (Fig. 163). (c) Exposed to Venusian surface conditions for 42 days (Fig. 164).

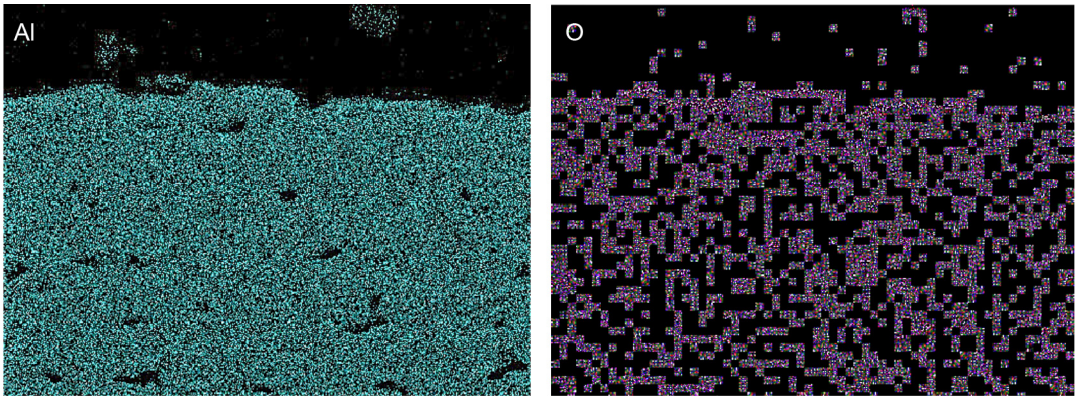


Figure 166.—X-ray elemental images of alumina sample exposed to Venusian surface conditions for 10 days (area mapped is that of Fig. 163). Each pixel represents information gathered by spectrometer at Al and O Kα line.

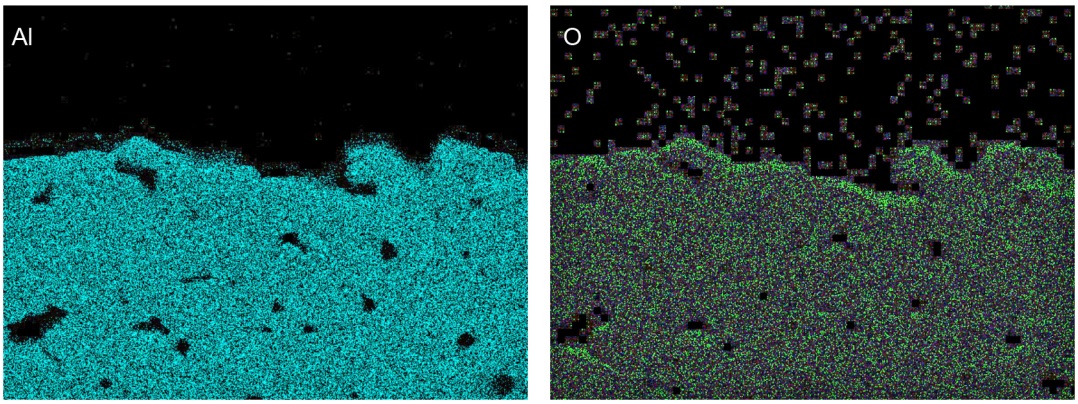


Figure 167.—X-ray elemental images of alumina sample exposed to Venusian surface conditions for 42 days (area mapped is that of Fig. 164). Each pixel represents information gathered by spectrometer at Al and O Kα line.

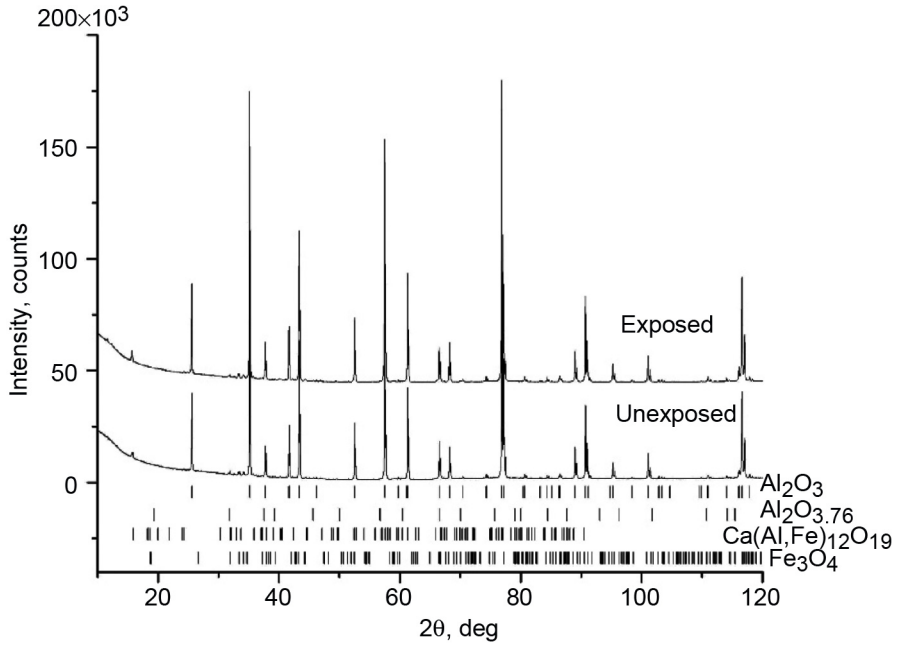


Figure 168.—X-ray diffraction patterns of alumina samples, unexposed and exposed to Venusian surface conditions for 42 days.

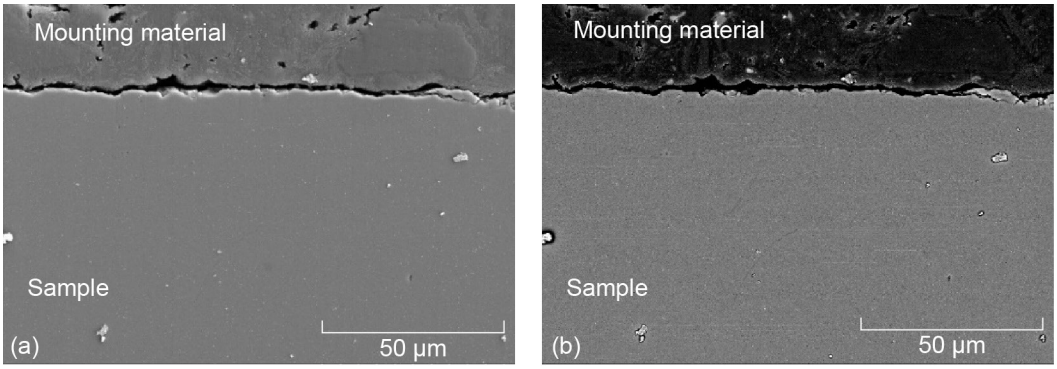


Figure 169.—Cross-sectional images of silicon nitride exposed to Venusian surface conditions for 10 days. (a) Scanning electron microscopy image. (b) Backscattered-electron image.

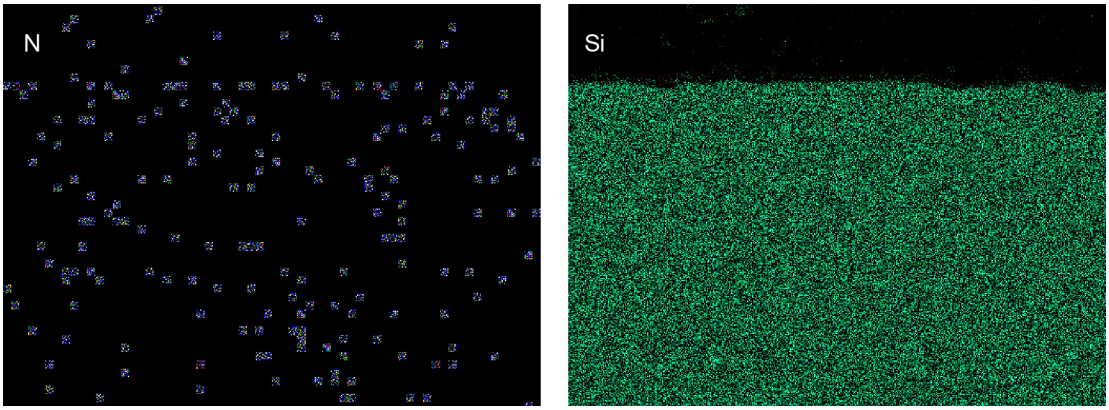


Figure 170.—X-ray elemental images of silicon nitride exposed to Venusian surface conditions for 10 days (area mapped is that of Fig. 169). Each pixel represents information gathered by spectrometer at N and Si Kα line.

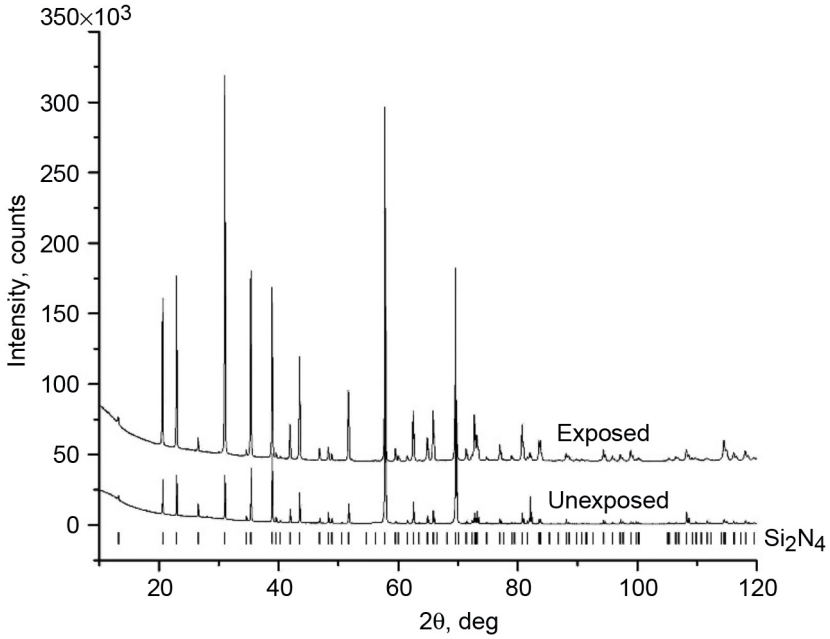


Figure 171.—X-ray diffraction patterns of silicon nitride samples, unexposed and exposed to Venusian surface conditions for 42 days.

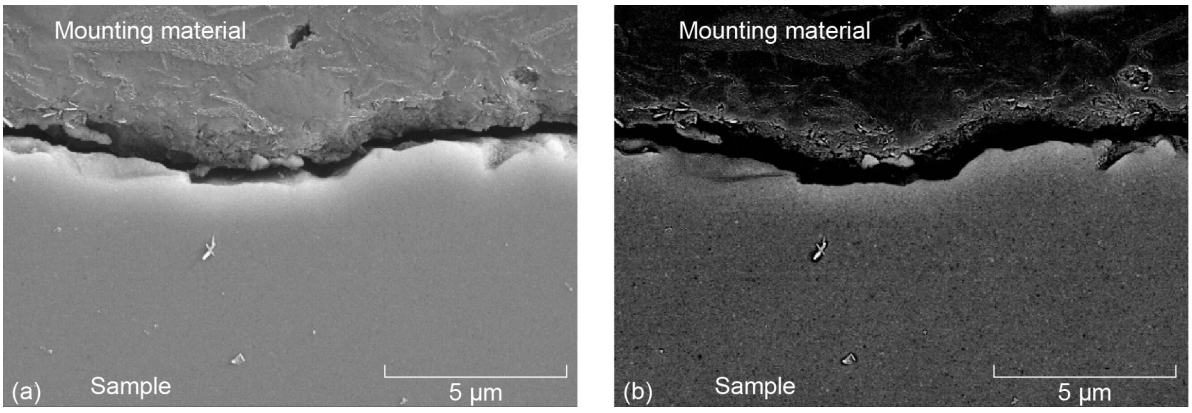


Figure 172.—Cross-sectional images of unexposed silicon carbide. (a) Scanning electron microscopy image. (b) Backscattered-electron image.

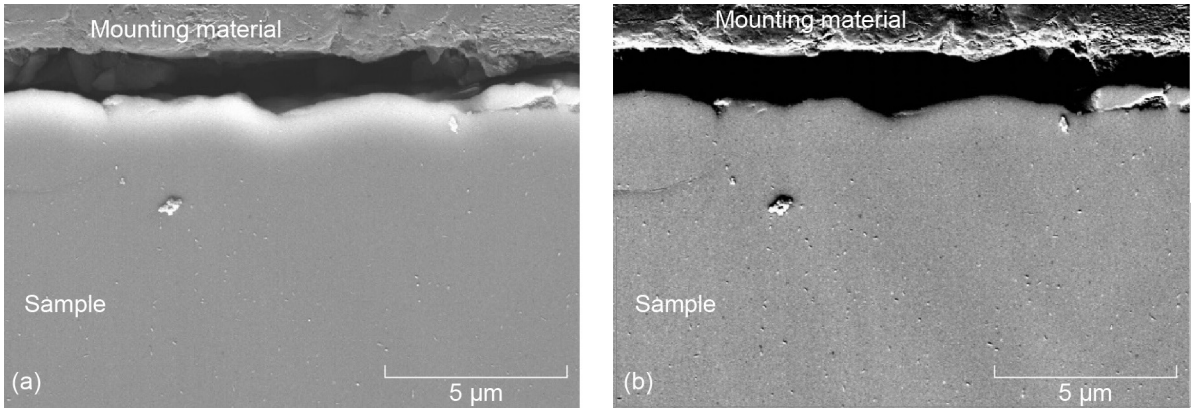


Figure 173.—Cross-sectional images of silicon carbide exposed to Venusian surface conditions for 10 days. (a) Scanning electron microscopy image. (b) Backscattered-electron image.

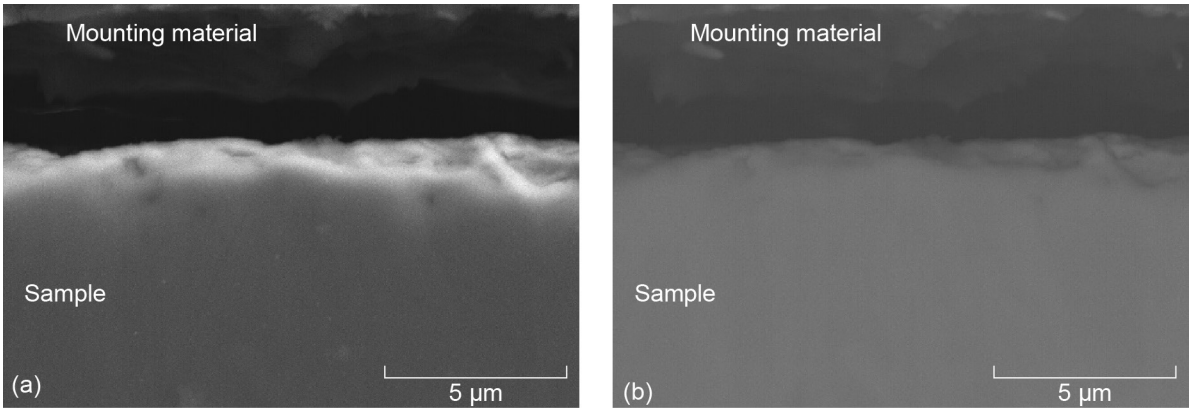


Figure 174.—Cross-sectional images of silicon carbide exposed to Venusian surface conditions for 42 days. (a) Scanning electron microscopy image. (b) Backscattered-electron image.

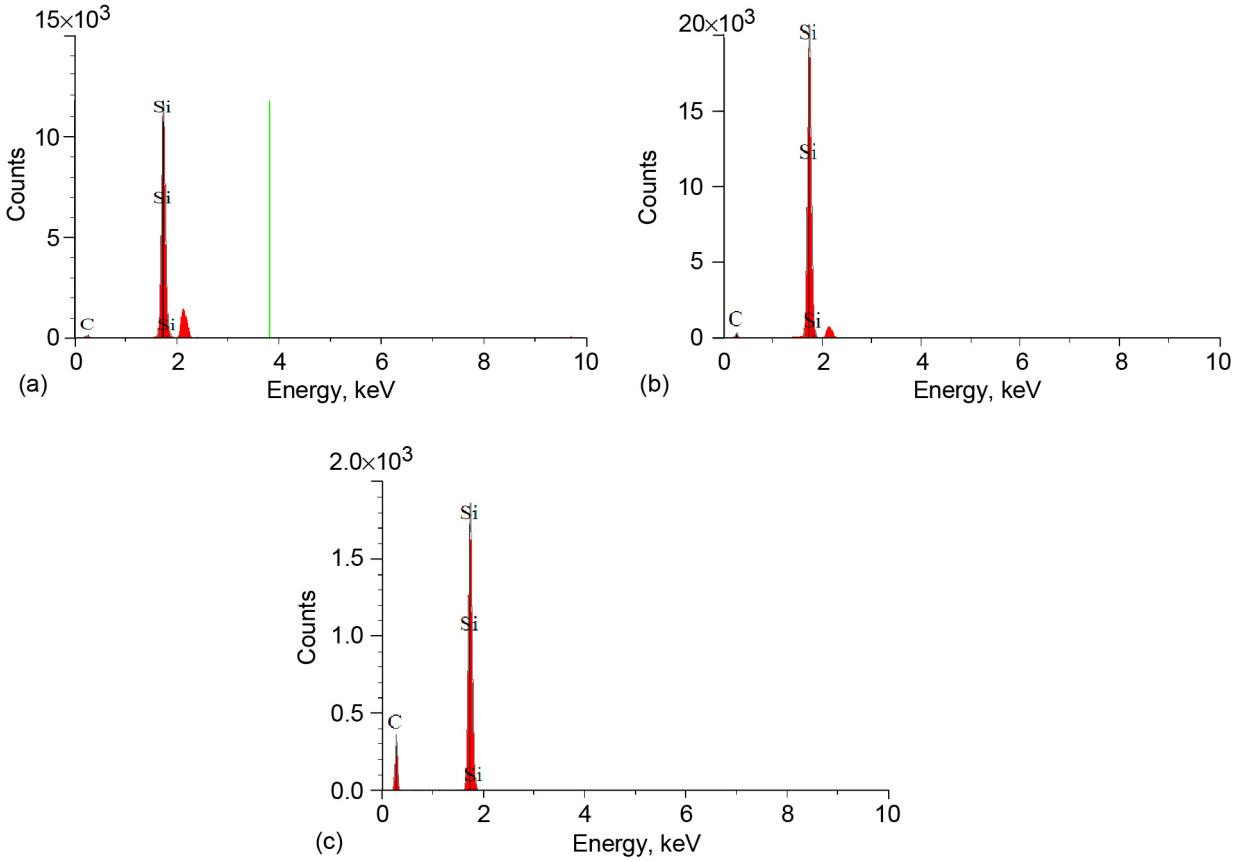


Figure 175.—Energy dispersive spectroscopy analysis of bulk (near edge of surface) silicon carbide. (a) Unexposed (Fig. 172). (b) Exposed to Venusian surface conditions for 10 days (Fig. 173). (c) Exposed to Venusian surface conditions for 42 days (Fig. 174).

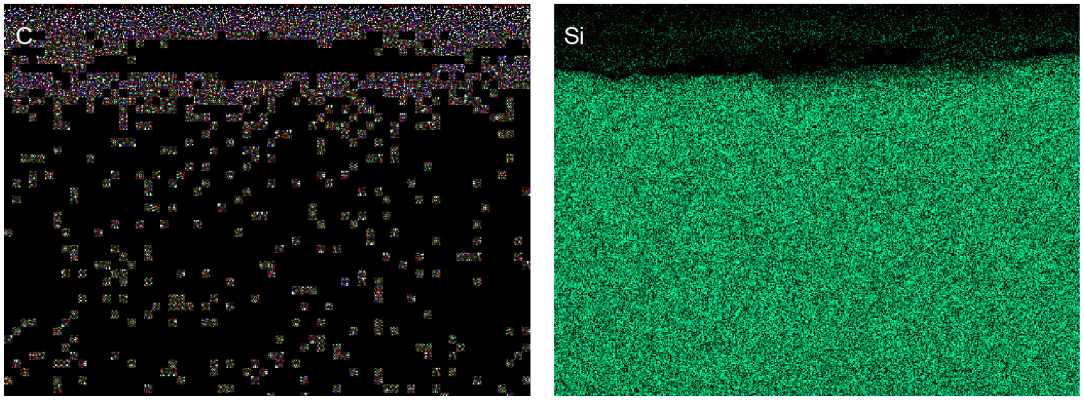


Figure 176.—X-ray elemental images of silicon carbide exposed to Venusian surface conditions for 10 days (area mapped is that of Fig. 173). Each pixel represents information gathered by spectrometer at C and Si Kα line.

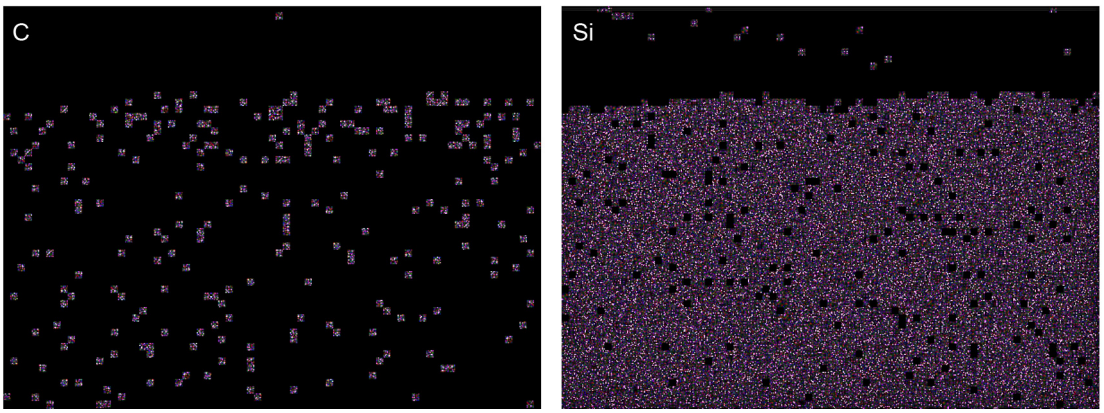


Figure 177.—X-ray elemental images of silicon carbide exposed to Venusian surface conditions for 42 days (area mapped is that of Fig. 174). Each pixel represents information gathered by spectrometer at C and Si Kα line.

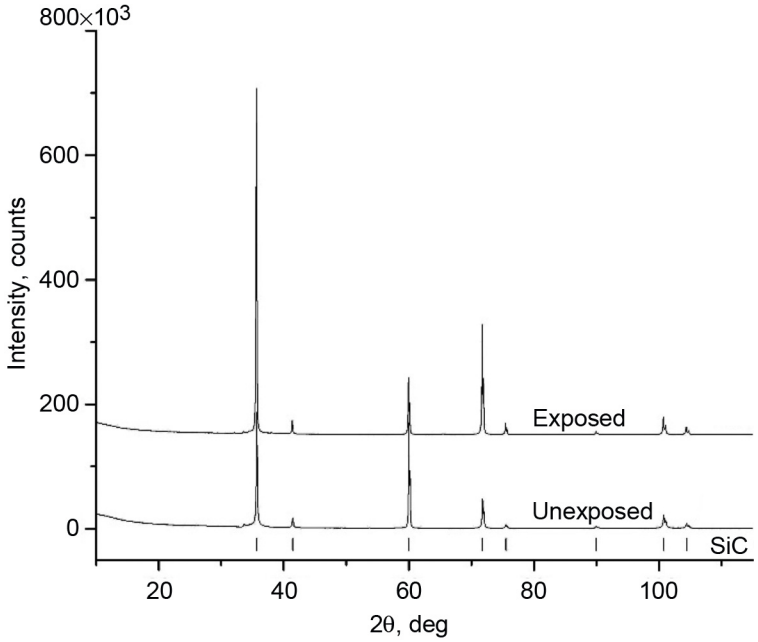


Figure 178.—X-ray diffraction patterns of silicon carbide samples, unexposed and exposed to Venusian surface conditions for 42 days.

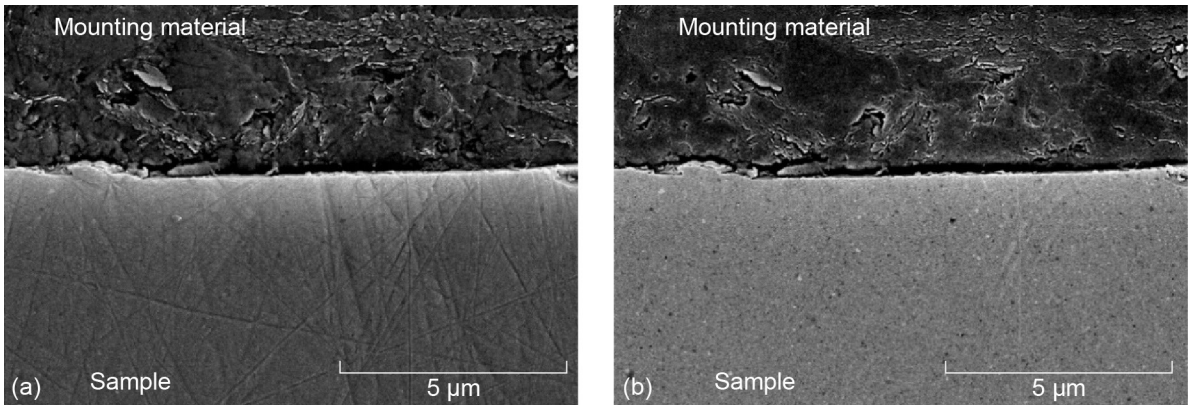


Figure 179.—Cross-sectional images of unexposed silica. (a) Scanning electron microscopy image. (b) Backscattered-electron image.

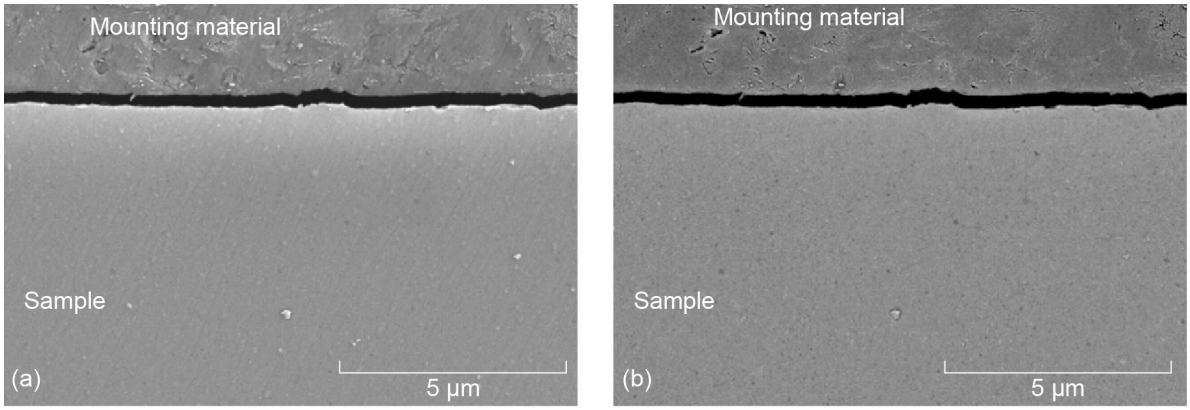


Figure 180.—Cross-sectional images of silica exposed to Venusian surface conditions for 10 days. (a) Scanning electron microscopy image. (b) Backscattered-electron image.

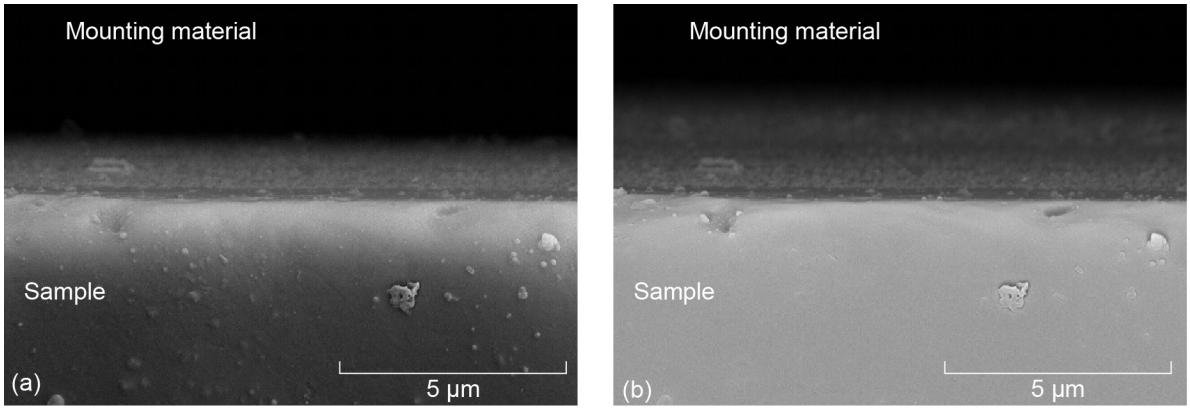


Figure 181.—Cross-sectional images of silica exposed to Venusian surface conditions for 42 days. (a) Scanning electron microscopy image. (b) Backscattered-electron image.

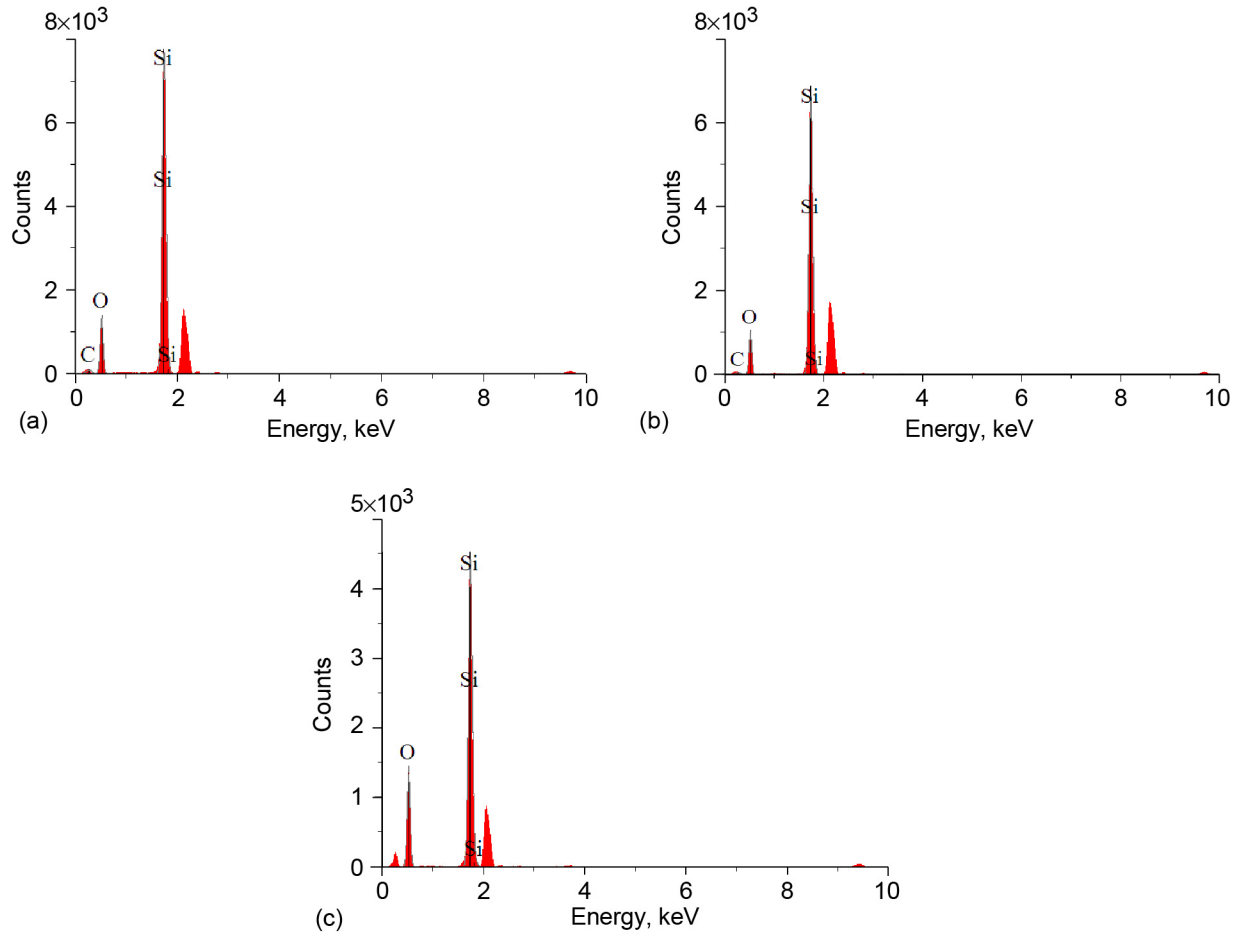


Figure 182.—Energy dispersive spectroscopy analysis of silica (near edge of surface). (a) Unexposed (Fig. 179). (b) Exposed to Venusian surface conditions for 10 days (Fig. 180). (c) Exposed to Venusian surface conditions for 42 days (Fig. 181).

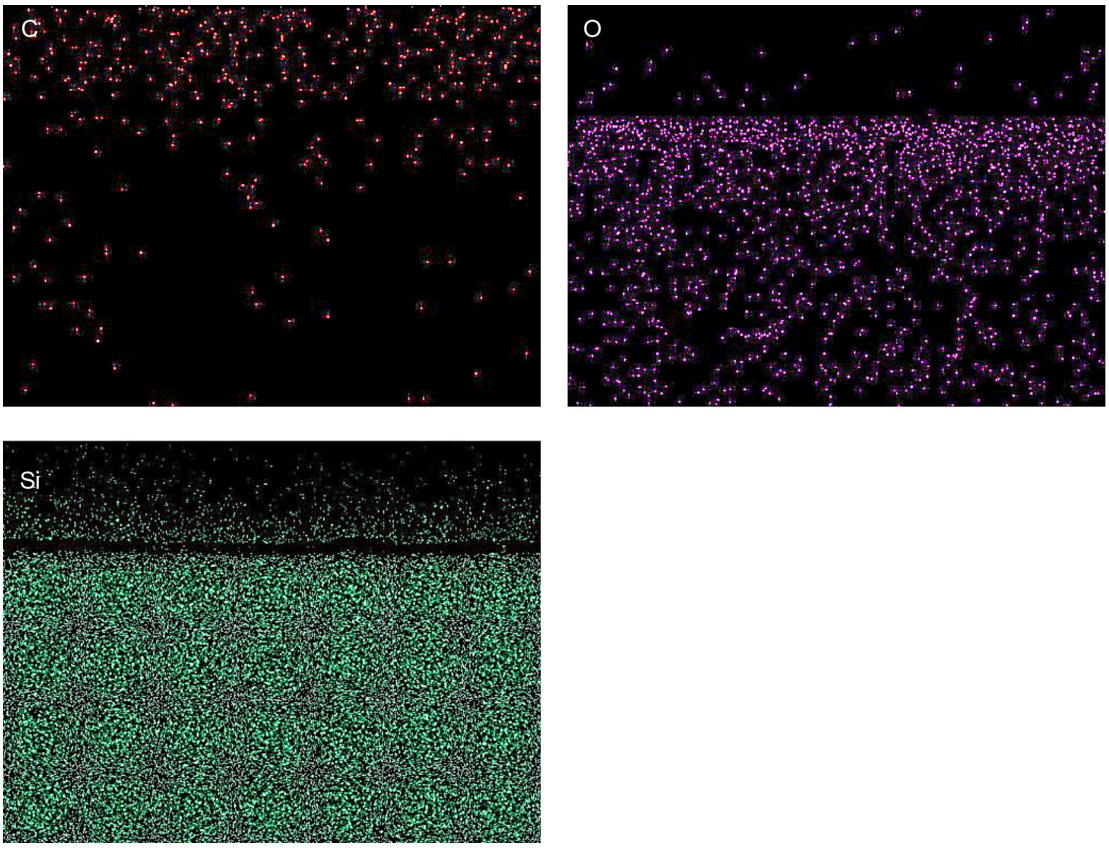


Figure 183.—X-ray elemental images of silica exposed to Venusian surface conditions for 10 days (area mapped is that of Fig. 180). Each pixel represents information gathered by spectrometer at C, O, and Si K$\alpha$ line.

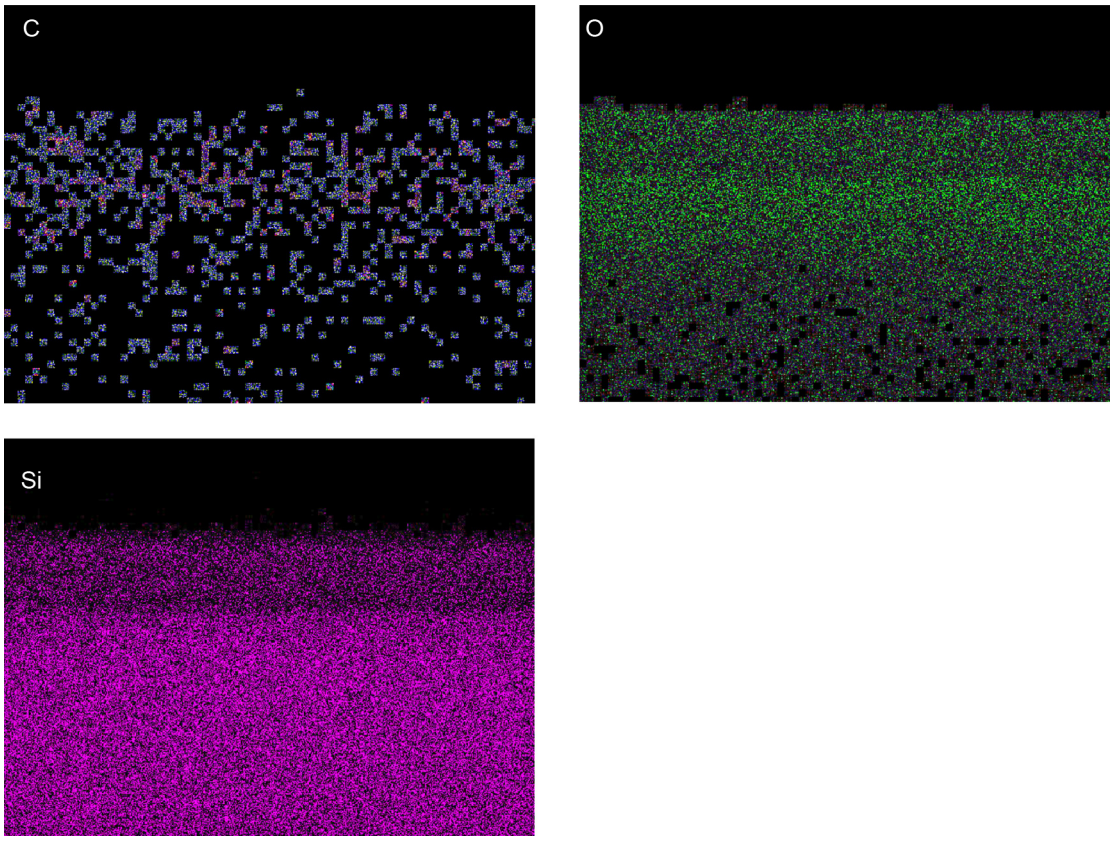


Figure 184.—X-ray elemental images of silica exposed to Venusian surface conditions for 42 days (area mapped is that of Fig. 181). Each pixel represents information gathered by spectrometer at C, O, and Si Kα line.

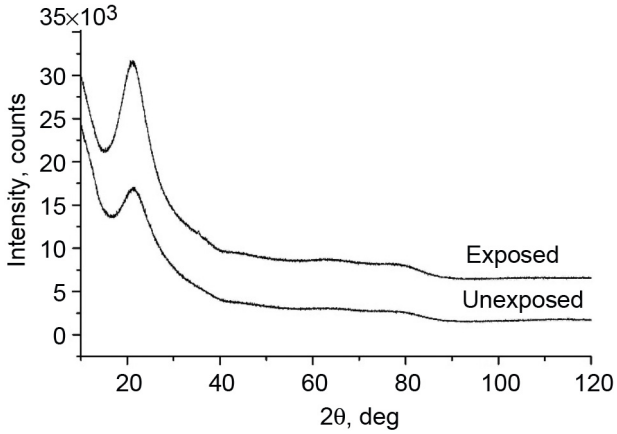


Figure 185.—X-ray diffraction patterns of fused silica samples, unexposed and exposed to Venusian surface conditions for 42 days.

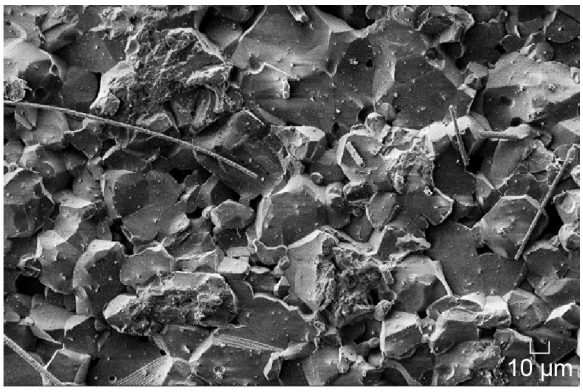


Figure 186.—Scanning electron microscopy image of surface of alumina exposed to Venusian surface conditions for 42 days.

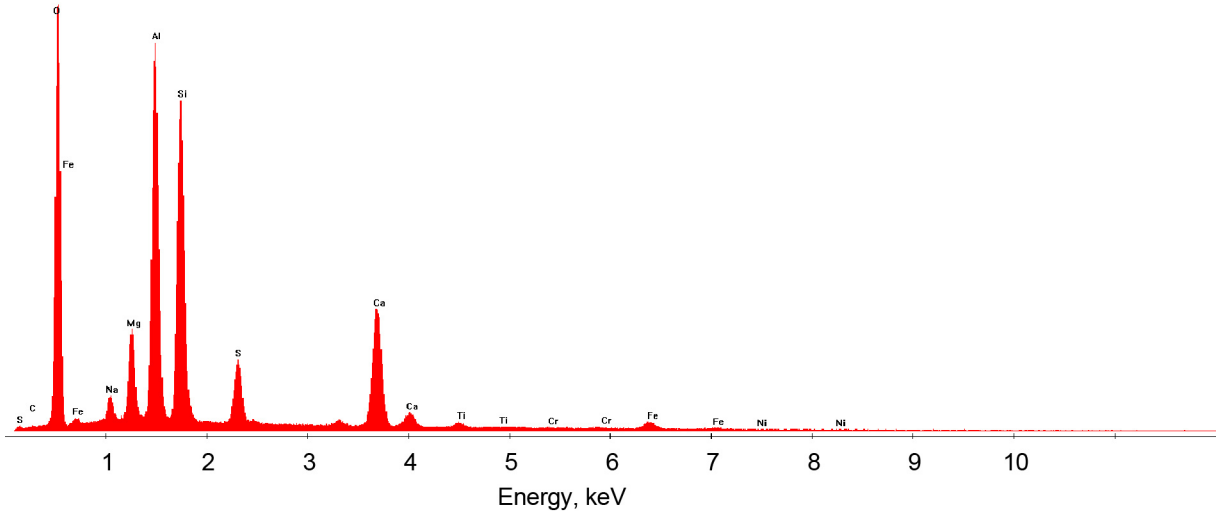


Figure 187.—Energy dispersive spectroscopy analysis of fiber-like material found on surface of alumina exposed to Venusian surface conditions for 42 days (Fig. 186).

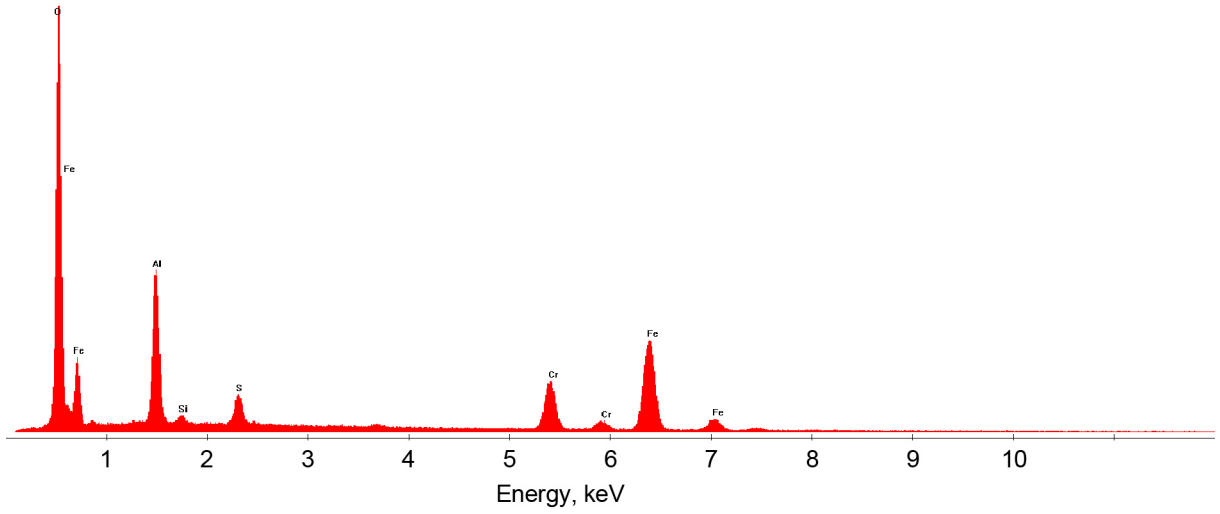


Figure 188.—Energy dispersive spectroscopy analysis of particulate-like material found on surface of alumina exposed to Venusian surface conditions for 42 days (Fig. 186).

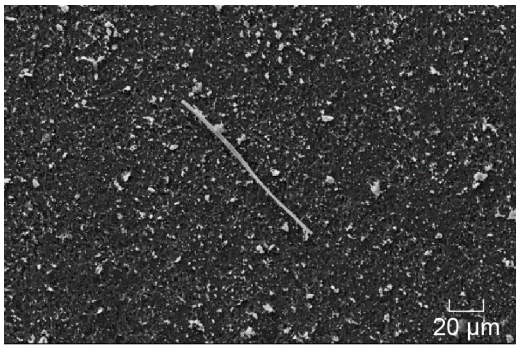


Figure 189.—Scanning electron microscopy image of surface of silicon nitride exposed to Venusian surface conditions for 42 days.

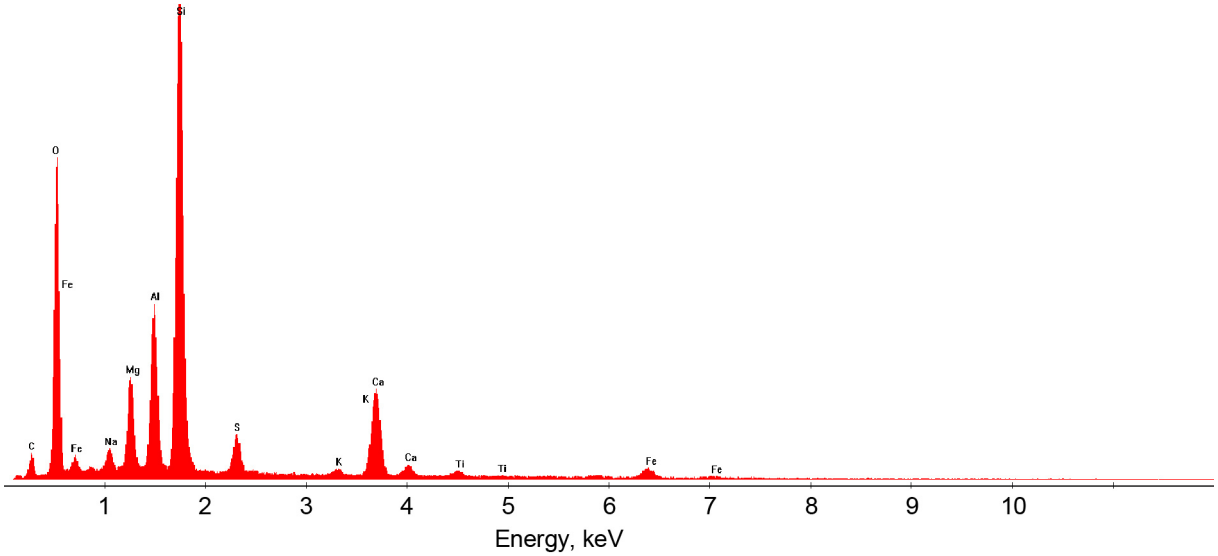


Figure 190.—Energy dispersive spectroscopy analysis of fiber-like material found on surface of silicon nitride exposed (Fig. 189) to Venusian surface conditions for 42 days.

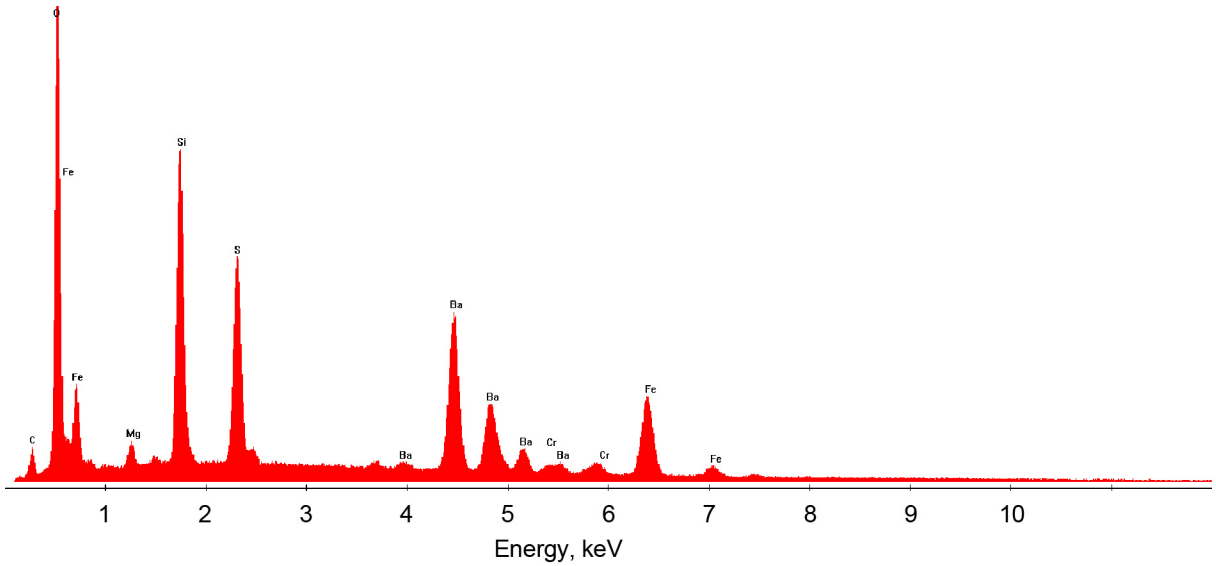


Figure 191.—Energy dispersive spectroscopy analysis of particulate-like material found on surface of silicon nitride exposed (Fig. 189) to Venusian surface conditions for 42 days.

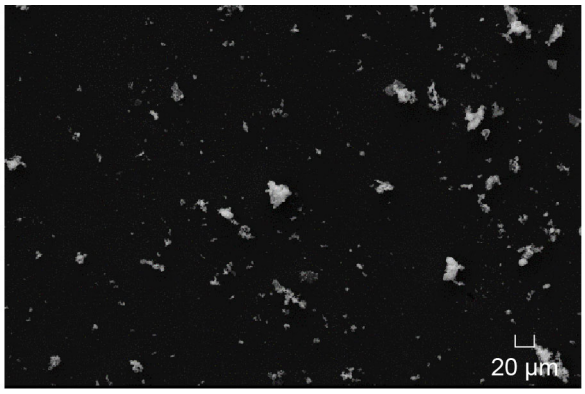


Figure 192.—Scanning electron microscopy image of surface of amorphous silica exposed to Venusian surface conditions for 42 days.

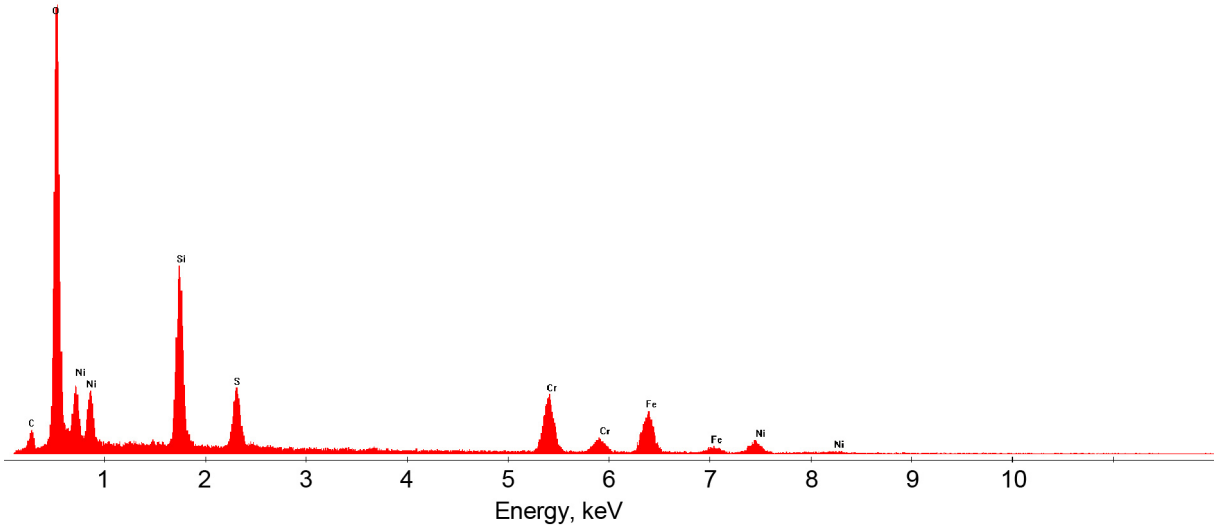


Figure 193.—Energy dispersive spectroscopy analysis of particulate-like material found on surface of amorphous silica exposed to Venusian surface conditions for 10 days (Fig. 192).

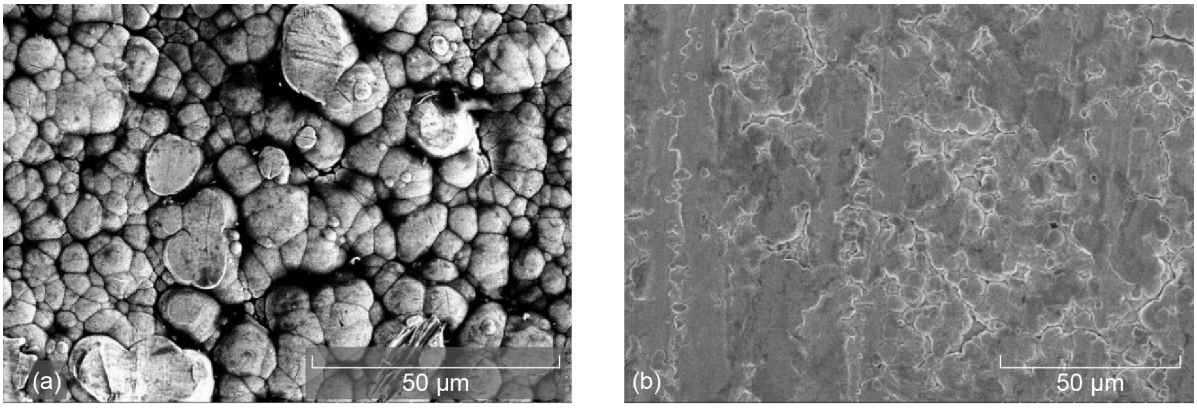


Figure 194.—Scanning electron microscopy images of surface of gold coating electrodeposited on 316 stainless steel rod. (a) Unexposed. (b) Exposed to Venusian surface conditions for 10 days.

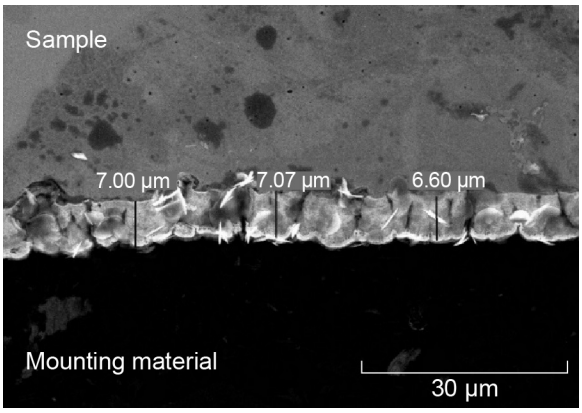


Figure 195.—Cross-sectional scanning electron microscopy images of stainless steel 316 rod with electrodeposited gold on its surface, exposed to Venusian surface conditions for 10 days.

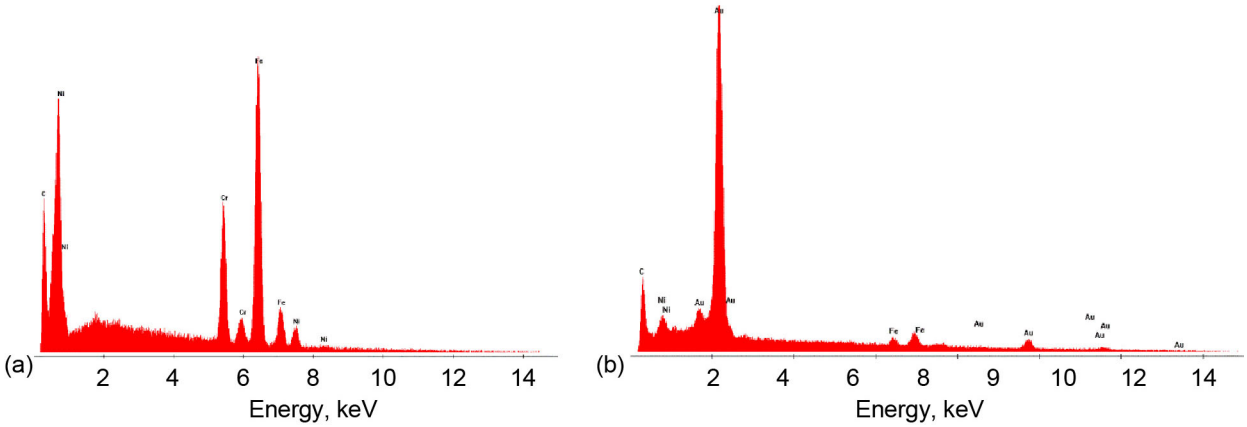


Figure 196.—Energy dispersive spectroscopy analysis of bulk 316 stainless steel and gold coating (Fig. 195), exposed to Venusian surface conditions for 10 days. (a) Bulk 316. (b) Gold coating.

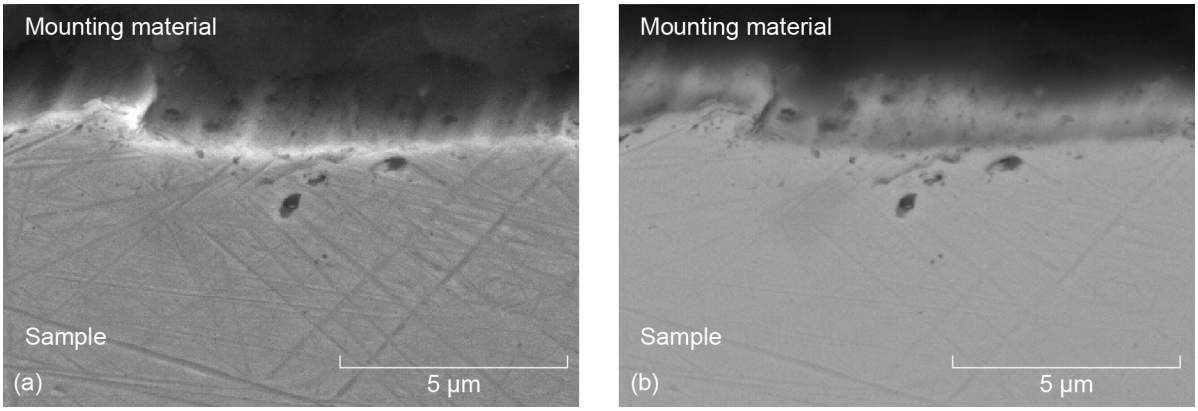


Figure 197.—Cross-sectional images of Inconel wire used to hang samples in Glenn Extreme Environments Rig, exposed to Venusian surface conditions for 10 days. (a) Scanning electron microscopy image. (b) Backscattered-electron image.

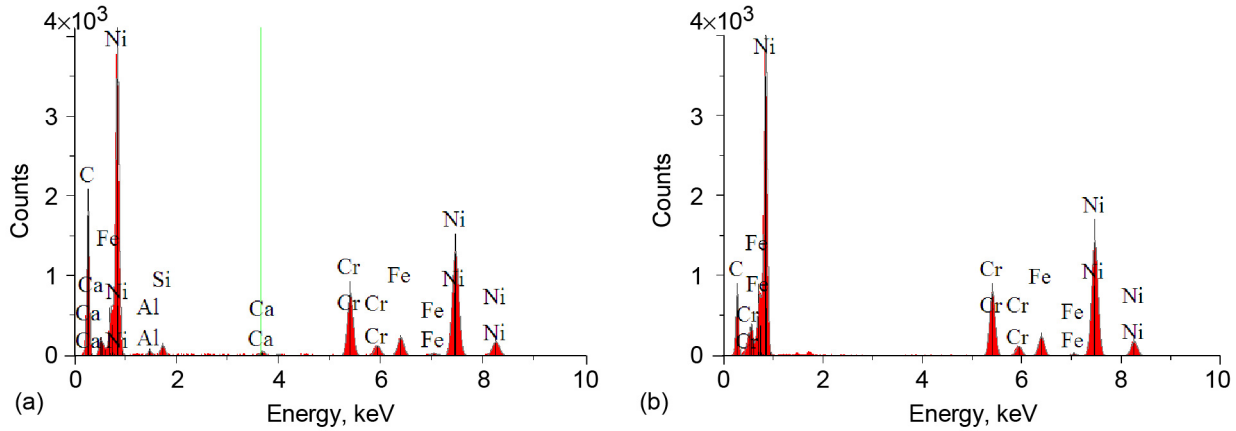


Figure 198.—Energy dispersive spectroscopy analysis of Inconel wire used to hang samples in Glenn Extreme Environments Rig, exposed to Venusian surface conditions for 10 days (Fig. 197). (a) Surface. (b) Bulk.

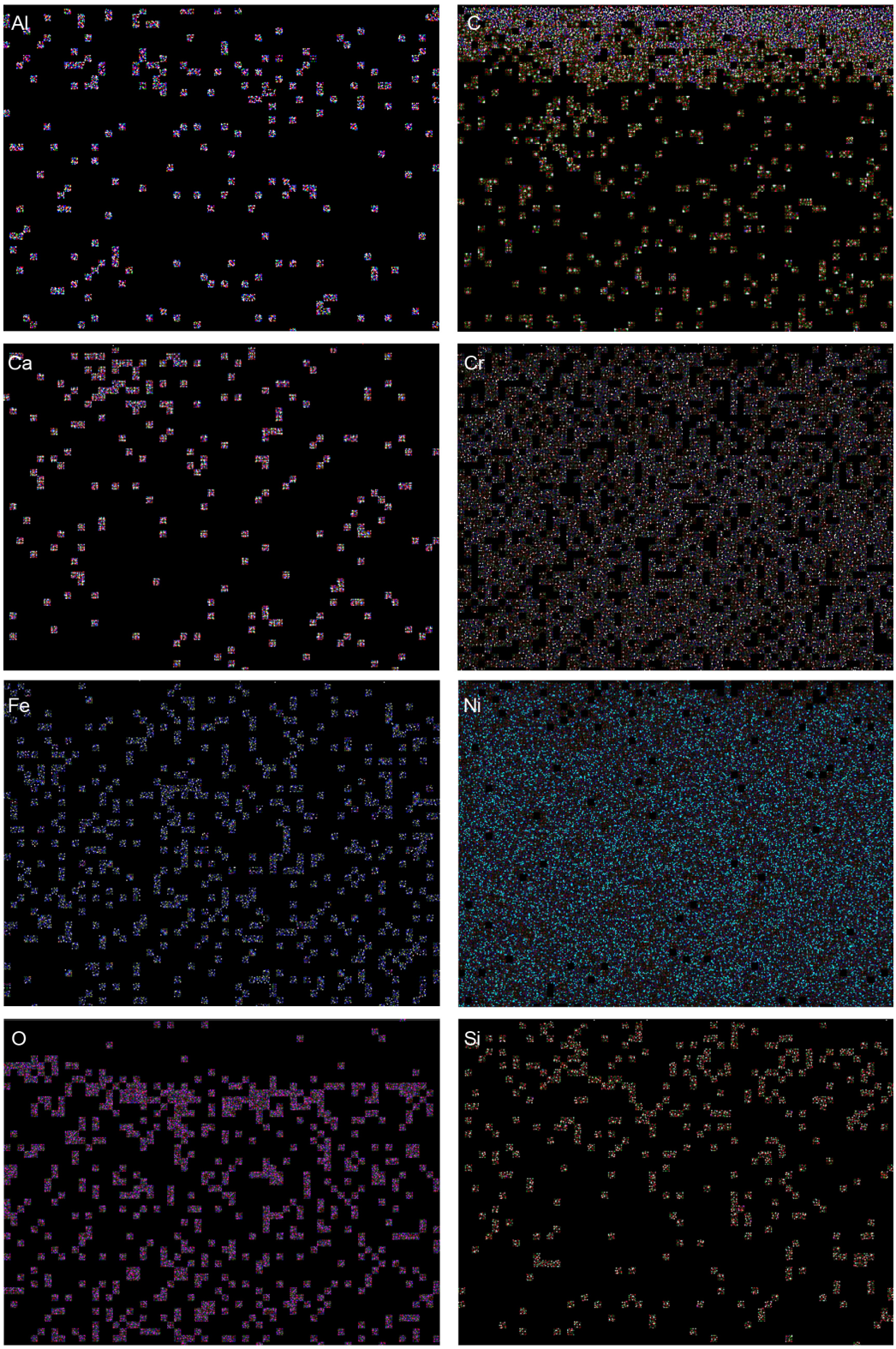


Figure 199.—X-ray elemental images of Inconel wire used to hang samples exposed to Venusian surface conditions for 10 days (area mapped is that of Fig. 197). Each pixel represents information gathered by spectrometer at C, Cr, Fe, Al, Ni, Si, and O Kα line and at Mo and Ta Lα line.